

MCR-73-97
NAS9-12182

CR-134157

Volume V

Earth
Storable
Design

October 1973

Final Report Acquisition/ Expulsion System for Earth Orbital Propulsion System Study

(NASA-CR-134157) ACQUISITION/EXPULSION
SYSTEM FOR EARTH ORBITAL PROPULSION
SYSTEM STUDY. VOLUME 5: EARTH STORABLE
DESIGN Final Report (Martin Marietta
Corp.) 240 p HC \$14.00

N74-12529

CSCL 22B

G3/31

Unclas
23521

MARTIN MARIETTA

MCR-73-97
NAS9-12182

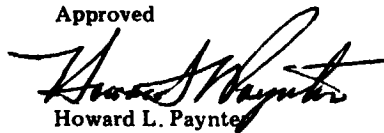
Volume V

Earth
Storable
Design

October 1973

**FINAL REPORT
ACQUISITION/EXPULSION
SYSTEM FOR EARTH
ORBITAL PROPULSION
SYSTEM STUDY**

Approved



Howard L. Paynter
Program Manager

Dale A. Fester
Technical Director
Earth Storable Systems Phase

Prepared for

National Aeronautics and Space Administration
Lyndon B. Johnson Space Center
Houston, Texas

Prepared by

MARTIN MARIETTA CORPORATION
DENVER DIVISION
Denver, Colorado 80201

FOREWORD

This document is submitted to the National Aeronautics and Space Administration, Johnson Space Center by Martin Marietta Corporation Denver Division, as part of the final report for Contract NAS9-12182, *Acquisition/Expulsion System for Earth Orbital Propulsion System Study*. The final report consists of five volumes as follows:

Volume I - Summary Report;

Volume II - Cryogenic Design;

Volume III - Cryogenic Test;

Volume IV - Flight Test Article;

Volume V - Earth-Storable Design.

This work was administered under the technical direction of Mr. Larry Rhodes, NASA-JSC Technical Monitor. Mr. Howard L. Paynter, Chief of the Thermodynamics and Fluid Mechanics Section, Propulsion Department, was the Martin Marietta Program Manager.

The following Martin Marietta personnel made significant contributions to the Phase B earth-storable design effort:

James R. Tegart	Parametric Design and Analysis, Representative System Designs
Preston E. Uney	Material Compatibility, Structural Design, Fabrication, Installation
Glenn F. Holle	Design Requirements and Ground Testing
E. Robert Wilson	Ground Test Detail Design
Dennis E. Gilmore	Representative System Detail Designs

CONTENTS

	<u>Page</u>
I. INTRODUCTION	I-1 thru I-3
II. SYSTEM DESIGN REQUIREMENTS	II-1
A. Acquisition/Expulsion Device Design Requirements	II-1
B. Propellant Physical Properties	II-4
C. Material Compatibility Requirements	II-12
III. PARAMETRIC DESIGN	III-1
A. Surface Tension System Parameters	III-1
B. Candidate Passive Designs	III-30
C. Concept Comparisons	III-36
D. Selection of Preferred Systems	III-60
E. Design Approach	III-62 thru III-72
IV. GROUND TESTING	IV-1
A. Multi-Screen Tests	IV-2
B. Acceptance, Ground Handling, and Inspection Testing	IV-52 thru IV-86
V. REPRESENTATIVE SYSTEM DESIGNS	V-1
A. Refillable Trap	V-1
B. Enlarged Trap	V-32 thru V-42
VI. DEVELOPMENT PLAN	VI-1
A. Objective, Guidelines, and Approach	VI-1
B. Prototype Development Requirements	VI-2
C. Development Program Schedule	VI-7
D. Development Program Cost	VI-8
VII. CONCLUSIONS AND RECOMMENDATIONS	VII-1
A. Conclusions	VII-1
B. Recommendations	VII-2
VIII. REFERENCES	VIII-1 thru VIII-4

Figure

I-1	Program Schedule	I-2
II-1	Propellant Density vs Temperature	II-6
II-2	Propellant Surface Tension vs Temperature	II-7
II-3	Propellant Viscosity vs Temperature	II-8
II-4	Properties of Propane	II-9
II-5	Liquid/Solid Contact Angle	II-11
III-1	Principal Radii of Curvature	III-2
III-2	Liquid/Gas Interface Shape	III-3
III-3	Partially Filled Propellant Tank	III-5
III-4	Stability of an Interface in a Cylindrical Tank	III-6
III-5	Stability of Liquid about a Post in a Spherical Tank	III-7
III-6	Capillary Barrier in a Propellant Tank	III-7
III-7	Lateral Stability of Capillary Barriers	III-9
III-8	Damping Performance of Selected Barriers	III-10
III-9	Damping Categories A thru G	III-11
III-10	Cross-Sectional Views of Various Screen Weaves	III-12
III-11	Categorization of the Initial Flow from a Flat Interface	III-14
III-12	Categorization of the Flow during Settling at the Tank Bottom	III-15
III-13	Categorization of Degree of Settling	III-16
III-14	Pressure Drop due to Hydrostatic Head	III-19
III-15	Retention Capability of Screens as a Function of Hydrostatic Head	III-20
III-16	Pressure Drop due to Area Change	III-21
III-17	Pressure Drop due to Friction - N_2O_4	III-22
III-18	Pressure Drop due to Friction - MMH	III-23
III-19	Pressure Drop due to Friction - N_2H_4	III-24
III-20	Pressure Drop due to Flow through Screen - N_2O_4	III-25
III-21	Pressure Drop due to Flow through Screen - MMH	III-26
III-22	Pressure Drop due to Flow through Screen - N_2H_4	III-27
III-23	Friction Factor due to Flow through Screen	III-28
III-24	Nonrefillable Trap	III-33
III-25	Refillable Trap	III-34
III-26	Liner	III-35
III-27	Effect of Burn Duration on Traps	III-39
III-28	Enlarged Trap Device	III-41
III-29	Propellant Offload Capability for a Liner System during 3-g Boost	III-42
III-30	Modified Liner Devices	III-43
III-31	Device Weight	III-47
III-32	Block Diagrams of Surface Tension Devices	III-50
III-33	Causes of Failure of Surface Tension Devices	III-52

III-34	Variations of Reliability with Operating Conditions	III-53
III-35	Space Shuttle Launch and Servicing Facilities	III-57
III-36	Map of Capillary System Applicability	III-61
III-37	Outline of Total Design Process	III-63
III-38	Refillable Trap Volume	III-65
III-39	Nonrefillable Trap Volume	III-66
III-40	Capillary Barriers	III-67
III-41	Annulus	III-68
III-42	Conical Coverplate for a Refillable Trap	III-69
III-43	Coverplate with Vent Tube	III-70
IV-1	Multiple Screen Performance Test Model	IV-4
IV-2	Bubble Point Test Schematic	IV-5
IV-3	Low-Pressure Test Apparatus	IV-6
IV-4	Assembled Multiple-Screen Test Model	IV-6
IV-5	Installation on the Rucker Centrifuge	IV-7
IV-6	Rucker 17.5-ft-Radius Arm Centrifuge in the Martin Marietta Environmental Test Laboratory	IV-7
IV-7	Multiple-Screen Performance Model, Bubble Point Tests of Typical Dutch-Twill Screen in Methanol	IV-15
IV-8	Multiple-Screen Performance Model, Bubble Point Tests of Square Weave Screen in Methanol	IV-16
IV-9	Average Bubble Point Test Data	IV-17
IV-10	Bubble Point Data from Multiple-Screen Tests	IV-19
IV-11	Apparent Pressure Retention Performance of the Multiple 325 x 2300 Dutch-Twill Screen Barriers under Lateral Acceleration	IV-22
IV-12	Apparent Pressure Retention Performance of the Multiple 180 x 180 Square Weave Screen Barriers under Lateral Acceleration	IV-23
IV-13	Gas Penetration vs Time, 325 x 2300 Dutch- Twill (Run 20)	IV-24
IV-14	Gas Penetration vs Time, 180 x 180 Square Weave (Run 17)	IV-25
IV-15	Gas Penetration Flux vs Time (Screen 1)	IV-26
IV-16	Gas Penetration Flux vs Time (Screen 2)	IV-27
IV-17	Gas Penetration Flux vs Time (Screen 3)	IV-28
IV-18	Gas Penetration Flux vs Time (Screen 1 & 2)	IV-29
IV-19	Gas Penetration Flux vs Time (Screen 3)	IV-30
IV-20	Gas Penetration Flux vs Time (Screen 1)	IV-31
IV-21	Gas Penetration Flux vs Time (Screen 2)	IV-32
IV-22	Influence of Lateral Acceleration Ratio on Initial Ingestion Constant	IV-35
IV-23	Prototype Multiple-Screen Liner for the OMS Monomethylhydrazine Tank	IV-46
IV-24	Performance Estimate Based on Multiple Screen Test Model Data	IV-47

IV-25	Performance Estimate Based on Multiple-Screen Test Model Data Modified for Lateral Acceleration Level	IV-48
IV-26	Inspection and Ground Handling Model	IV-54
IV-27	Screen Liner Components of Inspection and Ground Handling Model	IV-54
IV-28	Inspection and Ground Handling Test System Schematic	IV-56
IV-29	Drip Test for 250 x 1370 Dutch-Twill Screen Liner	IV-61
IV-30	Drip Test for 80 x 700 Dutch-Twill Screen Liner	IV-64
IV-31	Screen Liner Acceptance Drip Tests, Liquid Methanol in Ambient Air	IV-65
IV-32	Vertical Fill Test System Schematic	IV-68
IV-33	Vertical-Horizontal-Vertical Fill-Transport- Install Simulation	IV-69
IV-34	Horizontal Fill Test System Schematic	IV-70
IV-35	Horizontal-Vertical-Horizontal Fill-Transport- Install Simulation	IV-71
IV-36	Test System Schematic for Negative 1-g Expulsion Inspection	IV-73
IV-37	Negative 1-g Expulsion Test	IV-74
IV-38	Test System Schematic for Liquid Spray Remote Inspection Technique	IV-76
IV-39	Determination of System Integrity by Liquid Spray Remote Inspection Technique, Continuous Pressurization	IV-77
IV-40	Determination of System Integrity by Liquid Spray Remote Inspection Technique, Stepwise Pressurization	IV-78
IV-41	Refillable Trap System Installed in Foreshortened Cylindrical Test Tank	IV-80
IV-42	Transparent Fill/Catch Tank	IV-81
IV-43	Fill Mode Schematic	IV-82
IV-44	Expel Mode Schematic	IV-82
IV-45	Completion of Device/Tank Fill Operation	IV-84
IV-46	Minus 1-g Test Configuration	IV-84
IV-47	Lateral 1-g Test Configuration	IV-85
IV-48	Gas-Free Liquid Expulsion under Minus 1-g	IV-85
IV-49	Gas-Free Liquid Expulsion under Lateral 1-g	IV-86
IV-50	Trap Refill Operation Showing Gas Purging through Vent Tube	IV-86
V-1	Refillable Trap	V-3
V-2	Upper and Lower Cone Barriers	V-9
V-3	Welding of Screen to Perforated Plate	V-9
V-4	Lower Cone Barrier Ready for Bubble Point Testing	V-11
V-5	Welded Outlet Assembly	V-12

V-6	Lower Cone Barrier Showing Support Tube/ Outlet Assembly	V-13
V-7	Inner and Outer Perforated Side Rings	V-14
V-8	Welding the Lower Cone Barrier Subassembly to the Inner Ring/Upper Cone	V-15
V-9	Welding the Vent Tube Perforated Cap to the Vent and Support Tube	V-16
V-10	Top View of Trap Showing Small Vent Hole Screens Attached	V-17
V-11	Completed Subscale OMS Trap	V-18
V-12	Capillary Stability of N_2O_4	V-24
V-13	Pressure Retention of N_2O_4	V-25
V-14	Enlarged Pore in Capillary Barrier	V-26
V-15	Enlarged Pore in Annulus Screen	V-28
V-16	Enlarged Pore in Annulus under Flow Conditions	V-29
V-17	Effect of Hole Size on Liquid Quality in a Flowing Annulus	V-30
V-18	Enlarged Trap	V-35
VI-1	Subscale Trap Model	VI-5
VI-2	Minus 1-g Outflow	VI-5
VI-3	Earth-Storable OMS Acquisition/Expulsion System Development Schedule	VI-7

Table

II-1	Representative OMS Mission Criteria	II-2
II-2	Performance Parameters for Propellant Combinations . . .	II-3
II-3	Representative OMS Mission Duty Cycles	II-4
II-4	Properties of Propellants at 20°C (68°F)	II-5
II-5	Vapor Pressure of Propellants	II-11
II-6	Material Compatibility	II-12
III-1	Screen Pressure Retention Data	III-4
III-2	Pressure Retention Capability of Various Screen Meshes, N/cm ² (psi)	III-17
III-3	Recommended Joining Methods for Surface Tension Devices	III-48
IV-1	Candidate Screen Materials for Earth Storable Propellant Acquisition/Expulsion Devices	IV-4
IV-2	Rucker Centrifuge Characteristics	IV-8
IV-3	Multiple-Screen Bubble Point Data	IV-14
IV-4	Properties and Deterioration of Bubble Point Effective- ness of the Multiple-Screen Barriers	IV-18
IV-5	Summary of Lateral Stability Testing of the Multiple-Screen Model	IV-20
IV-6	Constants for Gas Penetration Analysis through Multiple-Layer Screens, Basic Model	IV-34
IV-7	Constants for Gas Penetration Analysis through Multi-Layer Screens for Generalized Relationship . . .	IV-36
IV-8	Comparison between Breakdown Characteristics for Bubble Point Tests and Lateral Stability Tests	IV-37
IV-9	Lateral Acceleration Environment of the Prototype Multiple-Screen Liner	IV-49
IV-10	Lateral Stability of the Screen Liners Tested in the Inspection and Ground Handling Model under a Static 1-g Environment	IV-57
IV-11	Submerged Bubble Point Test Results	IV-60
IV-12	Drip Test Results	IV-63
IV-13	Acceptance Test Evaluation Summary	IV-66
IV-14	Ground Test Results	IV-72
IV-15	Remote Inspection Test Results	IV-79
IV-16	Location of Leak Points	IV-80
V-1	Refillable Trap Parameters	V-2
V-2	Material Selection	V-6
V-3	Enlarged Trap Parameters	V-33
VI-1	Device/Tank Development Summary	VI-3
VI-2	Fabrication Development Summary	VI-4
VI-3	Development Program Cost	VI-8

SUMMARY

A comprehensive analysis and parameteric design effort was conducted under the earth-storable phase of the program. Passive acquisition/expulsion system concepts, representing all known developed capillary systems, were evaluated for a reusable Orbital Maneuvering System (OMS) application. The passive surface tension technique for providing gas-free liquid on demand is superior to other propellant acquisition methods. Systems using capillary pumping to orient the propellant were not serious contenders since they are not capable of functioning properly in the OMS system environment where Reaction Control System (RCS) operation can impose upsetting perturbations at any time. On the other hand, systems using fine-mesh screen can provide the requisite stability and satisfy OMS mission requirements. Both fine-mesh screen liner and trap systems were given detailed consideration in the parametric design, and trap systems were selected for this particular application. These systems are compatible with the 100- to 500-manned mission reuse requirements. They allow simple ground checkout, maintenance, and servicing procedures and provide no restraints on tank loading, transporting, and orbiter installation operations. Although the design depends on engine duty cycle, sufficient flexibility can be designed into a trap device to accommodate the expected variations in number and duration of OMS engine burns. In addition, the trap systems are simple, reusable, inspectable, lightweight, insensitive to propellant offloading, and can be modularly installed.

Two representative fuel and oxidizer trap designs were accomplished for satisfying mission requirements. The preferred approach for the baseline mission is a small, modular trap system that passively refills (purges any ingested gas) during OMS engine burn. The second, larger system is not refillable during mission operation and is assembled in a modular fashion inside the tank. It provides the advantage of being less dependent on mission duty cycle and can accommodate a large number of small engine burns not presently included in the baseline missions. These earth-storable systems are current state of the art. Fabrication techniques are developed. The systems can be acceptance tested and the design can be verified through ground testing. A 13-month program, costing an estimated \$350,000 is required for system development.

A ground test program was conducted to provide supporting information to the system design activity. Lateral stability tests with multiple-screen barriers showed that the extent of gas

ingestion is time dependent and that both transient and steady-state performance must be considered in system design, e.g., only three screen layers may be required to meet the propellant off-load conditions during 3-g boost. Other tests conducted with model trap and liner devices showed these systems to be compatible with expected ground handling operations. Tank fill and drain were demonstrated and transportation and installation on the orbiter were simulated. Acceptance, inspection, and performance tests were performed, showing the designs can be verified through ground testing. Remote inspection of the system installed in the tank was demonstrated; this is particularly pertinent to system reuse.

The surface tension propellant acquisition/expulsion systems designed in this study should be considered for any earth-orbital propulsion system having similar mission criteria. A specific, immediate application is the OMS for the Space Shuttle orbiter. Because of the promising results obtained in the multiple-screen barrier tests, a broader, in-depth experimental program to assess multiple-screen system performance is indicated.

I.

INTRODUCTION

The objective of this three-phased program was to design and verify passive acquisition/expulsion devices for liquid propulsion systems for earth-orbiting vehicles. Phase A of the program was limited to cryogenic propellants, while the Phase B effort was concerned with earth storables. An orbital test plan to verify the passive tank/feedline design for cryogens selected in Phase A was developed under Phase C. This report documents the effort conducted under Phase B.

The specific objective of Phase B was to define the design parameters for an earth-storable orbital maneuvering system (OMS) through analysis and testing. This objective was accomplished in performing the four Phase B tasks, Tasks I thru IV, as shown by the program schedule in Fig. I-1. The schedule for the 23-month technical effort shows the relationship between the Phase B tasks and those of the other two phases. Task I, begun in March 1972, was a four-month effort to establish system design requirements. The results of this activity were assembled into a design requirements document (Ref I-1) to complete Task I. Following publication of Reference I-1, updated criteria for the Shuttle OMS system were obtained and reviewed to assure that the parametric designs reflected the full range of probable earth-orbital vehicle requirements. The design requirements for the earth-storable OMS used in Phase B are presented in Chapter II.

Task II was begun in May 1972 to perform parametric analyses and design of earth-storable acquisition/expulsion systems per the design requirements criteria. Both trap and liner acquisition/expulsion systems were baselined. Various devices representing all known capillary systems developed or under development were compared and evaluated for the earth-storable OMS application. An interim report published in April 1973 summarized the results of the system comparison (Ref I-2). The parametric design effort is discussed in Chapter III of this volume.

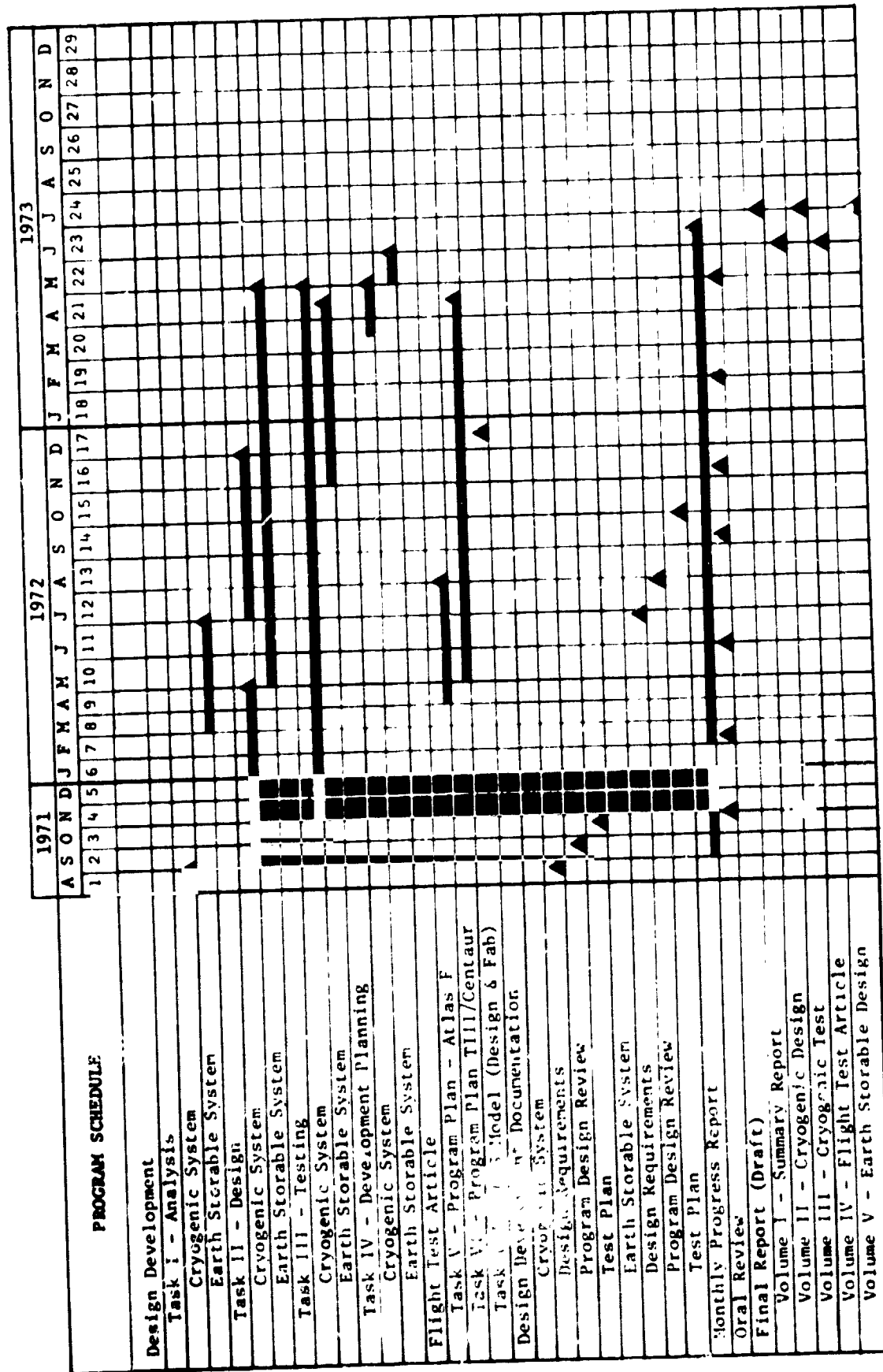


Figure 1-1 Program Schedule

The Task II design activity was supported by selected subscale ground tests (Task III). The experiments in support of the Phase B program comprised the tests needed to verify analytical predictions or to provide data in support of the design activity. A test plan was published in September 1972 to direct the experimental effort (Ref I-3). It was reviewed and approved by NASA-JSC and the Task III testing effort was initiated at the beginning of November 1972. Testing was conducted with multiple-screen barriers to compare actual performance with predicted lateral stability and to obtain information on the gas ingestion rate. Other tests were conducted with a subscale screen trap and models of complete screen liners to develop and demonstrate acceptance test procedures and functional inspection techniques. The models were also subjected to the expected ground handling operations, including vertical fill and drain, horizontal transport, and orbiter installation. All test models were fabricated by Martin Marietta using specially developed manufacturing techniques. Details of the tests and the results obtained are presented in Chapter IV.

Using the preferred systems resulting from the parametric design and the ground test results, two representative acquisition/expulsion system designs were prepared for the earth-storable OMS to complete Task II. These designs are presented and discussed in Chapter V. Considerations included fabrication and installation, acceptance testing, ground and flight operations, reusability and inspection, mass, reliability, and a failure modes and effects analysis (FMEA).

Task IV, a one-month development planning activity, was conducted during May 1973 to define the development program required for an earth-storable OMS acquisition/expulsion system. Using existing design and fabrication techniques, the program would develop the fabrication, quality control, acceptance, and fit test procedures for the specific system. Structural and fluid performance testing would be included, along with a detailed design of the developed system. This development plan is presented in Chapter VI. It includes a description of the program, together with the estimated cost and schedule.

Conclusions and recommendations resulting from the earth-storable phase of the program are presented in Chapter VII. References for this volume are contained in Chapter VIII.

II. SYSTEM DESIGN REQUIREMENTS

The criteria used in the parametric evaluation of the surface tension devices are presented in this chapter. First, the mission criteria and requirements for a typical earth-orbital propulsion system are defined. Propellant properties important to the design of surface tension devices are then discussed. Finally, the compatibility of propellants with materials of construction is summarized.

A. ACQUISITION/EXPULSION DEVICE DESIGN REQUIREMENTS

The propulsion system considered in this study provides large, on-orbit ΔV maneuvers for an earth-orbital spacecraft using earth-storable propellants. The highly maneuverable spacecraft is manned and reusable. Since the Space Shuttle orbital maneuvering system (OMS) is typical of this class of propulsion systems, Shuttle OMS mission criteria and requirements were used as guidelines to establish design requirements. Since these criteria are general in nature, the study results can be applied to a wide range of earth-orbital propulsion systems.

Initially, the design criteria were based primarily on the results of a Space Shuttle OMS tradeoff study conducted by McDonnell Douglas Corporation. These criteria were published in the design requirements document (Ref I-1). As the Space Shuttle OMS evolved and Rockwell International was selected by NASA as the prime contractor, the criteria and requirements for this study were updated accordingly. The mission criteria important to the design of surface tension propellant acquisition systems are summarized in Table II-1.

1. Propulsion System Criteria

The typical propellant combination given primary emphasis in this study was N_2O_4 and MMH. Other fuels considered included N_2H_4 , UDMH, A-50, RP-1, and propane.

The OMS system has two engines, each fed by its own separate fuel and oxidizer tanks. A specific tank size shown in Table II-1 was identified for use in preliminary design studies. Elliptical end domes as well as hemispherical domes were considered. Tank size and volume can vary depending on the specific propellants, packaging requirements, and mission ΔV requirements.

Table II-1 Representative OMS Mission Criteria

Spacecraft Parameters	
Weight at End of Boost	125,700 kg (277,200 lbm)
Dry Weight	77,100 kg (170,000 lbm)
Main Engine Thrust	26,700 N (6000 lbf)
Reaction Control System (RCS) Engine Thrust	4,890 N (1100 lbf)
Tanks - Cylindrical with Hemispherical End Domes	
- Size, 1.016 m (40 in.) diameter by 3.94 m (155 in.) long	
- Volume, 2.92 m ³ (103 ft ³)	
Acceleration Environment	
Boost	+3 g
Main Engines	+0.02 to 0.07 g
RCS Engines	+0.008 to 0.026 g
Coast	+~10 ⁻⁴ to 10 ⁻⁶ g

Due to such effects as aerodynamic heating, engine heat soak-back, and solar radiation, the propellant temperatures were assumed to range from 0°C (32°F) to 50°C (122°F).

Based on a 26700-N (6000-lbf) thrust engine, the propellant flow rate for each of the propellants considered is listed in Table II-2.

2. Acceleration Environment

The typical mission accelerations are listed in Table II-1. Accelerations produced during boost and by the main engines are axial and positive. They tend to settle the propellant within the OMS tanks over the outlet. Reaction control system (RCS) accelerations can act in any direction and are of the same order of magnitude as those produced by the main engines.

Table II-2 Performance Parameters for Propellant Combinations

Propellant Combination	Specific Impulse, Ns/kg (lbf-s/lbm)	Mixture Ratio, kg Oxidizer/kg Fuel	Flow Rate, kg/s (lbm/s)
N ₂ O ₄ .MH	3020 (308)	1.63	5.47 (12.1) 3.36 (7.40)
N ₂ O ₄ N ₂ H ₄	3099 (316)	1.11	4.52 (9.98) 4.08 (9.00)
N ₂ O ₄ A-50	3079 (314)	1.60	5.34 (11.8) 3.33 (7.34)
O ₂ UDMH	3265 (333)	1.68	-- -- 3.05 (6.72)
O ₂ RP-1	3148 (321)	2.63	-- -- 2.34 (5.15)
O ₂ Propane	3226 (329)	2.80	-- -- 2.17 (4.80)

While coasting in orbit, various forces (due to the interactions of the space vehicle with the atmosphere, the gravitational field, and the electric fields of space) will accelerate the vehicle. Typical values of these accelerations range from 10^{-4} g to 10^{-11} g, with the aerodynamic drag being the most significant (Ref II-2). For an orbiter in a 185-km (100-n-mi) orbit, it is estimated that drag will produce an acceleration of 3×10^{-6} g for a zero angle of attack, and 1.6×10^{-5} g for a 90° angle of attack. Docking and deployment of payloads, based on cargo manipulating systems presently being considered (Ref II-3), will produce accelerations on the order of 6×10^{-5} g. Movement of the crew within the spacecraft is expected to produce an acceleration of approximately 2×10^{-4} g (Ref II-4).

3. Mission Duty Cycle

Table II-3 summarizes the mission duty cycle for three typical Shuttle orbiter missions. Since the spacecraft is manned and highly maneuverable, considerable variation in the duty cycle is possible.

Table II-3 Representative OMS Mission Duty Cycles

Engine Burn	Due East Mission				Resupply Mission				Polar Mission			
	Elapsed Time from Launch			Burn Duration, s	Elapsed Time from Launch			Burn Duration, s	Elapsed Time from Launch			Burn Duration, s
	hr	min	s		hr	min	s		hr	min	s	
1	00	42	43	98	00	50	48	127	00	42	37	89
2	01	26	56	24	22	15	54	274	48	02	42	50
3	135	00	00	34	23	01	42	232	48	46	53	50
4	135	54	41	60	24	35	57	17	50	44	29	16
5	136	29	44	36	70	18	51	414	166	45	20	140
6	138	26	48	16								
7	145	25	00	80								
8	164	51	35	157								

The amount of propellant loaded may depend on the mission duty cycle when the same space vehicle must perform many varied missions. Partial propellant loads as small as 25% of the tank volume are possible.

B. PROPELLANT PHYSICAL PROPERTIES

The propellants considered in this study were:

Oxidizer - Nitrogen tetroxide, N_2O_4 ;

Fuels - Hydrazine, N_2H_4 ,
 Monomethylhydrazine (MMH), $CH_3N_2H_3$,
 Unsymmetrical dimethylhydrazine (UDMH), $(CH_3)_2N_2H_2$,
 Aerozine-50 (A-50), a 50-50 mixture by weight of
 N_2H_4 and UDMH,
 Kerosene (RP-1), $(CH_2)_x$,
 Propane, C_3H_8 .

Some possible combinations of these propellants and their performance are shown in Table II-2. Monomethylhydrazine, N_2H_4 , and A-50 can be used in combination with N_2O_4 , while UDMH, RP-1, and C_3H_8 provide better performance with liquid oxygen (LO_2). Since propellant acquisition for a cryogenic oxygen system was evaluated in Phase A of this program, N_2O_4 was the only oxidizer considered in Phase B.

Table II-4 Properties of Propellants at 20°C (68°F)*

Propellant	Density, ρ		Surface Tension, σ		Kinematic Surface Tension, β		Viscosity, μ		Kinematic Viscosity, ν	
	$\frac{gm}{cm^3}$	$\frac{lbm}{ft^3}$	$\frac{dynes}{cm}$	$\frac{lbf}{ft} \times 10^3$	$\frac{dyne\ cm^2}{gm}$	$\frac{lbf\ ft^2}{lbm} \times 10^5$	Centipoise (cp)	$\frac{lbf\ ft-s}{x\ 10^3}$	Centistoke (cs)	$\frac{ft^2}{s} \times 10^5$
<u>Oxidizer</u>										
N_2O_4	1.447	90.2	27.4	1.88	18.94	2.08	0.421	0.283	0.291	0.314
<u>Fuels</u>										
N_2H_4	1.007	62.8	63.2	4.33	62.76	6.89	0.974	0.654	0.968	1.041
MMH	0.880	54.9	34.3	2.35	38.98	4.28	0.860	0.578	0.977	1.052
UDMH	0.791	49.4	28.0	1.92	35.40	3.89	0.550	0.370	0.695	0.750
A-50	0.904	56.4	30.2	2.07	33.41	3.67	0.870	0.585	0.965	1.040
RP-1	0.808	50.4	27.0	1.85	33.42	3.67	1.760	1.180	2.180	2.340
$C_3H_8^*$	0.584	36.4	15.4	1.06	26.37	2.91	0.210	0.141	0.360	0.388

*The properties of C_3H_8 are given at its normal boiling point, -42°C (-44°F).

The propellant properties important to the design of a propellant acquisition system are density, surface tension, and viscosity. The values of these properties are listed in Table II-4 and are plotted as a function of temperature in Fig. II-1 thru II-4. The variation of these properties with pressure is small and can be neglected. The temperature range selected (0 to 60°C or 40 to 160°F) represents the possible extremes in the typical operating environment for all propellants with the exception of propane. Since propane has a normal boiling point of 231°K (416°R), it would be stored at temperatures lower than those of the other propellants. The properties of propane were obtained from Reference II-5, while the properties of the other propellants were obtained from Reference II-6.

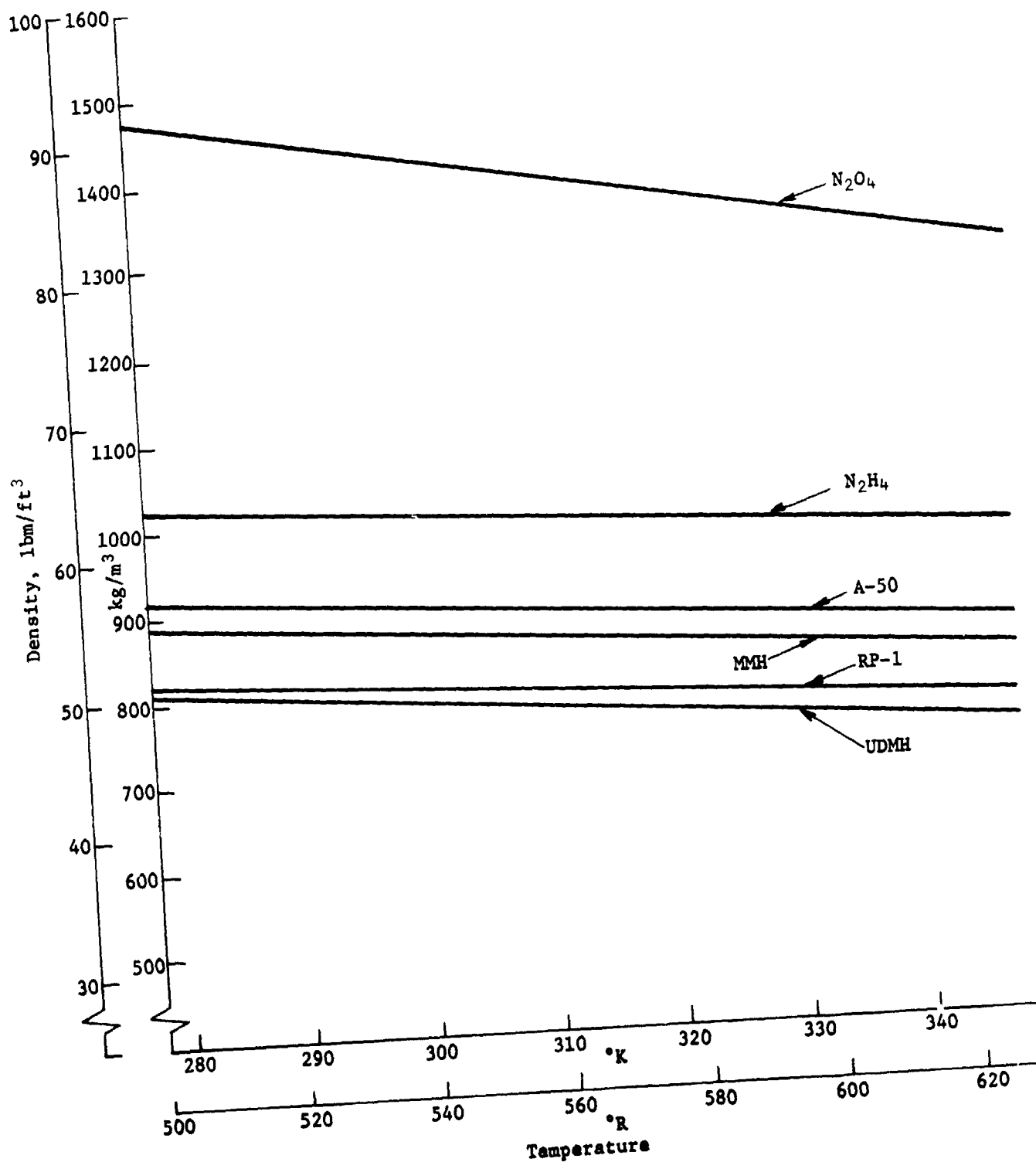


Fig. II-1 Propellant Density vs Temperature

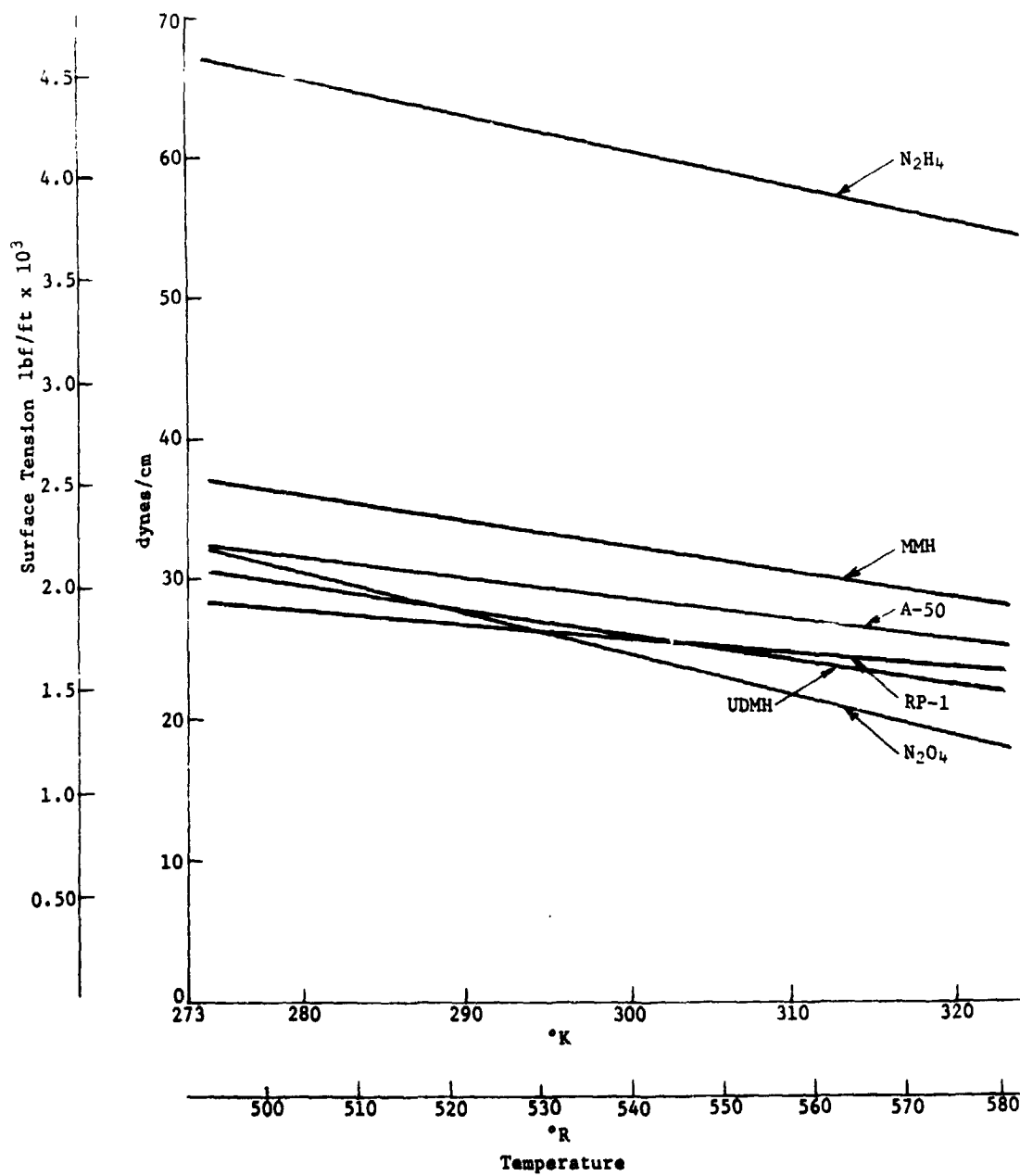


Fig. II-2 Propellant Surface Tension vs Temperature

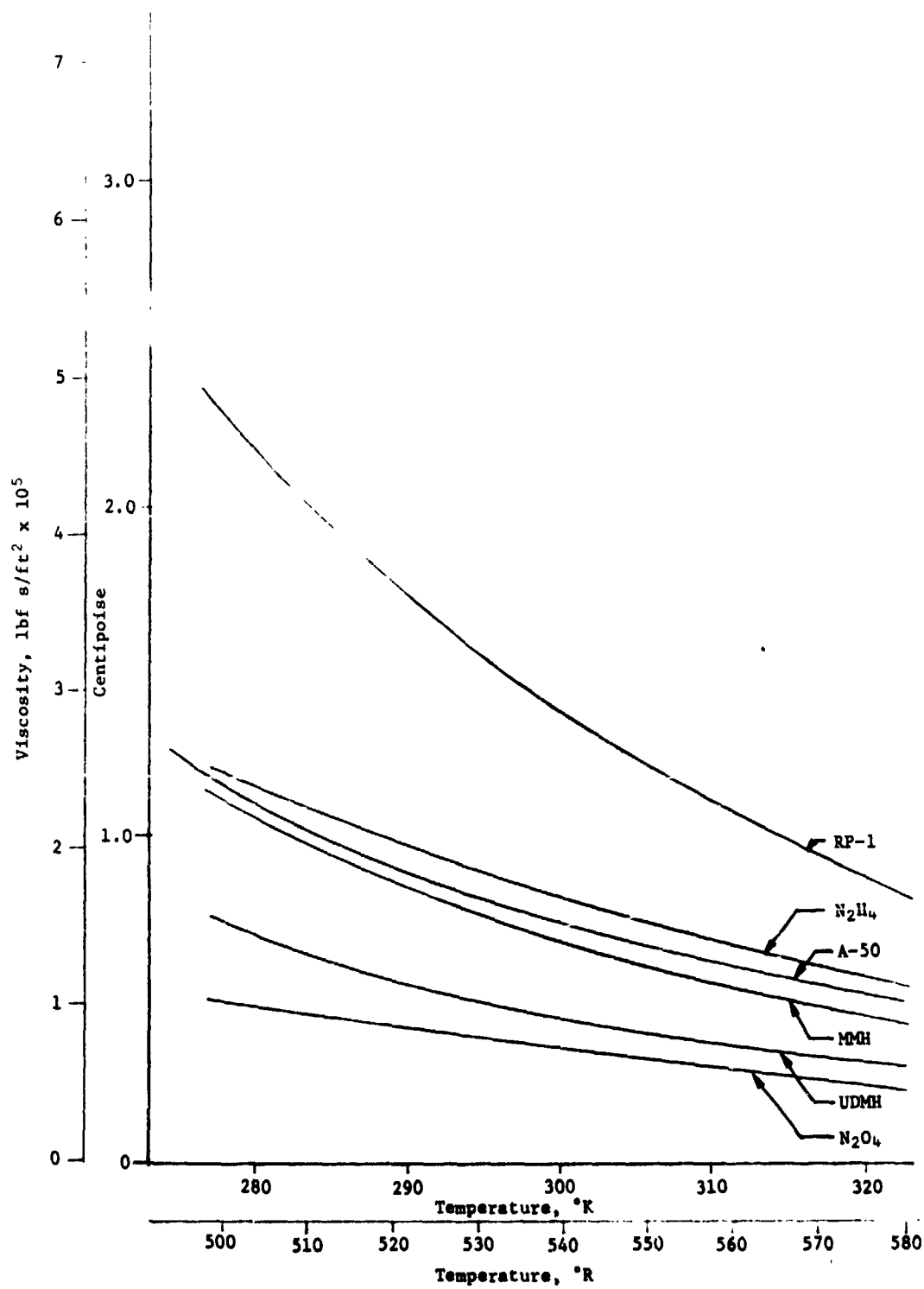


Fig. II-3 Propellant Viscosity vs Temperature

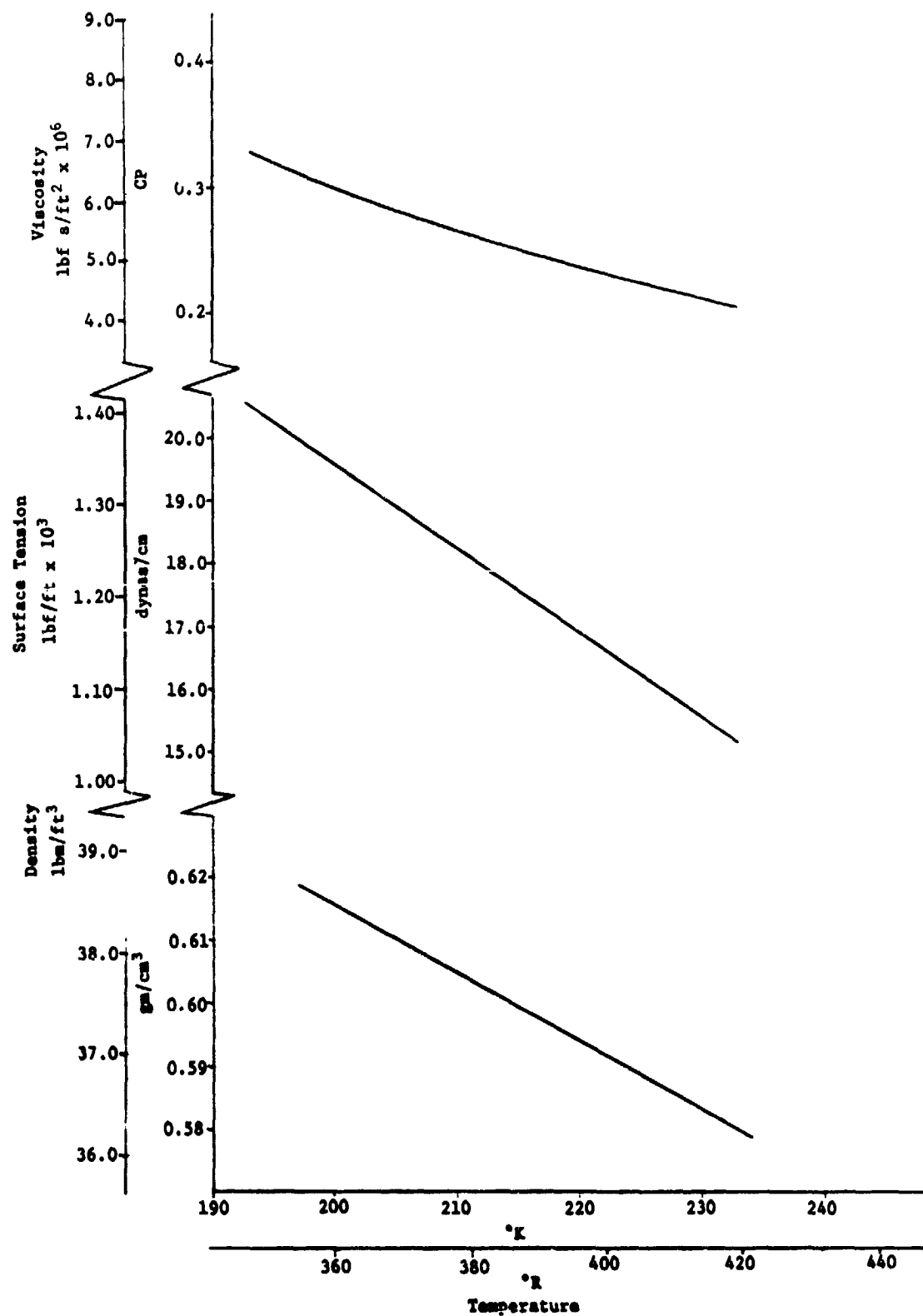


Fig. II-4 Properties of Propane

An examination of propellant properties shows that most have similar characteristics. Hydrazine has the highest surface tension, 70% higher than MMH, and propane has the lowest surface tension. The kinematic surface tension (γ/ρ) is usually of greater interest since body forces will be involved in addition to capillary forces in any application. Hydrazine has the highest kinematic surface tension and N_2O_4 has the lowest value. RP-1 has the highest viscosity, being 80% more viscous than N_2H_4 , while propane is the least viscous. Comparing kinematic viscosities (μ/ρ), RP-1 has the highest value and N_2O_4 the lowest. With a few exceptions, most of the propellant properties are comparable. The exceptions and specific implications are as follows:

- 1) N_2O_4 has a density at least 40% higher than the other propellants. For a given volumetric flow rate, it will produce greater pressure losses;
- 2) N_2O_4 has a kinematic surface tension about one-half the others. This makes it the most difficult of the propellants for a surface tension system to retain;
- 3) RP-1 has the highest kinematic viscosity, more than twice as great as the others. Frictional pressure losses due to flow will be high with this liquid.

The liquid/solid contact angle is another property that is important to the operation of capillary systems. This angle, θ , is defined in Fig. II-5. A liquid that readily wets a surface, i.e., has a near-zero contact angle, is the most desirable for a capillary system. Contact angle is independent of pressure and temperature, but is sensitive to the purity of the propellant and the cleanliness of the solid surface. On a previously wetted clean metal surface, all of the candidate propellants will have contact angles of 2 degrees or less.

The temperature at which these propellants must be stored is another important consideration. Table II-5 lists the vapor pressure of the liquids at 20°C (68°F). Propane must be stored at lower than ambient temperatures, near its normal boiling point. Tank insulation and/or some form of thermal control will be necessary. The normal storage precautions are required with the other propellants.

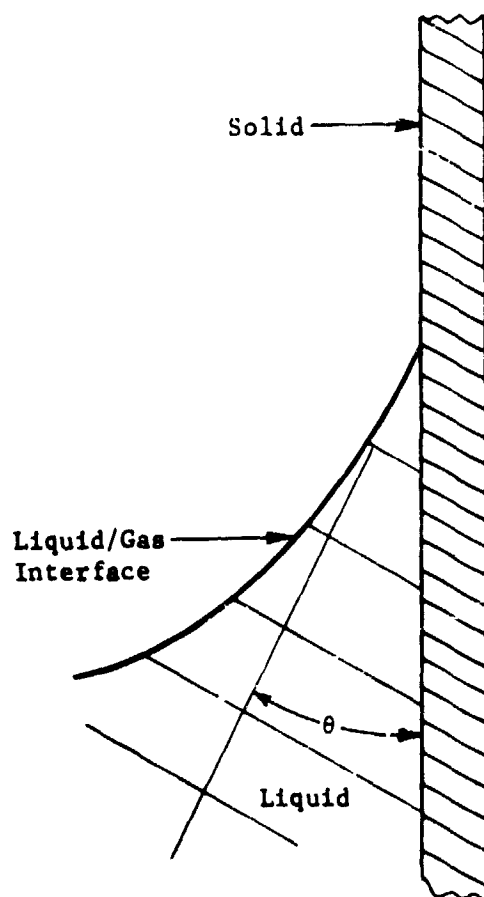


Fig. II-5 Liquid/Solid Contact Angle

Table II-5 Vapor Pressure of Propellants

Propellant	Vapor Pressure at 20°C (68°F), N/cm ² (psia)
N ₂ O ₄	9.79 (14.2)
A-50	1.59 (2.3)
MMH	0.55 (0.8)
N ₂ H ₄	0.14 (0.2)
UDMH	1.72 (2.5)
RP-1	0.14 (0.2)
C ₃ H ₈	85.49 (124.0)

The propellants are similar from the standpoint of the design or operation of a subsonic tension propellant acquisition/expulsion system. No unusual properties are exhibited by any of the fluids. In general, a design for one of the propellants is also applicable to the others.

C. MATERIAL COMPATIBILITY REQUIREMENTS

An important consideration in the design of propellant management devices is the compatibility of the construction materials with the propellants.

To aid in selecting materials and designing and evaluating the propellant management devices, available information was compiled on the compatibility of spacecraft materials with the propellants of interest. Table II-6 summarizes this information for the more commonly used aerospace materials. The information was obtained primarily from References II-6 thru II-10. Compatibility of a material with a propellant was based on the criteria that the material be essentially unaffected by propellant exposure (negligible corrosion for metals and negligible loss of physical properties for nonmetals) and that it should not significantly affect either the physical properties or the stability of the propellant. Reference II-7 should be consulted for a more detailed discussion of propellant/material compatibility.

Table II-6 Material Compatibility

Material	Propellant						
	N ₂ O ₄	N ₂ H ₄	MMH	UDMH	A-50	RP-1	C ₃ H ₈
Aluminum							
1100, 2219, 6061	B	A	A	A	A	A	A
Stainless Steel							
304, 321, 347	B	B	A	A	A	A	A
316	B	C	C	B	C	A	A
6Al-4V Ti	A	A	A	A	A	A	A
Nonmetals							
Teflon	B	A	A	A	A	A	A
Kel-F	C	A	C	C	C	B	B
EPR	C	B	B	B	B	B	C
Legend: A - Good B - Acceptable C - Undesirable							

III. PARAMETRIC DESIGN

A parametric approach to the selection and design of a surface tension propellant acquisition system is presented in this chapter. The system selected must be capable of meeting the general design requirements presented in the previous chapter. First, the parameters essential to the operation of surface tension devices are presented and their features and sensitivities are compared. Based on the comparison a preferred system was selected. Finally, the general approach to designing the selected system is discussed.

A. SURFACE TENSION SYSTEM PARAMETERS

The design of surface tension devices is based on the application of established design parameters and analysis of the flow of liquid within both the device and the propellant tank. The most basic of these parameters are presented in the following paragraphs.

1. Design Parameters for Screen Systems

The operation of surface tension devices using fine-mesh screen material depends on the interaction of the gas/liquid interface with the device. The pressure differential across the screen can be used to retain and orient the propellant within the tank. It is essential that the interface be both hydrostatically and hydrodynamically stable before the pressure differential can be used.

a. *Pressure Retention* - A pressure differential exists at any curved gas/liquid interface due to intermolecular forces. This capillary pressure difference ΔP_c may be expressed at any point across the interface as

$$\Delta P_c = \sigma \left(\frac{1}{R_1} + \frac{1}{R_2} \right) \quad [1]$$

where σ is the liquid/gas surface tension and R_1 and R_2 are the principal radii of curvature of the interface. The two principal radii are defined for a given point A on the interface as shown in Fig. III-1. The centers of the arcs lie on a line AB perpendicular to the surface and passing through the point A on the surface. R_1 and R_2 lie in planes that are perpendicular to one another; the intersection of the planes forms line AB. For a flat interface, R_1 and R_2 become infinite so the pressure difference is zero.

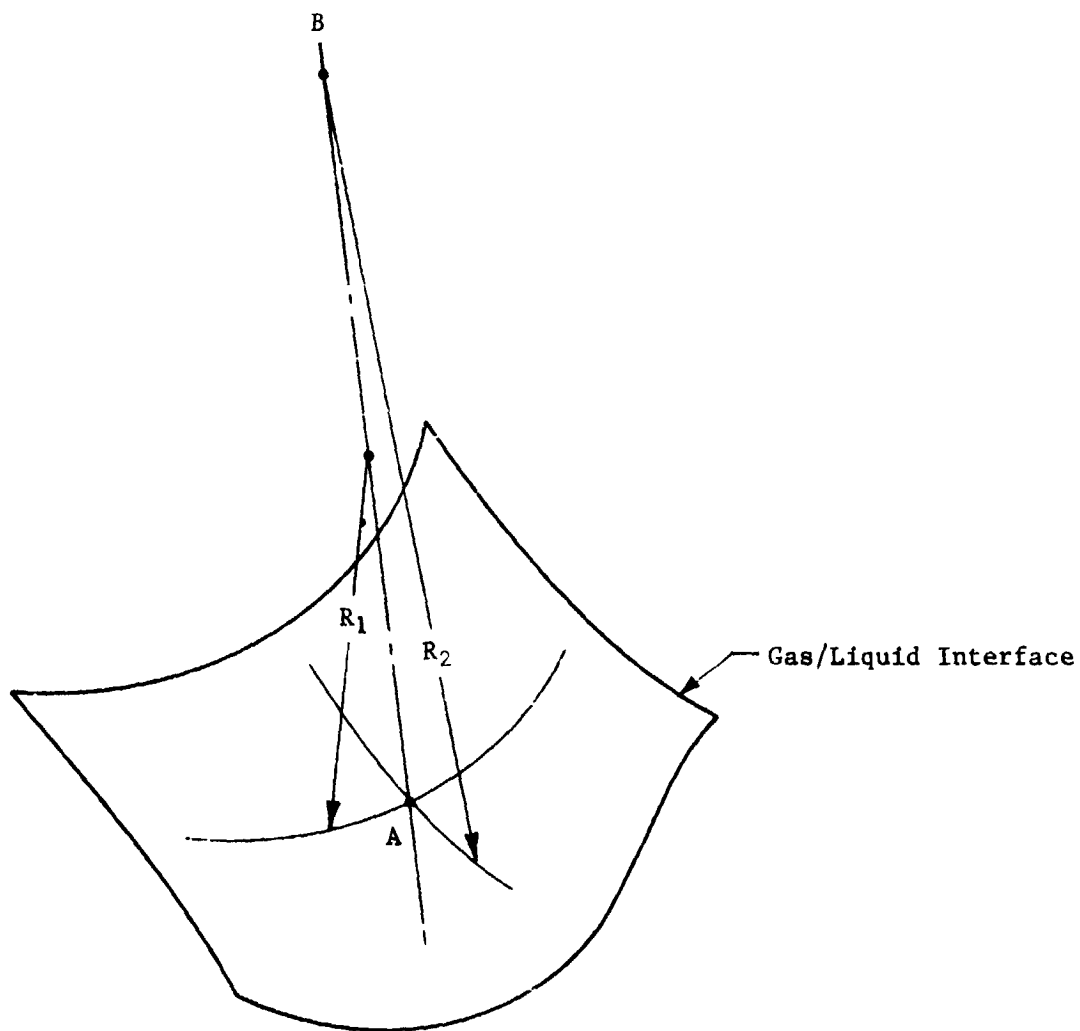


Fig. III-1 Principal Radii of Curvature

For a spherical interface, R_1 equals R_2 and the pressure difference is

$$\Delta P_c = \frac{2\sigma}{R_s} \quad [2]$$

where R_s is the radius of curvature. The capillary pressure difference can be related to a dimension (other than the radius of curvature) such as the pore radius R and a second parameter, the liquid-to-solid contact angle θ . This is done by introducing

the relationship between R , θ , and R_s as shown in Fig. III-2.

Then, rewriting Equation [2] as

$$\Delta P_c = \frac{2\sigma}{R} \cos\theta, \quad [3]$$

the designer can easily calculate the capillary pressure difference from measurable parameters. Surface tension and contact angle values for the propellants of interest were presented in Chapter II.

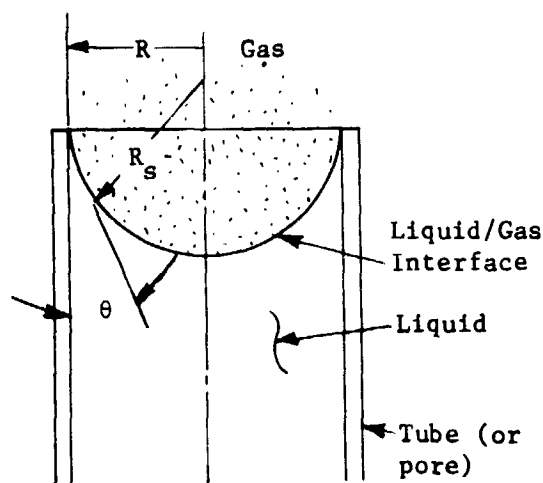


Fig. III-2 Liquid/Gas Interface Shape

The capillary pressure difference for a circular pore, as in a perforated plate, can be determined from equation [3]. Capillary pressure retention for pore geometries other than circular is more accurately determined empirically. The accepted technique is the so-called "bubble point" method. The screen material is covered by a thin layer of liquid, usually alcohol, and its underside is pressurized slowly with air or gaseous nitrogen. The pressure difference at which the first bubble passes through the material is termed the bubble point (BP). The pressure retention capability for various screen mesh sizes, as determined by Martin Marietta using the BP technique, is presented in Table III-1.

Table III-1 Screen Pressure Retention Data

Screen Material	Screen Mesh	Bubble Point, BP, mm (in.) of H ₂ O		
		As-Received	Vapor-Degreased	Ultrasonically Cleaned
Stainless Steel	30x30	17.3 [2]* (0.68)	17.3-17.5 [3] (0.68-0.69)	--
Stainless Steel	50x50	30.2-30.5 [2] (1.19-1.20)	31.0-31.2 [6] (1.22-1.23)	--
Stainless Steel	60x80	44.5-45.7 [2] (1.75-1.80)	45.7-47.0 [6] (1.80-1.85)	--
Stainless Steel	100x100	55.9-57.9 [4] (2.20-2.28)	55.9-56.4 [5] (2.20-2.22)	--
Stainless Steel	150x150	69.3-81.3 [4] (2.73-3.20)	78.7-79.2 [5] (3.10-3.12)	--
Stainless Steel	200x200	95.3-116.3 [11] (3.75-4.60)	98.8-111.8 [12] (3.89-4.40)	--
Aluminum	120x120	52.3-56.9 [13] (2.06-2.24)	55.1-54.8 [16] (2.17-2.55)	--
Aluminum	30x250	63.5-68.6 [6] (2.50-2.70)	66.8-68.8 [7] (2.63-2.71)	--
Aluminum	200x1400	414.0-416.6 [2] (16.30-16.40)	-- --	--
Stainless Steel	24x110	50.5-53.1 [5] (1.99-2.09)	49.8-53.8 [12] (1.96-2.12)	--
Stainless Steel	30x250	65.5-53.1 [5] (2.58-2.65)	64.5-76.2 [15] (2.54-3.00)	--
Stainless Steel	80x700	161.8-164.6 [5] (6.37-6.48)	64.5-76.2 [6] (6.28-6.36)	--
Stainless Steel	165x800	198.6-210.8 [17] (7.82-8.30)	200.7-209.0 [14] (7.90-8.23)	199.4-207.3 [15] (7.85-8.16)
Stainless Steel	200x1400	424.2-442.0 [18] (16.70-17.40)	424.2-432.8 [15] (16.70-17.04)	433.8-438.2 [17] (17.08-17.25)
Stainless Steel	250x1370	535.9-579.5 [12] (21.10-22.83)	528.3-563.9 [13] (20.80-22.20)	543.6-569.0 [20] (21.40-22.40)
Stainless Steel	325x2300	629.9-679.5 [18] (24.80-26.75)	638.8-670.6 [16] (25.15-26.40)	655.8-678.2 [21] (25.82-26.70)

*Numbers in brackets are the number of samples tested in methanol.

The pressure retention for a given screen material and mesh size can be determined for other liquids from

$$(BP)_{\ell} = \frac{\sigma_{\ell}}{\sigma_{t\ell}} (BP)_{t\ell} \quad [4]$$

where the subscripts refer to the other liquid ℓ and to the test liquid $t\ell$.

b. *Hydrostatic Interface Stability* - Figure III-3 shows a partially filled cylindrical tank. The acceleration vector is parallel to the tank axis and tends to reorient the propellant to the opposite end of the tank. However, if the proper relationship between fluid properties (surface tension and density) and system geometry (tank radius) exist, the liquid/gas interface will be stable and the liquid will remain as shown. The criterion for determining hydrostatic interface stability is the Bond number (Bo), a dimensionless ratio of body forces to capillary forces:

$$Bo = \frac{\rho a L^2}{\sigma} \quad [5]$$

The characteristic system dimension L is the tank radius (r) for the system shown.

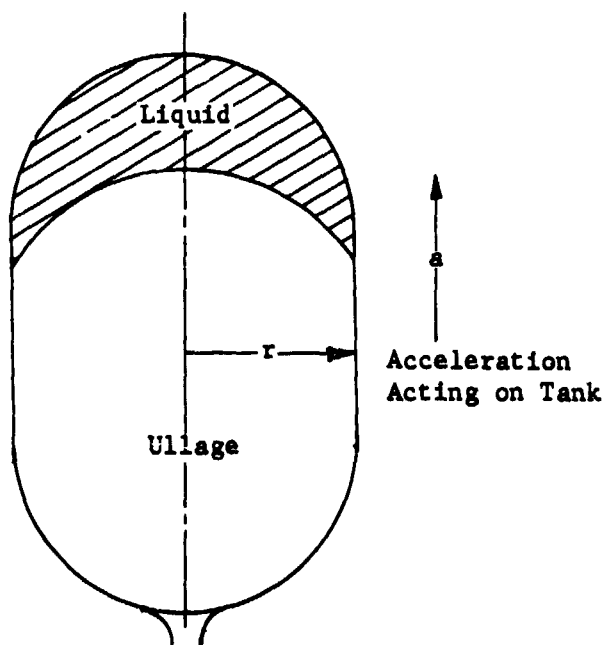


Fig. III-3 Partially Filled Propellant Tank

Under Contract NAS8-11328 (Ref III-1), the behavior of a gas/liquid interface in a cylindrical tank was investigated using the drop tower. It was found that the interface was stable for $Bo \leq 0.84$. The stability of an interface can be calculated (Ref III-2), yielding a curve for the critical Bond number as a function of contact angle as shown in Fig. III-4. An interface in a bare spherical tank will never be stable when an acceleration is tending to displace the liquid. However, the addition of an object that changes the internal geometry of the spherical tank will provide some stability. For example, a cylindrical post over the outlet gives the stability shown in Fig. III-5 (Ref III-2).

Next, consider the stability of a capillary barrier located within a tank as shown in Fig. III-6. When the acceleration is axial and the pores in the capillary barrier are circular, the results obtained above for a cylindrical tank also apply, i.e., the critical Bo is 0.84 when the contact angle is zero. This has been verified by drop tower tests of capillary barriers, which have also shown that the critical Bo for a square weave screen is 0.45 (Ref III-3).

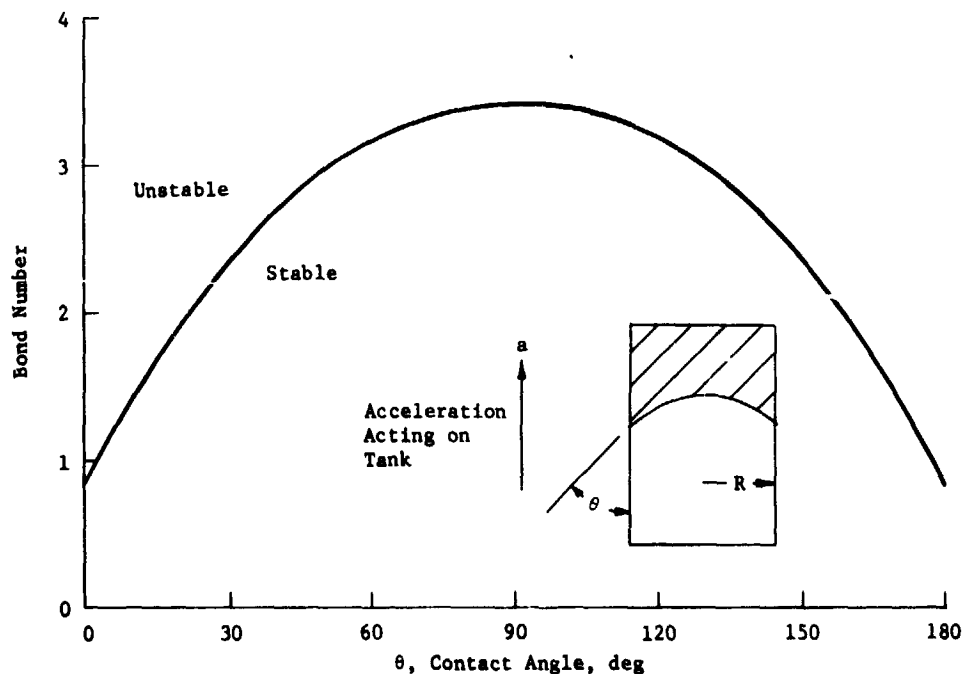


Fig. III-4 Stability of an Interface in a Cylindrical Tank

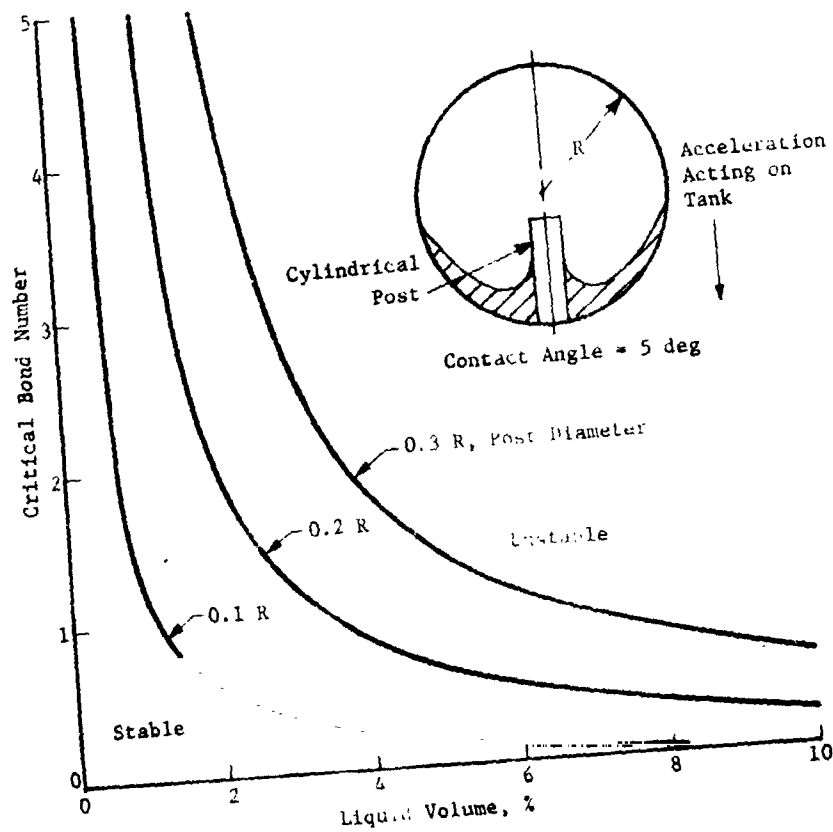


Fig. III-5 Stability of Liquid about a post in a spherical Tank

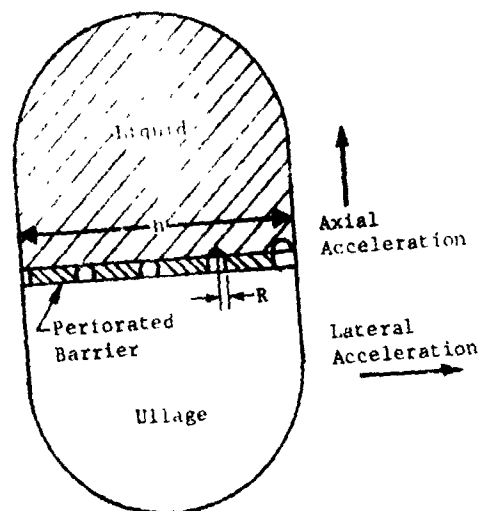


Fig. III-6 Capillary Barrier in a Propellant Tank

When the acceleration is acting laterally (parallel to barrier), the stability is expressed using a modified Bo number termed the ϕ number:

$$\phi = \frac{\rho a h R}{\sigma} \quad [6]$$

where the characteristic system dimensions are both the width of the barrier h and the radius of a pore in the barrier R . The experimentally determined lateral stability of various capillary barriers is shown in Fig. III-7 (Ref III-3).

c. Hydrodynamic Stability Criteria - Capillary barriers must also damp and control the motion of liquid within a propellant tank. Experimental work shows that the Weber number (We) can be used to predict low-g hydrodynamic stability (Ref III-3). The critical We number, a ratio of inertia to capillary forces, is

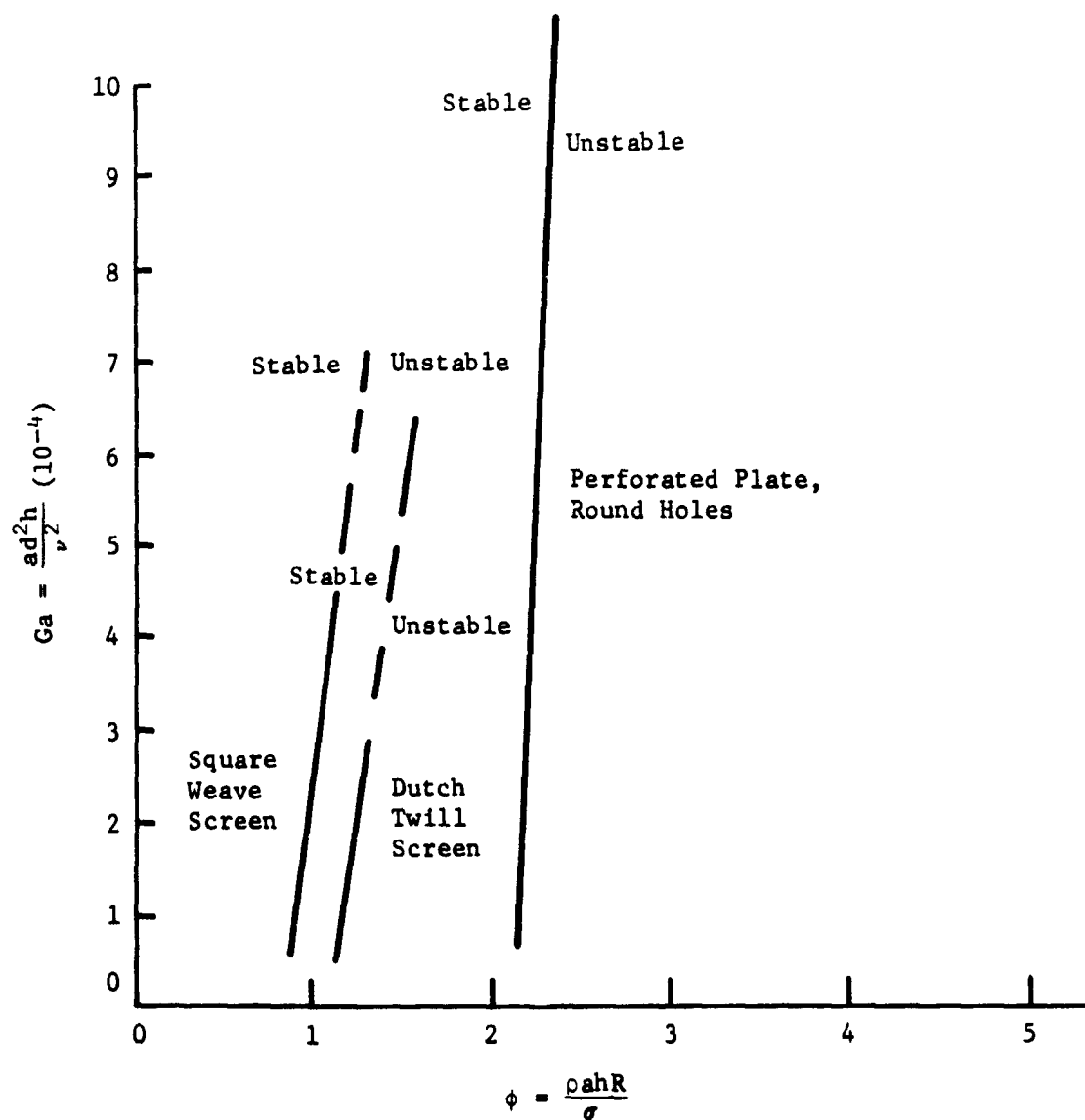
$$We_c = \frac{V_c^2 L}{\beta} \quad [7]$$

where L is the characteristic dimension of the screen material (pore radius, for example), V_c is the liquid impingement velocity, and β is the kinematic surface tension (σ/ρ). The damping performance of various capillary barriers is shown in Fig. III-8. The damping categories are defined by Fig. III-9.

d. Screen Materials - Materials used in the fabrication of capillary devices can range from perforated plate to square-weave screens to the fine-mesh screens using various types of twill weaves. Perforated plate is used when pore radii on the order of 3 mm (0.118-in.) and larger are required. Square-weave screens will provide pore radii down to approximately 40 μ (0.0016 in.). A Dutch-twill weave can provide the smallest pore size, about 10 μ (3.94×10^{-4} in.). The various types of weaves in which screen materials are available are shown in Fig. III-10.

The finer mesh screens are not available in all materials. The ductility of the metal determines how fine a weave can be made. Although stainless steel has been woven into screen as fine as 450 x 2750* Dutch twill, 325 x 2300 Dutch twill is a more realistic limit, considering both flaws in the "as-received" material and practical fabrication techniques. Aluminum can be obtained in a 200 x 1400 Dutch twill, while the finest titanium is only a 180 x 180 twill.

*Screen material is specified by the number of warp and shute wires per lineal inch.



where

a = acceleration,	ν = kinematic viscosity,
d = pore diameter,	σ = surface tension,
R = pore radius,	ρ = density
h = barrier width,	

Fig. III-7 Lateral Stability of Capillary Barriers

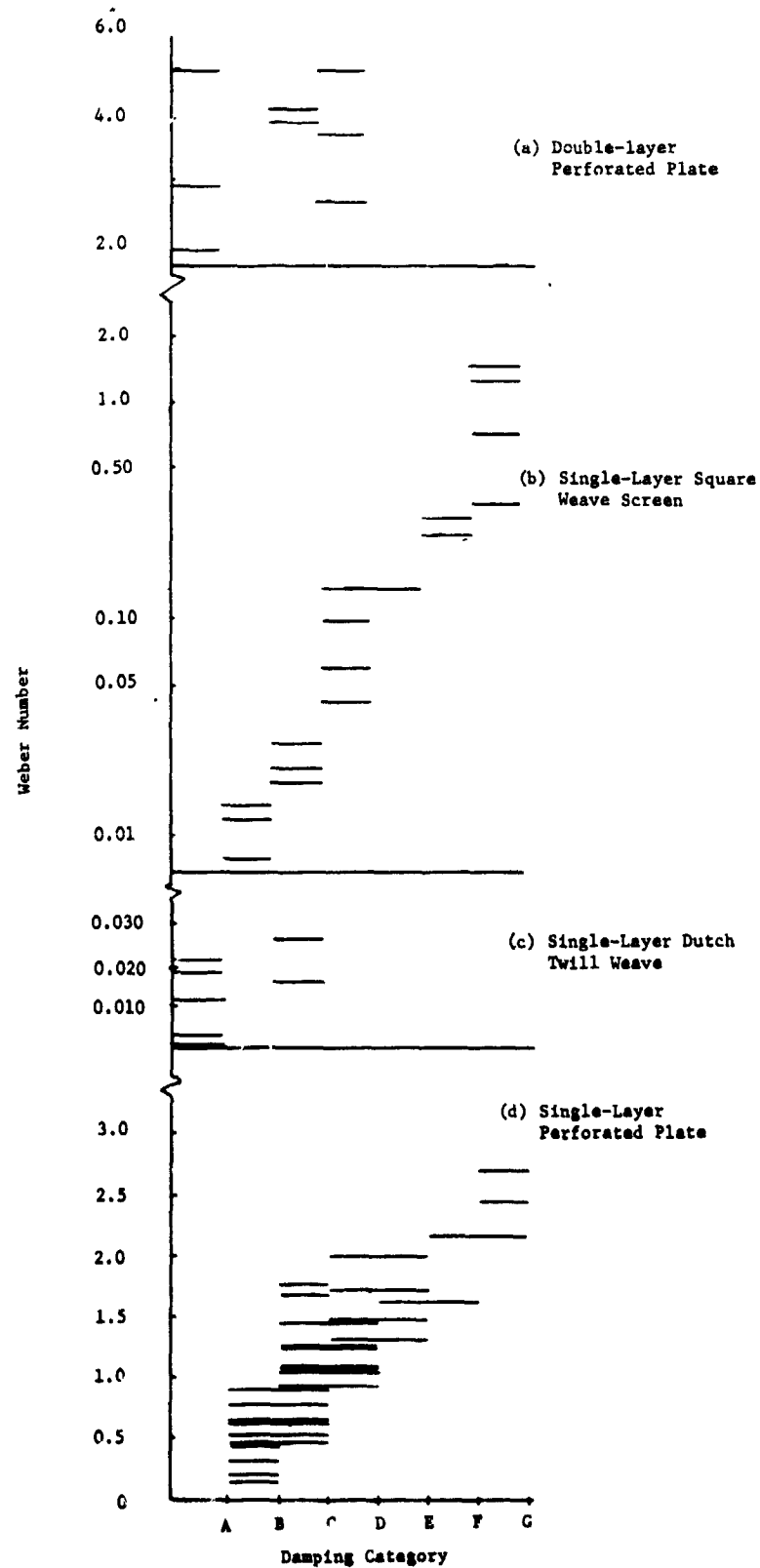
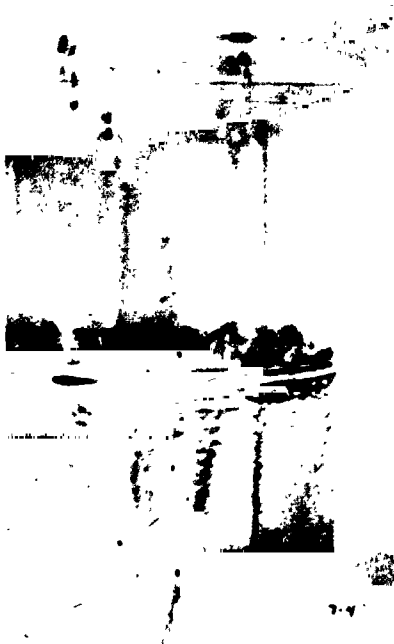


Fig. III-8 Damping Performance of Selected Barriers
III-10



Category A



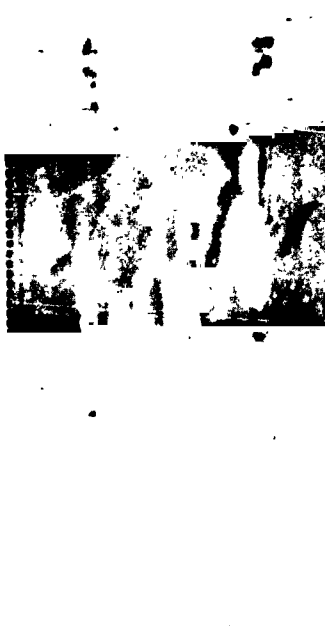
Category B



Category C



Category D



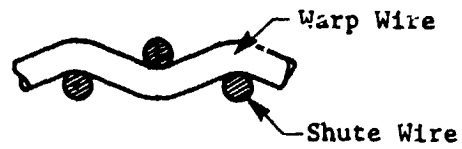
Category E



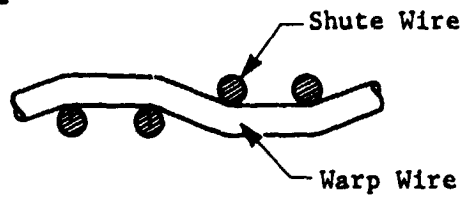
Category F or G

Fig. III-9 Damping Categories A thru G

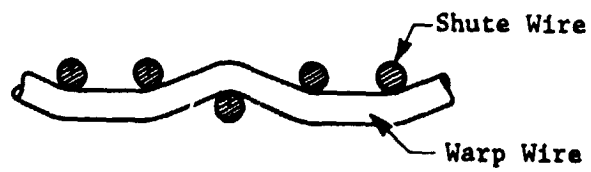
(a) Plain Square Weave



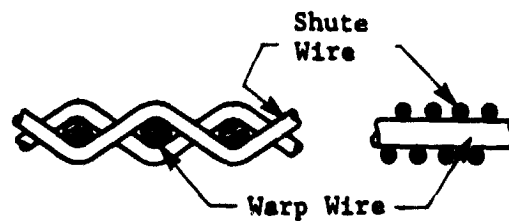
(b) Full Twill Weave



(c) Semitwill
Fourdrinier Weave



(d) Plain Dutch Weave



(e) Dutch Twill Weave

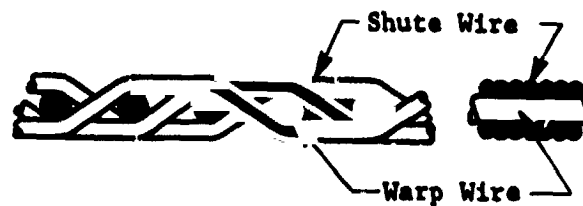


Fig. III-10 Cross-Sectional Views of Various Screen Weaves

2. Low-g Fluid Mechanics

a. *Propellant Settling* - Settling of the liquid within the propellant tank is a primary concern in design of the trap-type propellant acquisition device. How the liquid moves during settling and the rate at which liquid accumulates over the tank outlet are the important parameters. It is assumed that the accelerations occurring during coast caused by drag will orient the liquid within the tank to the end opposite the outlet. When the spacecraft engine starts, this liquid will be reoriented to the tank outlet.

The way in which the liquid moves during settling depends on a number of parameters. One is the shape of the interface before settling begins. If the interface is flat because of a relatively large adverse coast acceleration, the manner in which the liquid reorients depends on the settling Bond number:

$$Bo = \frac{\rho a R^2}{\sigma} \quad [8]$$

where ρ = liquid density,
a = settling acceleration,
R = tank radius,
 σ = liquid surface tension.

Figure III-11 shows the different settling regimes as a function of Bond number (Ref III-1). When Bo is approximately 20 or greater, a significant portion of the settling liquid is in the form of a dome that progresses down the center of the tank. When the interface is initially curved (concave) as it would be under very low-g conditions, the flow of the liquid will be along the walls of the tank without formation of a central dome (Ref III-4).

As the liquid reaches the bottom of the tank, the manner in which it flows can be predicted by the Weber number

$$We = \frac{\rho V^2 R}{\sigma} \quad [9]$$

where V = velocity of the leading edge of the settling liquid.

It has been shown that the velocity, V , is equal to 7/8 of the free-fall velocity (Ref III-5). The flow can be categorized as shown in Fig. III-12 (Ref III-6). When the Weber number is greater than about 10, a geyser, which is a central column of liquid rising from the tank bottom, will form. A geyser will return a considerable portion of the settling liquid to the top of the tank reducing the amount of liquid that initially accumulates.

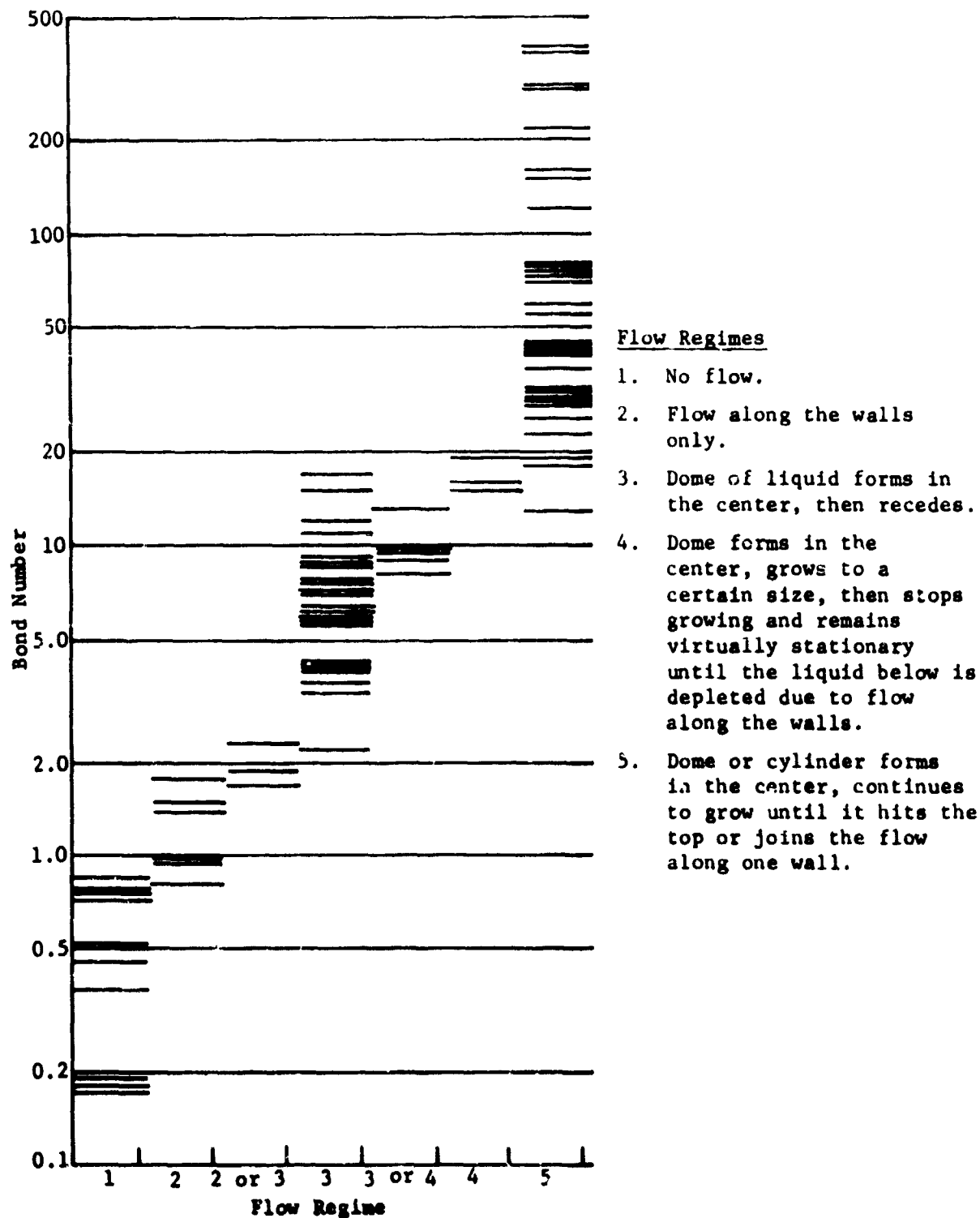


Fig. III-11 Categorization of the Initial Flow from a Flat Interface (Ref III-1)

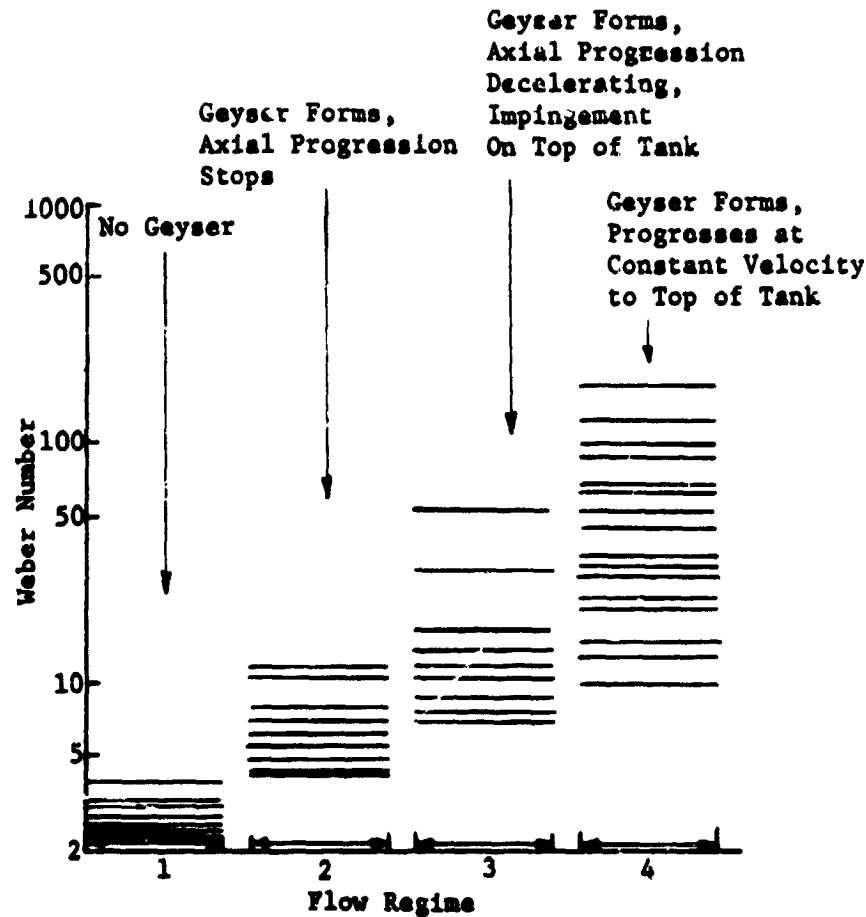


Fig. III-12 Categorization of the Flow during Settling at the Tank Bottom (Ref III-C)

The various correlations presented can be used to predict the time at which certain events occur during the settling of the liquid. Based on the velocity of the ullage bubble (buoyant rise opposed by viscous drag), the time for the bubble to travel some specified distance can be predicted (Ref III-7). The time of liquid impact at the tank bottom, time of geyser initiation, time when tank top is clear of liquid, etc, can be predicted with the equations in Reference III-4. Predicting the rate of liquid accumulation at the tank bottom is more difficult. Geysering, slosh, and the formation of gas bubbles within the settled liquid influence the accumulation rate.

A simple approach to determining the rate of liquid accumulation is based on a correlation of the degree to which settling is complete. The correlation uses free-fall periods as its base, which is defined as

$$t_o = \sqrt{\frac{2h}{a}} \quad [10]$$

where h = distance over which liquid must settle,

a = settling acceleration,

t_o = time required for a particle to free-fall the distance h .

After examining the data from a number of tests, the degree to which the liquid has settled can be categorized as shown in Fig. III-13 (Ref III-8), where τ is the number of free-fall periods that have elapsed since the settling began. After one free-fall period ($\tau = 1$), the liquid first reaches the bottom of the tank. At $\tau = 2$, the liquid is violently rebounding with little accumulation. At $\tau = 3$, the liquid is partially collected but may contain large pockets of gas. Between $\tau = 3$ and $\tau = 5$, the liquid becomes contiguous but has trapped many gas bubbles. The liquid is still very turbulent at this time, the bubbles may be carried from the surface to the outlet area. By $\tau = 10$, the liquid is clear at the bottom with only a few bubbles remaining at the liquid surface (Ref III-8).

Note: τ = number of free-fall periods elapsed since start of settling.

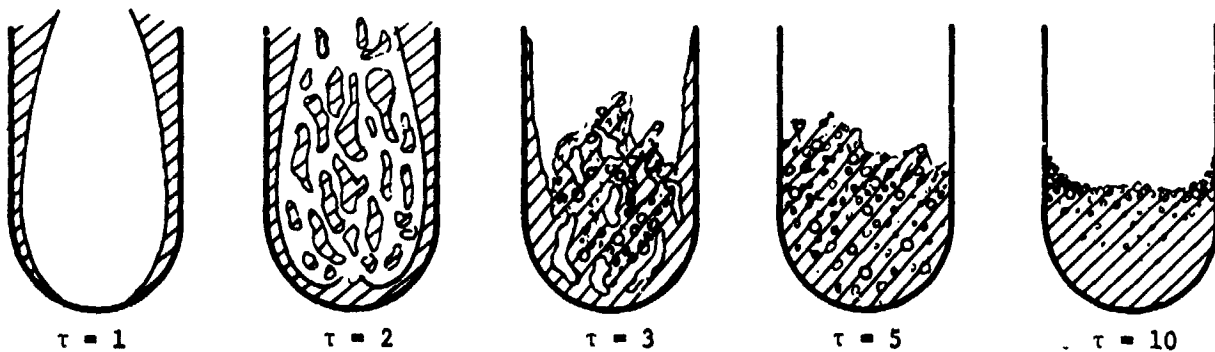


Fig. III-13 Categorization of Degree of Settling (Ref III-8)

b. *Flow in an Annulus* - Most propellant acquisition system concepts use some form of annular passage through which liquid flows to the tank outlet. Portions of the annular surface are covered with screen material to allow liquid entry. Proper operation of these concepts requires that the annulus be initially filled with liquid and remain full until tank depletion. Therefore the screen material must retain liquid in the annulus under all flow conditions.

As discussed previously, pressure retention capability of the screen is measured by the bubble point test. This capability can be expressed as a pressure differential for each propellant. Some typical examples of available pressure differential data are shown in Table III-2. This available pressure retention capability must exceed the sum of all the possible pressure drops or losses that occur at any point within the annulus. Retention of liquid is possible when the following equation is satisfied:

$$\Delta P_c > \Delta P_h + \Delta P_f + \Delta P_e + \Delta P_a \quad [11]$$

where ΔP_c = screen pressure retention capability, bubble point,
 ΔP_h = pressure drop due to hydrostatic head,
 ΔP_f = pressure loss due to friction,
 ΔP_e = pressure loss due to flow through screen,
 ΔP_a = pressure drop due to change in flow area.

Table III-2 *Pressure Retention Capability of Various Screen Meshes, N/cm² (psi)*

Screen Mesh	N ₂ O ₄	MMH	N ₂ H ₄
325 x 2300	0.755 (1.095)	0.944 (1.369)	1.739 (2.522)
200 x 1400	0.514 (0.745)	0.642 (0.931)	1.182 (1.715)
165 x 800	0.241 (0.350)	0.302 (0.438)	0.556 (0.807)
200 x 200	0.121 (0.175)	0.151 (0.219)	0.279 (0.404)

Each of the four pressure losses are discussed in the following paragraphs. Three propellants, N₂O₄, MMH, and N₂H₄, are used as examples in this discussion. N₂O₄ and MMH are a typical bipropellant combination. N₂H₄ has the highest kinematic surface tension and is the easiest of the propellants being considered to retain, while N₂O₄ has the lowest kinematic surface tension and is the most difficult to retain.

- 1) *Pressure Drop due to Hydrostatic Head* - An acceleration acting on the spacecraft produces a hydrostatic pressure difference within the annulus. Figure III-14 shows the pressure difference for the three propellants as a function of the product of the acceleration and the distance over which it could act. The distance h is measured along the annulus in the direction in which the acceleration a is acting. The pressure difference is measured from one end of h to the other. For example 0.25 g acting over a N_2O_4 -filled annulus that has a height of 2 m (6.56 ft), i.e., $ah = 0.5 \text{ g-m}$ (1.65 g-ft), would produce a pressure differential of 0.71 N/cm^2 (1.03 psi). Considering only this pressure differential, Table III-2 shows that 325 x 2300 mesh screen would be necessary to retain the liquid. Figure III-15 combines Fig. III-14 and Table III-2 to show a direct comparison of hydrostatic head and screen retention capability for any propellant.
- 2) *Pressure Drop due to Area Change* - This pressure drop refers to the change in momentum of the liquid. The pressure drop occurs between liquid at rest and liquid flowing in an annulus at some flow rate Q and through some area A . The pressure drop resulting from changing pressure head to velocity head is shown in Fig. III-16 as a function of liquid velocity in the annulus.
- 3) *Pressure Loss due to Friction* - Viscous losses due to flow within the annulus will cause a pressure loss. The length of the flow path L and the hydraulic diameter D determine the magnitude of the loss, which is shown in Fig. III-17, III-18, and III-19 for N_2O_4 , MMH, and N_2H_4 , respectively. A value of 0.03 was used for the friction factor (Darcy-Weisback equation) based on an estimated relative roughness of 0.001 and assuming flow to be in the transition or turbulent regime.
- 4) *Pressure Loss due to Flow through Screen* - A pressure loss occurs as liquid flows through a screen. The flow rate Q and the screen area A through which the liquid is flowing determine the magnitude of the pressure loss for any given screen mesh, as shown in Fig. III-20, III-21, and III-22 for N_2O_4 , MMH, N_2H_4 , respectively. A correlation for the friction factor of a screen has been developed (Ref III-9) and verified with flow tests at Martin Marietta, as shown in Fig. III-23 (Ref III-10).

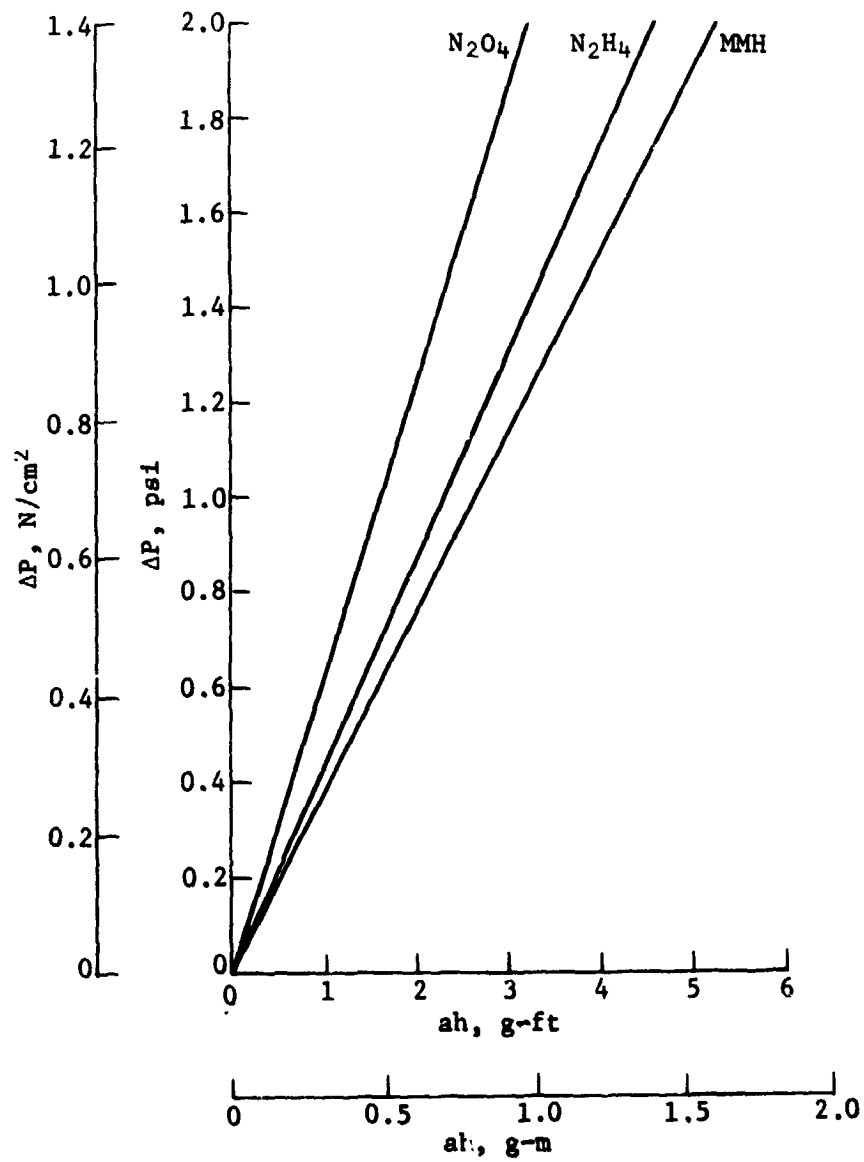


Fig. III-14 Pressure Drop due to Hydrostatic Head

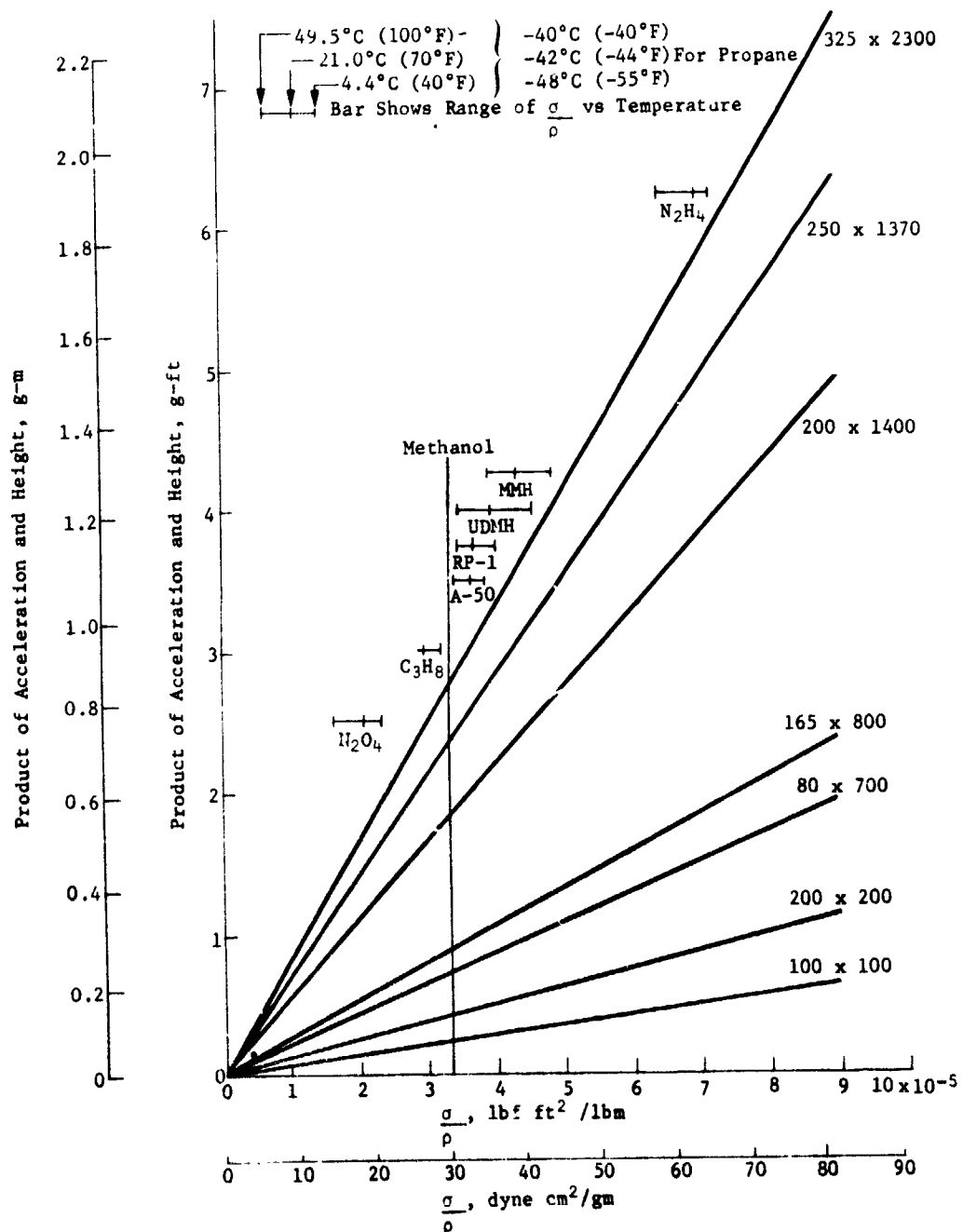


Fig. III-15 Retention Capability of Screens as a Function of Hydrostatic Head

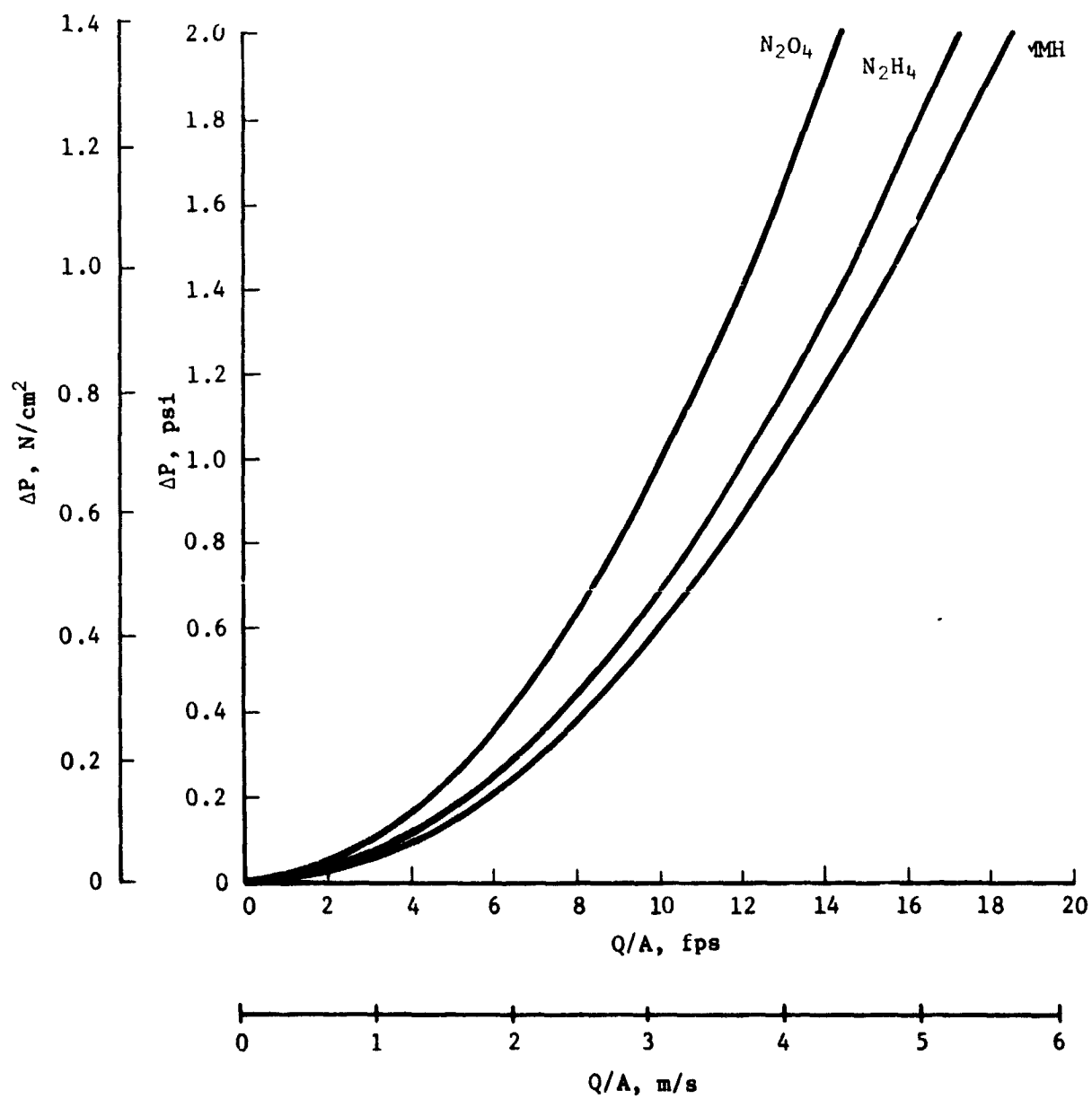


Fig. III-16 Pressure Drop due to Area Change

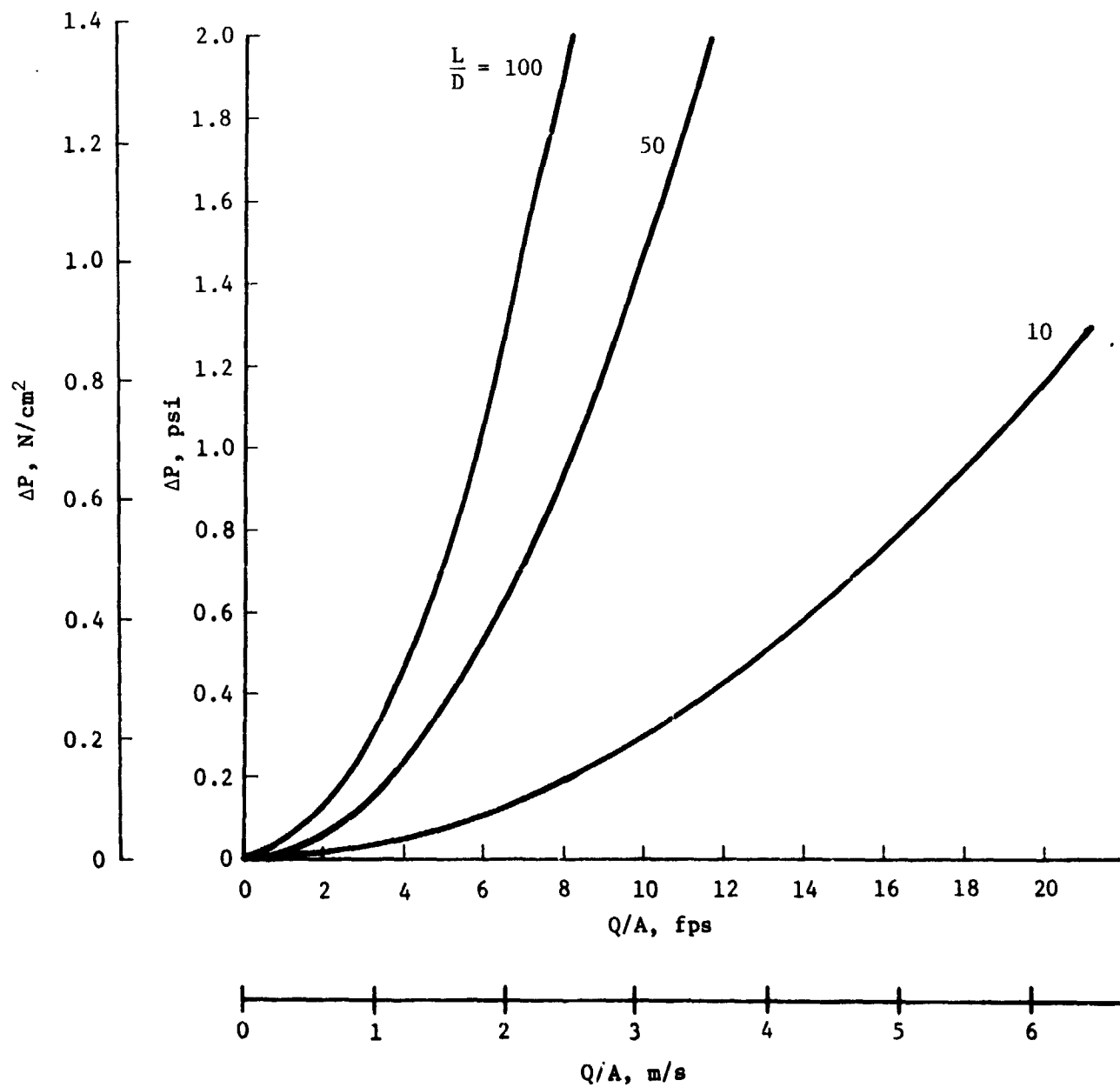


Fig. III-17 Pressure Drop due to Friction - N_2O_4

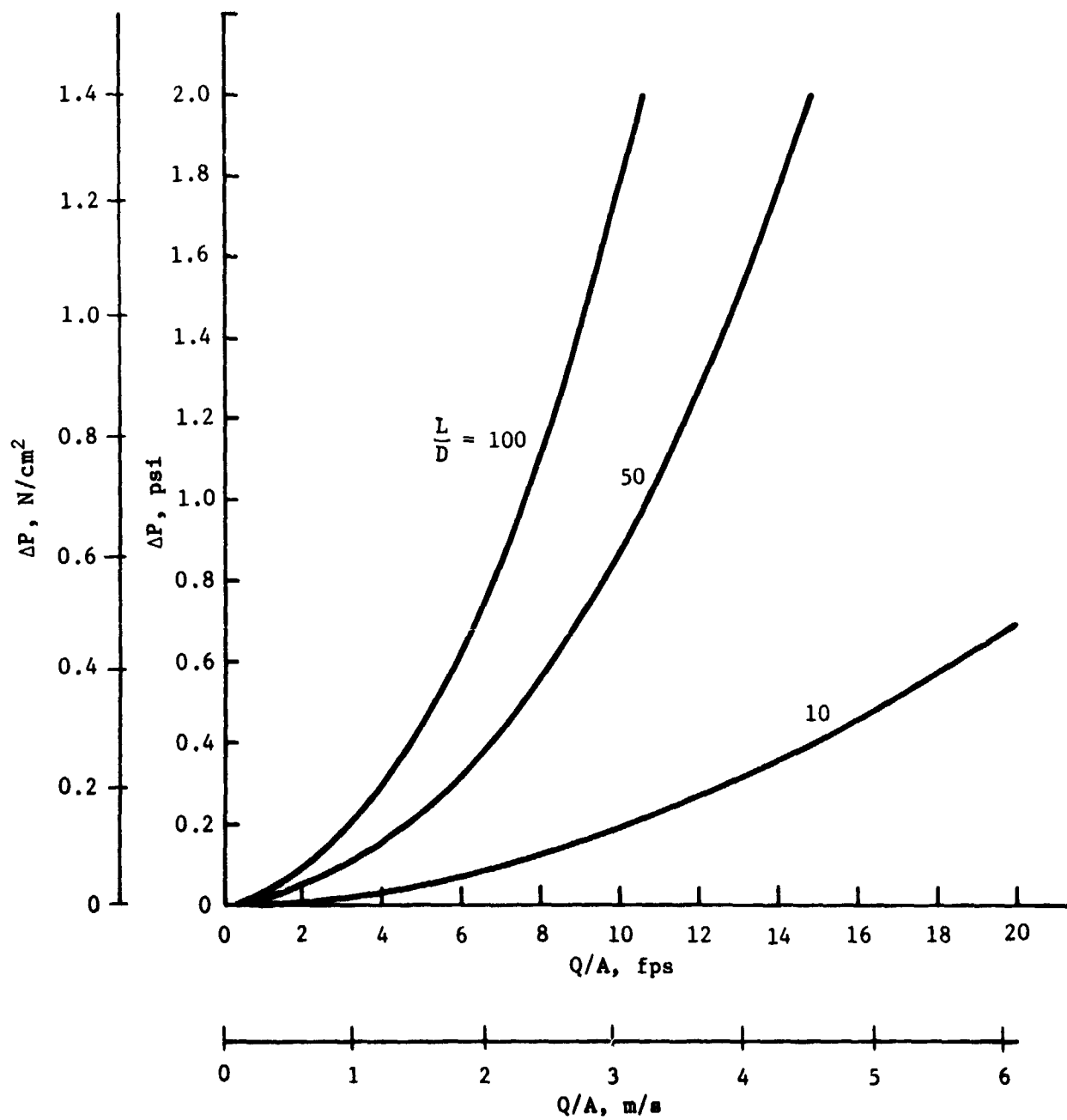


Fig. III-18 Pressure Drop due to Friction - MMH

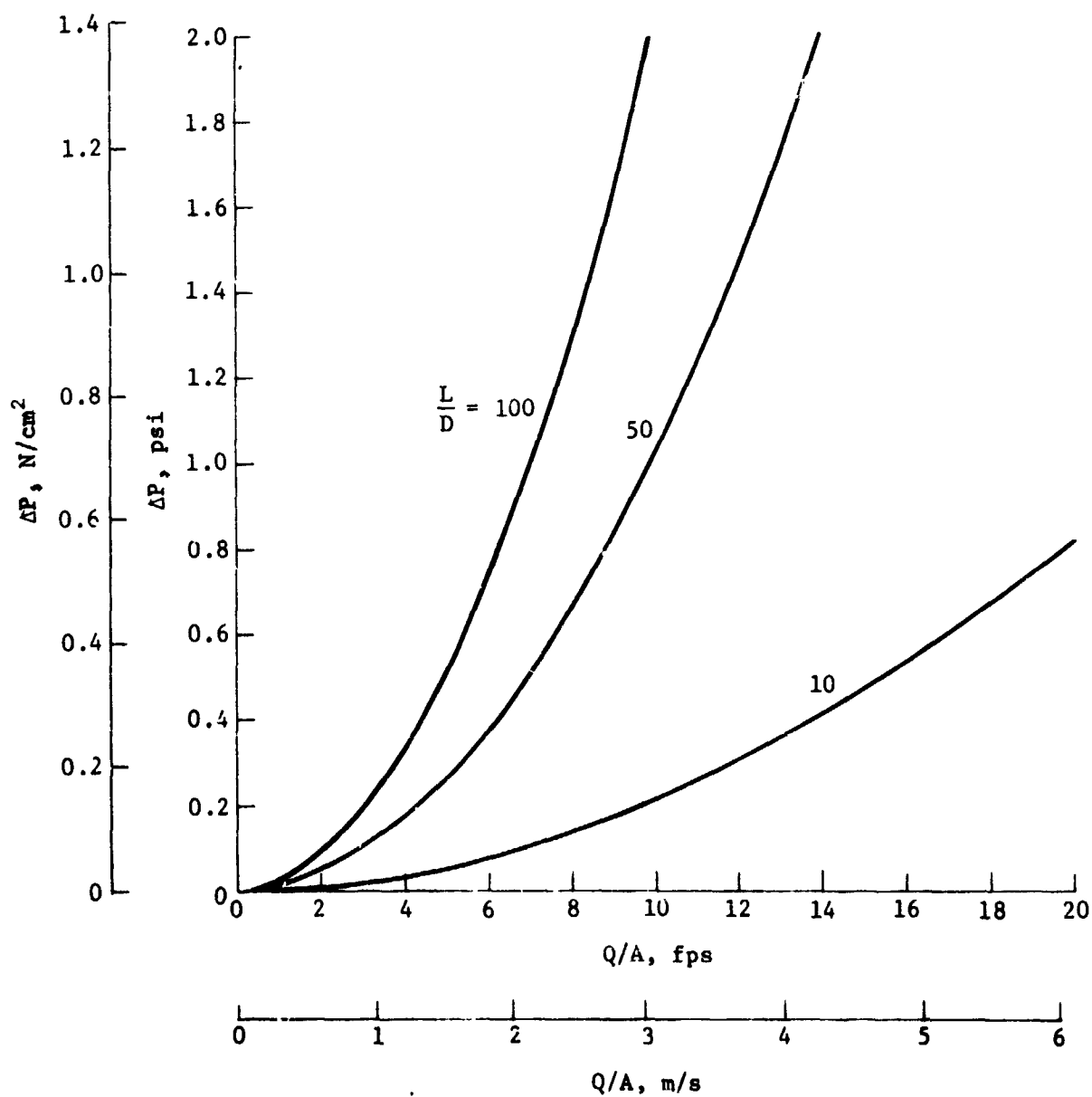


Fig. III-19 Pressure Drop due to Friction - N_2H_4

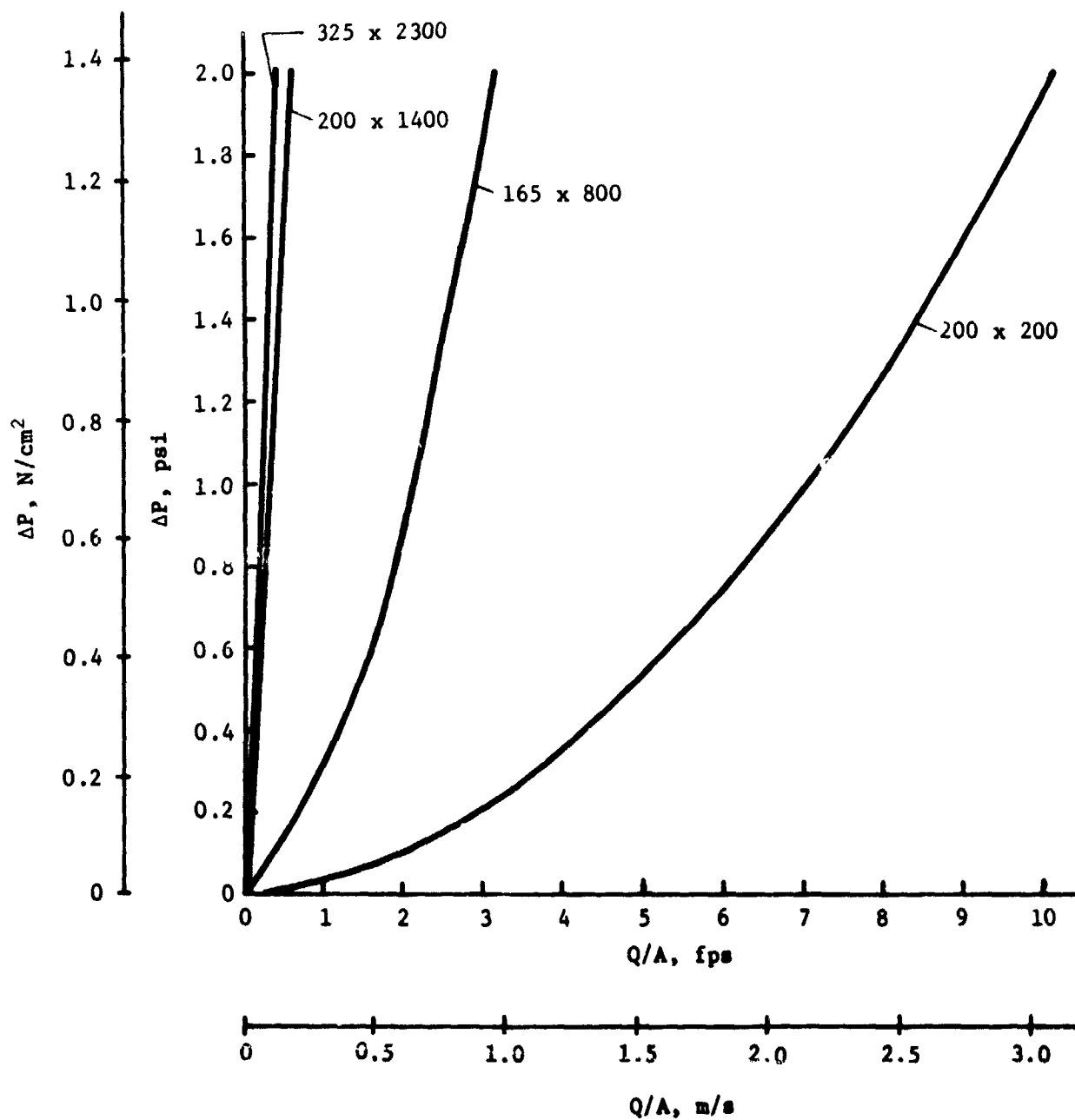


Fig. III-20 Pressure Drop due to Flow through Screen - N_2O_4

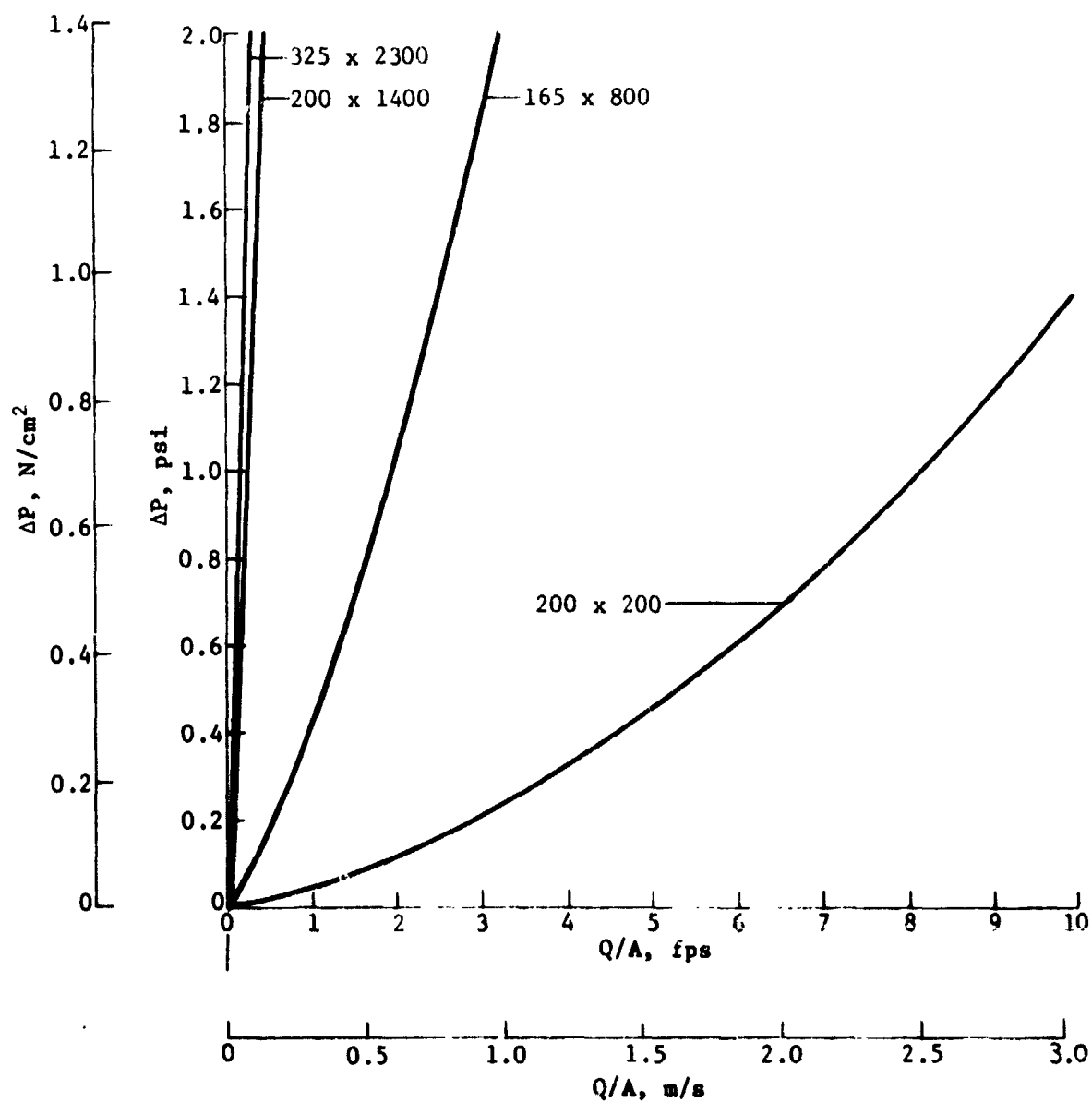


Fig. III-21 Pressure Drop due to Flow through Screen - MMH

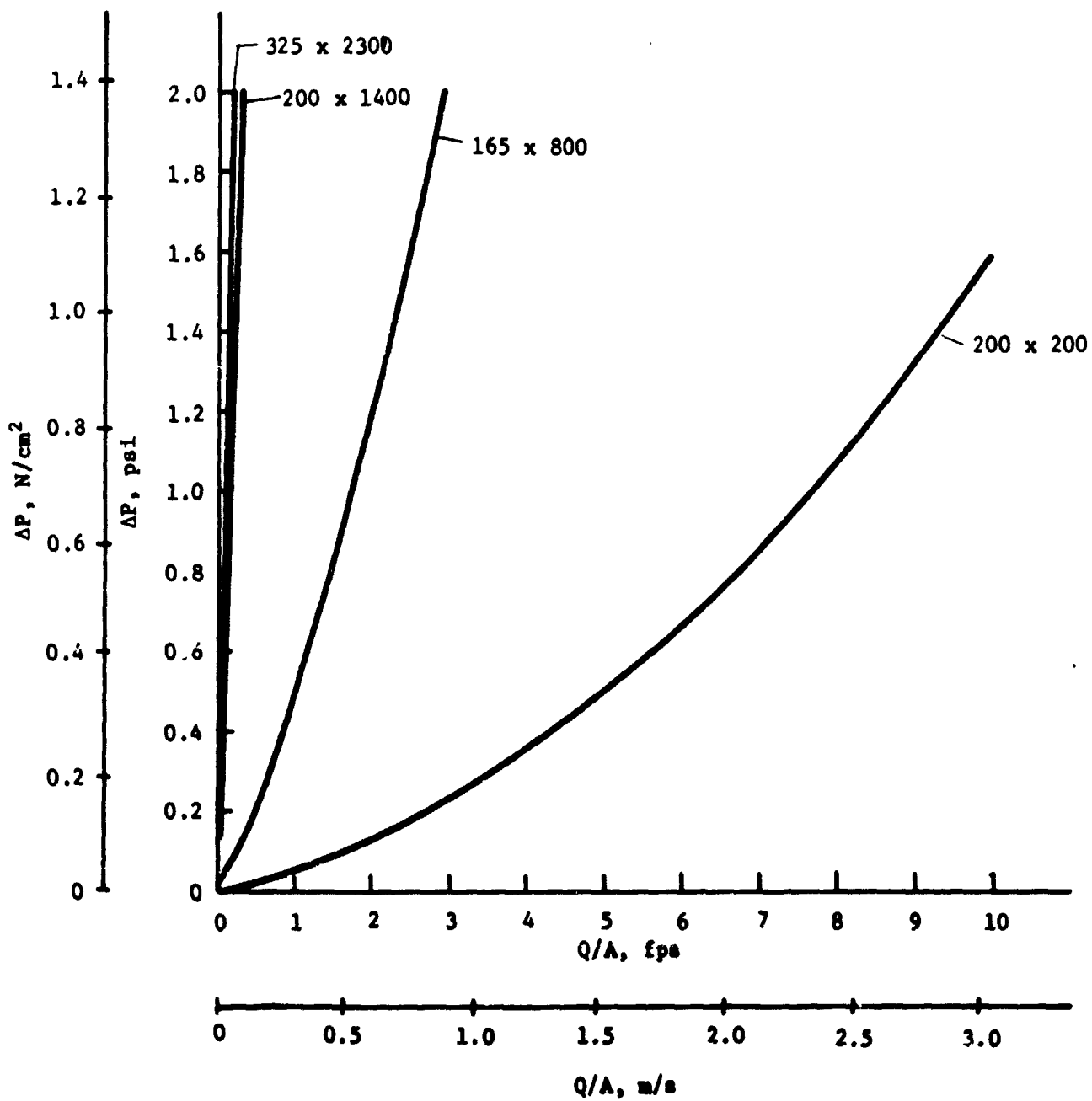


Fig. III-22 Pressure Drop due to Flow through Screen - N_2H_4

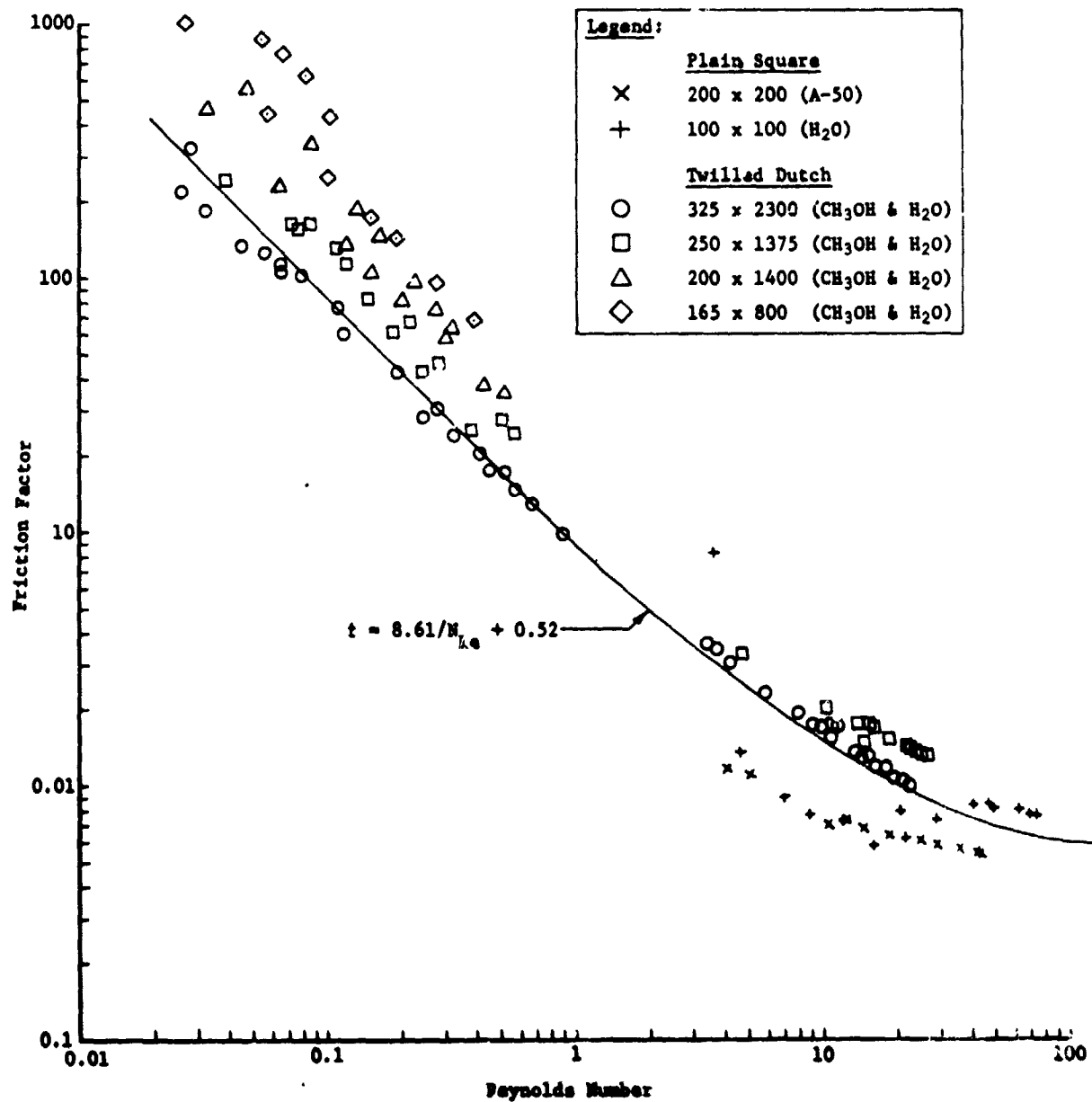


Fig. III-23 Friction Factor due to Flow through Screen

c. *Capillary Pumping* - Liquid will preferentially reorient within a propellant tank by capillary pumping if the system is in a low-g environment where the capillary forces exceed all other forces acting on the liquid. A surface tension device can reduce the pressure of the liquid adjacent to and within the device to a value lower than the pressure of the liquid located away from the device. This low-pressure region will be created when the device causes the curvature of the interface about the device to be large (small radius of curvature) in comparison to the curvature of the liquid elsewhere in the tank. As a result, liquid will flow toward the device until the pressure throughout the tank reaches equilibrium.

As previously discussed, the pressure difference across the gas/liquid interface is given by

$$\Delta P_c = \sigma \left(\frac{1}{R_1} + \frac{1}{R_2} \right) \quad [12]$$

where $\Delta P_c = P_g - P_l$,

P_g = ullage pressure,

P_l = liquid pressure.

It is assumed that hydrostatic pressures due to accelerations acting on the tank are negligible. Let

$$C = \frac{1}{R_1} + \frac{1}{R_2} \quad [13]$$

where C is the curvature of the interface. A flat interface has a curvature of zero and the more curved the surface (smaller radii of curvature R_1 and R_2), the higher the curvature.

For two separate volumes of liquid, the pressure of each with respect to a common ullage is determined by the curvature of the interface of each volume:

$$P_g - P_{l_1} = \sigma C_1, \quad [14]$$

and

$$P_g - P_{l_2} = \sigma C_2. \quad [15]$$

With respect to each other, the pressure differential is

$$P_{\ell_1} - P_{\ell_2} = \sigma(C_2 - C_1). \quad [16]$$

If a surface tension device creates a large curvature of the liquid in one volume, a pressure gradient tending to make the liquid flow toward the device will be established. The magnitude of the pressure difference is a function of the surface tension of the liquid and the difference in curvature between the volumes. This pressure difference will have an effect only if the two liquid volumes are in communication. Under near-zero-g conditions, spreading of the liquid as it wets the tank walls will usually bring the liquid into communication with the surface tension device. If this is not possible, some sort of communication channel must be provided.

With a communication path provided, liquid will be transferred until the curvature of the interface throughout the tank is the same, i.e., pressure is uniform. The surface tension device is designed so the curvature of the interface remains high until the device has filled with liquid. In comparison, liquid in contact with only the tank wall has a relatively low curvature.

B. CANDIDATE PASSIVE DESIGNS

Surface tension devices are attractive propellant acquisition systems for many different spacecraft applications. Some devices have been flight-qualified and flown, and many others have been built or are in the conceptual stage. In selecting the preferred surface tension device for a typical OMS application, the entire spectrum of devices was considered.

In general, surface tension devices can be divided into two categories--devices that use fine-mesh screens and those that do not. The devices that do not use screens use open sheet metal structures to orient and retain the liquid. The characteristic dimension of the capillary system, pore size, is the significant parameter that differentiates the two concepts. Screen systems can have pore sizes as small as 10μ (4×10^{-4} in.), while a practical pore size limit for a sheet metal baffled tank device is on the order of 2 cm (0.79 in.). Since the pressure retention capability is related to pore size, the acceleration environment in which the system can operate also depends on pore size. Therefore, the screen systems can operate over a wide

range of accelerations, but the sheet metal systems, with larger pores, will only operate in a low-g environment.

The nonscreen systems use capillary pumping and other low-g fluid mechanics phenomena to orient the liquid. Coast accelerations, when none of the spacecraft engines are operating, would be low enough to permit capillary pumping and orientation of the liquid into a nonscreen device. Typical systems require g-levels less than 10^{-4} g and it is estimated that the g-level for a coasting OMS would be 10^{-5} g. However, the random occurrence of RCS engine firings would upset the capillary pumping and cause displacement of liquid from the device. The pore size is not small enough to retain the liquid under such accelerations. Once the liquid has been perturbed, the propellant motion will continue for hours, even days, in the low-g orbital condition since viscous forces will be the primary energy dissipation (damping) mechanism. This motion further complicates the capillary pumping and orientation of the propellant. While such systems are attractive in certain applications such as deep space probes, they would not be considered for an OMS as it has been defined here. As shown in the criteria, perturbations up to 0.03 g may be acting on the system between engine burns. The retention capability of the screen is necessary to keep the propellant properly oriented. For this reason, only the fine-mesh screen systems were considered.

Screen systems can take many different forms, each with its own unique capabilities and performance. All screen devices function essentially the same--they position a volume of liquid in a specified location in the tank. Screen devices can be arbitrarily divided into two general categories. One, the trap, positions a volume of liquid directly at the tank outlet in the form of a reservoir. The other category, the liner, positions the liquid to form a flow annulus to the tank outlet. Because of the many variations in the configuration of the devices, the identification of a device as a trap or liner becomes a matter of semantics.

1. Traps

A trap device holds a specified volume of liquid over the tank outlet. This trapped propellant volume supplies the engine until the bulk propellant can be settled to maintain the supply of liquid to the engine. Two different types of traps were considered--one that cannot be refilled during flight and one that will refill during OMS engine burn.

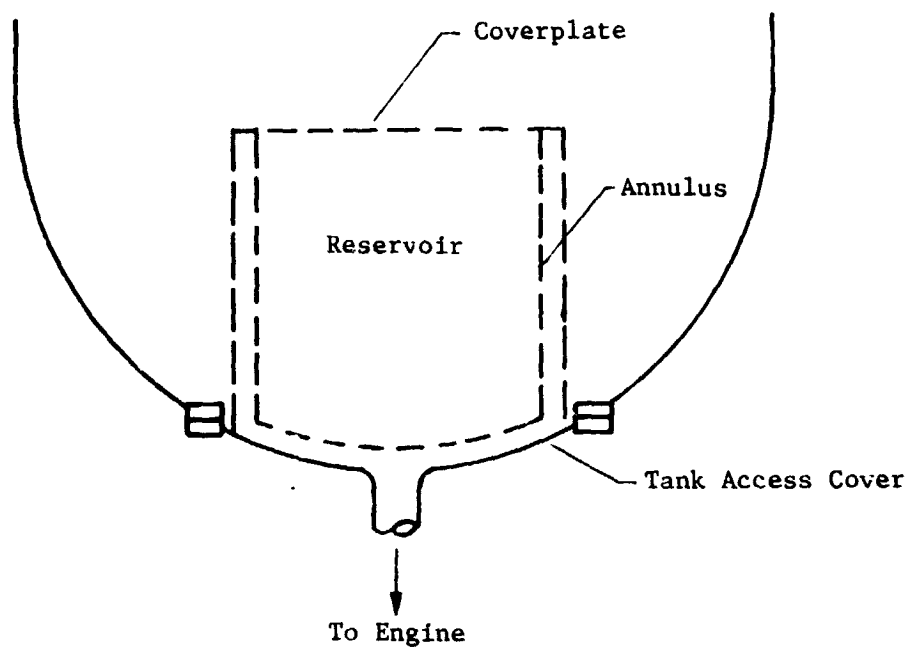
a. *Nonrefillable Trap* - The nonrefillable trap is shown schematically in Fig. III-24. Two concepts are shown--one that could be modularly installed and another that could be built into the tank. Dashed lines indicate screen surfaces. The device consists of two elements--the coverplate that retains liquid within the reservoir, and the annulus that forms a flow path from liquid in the reservoir to the tank outlet.

Both the reservoir and annulus are filled with liquid during propellant loading. Throughout the mission liquid is retained by the coverplate so no liquid can be lost from the reservoir. When the engine is started, liquid feeds from the reservoir through the annulus and to the engine. If none of the liquid located outside the trap is in contact with the device during engine start, gas will enter the reservoir as the liquid in the reservoir is being used. The annulus screen prevents any gas from entering the flow annulus and reaching the tank outlet, however. Once the bulk liquid is settled, bringing it into contact with the trap, this bulk liquid can continue to supply the engine and gas will cease to enter the reservoir. Adverse accelerations caused by drag forces acting on the spacecraft during coast will tend to orient the bulk liquid away from the trap. Therefore, it must be assumed that some gas will enter the reservoir with each engine start. The amount of gas that enters depends on the time required to settle the propellant.

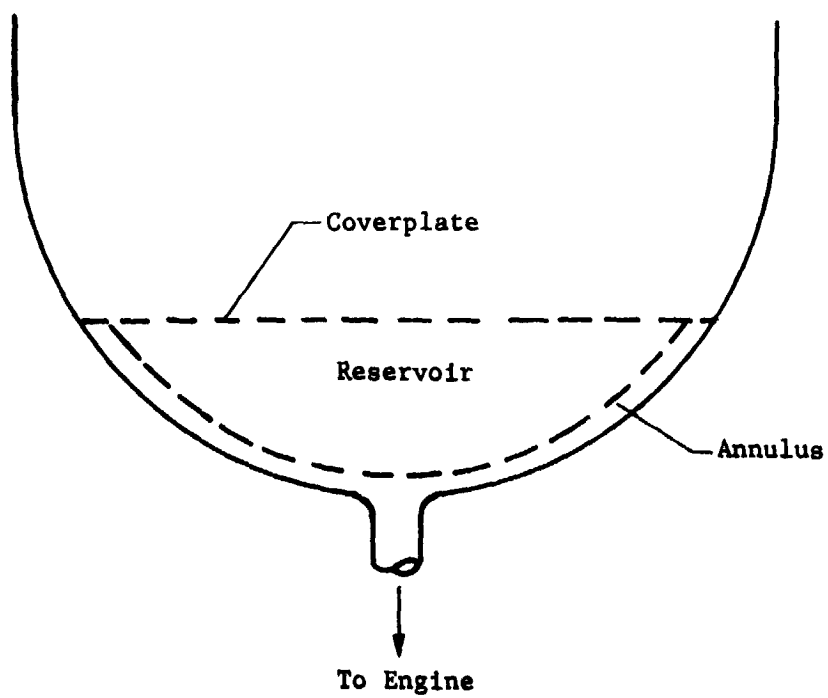
b. *Refillable Trap* - This trap device (Fig. III-25) can be refilled during a settling engine burn. It is similar to the nonrefillable trap except that the reservoir refills (purging ingested gas) after the bulk liquid has been settled. If the duration of the burn is adequate, the reservoir will completely refill. The coverplate must be capable of both retaining the reservoir of liquid and becoming unstable, allowing refill, during the engine burn. Sloping the coverplate or adding a vent tube are two methods for providing this refill capability.

2. Liners

A liner device maintains communication with the bulk liquid, regardless of its location, and provides a flow passage from the liquid to the tank outlet. The basic nonrefillable liner is shown in Fig. III-26. The channels of the device form annuli that encircle the tank, connecting with the outlet. During the entire process of engine start and propellant settling, and continuing after the liquid is settled, the channels feed gas-free liquid to the engine. No gas enters the channels and reaches the outlet until breakdown (gas ingestion) occurs at propellant depletion.



(a) Removable



(b) Integral

Fig. III-24 Nonrefillable Trap

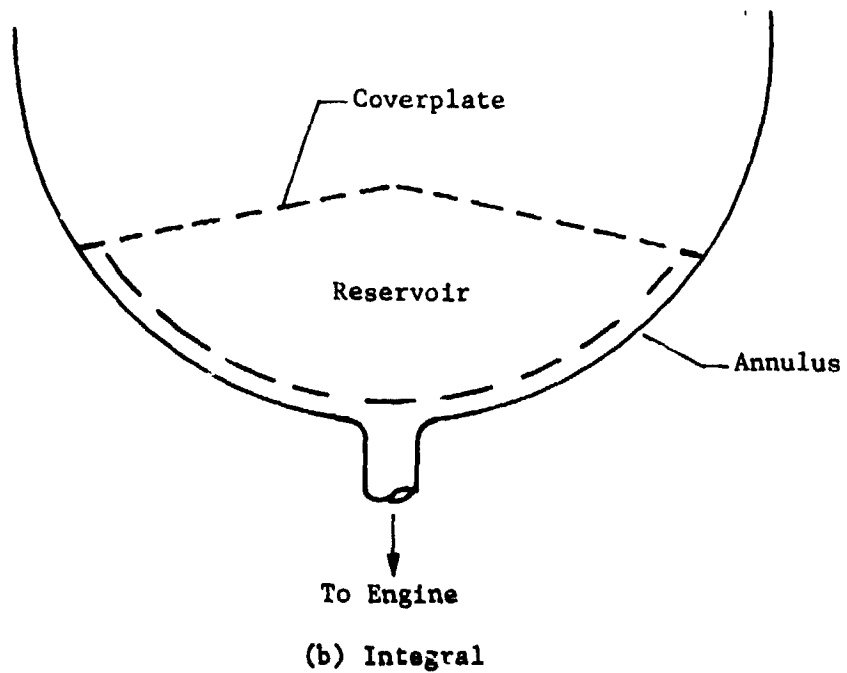
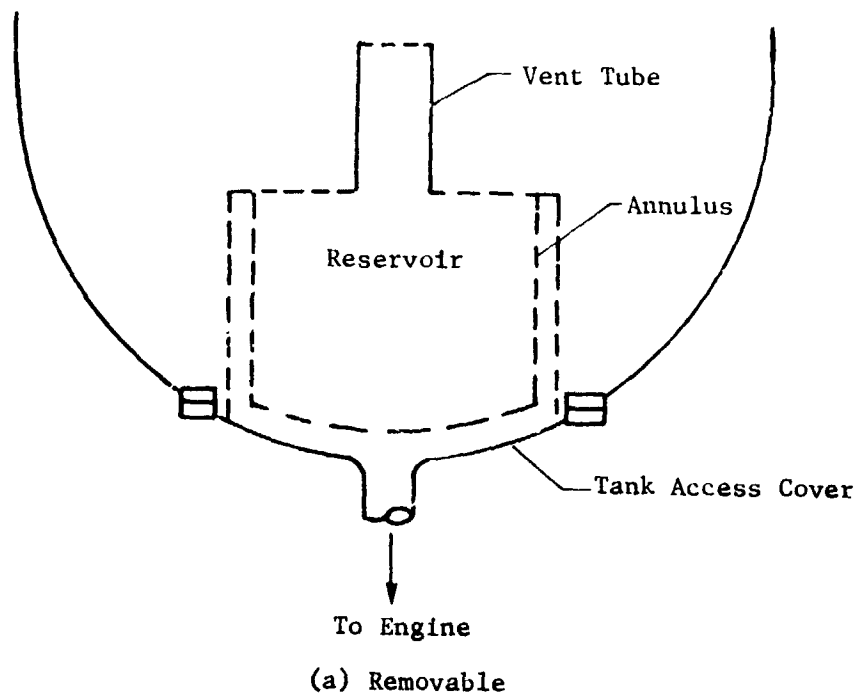


Fig. III-25 Refillable Trap

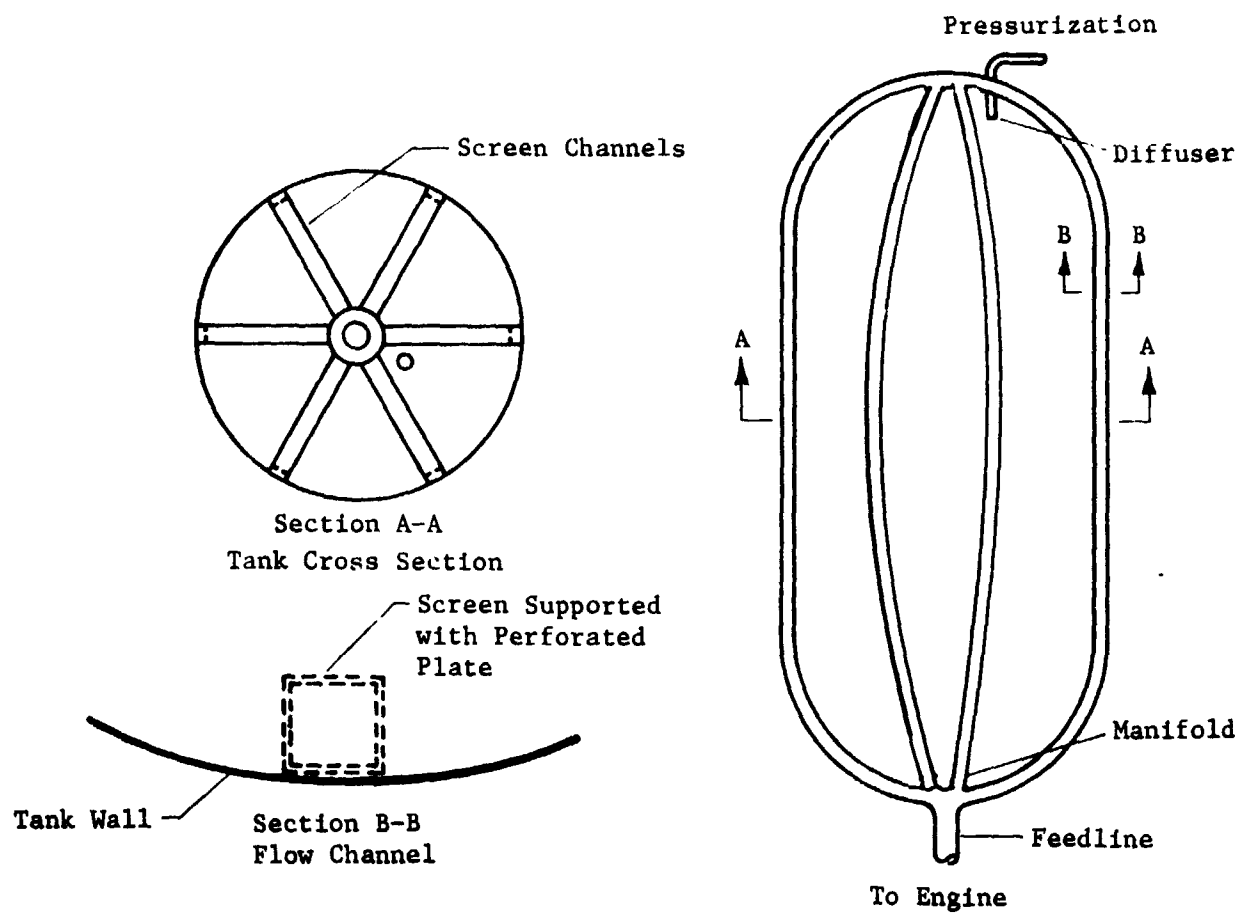


Fig. III-26 Liner

The channels are filled with liquid during propellant loading and remain full throughout the mission. This requires that the screen on the channels be capable of retaining the liquid under the worst-case condition. During the boost phase of the mission, the upper portions of the channels are exposed to the initial ullage volume, which could be up to 75% of the tank volume if only a partial propellant load is carried. During the final burn, practically the entire length of the channels must remain stable while exposed to ullage during the OMS engine burn.

C. CONCEPT COMPARISONS

Selection of the preferred surface tension device was based on evaluation of a number of factors. The factors in the comparison of the trap and liner systems were:

- 1) Flexibility - Sensitivity to engine duty cycle and propellant offloading;
- 2) Performance - System volumetric efficiency and expulsion efficiency;
- 3) System mass - Dry (hardware) mass and wet (hardware plus residual propellant) mass;
- 4) Structural design and fabrication - Materials and forming and joining techniques;
- 5) Reliability - Active/passive, functional elements, mechanics of operation;
- 6) Compatibility - Material/propellant interaction, cleanliness;
- 7) Loading and handling - Handling prior to tank installation and following propellant loading, loading technique;
- 8) Reusability - Expulsion cycle capability, operational life-time, accessibility, inspectability;
- 9) Development status - Flight-qualified, fabricated and tested, or in conceptual stage.

Specific values for some of the mission criteria presented in Chapter II (Table II-1) were used in this comparison. These criteria are representative of a Space Shuttle OMS. Nitrogen tetroxide and MMH were used as the propellants because they are the most common combination. Since N_2O_4 is the most difficult of the propellants to retain in a capillary system, a system designed for N_2O_4 would function with any of the propellants being considered. A specific representative tank size and acceleration environment is also specified in the table. While the criteria in Table II-1 provided a specific example, the general criteria in Chapter II were continually reviewed so the more stringent conditions would not be overlooked.

1. System Flexibility

The flexibility of a surface tension concept is a measure of its capability to accommodate changes in mission requirements. An OMS is intended to be part of a highly maneuverable spacecraft capable of many varied missions. Specifically, this would imply that the engine duty cycle would be changed from mission to mission. To minimize the spacecraft weight, the propellant tanks would not have to be fully loaded for every mission. The effect of propellant offloads as high as 75% were considered.

a. Mission Duty Cycle - The number of burns, duration of each burn, and the time between each burn or perturbation are all elements of the mission duty cycle. The direction in which the thrust acts with respect to both the tank and the surface tension device was also considered as part of the mission duty cycle.

Liner devices are completely independent of (insensitive to) the mission duty cycle. Because the device is always in communication with the liquid, it can feed propellants at any time and for any duration regardless of the direction of the thrust vector. Trap devices depend on the mission duty cycle because they require propellant settling; the thrust vector must act to settle propellant over the device. This is not a limitation for the OMS propulsion system because the vector is fixed and will always tend to settle the propellant.

Trap devices are highly sensitive to the number and duration of engine burns, which is reflected in the size of the trap reservoir. By increasing the volume of the trap, the flexibility of the device can be improved, but weight and other factors limit the extent to which the volume can be increased. Once a trap volume has been selected, the degree of flexibility has also been established.

A few simple examples will show how two factors, burn duration and number of burns, affect trap volume. First, consider the refillable trap. It will be assumed that 10 s is required to settle the propellant and 15 s is required to refill the trap, where both times are referenced to the initiation of engine thrust. This example represents the worst-case condition of a nearly empty tank; the settling time will be less when the volume of liquid in the tank is greater. As the liquid accumulates at the bottom of the tank during settling, there is a short delay before refill begins. Using a propellant outflow rate of 3823 cc/s ($0.135 \text{ ft}^3/\text{s}$), the curve shown in Fig. III-37(a) can be constructed. The curve shows the increment that must be added to the basic trap volume to accommodate short-duration burns. If the burn duration is greater than 15 s, no increment is required. After 15 s of burn time, any liquid used from the reservoir has been replaced when the trap refills. When the burn duration is less than 15 s, liquid is used from the reservoir and either refill does not occur or the refill is only partial.

Consider the effect of four consecutive 3-s burns. Each burn would require an increment of 0.011 m^3 (0.4 ft^3), with a total increment of 0.045 m^3 (1.6 ft^3). This increment would be added to the basic trap volume to design a trap that could accommodate four consecutive 3-s burns. These four burns could be accomplished between any two burns that completely refill the trap. Therefore although the number of 3-s burns possible during the mission could be large, the trap has been sized to accomplish only four of these burns between any two complete refill burns.

The effect is greater in the case of the nonrefillable trap. The curve in Fig. III-27(b) was constructed using the same settle time and outflow rate. Liquid is used from the reservoir until the propellant has settled, but no refill occurs. Burn durations equal to and greater than 10 s use the same amount of liquid from the reservoir because the bulk propellant is settled in 10 s and supplies the liquid to the outlet after this time period. For shorter duration burns, the bulk liquid does not reach the trap during settling so the amount of liquid outflowed from the reservoir during the burn represents the volume increment. Each burn must be considered; the sum of all the increments yields the trap volume.

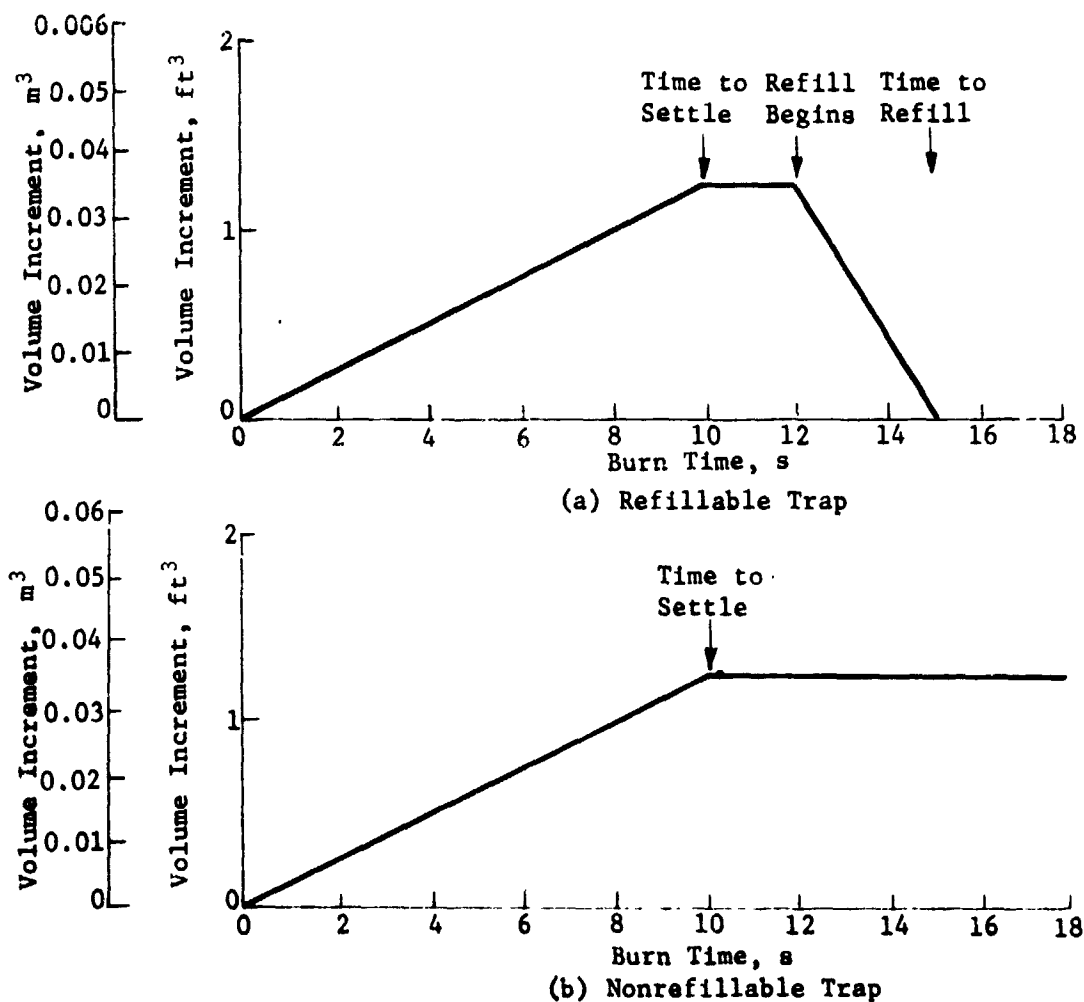


Fig. III-27 Effect of Burn Duration on Traps

To summarize, the refillable trap is sensitive to the duration of the burn if the duration is less than the time required to refill. If there are such burns, the maximum number that could occur between complete refills must be known. In the case of the nonrefillable trap, the number of burns and the duration of each burn must be known. If the duration is greater than the settle time, the actual duration does not have to be known.

Referring to the typical mission duty cycles discussed in Chapter II, the minimum burn time for all three missions is 16 s. If the maximum time to refill the refillable trap is actually 15 s, no volume increments would be required and there would be no limitation in the flexibility of the device. However, it is recognized that there may be other missions requiring shorter duration burns.

Considering the nonrefillable trap, the mission duty cycles indicate that the maximum number of burns is eight and all the burns have a duration greater than the maximum settle time (10 s). Using the curve in Fig. III-27(b), the trap volume would be equal to eight of the maximum volume increments, i.e., 8 times 0.0382 m^3 (1.35 ft^3) or 0.306 m^3 (10.8 ft^3). Again, there may be missions with a greater number of burns.

A high degree of flexibility can be achieved with the trap device by oversizing the reservoir volume. Such a device would permit any reasonable combination of burn and burn duration. There will always be a sufficient number of longer duration burns, with complete settling of the propellant so no liquid will be left above the trap. The three mission profiles show that the first burn and the last burn (deorbit) are always large burns. An example of an enlarged trap device is shown in Fig. III-28. Channels are used to form the annulus to minimize weight.

b. Propellant Offloading - To provide the maximum payload capability, only the amount of propellant required for the specific mission would be loaded. Because of the wide range of mission and propellant requirements, propellant offloads as high as 75% could be expected.

Portions of both the trap and liner devices (the annulus or channels) must remain full of liquid throughout the mission. When a portion of the annulus is exposed to ullage, the screen must be able to retain the liquid under the applied hydrostatic head. Near the end of the mission when the amount of remaining propellant is small, nearly the entire annulus is exposed to the ullage. But the device can be designed to remain stable under this 0.1-g on-orbit operating condition. A much worse case may occur during the 3-g boost phase of the mission. If the tanks are full during boost, this is no problem. But offloading can expose the annulus, creating large hydrostatic heads that must be supported by the screen.

Using the tank size specified in Table II-1, the amount of propellant offload that could be accommodated by a liner system during a 3-g boost can be predicted. Figure III-29 shows the percent of offload as a function of the screen mesh used in the liner. A liner system, using a single layer of the finest mesh screen, would permit a 5% offload of the fuel tank and a mere 1.5% offload of the oxidizer tank.

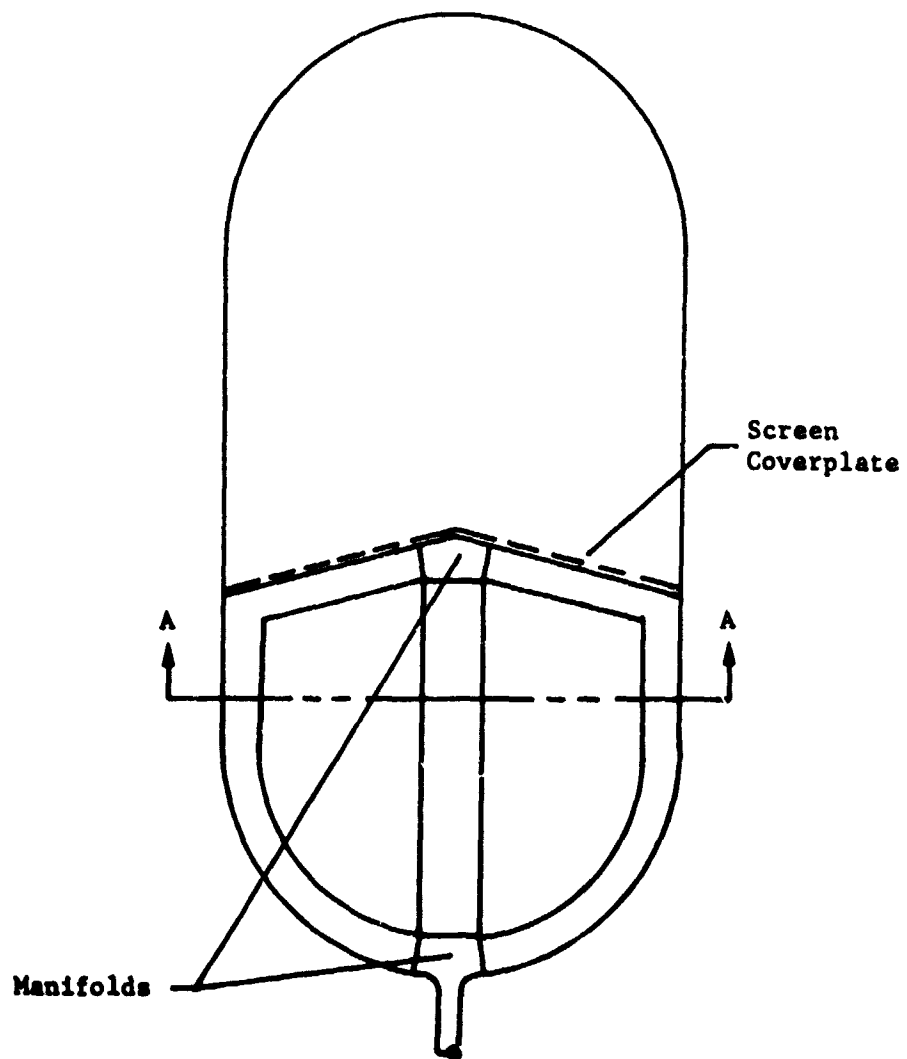
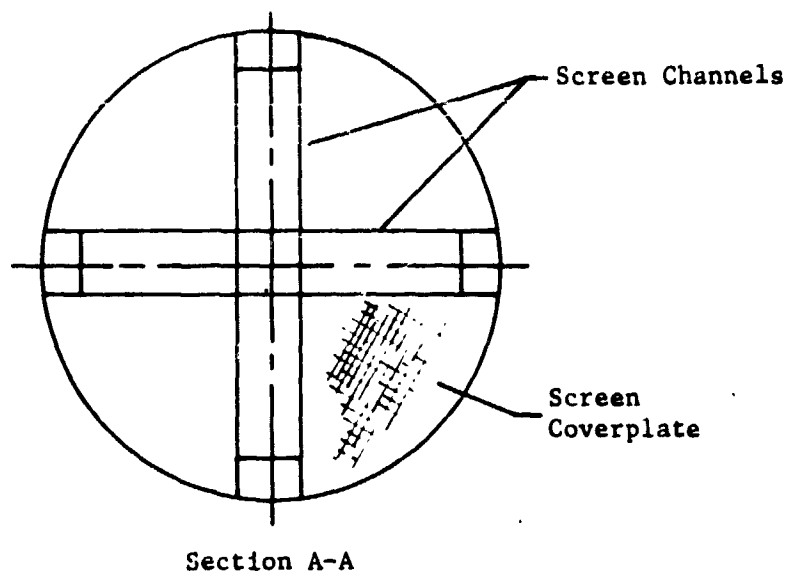


Fig. III-28 Enlarged Trap Device

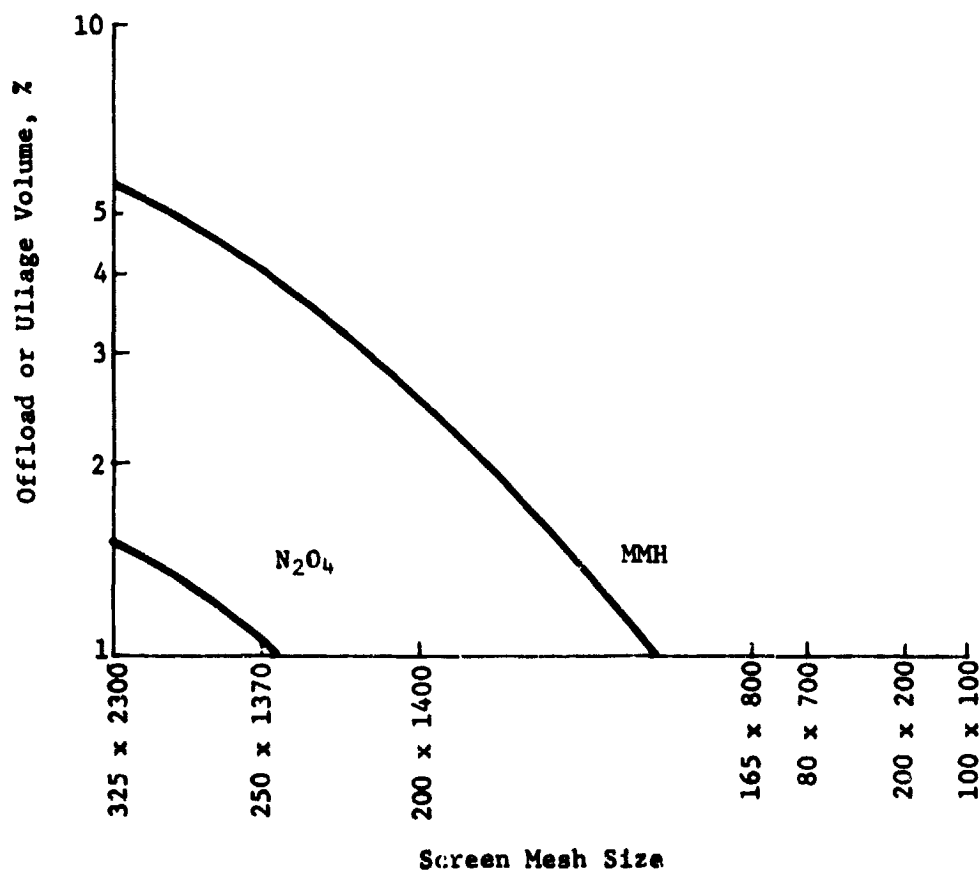


Fig. III-29 Propellant Offload Capability for a Liner System during 3-g Boost

Various modifications can be incorporated in the liner device to overcome its sensitivity to offloading. Two of these modifications are shown in Fig. III-30. By placing a capillary barrier across the tank, it is effectively divided into compartments. The device in Fig. III-30 (a) has a valve located in a central feeder tube. This coverplate is located at the level of the partial propellant load. When the tank is fully loaded, the valve is open, the barrier has little effect on the operation of the device, and it will function in the same manner as the basic liner.

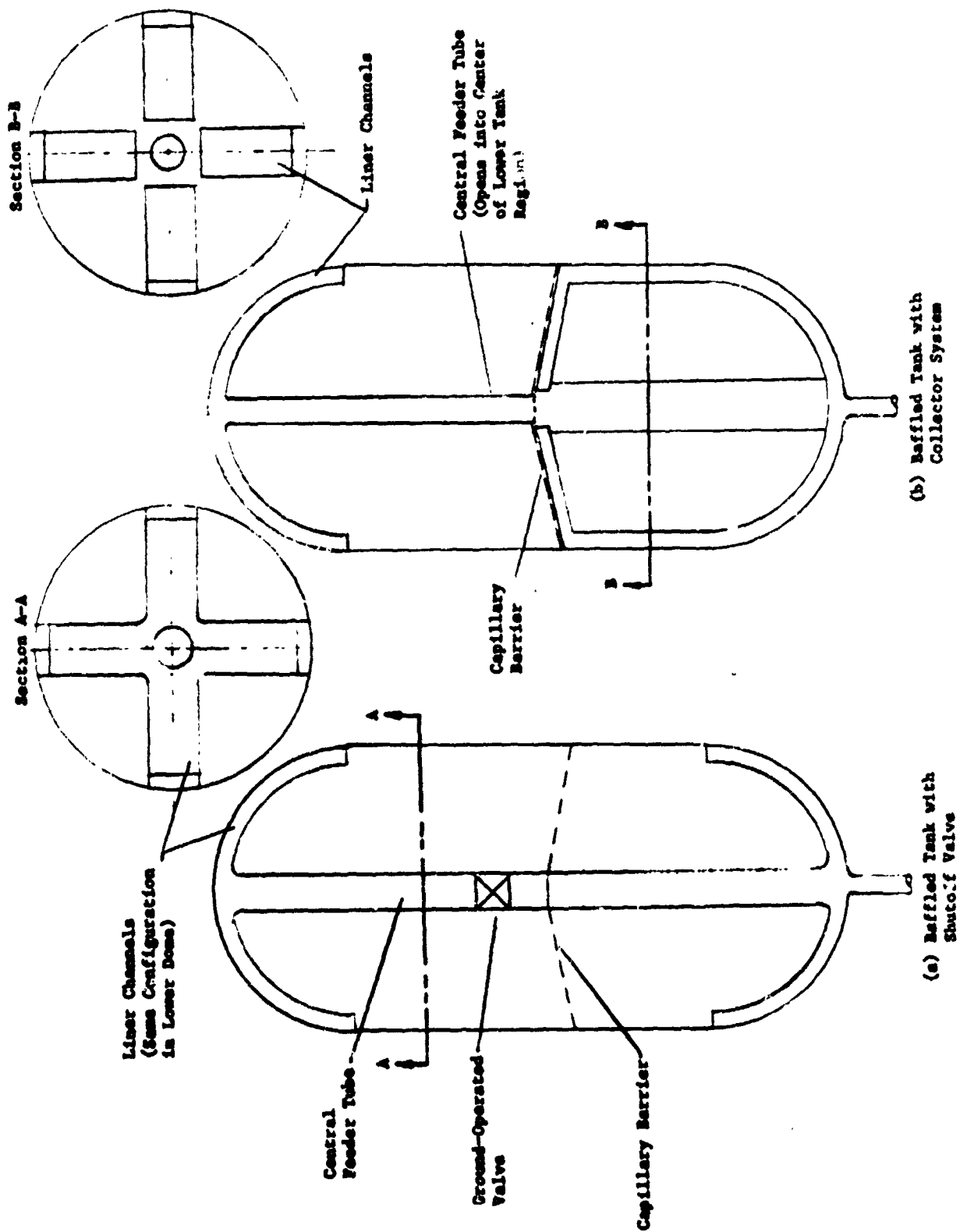


Fig. III-30 Modified Liner Devices

When the tank is offloaded, the valve is closed and the barrier keeps the liquid at the bottom of the tank. The portion of the device below the valve would function like the basic liner. Only two different loads can be handled by this device--a full load and the offload determined by the location of the barrier. Although adding more valves and barriers would permit loads of other sizes to be accepted, this would increase the weight and complexity of the system. This is not considered a reasonable approach for providing an offload capability.

The modification shown in Fig. III-30(b) is more promising. The barrier is located at the level of the maximum offload. The channels above the barrier are capable of collecting the liquid located above the barrier and transferring it to the central region of the lower compartment. Since the upper compartment does not feed directly into the annulus of the lower compartment, it can transfer two-phase fluid to the lower compartment without compromising the outflow of gas-free propellant. The annulus of the upper compartment does not have to remain full of liquid. Any offload, up to the volume determined by the location of the barrier, can be accommodated.

Another modification is the use of multiple-screen layers instead of a single layer on the annulus of the basic screen liner. The multiple-screen system was tested and the performance data are reported in Chapter IV. The retention capability of an annulus can be increased by adding screen layers. Results of the tests indicate that the increase is not linear, i.e., adding a screen layer increases the bubble point of the stack by a value less than the bubble point of the added layer. It was also found that, under transient high-g conditions, the rate at which a stack of screens breaks down depends on the rate at which gas penetrates the screen layers. A stack of screen layers that would be unstable under a steady acceleration will remain stable for a period of time as the layers fill with gas. Based on the multiple-screen test results presented in Chapter IV, a liner with three layers of screen would remain stable during the boost phase of the mission with a large propellant offload. The retention capability is only one aspect of the performance of multiple-screen systems. Other questions, such as the effect of the gas that enters the screen layers on the flow of liquid into the annulus, remain to be investigated. Additional testing and analysis are necessary before the characteristics of a multiple-screen system are completely understood.

Trap devices are completely insensitive to propellant offloading. Unless the trap volume is greater than 25% (considered to be the minimum propellant load), the device will always be submerged in the propellant during the boost phase of the mission.

2. Performance

The most important aspect of the performance of a surface tension device is its ability to provide the required gas-free liquid to the engine throughout the mission. This ability is given primary emphasis in design of the device. While certain engines can tolerate small amounts of gas entrained with the propellant, surface tension devices are designed to provide pure liquid to the engine. Both trap and liner systems can be designed to comply with this requirement.

Other performance aspects are volumetric efficiency and expulsion efficiency. Volumetric efficiency is defined as the total possible volume of propellant that can be loaded into a given tank divided by the total volume of the propellant tank. For a surface tension system, this becomes a measure of the volume of the device material compared to the tank volume:

$$\eta_v = 100 \left(1 - \frac{\text{volume of device material}}{\text{volume of tank}} \right).$$

For the capillary systems under consideration, volumetric efficiency ranges from 99.7% for a liner to greater than 99.9% for a trap. Although the smaller, compact trap concepts have a slight advantage, volumetric efficiency is not considered a major factor in the selection of a capillary propellant acquisition system.

Expulsion efficiency is a measure of the propellant residual, defined as

$$\eta_e = 100 \left(1 - \frac{\text{volume of residual propellant}}{\text{volume of tank}} \right).$$

The expulsion efficiencies of the concepts being considered range from 98% for a liner to greater than 99.5% for a trap. Because these values are based on depletion of all bulk propellant from the tank, the residual propellant is either the volume of the trap annuli or the volume of the liner channels. In reality the entire bulk propellant cannot be drained because of the pressure drop that occurs as the liquid flows from the bulk region into the annulus. However, the quantity of bulk propellant remaining is usually small. Using the criteria in

Chapter II, a minimum flow area of 0.014 m^2 (0.5 ft^2) would be required for N_2O_4 flowing through 325 x 2300 mesh screen (a worst-case condition). The amount of oxidizer left in the bulk region when the flow area is reduced below this value would have a small effect on expulsion efficiency.

3. System Mass

Since the screen material of the surface tension devices is relatively lightweight, the structural support for the screen is the predominant factor in determining the mass of the device. As the device becomes large, increasing the amount of structure, the devices can become heavy. Figure III-31 shows the mass of representative liner and trap systems for the tank sizes given in Table II-1 plotted versus the volume of the device. Both the dry mass (simply the hardware mass) and the wet mass (hardware plus the residual propellant) are included.

Because of their size, liners tend to be heavier than traps. The use of multiple-screen layers will further increase the liner weight. The volume of the liner increases as the flow area of the channels and the number of channels is increased. Weight increases rapidly as the volume of the liner increases. However, the volume of a liner device is usually small, on the order of 2 to 3% of the tank volume, preventing their weight from becoming too large.

Typical trap volumes may range from 2 to 10% of the tank volume, but the weight of the trap grows slowly as its volume increases. To provide greater flexibility, trap volume must be increased. When the trap volume reaches 25% or more of the tank volume, the weight advantage of a trap device is not as significant.

4. Structural Design and Fabrication

The structure of a surface tension device must be capable of withstanding the imposed loads. Reusability and the need to withstand reentry and landing loads are new requirements for propellant acquisition systems. During reentry the device will not be cushioned within the liquid as it is during boost. The multiple-reuse requirement dictates that the structure be capable of withstanding cycling and handling loads over a long period of time. In general, a conservative approach to structural design would be necessary. Perforated plate would be used to support the screen material.

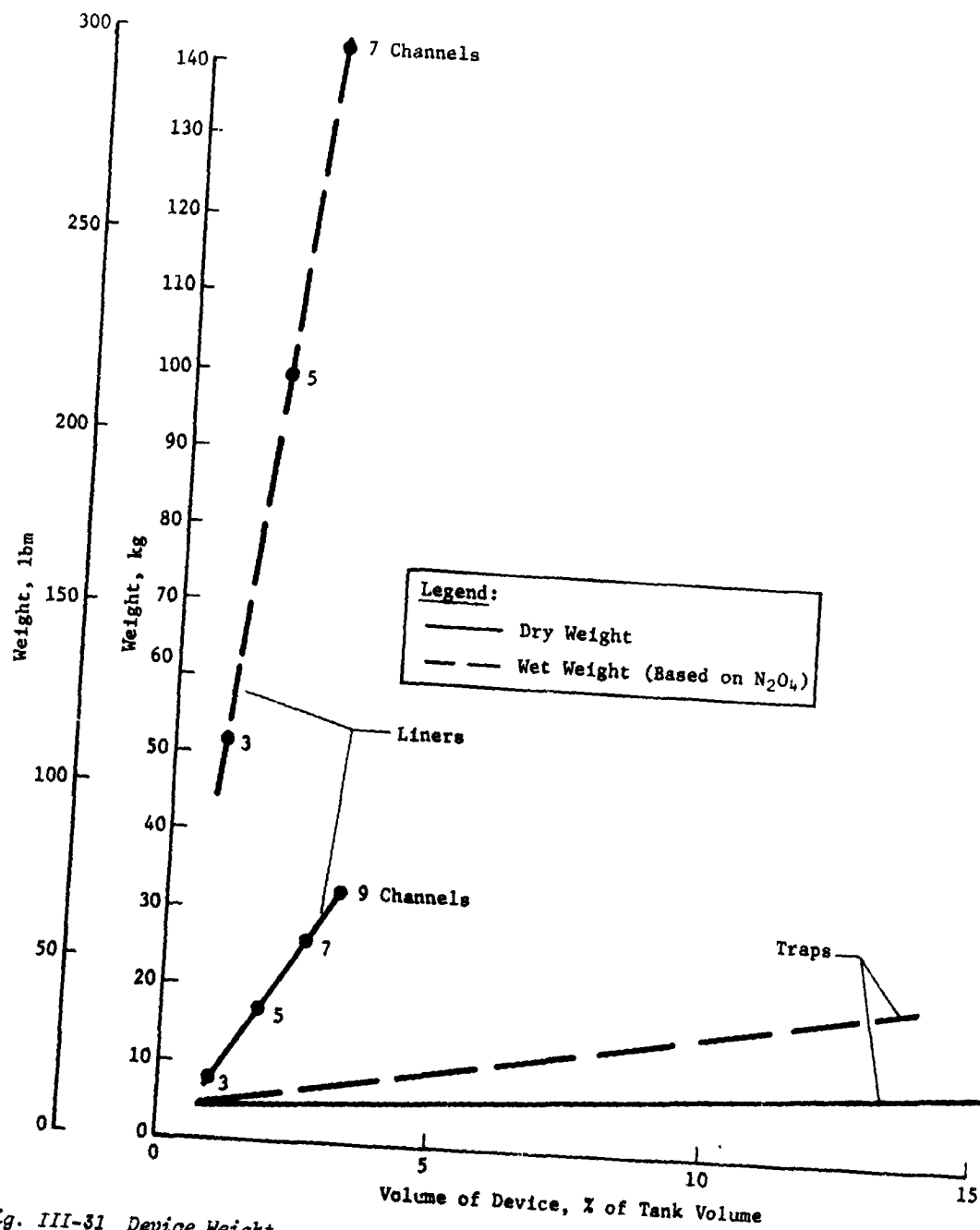


Fig. III-31 Device Weight

In fabricating surface tension devices, the joining of screen-to-screen and screen-to-plate is of primary concern. Techniques for accomplishing such joints have been developed at Martin Marietta. Sample joints have been made and tested for strength (Ref III-11). Complete devices made of stainless steel and aluminum have been fabricated (Ref III-12 and Vol II and III of this report).

The recommended methods of joining each of the materials (stainless steel, aluminum, and titanium) are shown in Table III-3. Resistance welding is the most desirable method of making the joints. A continuous seam is formed by slightly overlapping each of the spot welds, forming a uniform joint that can easily be cleaned. Fusion welding is not desirable because the high temperatures will readily destroy the screen. Fusion-welded joints have been successfully made by sandwiching the screen between two plates and melting the three together. Although no development work in electron beam welding has been conducted, it seems to be a good method for making stainless steel and titanium screen joints. Since aluminum tends to crack when electron-beam-welded, the method is not recommended for this material.

Table III-3 Recommended Joining Methods for Surface Tension Devices

	Material					
	Stainless Steel		Aluminum		Titanium	
	Screen-to-Screen	Screen-to-Plate	Screen-to-Screen	Screen-to-Plate	Screen-to-Screen	Screen-to-Plate
Resistance Welding	X	X	X	X	X	X
Fusion Welding						
Electron Beam Welding	X	X			X	X
Brazing		X		X		
Soldering		X		X		
Mechanical Fastening		X		X		X

Brazing is attractive for screen-to-plate joints, especially for intricate joints difficult to reach by the welding methods. Compatibility of the braze alloy with the propellant and the possible need to anneal the device after brazing are problem areas that must be considered.

Soldering does not produce as strong a joint as the other methods, but is a simple means for building various development devices. It is also a good method for repairing small holes in a screen surface. Compatibility of the solder must be considered.

Mechanical fastening could be used for screen-to-plate joints if mounting plates with gaskets are used. This would allow sections of a screen device to be easily removed and replaced. However, it is less reliable than the permanent joining methods.

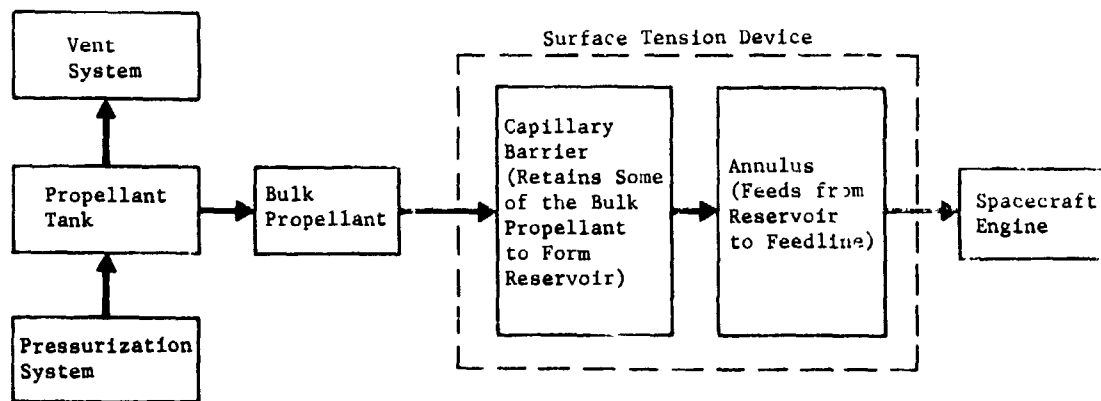
Both trap and liner systems would be structurally designed and fabricated in a similar manner. As far as this factor is concerned, there are no differences between the two types of devices.

5. Reliability

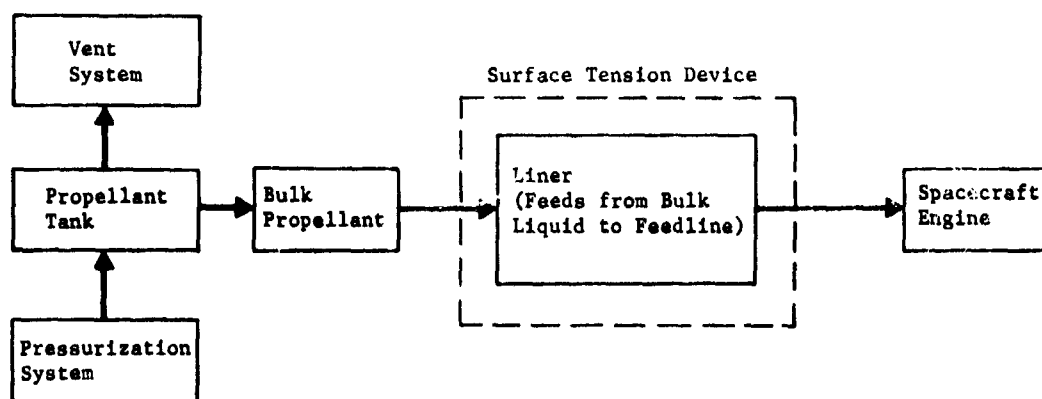
Reliability means the probability of a device performing its function adequately for the period of time intended under the operating conditions encountered. The reliability of many active systems and components has been analyzed, verified with functional tests, and reduced to a prediction of a "mean time between failure." On the other hand, passive systems that have no moving parts do not always lend themselves to such an analytical or experimental approach. The surface tension devices considered in this study are passive systems consisting of screen material supported by a structure. Since the design of surface tension systems requires a knowledge of the operating environment, the system's reliability primarily depends on how well the operating environment is understood. The following discussion is aimed at developing a rationale for evaluating the reliability of surface tension devices.

The two surface tension devices considered are traps and liners. The block diagrams in Fig. III-32 show how the devices fit into the propulsion system and how they function. The diagrams illustrate the primary function of the device--to provide gas-free liquid to the spacecraft engine on demand throughout the mission. Although a surface tension device can have other secondary functions such as controlling the liquid center of gravity and venting gas, this discussion will concentrate only on the devices' primary purpose.

A trap device has two elements--a capillary barrier that retains a given amount of liquid in the vicinity of the tank outlet, and an annulus that feeds liquid from the reservoir formed by the capillary barrier to the outlet. Both elements must operate if the trap is to function normally. The liner device has a single element--the liquid flow annulus.



(a) Trap Device



(b) Liner Device

Fig. III-32 Block Diagrams of Surface Tension Devices

A surface tension device has a single failure mode that occurs when operation of the device has been sufficiently degraded that gas enters the feedline. The possible causes of this failure mode can be broken down into the three levels shown in Fig. III-33. The right-hand column of the figure lists the possible basic causes of failure of a surface tension device. These causes are the result of an unexpected or excessively severe environmental condition for which the device was not designed. If the loads acting on the device exceed those expected, failure of the structure could occur. If the accelerations acting on the spacecraft exceed those expected, the capillary barriers may not be able to retain the liquid. Thermal environment, corrosion, contamination, and fluid behavior are additional environmental factors that could cause failure of the device.

The device is designed to function over a range of environmental conditions and will fail when the conditions reach some degree of severity. Between these two extremes there is a gradual reduction of reliability as the conditions become worse. A hypothetical case of this variation in reliability is illustrated in Fig. III-34. It is assumed that the period during which the device must successfully operate is fixed.

Under ideal operating conditions, the device would be 100% reliable, while the reliability would be somewhat less under nominal operating conditions. As the operating conditions become worse, the reliability decreases. Overdesign of the device extends its capability beyond the design range. Marginal operation, meaning the device has failed to some extent and degraded the capabilities of the propulsion system, extends the operating range. Further worsening of the operating conditions eventually reduces the reliability to a point that the device cannot be expected to continue operating over the required period and failure will occur. For the duration or the number of missions considered, the probability that the device will function can be selected as a design goal; i.e., one failure in 500 missions. This would set a lower limit for the curve in Fig. III-34.

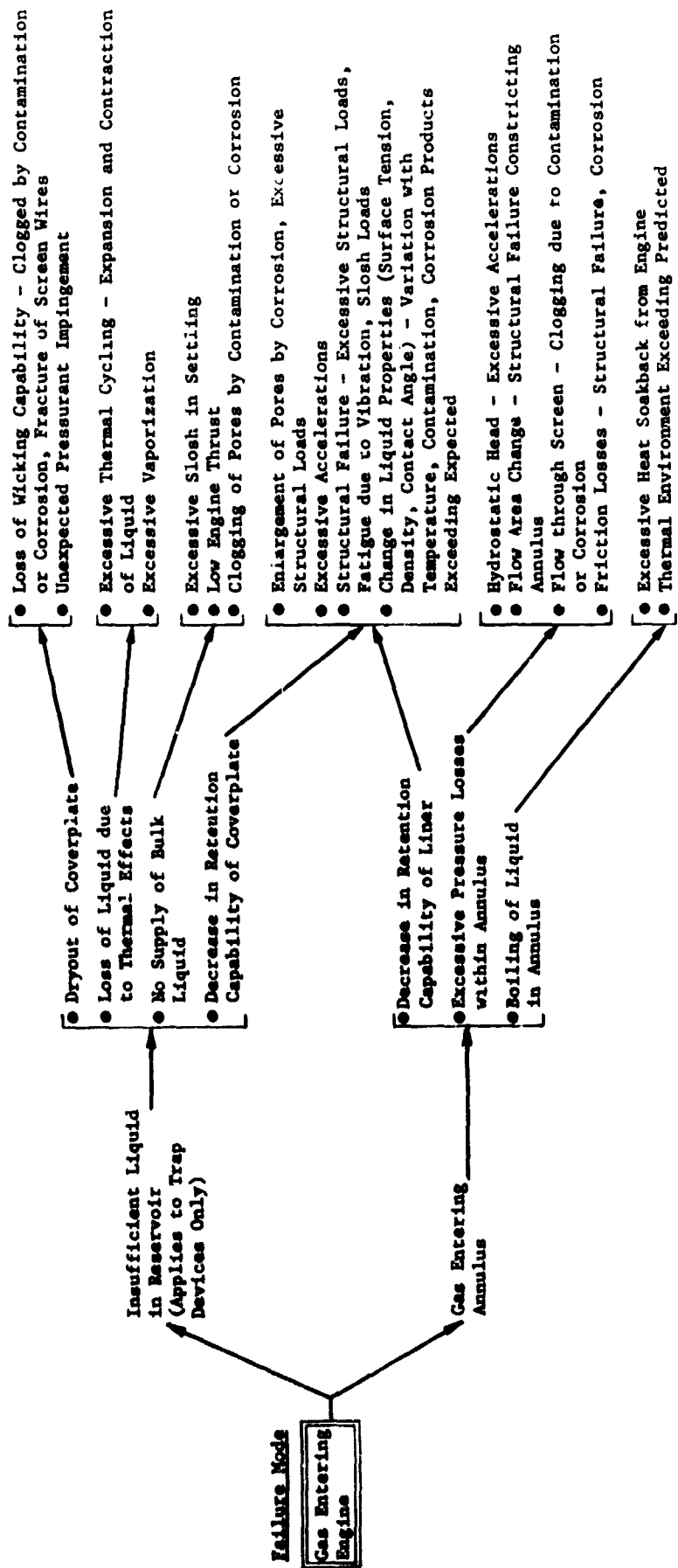


Fig. III-33 Causes of Failure of Surface Tension Devices

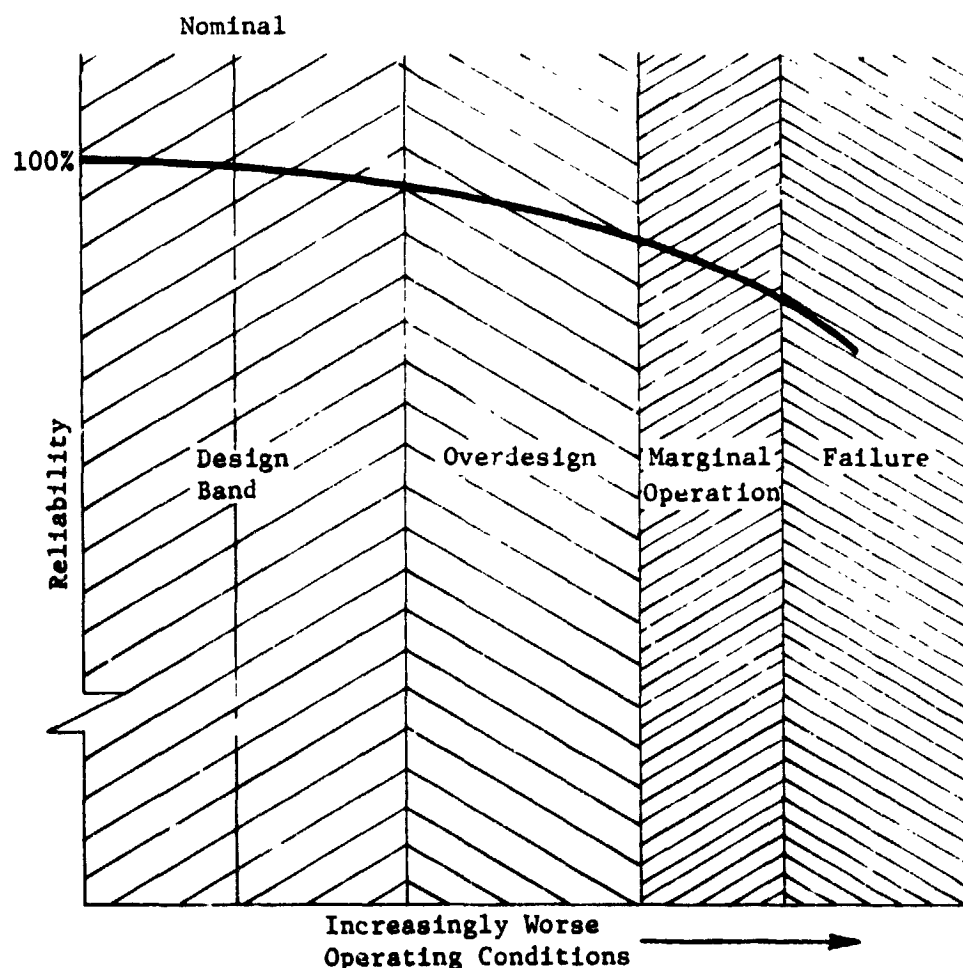


Fig. III-34 Variation of Reliability with Operating Conditions

If the curve falls above this lower limit, it is more probable that the device will function under the worst-case operating conditions without failure. The design approach is to extend the various bands as far as reasonable so the failure limits far exceed the anticipated operating conditions. Each of the possible causes of failure listed in Fig. III-33 are approached from this standpoint to determine how the design can maintain a high degree of reliability under all anticipated operating conditions. Inherently, the general level of reliability should be high since the device is passive. It is reasonable to expect that the reliability of the surface tension device will be on the same level as that of the propellant tanks.

The causes of failure listed in Figure III-33 can be summarized as the following excessive or unanticipated conditions. The general design approach to these environmental conditions is discussed in Section E of this chapter. The aspects related to a high degree of reliability are summarized in the following paragraphs.

1) *Structural loads* - Since the basic screen material of the device is very lightweight, substantial supporting structure can be added while maintaining a relatively small total weight. The screen alone can support typical low-g loads, and the supporting structure is added primarily for boost- and reentry-type loads. Using safety factors etc, a structure can be designed to yield a reliability essentially equal to, or greater than, that of the tank itself;

2) *Contamination* - Both the tank and the propellant acquisition device would be cleaned following fabrication and after any operation that could introduce contamination. Maintenance and servicing operations would be controlled to prevent the introduction of contaminants. Gases and liquids used in the system would be sampled before use to eliminate excessive contamination. With these procedures, contamination problems can be kept to a minimum. If any contaminants do collect within the device, their presence could be detected by an outflow test. An increased pressure loss during flow between the ullage and the tank outlet indicates that the screen material may have become clogged with contaminants. In most surface tension systems, considerable contamination would be required before any significant pressure increase would be detected because of the large flow area available;

3) *Corrosion* - The effect of corrosion can be similar to that of contamination--the corrosion products could clog the screen. Enlargement of the screen pores from corrosion is another concern. Corrosion could be controlled by using compatible materials and proven techniques. The compatibility of various materials with the propellants of concern was summarized in Chapter II. Based on this information, all of the common materials of construction are suitable for this application. Some control of the propellant quality will also be required, e.g., the amount of NO in N_2O_4 . These controls, combined with monitoring for any evidence of corrosion, should eliminate this problem;

4) *Thermal Environment* - The effect of the thermal environment on the properties of the propellant is the primary concern. Properties such as surface tension and density change with temperature and can either improve or degrade the performance of the device. Boiling and vaporization of the propellant must also be considered. Thermal analysis of the spacecraft will predict the expected range of temperatures for design of the surface tension device. Overdesign can be incorporated, depending on the confidence associated with the predicted thermal environment;

5) *Acceleration Environment* - The primary environmental factor influencing the design of a surface tension device is acceleration. All possible forces must be evaluated during the design.

Failure mode for surface tension devices and the possible causes of this failure mode have been identified. Inherently, the devices have a high reliability because their operation is entirely passive. By controlling the factors that influence each of the failure causes, an overall high degree of reliability can be obtained.

On a relative basis, it appears that a liner would be somewhat more reliable than a trap. A liner has a single operating element, the annulus, while the trap has two elements, the annulus and capillary barrier. Both elements of the trap must be functioning if the device is to operate normally.

6. Compatibility

The compatibility of the propellants being considered with the various materials of fabrication has already been discussed. To summarize, all of the combinations are sufficiently compatible. It would be most desirable to select a screen material that is of the same metal as the tank. However, the fineness of the screen mesh required will most likely be the determining factor. As discussed in Section A of this chapter, the mesh sizes available in aluminum, and especially titanium, are limited. These considerations do not produce any difference in capability between the traps and liners.

7. Loading and Handling

The problems involved in loading and handling the tanks for an OMS can be better appreciated by considering the facilities and procedures being considered for the Space Shuttle (Ref III-13). Figure III-35 shows a possible layout of the facilities at Cape Kennedy. After the Shuttle lands on the runway, the system would be safed and interface lines purged and disconnected. The pods containing the OMS would be removed from the vehicle and transported to the Hypergolic Test and Servicing Facility. All servicing and maintenance of the OMS is to be conducted in this facility. The pods would be stored at the facility until needed, then loaded with the tanks oriented vertically.

The loaded pods would be transported either vertically or horizontally to the Vehicle Assembly Building (VAB). The pods would be mated with the Shuttle orbiter and the interfaces verified. The orbiter could be either horizontal, prior to installation on the Launch Umbilical Tower (LUT), or vertical after installation on the LUT when the pods are attached. After assembly of the entire Shuttle vehicle, it would be transported on a crawler to the launch pad for final checkout and launch. Although the possibility of loading the OMS on the launch pad is still being considered, loading at the hypergolic facility (removing as much servicing from the pad as possible) is the desirable approach. Another alternative would be to load at the hypergolic facility and install on the orbiter at the launch pad, thereby eliminating hypergolic propellants from the VAB.

The annulus of a surface tension device must be filled during loading, but otherwise loading a tank containing a screen device is the same as loading a bare tank. The annulus in a trap can be filled using a number of techniques. A vent line at the high point of the annulus would be the easiest way to guarantee complete filling. Loading a tank with a liner device would be similar. However, the tank would have to be completely filled to fill the liner annulus; then the tank would be offloaded to the desired level.

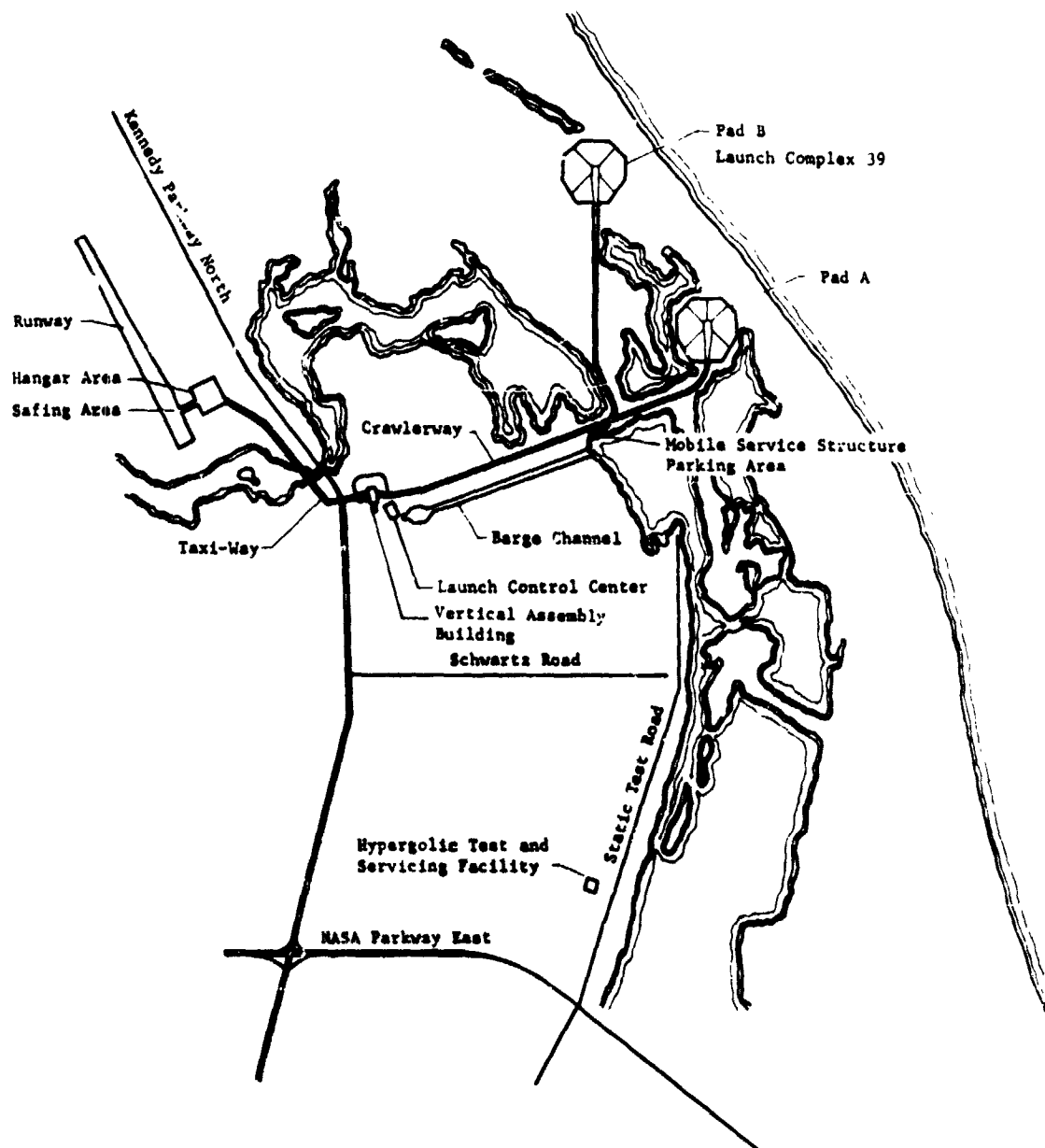


Fig. III-56 Space Shuttle Launch and Servicing Facilities

Handling of the system would involve rotating the tanks from vertical to horizontal, and vice versa, and transporting them from one facility to another. During this handling, the trap will remain completely or partially in the propellant and will not present any problem. The liner is more sensitive to handling since portions of the annulus will always be exposed to the ullage. Vibration and impact loads could cause some loss of liquid from the annulus. Both the liner and trap systems were tested, demonstrating loading and handling (see Chapter IV). These tests show that such operations can be accomplished without degrading device performance.

8. Reusability

After each use, the spacecraft will be tested and refurbished, as required, for the next use. The life of the system could extend over a period of 10 years, including 100 to 500 missions. The current philosophy envisioned for Space Shuttle was used to evaluate the reuse of surface tension devices. NASA Kennedy Space Center personnel, who are developing the facilities and philosophies for Shuttle, were contacted to obtain this information (Ref III-13).

It is expected that all systems will be carefully inspected between flights during the developmental period to establish performance trend data. An operational philosophy will be developed that will probably not require detailed inspection between flights. Once the Space Shuttle is fully operational, minimum refurbishment and verification testing would be required. Flight data from the previous flight would be used to determine the level of maintenance required.

Samples of residual propellants would be taken to determine whether the propulsion system had become contaminated. If no anomalies were detected, no maintenance or subsystem testing would be performed. The tanks would merely be reloaded for the next flight.

If problems related to the tankage or surface tension device were detected, the tanks would be purged and decontaminated. Maintenance would be performed, probably including replacement of the suspect components. Leak checks and functional checks would be conducted and the system would return to the normal operational cycle.

The success of this approach highly depends on the capabilities of the subsystems used in the vehicle. Surface tension devices will maintain a high degree of reliability after many missions and many years of use. A device that can withstand all imposed structural loads can be fabricated using state-of-the-art techniques. The materials used in the device will be compatible with the propellants for the time required.

Modular installation is highly desirable for a reusable system. Maintenance for a modular surface tension device would be accomplished on a remove-and-replace basis. The removed device could be repaired, inspected, tested, etc without interfering with the turnaround schedule of the spacecraft.

Because of their compact size, trap devices lend themselves to modular installation. The device is attached to an access cover so it can be bolted in place or removed as required. Modular installation of a liner is more difficult. Although the channels of the device could be removed individually, they would have to be interconnected and sealed within the tank.

Ease of inspection and test is also an important aspect of reusability. Both liners and traps can be tested with simple 1-g tests. Bubble point tests of the screen surfaces can be conducted. Outflow tests, with the device inverted so flow is against 1-g, will verify the retention capability of the system. Measuring the pressure drop between the ullage and the feedline during outflow will determine if any clogging of the screens has occurred. Procedures for checking the devices while installed in the tank have been developed and verified (see Chapter IV).

9. Development Status

Although both traps and liners use currently available technology, there is some variation in the development status of these systems. Nonrefillable traps have been flight-qualified. The applications include numerous flights on the Agena, Apollo LEM, Transtage, and several target drones. Refillable traps were also flight-qualified for such applications as Apollo SPS, improved Agena, and Mariner 9. Liner systems have been designed, fabricated, and tested in considerable depth. A flight-qualified liner is presently used in the P-95 program.

D. SELECTION OF PREFERRED SYSTEMS

The comparison of traps and liners in the previous section showed similar capabilities in many respects. Some of the minor differences are:

- 1) The expulsion efficiency of liners is less than that of traps;
- 2) Liner devices are somewhat heavier than traps;
- 3) Liners would tend to be more reliable than traps;
- 4) Traps are more easily adapted to modular installation.

One factor, flexibility, is considerably different for the two devices and will be the basis for the selection of the preferred systems. Liners are independent of mission duty cycle, while traps are highly dependent. Although trap flexibility can be improved by increasing the trap volume, a trap can never be as flexible as a liner. However, examination of typical OMS missions showed that a refillable trap, with possibly only a small increase in its basic volume, could accomplish all missions. Since the OMS engine burns tend to settle the propellant, there are no omnidirectional accelerations during outflow. Because the first and last burns are of long duration, complete settling during some of the burns is certain. This leaves the number of short-duration burns (too short for any settling or refill) as the only significant concern. By sufficiently oversizing the trap, this concern can also be eliminated.

Propellant offloading capability was the other aspect of flexibility also evaluated. The basic liner would not allow any offload. Modifications to the liner, such as compartments or multiple screens, would permit the tank to be offloaded but these modifications would increase the complexity and mass of the device. Traps are virtually insensitive to offloading.

Figure III-36 provides a summary of the applicability of the various candidate capillary devices. Regions within which the concepts are applicable as a function of adverse acceleration level, settling duration, and propellant offload are identified.

Based on these comparisons, traps were selected as the preferred system. Specifically, two trap devices are recommended for the type of mission being considered. One is the compact refillable

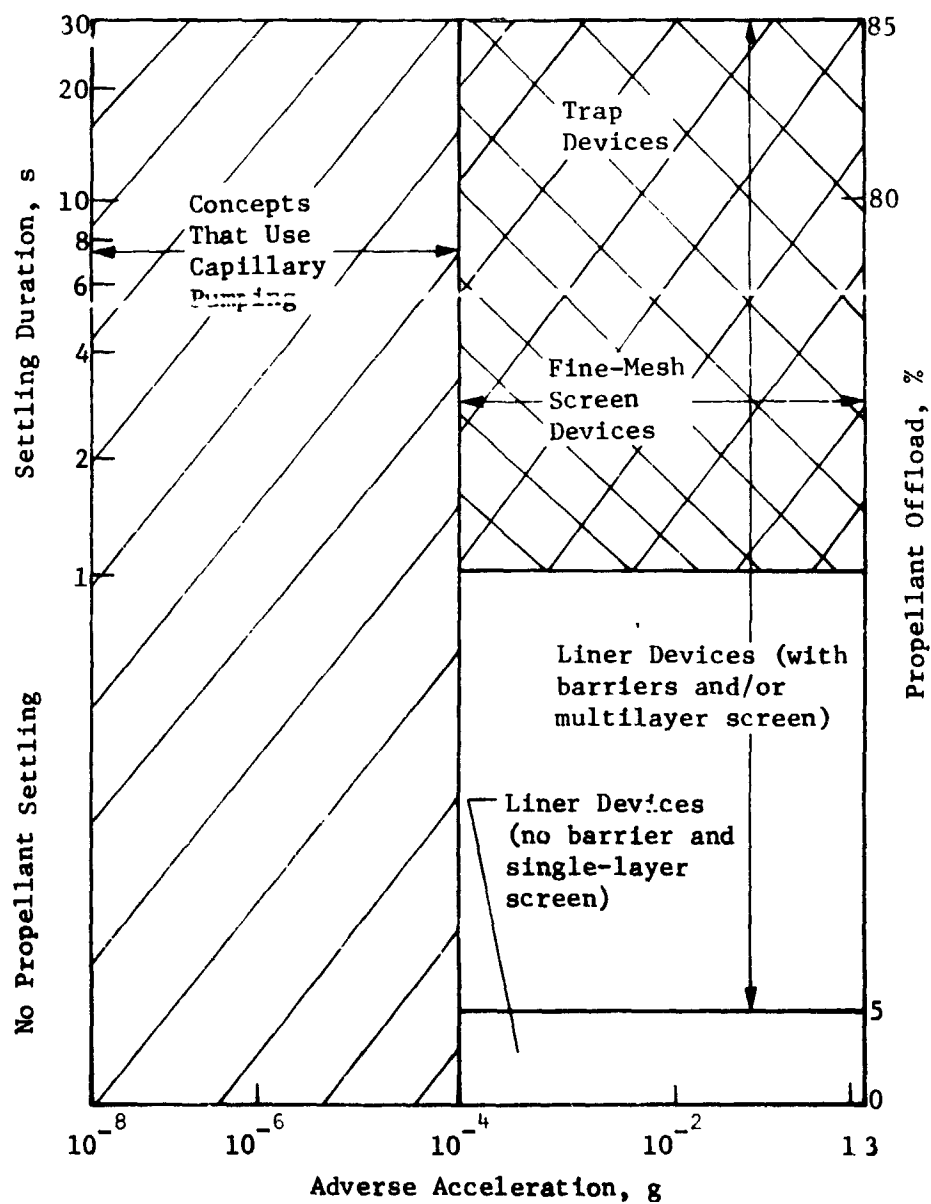


Fig. III-36 Map of Capillary System Applicability

trap similar to that shown in Fig. III-25. This device can meet the typical mission duty cycles with only a minimum variation. It can be easily installed and removed from the tank, tested, and inspected.

The second device is the enlarged trap, similar to the device shown in Fig. III-28. This is the recommended system if the typical duty cycles are only representative and a number of additional short-duration burns are possible during the mission. The trap volume is increased to accommodate additional burns and increase the flexibility of the system. Since the minimum propellant load would still be greater than the trap volume, offloading would not be a problem.

This enlarged trap device could be considered a shortened or truncated liner. In the lower part of the tank, the device has the configuration of a liner device. The upper portion of the liner has been removed and the lower portion is sealed with a coverplate. By eliminating the upper portion of the liner, problems caused by offloading the tank are eliminated. However, the device is not in communication with the entire tank and therefore is not as flexible as the basic liner.

E. DESIGN APPROACH

The design process presented in this section is applicable to any surface tension device for earth-storable propellants and for the mission criteria presented in Chapter II. The devices presented in previous sections of this chapter are typical examples. The purpose of this outline is to define the process and considerations involved in design of the devices.

Figure III-37 outlines the total design process. Only devices for earth-orbital missions are considered. Interplanetary missions (typically of long duration with very low g-l vels) and missions within the atmosphere (short duration, few restarts, and high g-levels) would require somewhat modified approaches.

The first step in the process, selection of either a trap or a liner, would be a comparative process similar to that presented in Section C. Each of the factors significant to the selection must be evaluated. The selection must be based on the mission parameters and criteria. A similar comparison would be required to select either the refillable or nonrefillable trap if a trap system were to be selected.

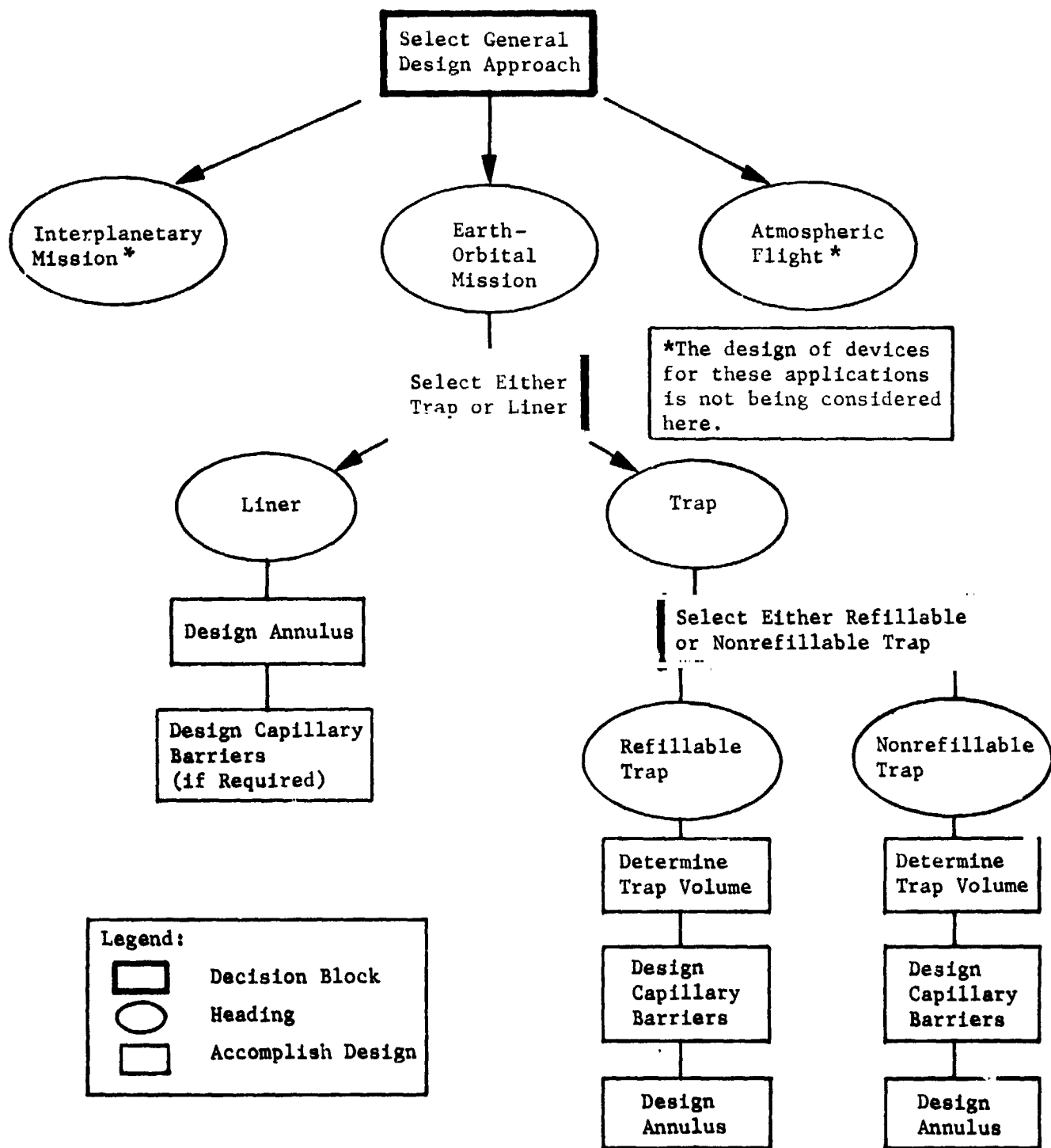


Fig. III-37 Outline of Total Design Process

The process for determination of trap volume, annulus, and capillary barriers is outlined in Fig. III-38 thru III-41. The parameters and phenomena discussed in Section A would be applied to the design process. Worst-case conditions should be used to provide the specific design criteria for components. For example, the maximum number of short-duration burns when determining trap volume, the maximum adverse accelerations when designing capillary barriers, and the worst-case engine start situation when designing the annulus should be considered.

In addition to those outlined in the figures, some special considerations must be applied to the design of refillable traps. The coverplate must be capable of retaining the liquid within the reservoir under the action of adverse axial and lateral accelerations, but allow gas to leave the reservoir and liquid to enter under the favorable settling acceleration during an engine burn.

First, the effect of adverse axial accelerations will be evaluated using the conical coverplate shown in Fig. III-42 as an example. The coverplate must be capable of retaining liquid when an adverse axial acceleration A_a is tending to displace liquid from the reservoir. The bubble point of the screen material used on the coverplate ΔP_c must be greater than the hydrostatic head

$$\Delta P_c > \rho A_a h_a \quad [14]$$

where ρ is the density of the liquid and h_a is defined in Fig.

III-42. This same screen must break down when the engine acceleration A_e is acting to settle liquid on top of the coverplate, as expressed by

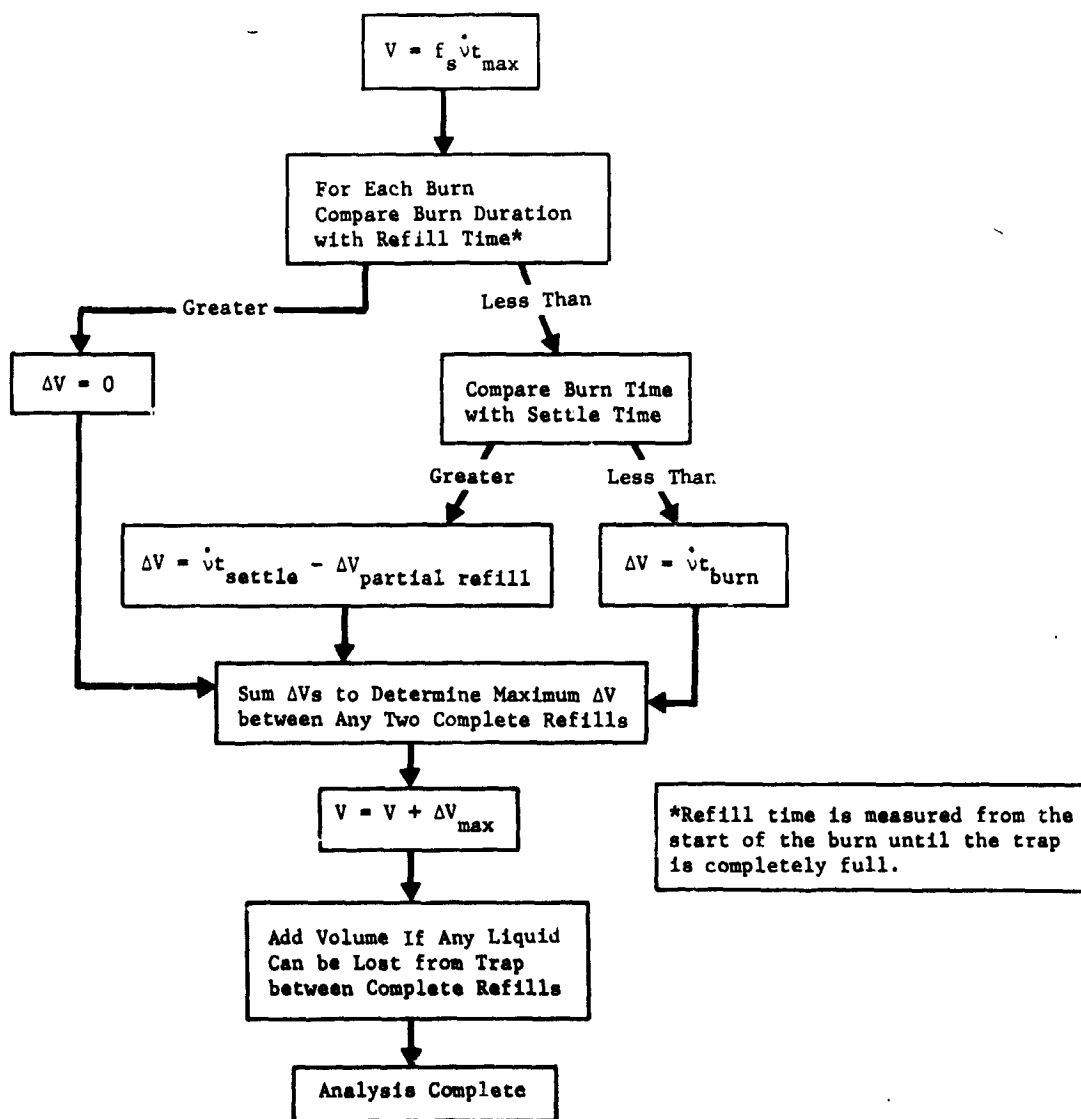
$$\Delta P_c < \rho A_e h_a .$$

Since the same value of ΔP_c is involved in both equations, the equations can be combined:

$$\rho A_e h_a > \rho A_a h_a$$

or

$$A_e > A_a . \quad [15]$$



Note: V = volume of liquid that must be retained in trap.
 f_s = safety factor,
 \dot{v} = volumetric flow rate,
 t_{max} = maximum settle time,
 t_{settle} = settle time, starting with flow of liquid from tank until gas ceases to enter trap.
 t_{burn} = duration of burn.

Fig. III-38 Refillable Trap Volume

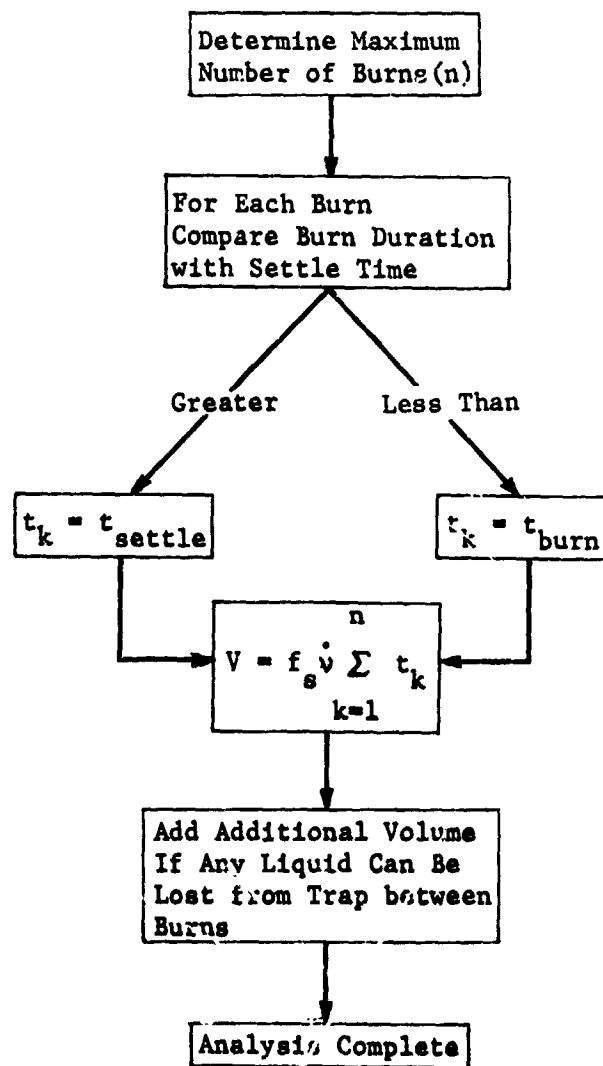
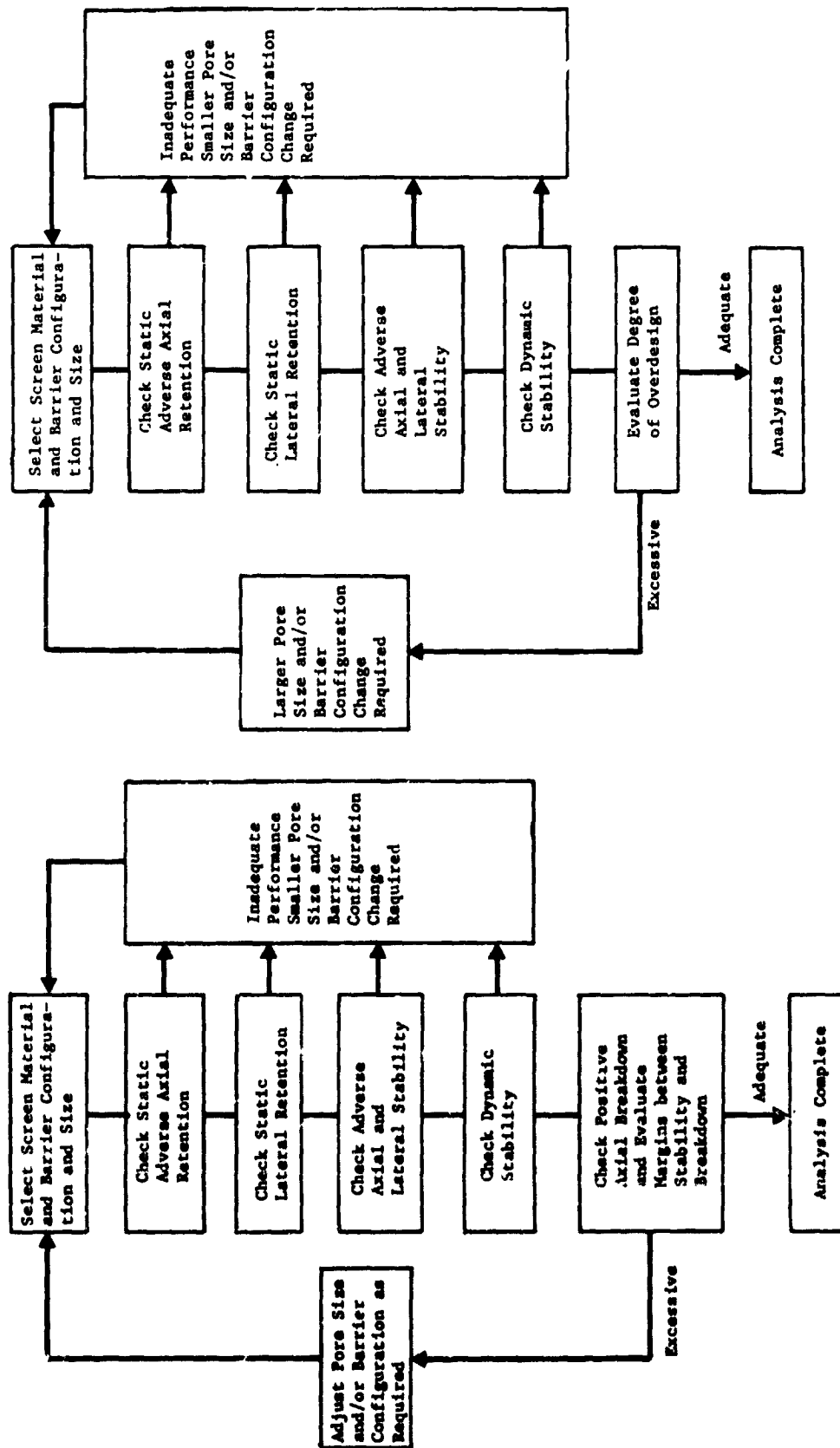


Fig. III-39 Nonrefillable Trap Volume



(b) Nonrefillable Trap or Compartment

(a) Refillable Trap or Compartment

Fig. III-40 Capillary Barriers

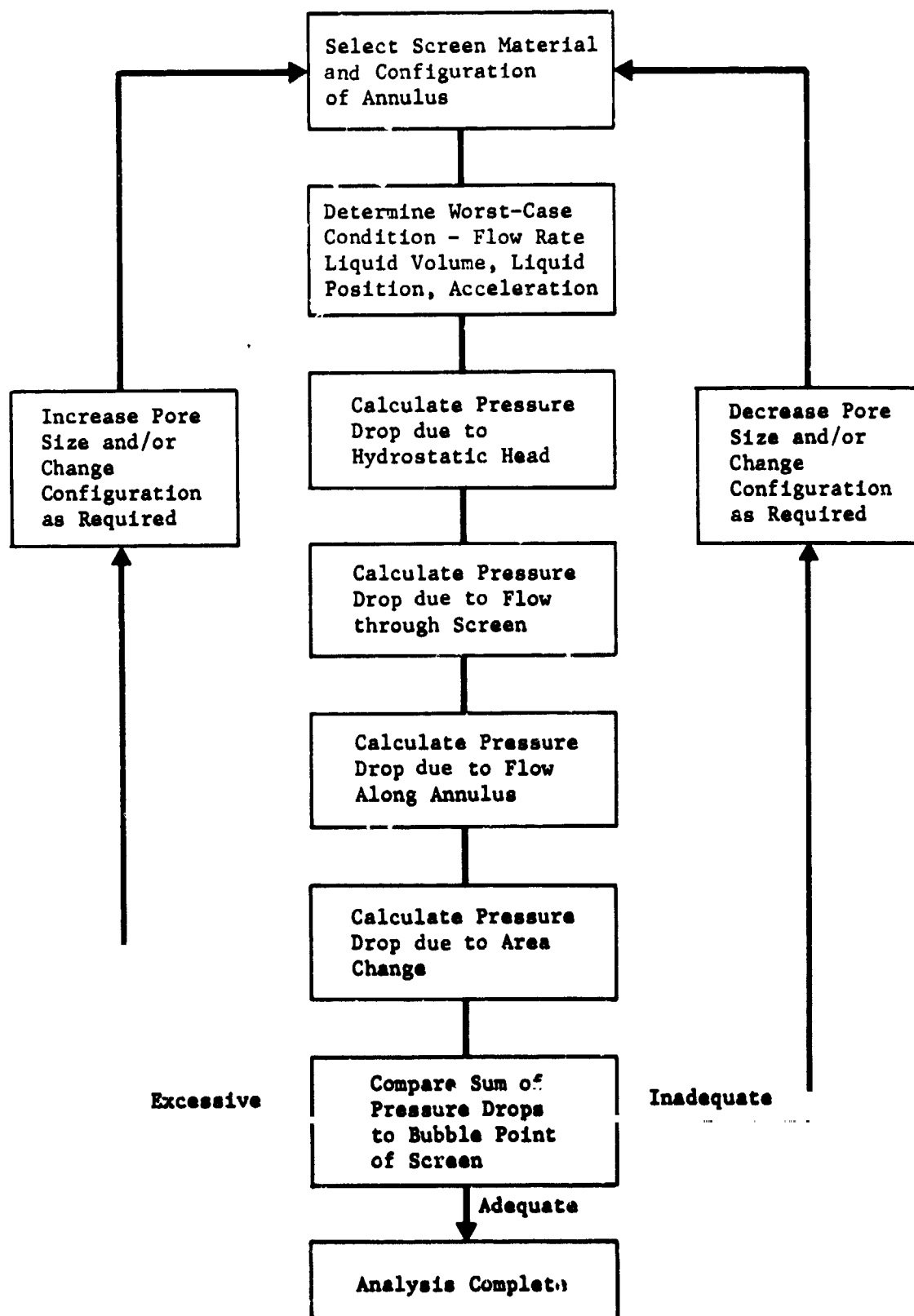


Fig. III-41 Annulus

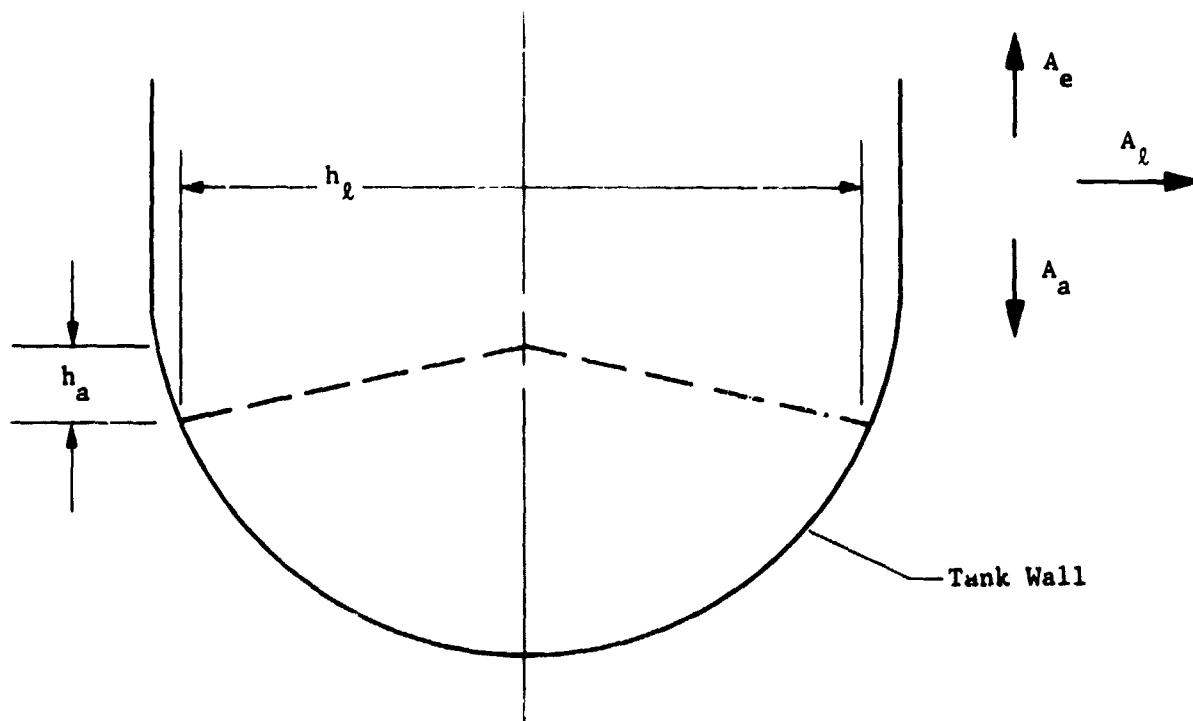


Fig. III-42 Conical Coverplate for a Refillable Trap

The engine acceleration must be greater than the adverse axial acceleration to permit refill for this coverplate configuration. Hopefully the accelerations will differ by at least an order of magnitude to allow selection of the screen material and operating margins.

The coverplate shown in Fig. III-43 makes it easier to satisfy the above requirement. A cylindrical vent tube is located in the center of the coverplate. Screen A on the top of the tube is coarser than Screen B on the coverplate. Screen B always remains stable, but Screen A breaks down when the engine is operating, permitting refill. The requirements become:

$$\text{For Screen B } (\Delta P_c)_B > \rho A_a h_a,$$

$$\text{For Screen A } (\Delta P_c)_A < \rho A_e h_a$$

$$\text{and } Bo = \frac{\rho A_a r^2}{\sigma} < 0.84.$$

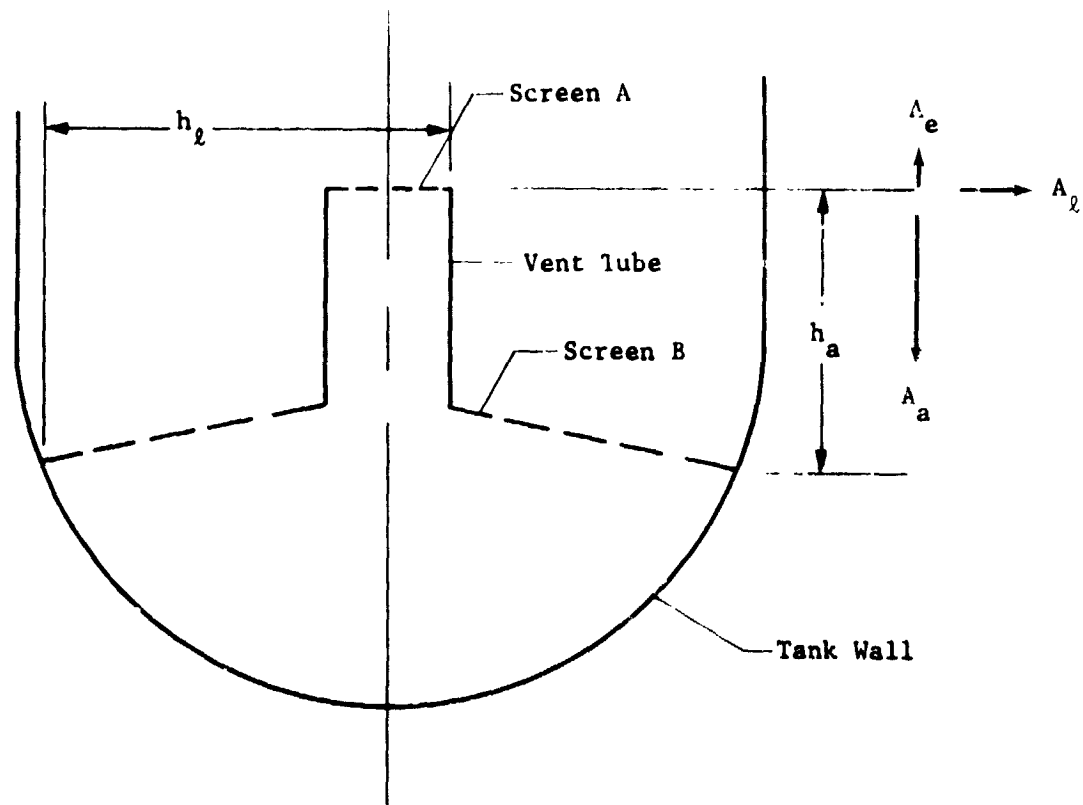


Fig. III-43 Coverplate with Vent Tube

With the adverse axial acceleration, the pressure differential across Screen A is zero, but the screen must satisfy the hydrostatic stability criteria. Although the Bond number (Bo), based on the screen pore radius (r), must be less than 0.84, this is an easily satisfied criterion. With this configuration, one screen does not have to satisfy two criteria. For typical coverplate designs, A_a can be the same as, or even slightly greater than, A_e and still satisfy the criteria of the above equations.

Now, the effect of lateral accelerations will be evaluated. For the coverplate configuration in Fig. III-42, the following criteria apply:

$$\Delta P_c > \rho A_l h_l,$$

while the previous criteria still apply,

$$\Delta P_c > \rho A_a h_a$$

and

$$\Delta P_c < \rho A_e h_e.$$

The added requirement is that

$$\rho A_e h_a > \rho a_l h_l$$

or

$$\frac{h_a}{h_l} > \frac{A_l}{A_e}.$$

The ratio of the accelerations establishes the criteria for the coverplate dimensions.

The same relation is obtained when Screen A or the coverplate in Fig. III-43 is evaluated:

$$(\Delta P_c)_A > \rho A_l h_l$$

and the previous equation,

$$(\Delta P_c)_A < \rho A_e h_a$$

so

$$\frac{h_a}{h_l} > \frac{A_l}{A_e}.$$

The distance h_l in this case is only about one-half that of the other coverplate. This helps to keep the ratio h_a/h_l large, which is essential if the ratio A_l/A_e is also large.

Another concern is associated with the criterion

$$\Delta P_c < \rho A_e h_a$$

as it applies to both coverplate configurations. The dimension h_a as shown in Fig. III-42 and III-43 assumes that the liquid level inside the trap is at or below the coverplate/tank wall attach point. As the trap fills and the liquid level increases along the coverplate, h_a is measured from the liquid level to the top of the coverplate (Fig. III-42) or to the top of the vent tube (Fig. III-43). As h_a decreases, a value will eventually be reached that satisfies the relation

$$\Delta P_c = \rho A_e h_a$$

and the screen that was unstable, allowing gas to leave the trap, becomes stable and stops the refill. This value of h_a determines how much of the trap device can be filled.

The representative system designs presented in Chapter V were based on this parametric design approach and the results of the ground test program (Chapter IV).

IV. GROUND TESTING

The earth-storable propellant system study was concerned with the performance, design, operation, and reuse of passive acquisition/expulsion devices. Complete tank liners and traps were selected as the two baseline designs for ground testing because their physical and performance characteristics tend to span the range of capillary devices for orbital low-g propellant management. A comprehensive evaluation of complete tank liners and traps for reuse in an earth-orbiting vehicle must consider failure modes and effects, the ground processing between flights, and fabrication or operational complexities introduced by the performance-oriented designs. In addition, a simple and reliable acceptance test procedure was required for the selected acquisition/expulsion device. The ground testing was conducted to provide qualitative and quantitative data for the design and the sensitivity analysis.

Three test programs were defined to provide information and experience necessary for the design (Task II) and development planning (Task IV) under the earth-storable study. All of the ground tests utilized Martin Marietta facilities. The performance of multiple-screen barriers was investigated by bubble point testing and lateral stability testing. Bubble point and centrifuge tests of the multiple-screen barrier model provided an empirical correlation with theoretical liquid retention and lateral stability predictions. A small model of a complete screen liner and a sub-scale trap, produced under an IR&D program, were used to study ground handling requirements and procedures. Acceptance tests, functional (flight readiness) inspections, and propellant loading and draining procedures were investigated in bench tests. The effects of vibration and shock environments during ground transportation and handling were determined using the same model. These qualitative tests were conducted to demonstrate capability and complement the quantitative evaluation of vibration effects conducted under the cryogenic phase of the program and presented in Volume III. The ground handling and acceptance tests were planned to emphasize the reusability and inspectability criteria.

The ground test program and results are presented in this chapter, which includes a discussion of the experimental approach and a description of the test apparatus, instrumentation, test procedures, and data obtained.

A. MULTIPLE-SCREEN TESTS

The complete tank liner device offers freedom from duty cycle limitations and is a flexible, attractive system for many applications, as discussed in Chapter III. A complete (noncompartmental) liner for the OMS application, however, requires a number of screen layers to provide liquid retention during the 3-g boost phase with offloaded tanks. From a steady-state standpoint, many layers of screen would be required to maintain liquid/gas interface stability under these conditions.

Extensive testing by Martin Marietta (Vol III) has demonstrated that the liquid retention capacity (bubble point) of stacked screens is approximately additive as long as the screens are separated by more than a pore diameter. The components of stacked screen barriers could be termed "overload screens" because they are not effective until breakdown (gas ingestion) reaches them. This liquid retention mechanism of multiple-screen barriers suggests that a response time is important to the performance of systems using multiple layers of screen. Gas ingestion and the resulting loss of liquid is a rate process that takes place over some period of time (Ref IV-1). If the rate of gas ingestion were slow enough or the duration of the upsetting perturbation short enough, the number of screen layers required could be reduced. For instance, the retention capability of two screens could be exceeded, gas would enter the first screen, and liquid would be lost from between the screens at some rate. However, if the conditions causing breakdown did not last long enough to cause gas ingestion through the second screen, a system employing two screen layers would meet the requirements. Therefore, both the transient and steady-state performance must be considered in the design of capillary systems.

Since no quantitative data were available for the transient performance of multiple-screen systems, tests were conducted to determine the rate at which stacked screen barriers break down (rate of gas ingestion) under excessive accelerations, the severity of the breakdown or quantity of gas ingested (which determines the subsequent flow blockage during outflow), and any reduction in stability margin caused by gas trapped between screens.

1. Objectives

The objectives of the multiple-screen performance tests (MSPTs) were to evaluate the operating characteristics of screen stacks under sustained lateral accelerations and to obtain performance data for propellant acquisition/expulsion system design, sensitivity evaluation, FMEA, and handling and operating procedure development.

2. Approach

The capillary dynamics of multiple-screen barriers were studied under conventional bubble point static pressure loading conditions and under sustained accelerations in the region of the barrier stability limits. The cumulative bubble point capability of the screen stacks was assessed using standard bubble point test procedures and performance definitions. A centrifuge was used to provide constant lateral acceleration loading for a test period long enough to allow the fluid dynamics of the screen stack to be characterized. These tests were supplemented by transient centrifuge acceleration tests covering the entire acceleration range. The acceleration range spanned the breakdown regime for the multiple-screen system so the rate of gas ingestion and depth of gas penetration into the barrier could be correlated.

3. Test System

The multiple-screen performance test system was composed of the test model, assembly hardware, and appropriate instrumentation for either the bubble point tests or the lateral stability tests. The test model, shown in Fig. IV-1, was transparent to allow visual observation of the screen barrier and liquid. As shown, it consisted of three subassemblies: (1) gas ullage compartment, (2) three-screen capillary barrier, and (3) bulk liquid compartment. The transparent model walls were 1.27-cm (1/2-in.) thick polycarbonate plastic to provide the strength, toughness, and resistance to chemical attack by the methanol test liquid. In the test orientation with the ullage compartment on the bottom, the horizontal screen barrier in the center, and the bulk liquid compartment on the top, the overall internal dimensions were:

- 1) Length parallel to induced lateral acceleration = 22.9 cm (9.0 in.);
- 2) Height aligned with gravity vector = 12.7 cm (5.0 in.);
- 3) Width normal to the resultant acceleration plane = 11.4 cm (4.5 in.).

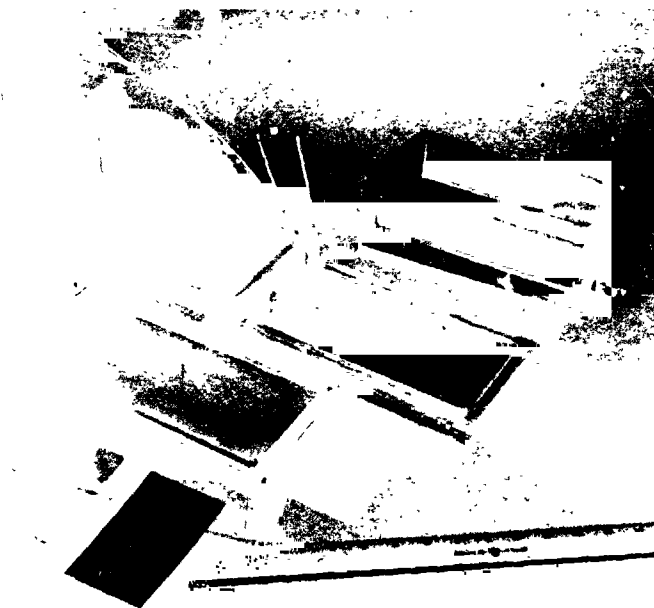


Figure IV-1 Multiple-Screen Performance Test Model

Three capillary barriers constructed of three layers of screen separated by 0.64-cm (1/4-in.) spacing were each tested in the assembled model. The three stainless steel screen barriers simulated the finest mesh screen material available in stainless steel, aluminum, and titanium, as shown in Table IV-1. This table also presents the single-layer bubble point and the lateral acceleration ranges required to test the three-screen-layer model with methanol for the 325 x 2300-mesh Dutch-twill screen, the 200 x 1400-mesh Dutch-twill screen, and the 180 x 180-mesh square weave screen. Methanol, which has a kinematic surface tension near the average for the candidate propellants (Chapter II), was used for the tests.

Table IV-1 Candidate Screen Materials for Earth Storable Propellant Acquisition/Expulsion Devices

Material	Screen Weave	Bubble Point,* cm H ₂ O (in. H ₂ O)	Predicted Lateral Acceleration Range for Three-Screen Barrier, g
Titanium (Pure)	180 x 180 Plain Square Weave	9.4 (3.7)	0.5 to 1.6
5056 Aluminum	200 x 1400 Dutch Twill	40.6 (16.0)	2.2 to 6.8
304L Stainless	325 x 2300 Dutch Twill	63.5 (25.0)	3.5 to 10.6
*Single-layer bubble point pressures in methanol.			

The model was located against a gusseted butt plate, which provided the mounting structure required for lateral stability testing. Assembly was accomplished by clamping the component parts between top and bottom aluminum plates with eight equally spaced tension rods. Sealing between parts was provided by two 0.16-cm (1/16-in.) thick neoprene gaskets. The configuration for the bubble point tests is shown schematically in Fig. IV-2 and the bubble point test instrument is pictured in Fig. IV-3. The assembled model ready for centrifuge testing is shown in Fig. IV-4. Installation on the Rucker centrifuge, used for the lateral stability tests, is shown in Fig. IV-5. The centrifuge is shown in Fig. IV-6 and its characteristics are listed in Table IV-2.

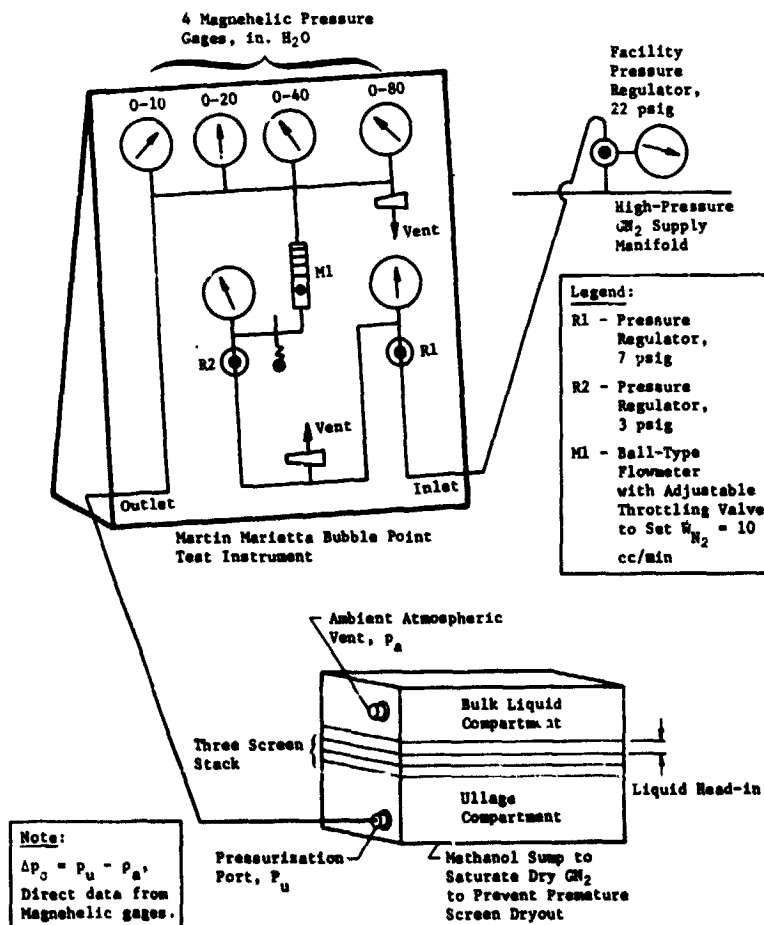


Fig. IV-2 Bubble Point Test Schematic

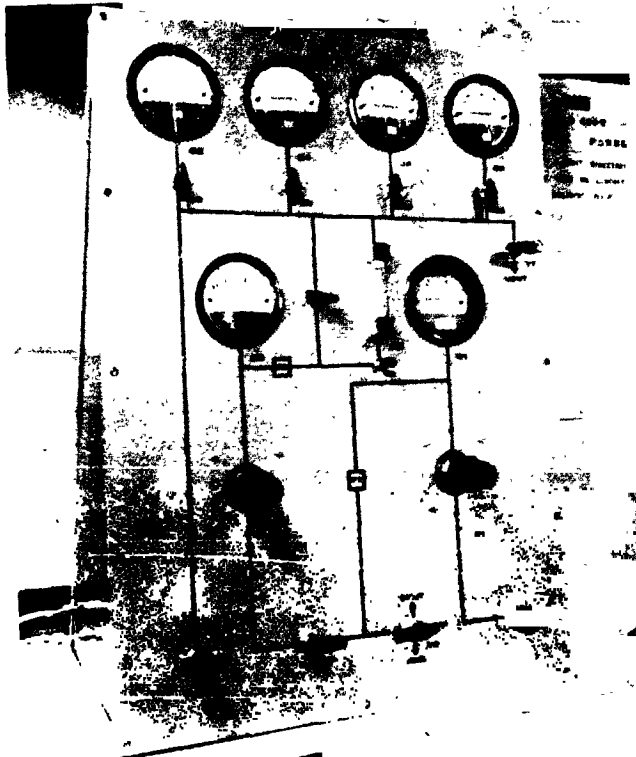


Figure IV-3 Low-Pressure Test Apparatus

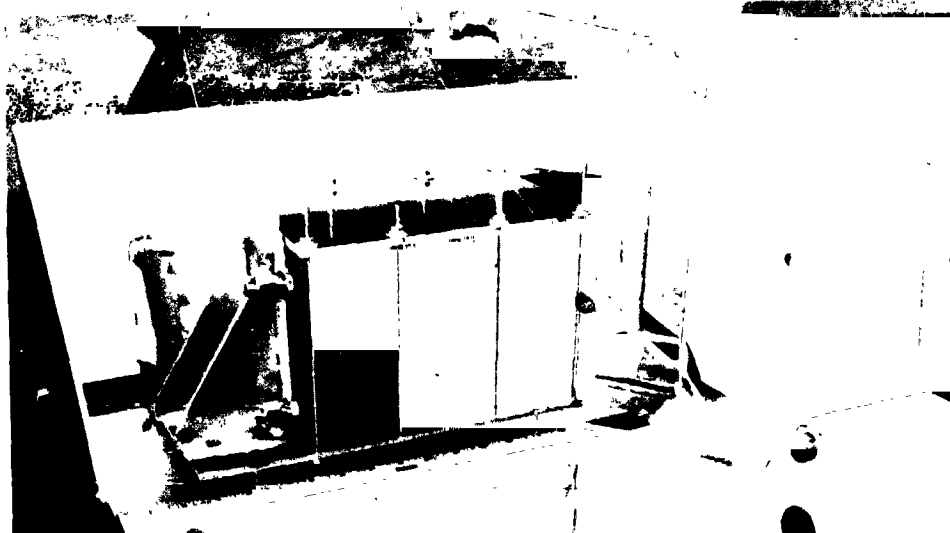
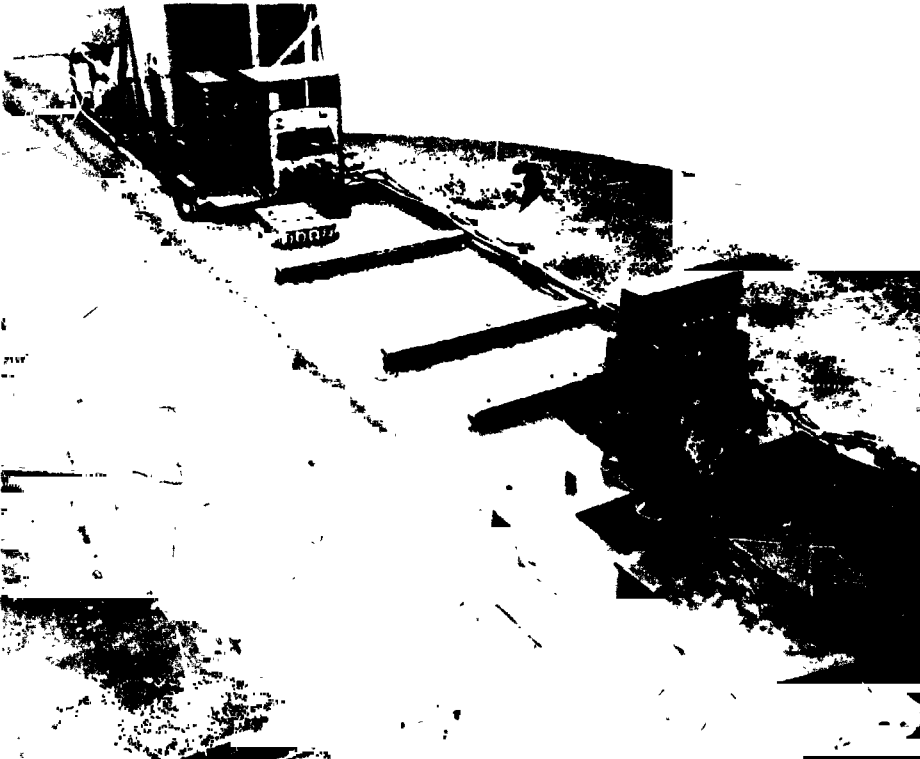


Figure IV-4 Assembled Multiple-Screen Test Model



Figure IV-5 Installation on the Rucker Centrifuge



*Figure IV-6 Rucker 17.5-ft-Radius Arm Centrifuge in the
Martin Marietta Environmental Test Laboratory*

Table IV-2 Rucker Centrifuge Characteristics

Radius Arm, m (ft)	5.34 (17.5)
Acceleration Range, g	0 - 25
Adjustment over Range	Infinite
Load Limit, g-kg (g-lbm)	3640 (8000)
Maximum Experiment Mass, kg (lbm)	182 (400)
Model cg Radius, cm (in.)	556 (219)
Acceleration Gradient over Model	$\pm 2\%$

System performance during lateral stability was filmed in slow motion at 64 frames per second using a 16mm DBM-3 movie camera with 100-ft roll film. The time correlation required for the multiple-screen barrier performance data was obtained from the films. The test acceleration level was determined directly from a tachometer that displayed centrifuge angular velocity. The high-speed movie camera, operating on 28-Vdc battery power, was focused on the spaces between the barrier screens from both directions at the inner end of the model where gas penetration occurred. A mirror provided a full view of the end of the MSPT model. The movie camera also recorded a 16-cm (6.3-in.) field of view along the 22.9-cm (9.0-in.) side of the model.

4.

Procedures

The techniques employed for filling the model with liquid methanol depended on the capillary barrier stability in the normal 1-g environment, but were the same for each model whether prepared for bubble point or centrifuge testing. The bubble point tests are conventional static tests with established criteria for operation and data evaluation. The lateral stability testing on the centrifuge is not as routine; these dynamic tests are closely related to model geometry for operation and data evaluation.

a. Filling Procedures - The model assembly and filling procedures in preparation for either bubble point or lateral stability testing are documented on 16mm color movie film. For the Dutch-twill screen barriers, filling was accomplished by pressurizing the liquid in the ullage compartment until liquid overflowed through the high-point vent holes between the screens. When the holes were capped, the stable barriers prevented liquid loss. For

bubble point testing, a thin layer of liquid was added to the ullage compartment for pressurant saturation and to the liquid compartment to keep the screens wet. For lateral stability testing, the ullage compartment was completely emptied and capped, and the bulk liquid compartment was completely filled and capped. Since the 180 x 180 square weave barrier was unstable in 1-g, it was completely filled with methanol, installed in the test position, and the ullage and the liquid compartment (for bubble point only) were drained to the desired levels.

b. Bubble Point Test Procedures - Eight bubble point tests were planned for each screen barrier, four with the barrier as initially installed (original) and four with the barrier inverted. The random, unstable breakdown characteristics encountered with the 180 x 180 plain square weave barrier resulted in only two extensive bubble point tests of this barrier.

The ullage compartment of the MSPT model was pressurized slowly at a constant $10 \text{ cm}^3/\text{minute}$ ($0.61 \text{ in.}^3/\text{minute}$) with GN_2 until general breakdown of the entire barrier occurred. The maximum pressure drop between the ullage compartment and the bulk liquid compartment, which was operating at ambient pressure, occurs at the equilibrium breakdown condition where enough pores in the upper screen are bubbling to vent the $10 \text{ cm}^3/\text{minute}$ ($0.61 \text{ in.}^3/\text{minute}$) GN_2 input. During each test, the progressive breakdown for each screen layer was observed and the gage pressure in the ullage compartment was recorded for each bubble point and maximum general breakdown. After steady-state breakdown to the bulk liquid compartment had been achieved, the ullage compartment was locked up and the pressure decay to upper screen bubble sealoff was recorded.

c. Centrifuge Test Procedures - Two different procedures were used to obtain lateral stability performance and breakdown transients for multiple-screen barriers. Steady-state lateral acceleration tests were performed at constant centrifuge speeds and transient lateral acceleration tests were conducted as the centrifuge was accelerated.

1) Steady-State Lateral Acceleration Tests - The steady-state lateral acceleration tests were run to provide quantitative data on the breakdown characteristics for each screen layer (gas penetration and accumulation rates) under constant lateral acceleration. Of the 20 centrifuge runs, 17 runs were of the steady-state acceleration type

$$a = R\omega^2$$

$$\alpha \equiv \frac{d\omega}{dt}, \quad \alpha \approx 0.$$

The centrifuge hydraulic motor bypass valve, which controls maximum angular velocity, was preset at a level well below the desired ω . When the preset ω stabilized, the bypass valve was stepped-closed in small increments until the desired ω was achieved. This procedure resulted in reduced initial acceleration α since the power was lower to obtain $\omega_{\text{preset}} < \omega_{\text{desired}}$. The acceleration component

$$a_R = R\alpha$$

was negligible from the small increases in hydraulic motor power and the subsequent restabilization periods that required 1 to 2 minutes of preliminary adjustment to reach ω_{desired} . After the preliminary centrifuge test condition adjustment, 60 s of film data were taken at

$$a = R\omega^2$$

2) *Transient (Increasing) Lateral Acceleration Tests* - The transient, increasing lateral acceleration tests were run to provide qualitative data on multiple-screen barrier breakdown characteristics. Runs 16 and 17, on the 180 x 180 square weave barrier, and Run 20, on the 325 x 2300 Dutch-twill barrier, were transient lateral acceleration tests:

$$a = \sqrt{(R\omega^2)^2 + (R\alpha)^2}$$

where

$$\alpha = \frac{d\omega}{dt}$$

acts normal to the radius arm to deflect the resultant lateral acceleration vector. The lagging angle is

$$\theta = \arctan \left(\frac{\alpha}{\omega^2} \right).$$

In the region of supercritical lateral accelerations, θ is much less than 26.6° , where θ is the model corner coordinate referenced to the model center origin. Then the exposed barrier length under the effects of the lateral acceleration is increased

$$\Delta h = \frac{\Delta h_x}{\cos \theta}.$$

However, the influence of the elongated barrier exposure is less than 1% for $\theta < 8^\circ$. It should be noted that the screen layer bubble point calculated from steady-state acceleration test data as

$$\Delta P_c = \rho (R\omega^2) \Delta h_x$$

becomes

$$\Delta P_c = \rho [(R\omega^2)^2 + (R\alpha)^2]^{1/2} \frac{\Delta h_x}{\cos \theta}$$

during the transient acceleration tests.

Since the maximum centrifuge acceleration in the region of the barrier breakdown was

Screen	Run	$\alpha, \frac{\text{rpm}}{\text{s}}$	$\alpha, \frac{\text{rad}}{\text{s}^2}$	a_R, g	θ, deg
180 x 180	17	1.0	0.1047	0.0594	6.91
325 x 2300	20	1.4	0.1466	0.0832	1.70,

the largest discrepancy incurred by neglecting the effects of α

$$\frac{\Delta P_c}{\Delta P_{cx}} = \frac{1}{\cos^2 \theta}$$

becomes

Screen	Run	$\cos \theta$	$\left(\frac{\Delta P_c}{\Delta P_{cx}} \right)$	$\left(\frac{\alpha}{a_\omega} \right)$
180 x 180	17	0.9927	1.0147	1.0073
325 x 2300	20	0.9996	1.0009	1.0004.

Since the transient acceleration data were to be used qualitatively and since the errors incurred by neglecting the effects of α were predicted to be within the accuracy of the test data ($\pm 2\%$), the data from the transient acceleration tests were reduced with the same procedures employed for the steady-state acceleration test data.

The centrifuge hydraulic motor bypass valve was preset for the maximum desired angular velocity. The maximum angular velocity was chosen to exceed the lateral stability of the complete barrier so that continuous layer-to-layer screen breakdown could be observed. The high maximum ω presetting on hydraulic motor power resulted in more rapid centrifuge acceleration α . Consequently, the multiple-screen barrier performance was influenced by $d\omega/dt$, both as α , which was minor, and ω , which was major.

The camera was initiated at centrifuge start so that film data of the barrier breakdown characteristics during transient lateral acceleration (t_T) to ω_{\max} and steady lateral acceleration (t_S) at ω_{\max} were obtained. Data were taken until 100 ft of film had been run at 64 frames per second (about 60 s). The data obtained are tabulated.

Weave	Run	ω_{\max} , rpm	t_T , s	t_S , s
180 x 180	17	10	15	52
325 x 2300	20	42	18	24

5. Test Results

The results of the bubble point tests and the lateral stability tests on the multiple-screen barriers provided (1) substantiation of earlier experimental findings, (2) the basic data from which a preliminary empirical model was formulated for predicting gas penetration transients through several layers of specific screen materials, and (3) the definition of parameters that require additional investigation to determine or clarify effects. The test data and analyses derived from the model experiments are presented as bubble point test results and lateral stability test results. The multiple-screen barrier performance and generalized model are analyzed and discussed under analysis of multiple-screen performance characteristics. The application of the empirical performance model is demonstrated and the implications of the solutions are discussed through a sample calculation. The conclusions derived from the multiple-screen performance tests are presented.

a. Bubble Point Test Results - The data obtained from the bubble point testing of the multiple-screen model provided substantiation for the bubble point performance of multiple-screen barriers measured in the earlier testing on another model (Volume III). The bubble point performance of the model formed the foundation for the correlation and analysis of the lateral stability test results.

Table IV-3 summarizes the bubble point test data, which have been corrected for the effect of the hydrostatic pressure produced by the methanol cover. The breakdown characteristics of the micropore Dutch-twill weave screens under the transverse pressure differences of bubble point testing were found to be essentially monotonic, smooth, and repeatable, as shown in Fig. IV-7. On the contrary, the bubble point breakdown of the plain square weave screens often proceeded erratically, unpredictably, and on a massive scale with the breakdown occurring suddenly and for short duration over an area of hundreds of contiguous pores. One such bubble point test of the square weave material is illustrated in Fig. IV-8. The cause of the disparity in bubble point behavior between the multiple-layer Dutch-twill screens and the multiple-layer square weave screens cannot be determined as a consequence of pore size, pore geometry, or the more general screen weave geometry from the limited testing done with the model. However, it may be germane to recall that, in addition to the larger pore size of the 180 x 180-mesh screen, square weave screens have been found not to wick liquid while the Dutch-twill weave screens exhibit good wicking properties. It is felt that the difference in observed performance was due to these differences in wicking characteristics.

Table IV-3 Multiple-Screen Bubble Point Data

Material	Test	Bubble Point, cm H ₂ O (in. H ₂ O)			
		Orientation	Screen 1	Screen 2	Screen 3
325 x 2300 Dutch Twill	1	Original	59.9 (23.6)	118.4 (46.6)	179.3 (70.6)
	2	Original	61.0 (24.0)	110.5 (43.5)	176.5 (69.5)
	3	Original	61.0 (24.0)	103.0 (42.5)	174.0 (68.5)
	4	Original	61.0 (24.0)	105.4 (41.5)	174.0 (68.5)
	5	Inverted	66.0 (26.0)	113.0 (44.5)	163.8 (64.5)
	6	Inverted	65.0 (25.6)	115.6 (45.5)	166.4 (65.5)
	7	Inverted	64.8 (25.5)	115.6 (45.5)	168.9 (66.5)
	8	Inverted	65.0 (25.6)	113.0 (44.5)	163.8 (64.5)
200 x 1400 Dutch Twill	1	Original	41.7 (16.4)	73.4 (28.9)	102.6 (40.4)
	2	Original	40.9 (16.1)	73.7 (29.0)	102.9 (40.5)
	3	Original	40.6 (16.0)	72.4 (28.5)	100.3 (39.5)
	4	Original	40.9 (16.1)	78.7 (31.0)	108.0 (42.5)
	5	Inverted	40.6 (16.0)	71.1 (28.0)	102.9 (40.5)
	6	Inverted	39.4 (15.5)	71.1 (28.0)	102.9 (40.5)
	7	Inverted	42.2 (16.6)	72.4 (28.5)	102.9 (40.5)
	8	Inverted	40.9 (16.1)	71.1 (28.0)	100.3 (39.5)
180 x 180 Square Weave	1	Original	11.7 (4.6)	14.2 (5.6)	19.6 (7.7)
	2	Original	9.7 (3.8)	16.5 (6.3)	22.1 (8.7)
Note: Three-Screen stacks in methanol at 0.64-cm (1/4-in.) spacing.					

All layers of every screen material tested demonstrated the classical bubble point behavior over at least the initial portion of the developing breakdown transient. After the bubble point of any layer in a multiple-screen barrier is reached, the larger screen pores break down into regular bubble formation followed by detachment. This bubbling between screens elevates the liquid from that space to the cover liquid until the gas accumulation becomes so large that liquid communication with the superior screen is lost. Then the gas pressure in the space between the screen undergoing breakdown and the superior screen begins to rise and the outer (lower) screen resistance to gas penetration deteriorates, probably as the result of progressive dryout. It is this loss of resistance to gas penetration as the gas accumulates behind the outer screen layers that causes the nonadditive bubble point performance shown in Fig. IV-9.

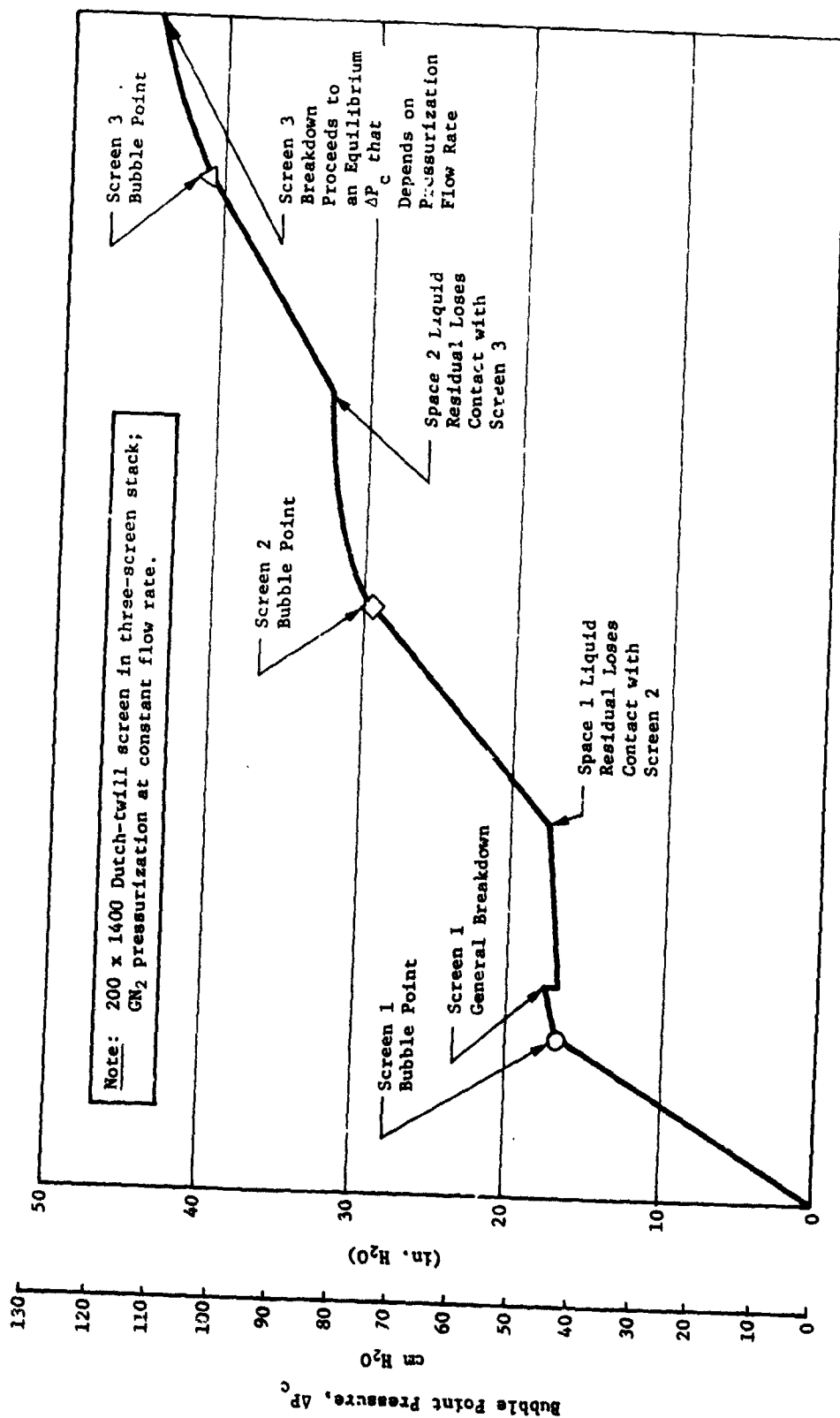


Fig. IV-7 Multiple-Screen Performance Model, Bubble Point Tests
of Typical Dutch-Twill Screen in Methanol

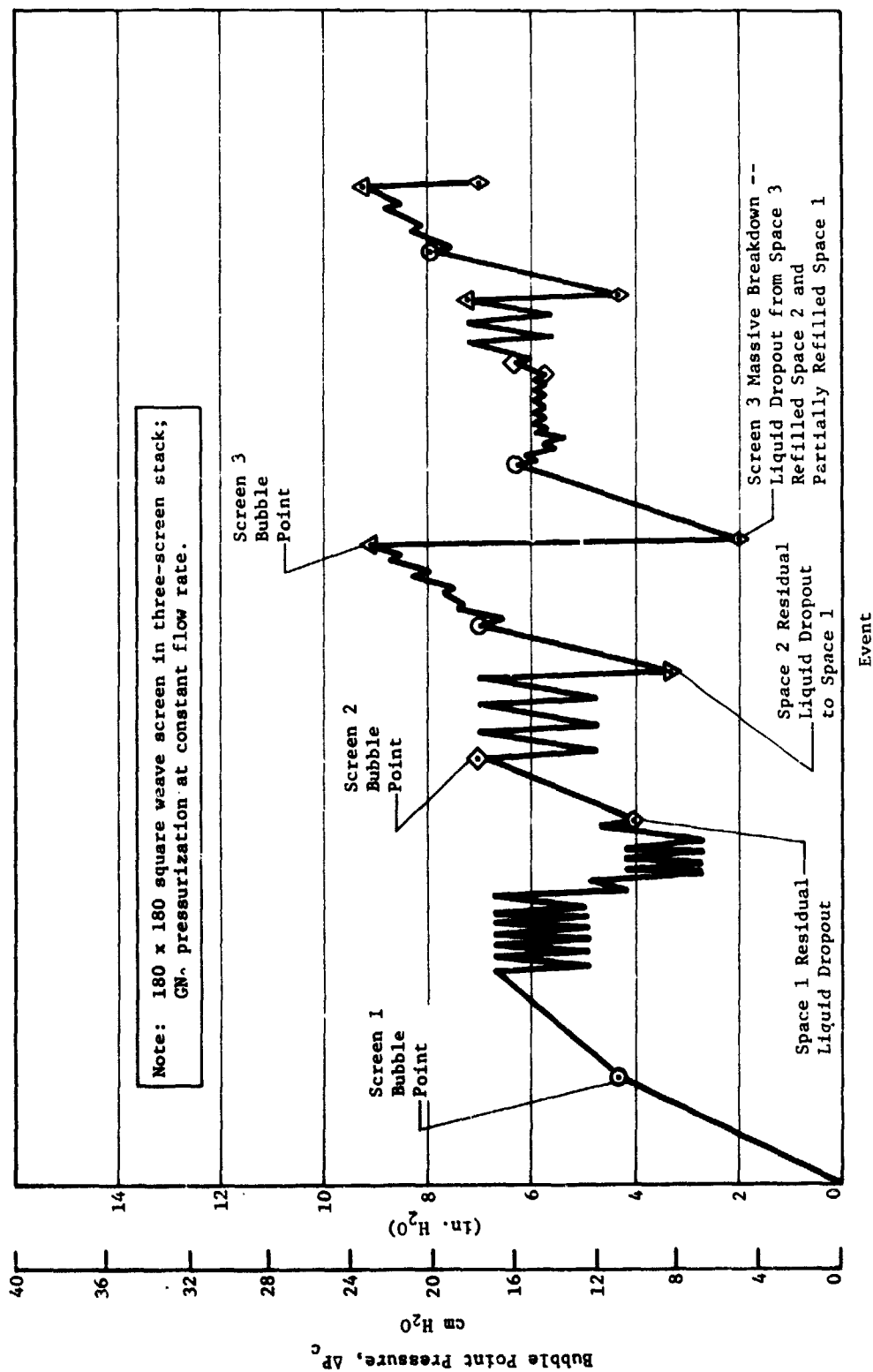


Fig. IV-3 Multiple-Screen Performance Model, Bubble Point Tests of Square Wave Screen in Methanol

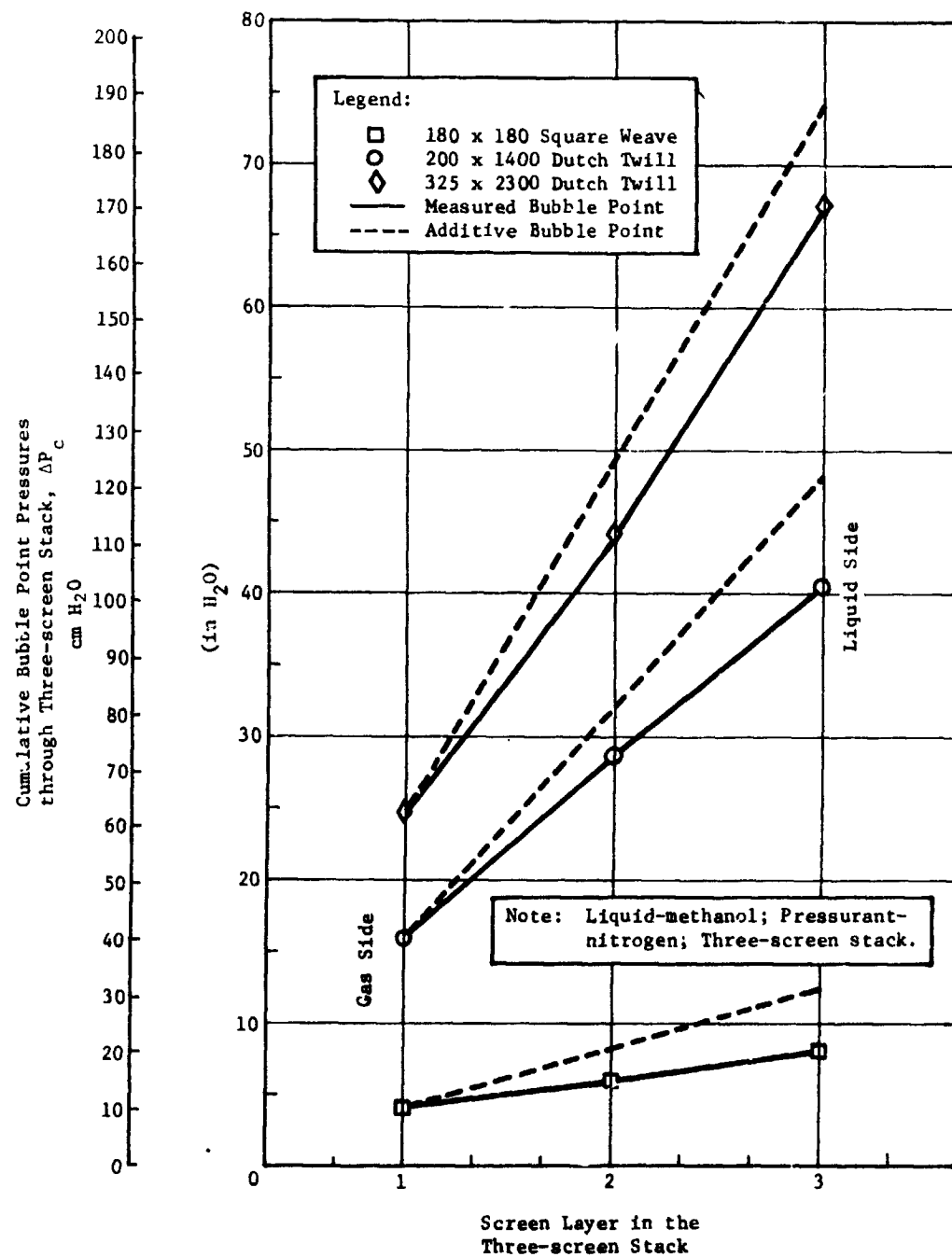


Fig. IV-9 Average Bubble Point Test Data

Although the individual bubble points for interior screens appear to be lower than expected, in reality each screen breaks down at its normal bubble point. The decreasing effectiveness of the outer layers to prevent gas penetration is the contributor to the less than ideal performance of multiple-screen barriers. Screen dryout characteristics could not be identified because of the difficulty of measuring gas penetration rates during multiple-screen bubble point transients. However, the measured bubble point deterioration (loss of screen effectiveness) through the multiple-screen barriers is tabulated in Table IV-4. These data agree well with the experimental results presented in Volume III as shown in Fig. IV-10.

Table IV-4 Properties and Deterioration of Bubble Point Effectiveness of the Multiple-Screen Barriers

Material	Nominal Bubble Point, cm H ₂ O (in. H ₂ O)	Approximate Effective Pore Diameter, cm (in.)	% Loss in Effective Bubble Point		
			Screen 1	Screen 2	Screen 3
325 x 2300 Dutch Twill	63.0 (24.8)	0.0015 (0.0006)	0	10.7	9.5
200 x 1400 Dutch Twill	40.9 (16.1)	0.0023 (0.0009)	0	10.9	16.1
180 x 180 Square Weave	10.7 (4.2)	0.0087 (0.0034)	0	28.0	35.0

b. Lateral Stability Test Results - The lateral stability tests, which were run over a range of accelerations, provided data on the behavior of the breakdown phenomena in multiple-screen barriers and correlations for the rate of gas penetration under supercritical lateral accelerations. Qualitative tests during centrifuge acceleration to high terminal conditions of lateral acceleration produced comprehensive information on the behavior of laterally unstable multiple-screen barriers over their entire breakdown regime. Quantitative tests of models that had been more gently accelerated to a constant lateral acceleration were the bases for the gas penetration data from which the empirical performance model was derived. The 20-run program, including test environments and barrier reactions, is summarized in Table IV-5.

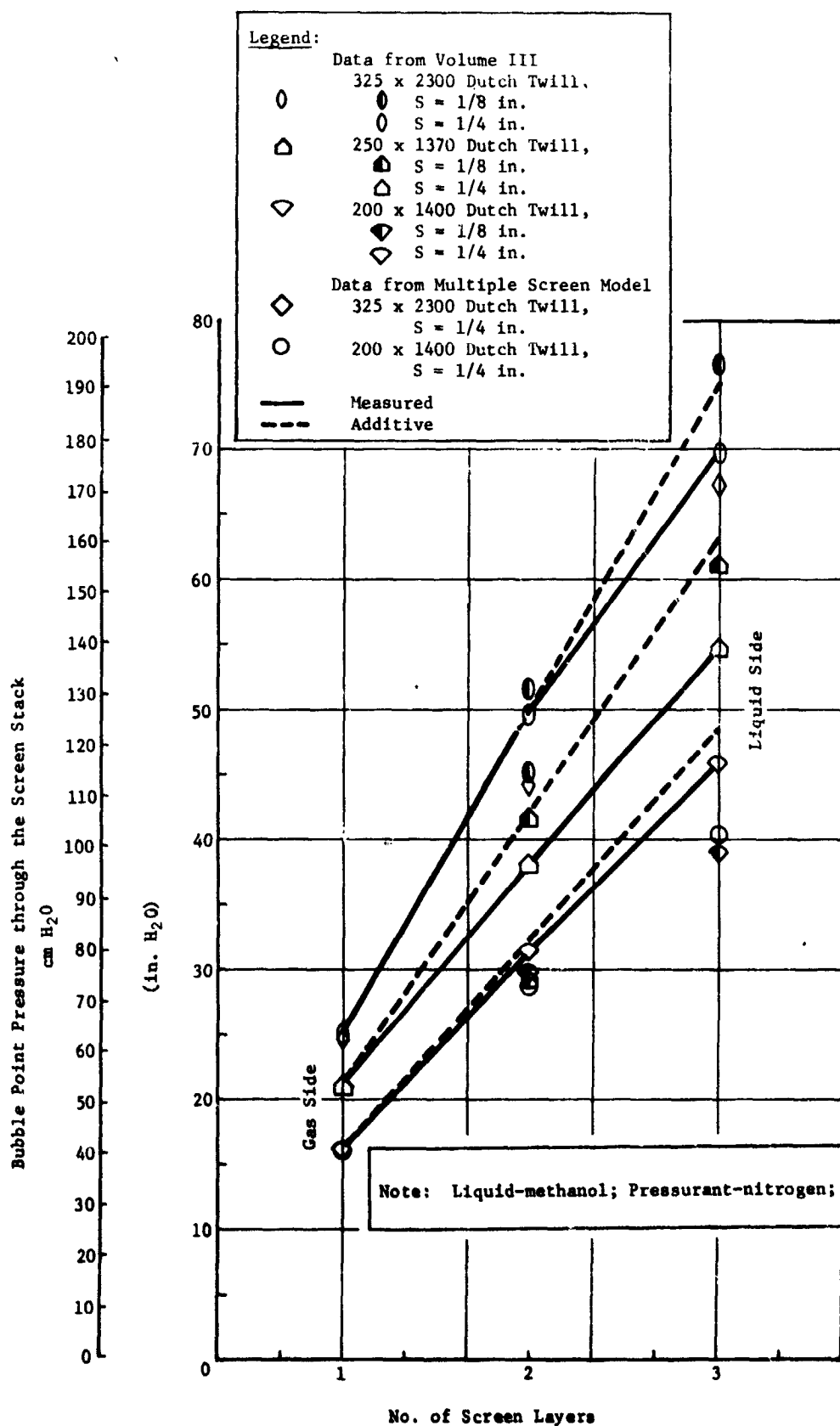


Fig. IV-10 Bubble Point Data From Multiple-Screen Tests

Table IV-5 Summary of Lateral Stability Testing of the Multiple-Screen Model

Material	Lateral Acceleration, g	Screen and Condition*			Run
		1	2	3	
325 x 2300 Dutch Twill	3.34	S	S	S	6
	3.52	B	S	S	11
	4.03	B	S	S	18
	5.23	B	S	S	7
	7.03	B	B	S	19
	8.24	B	B	B	8
	9.79	B	B	B	9
	0 to 11.08	B	B	B	20
	11.11	B	B	B	10
200 x 1400 Dutch Twill	2.20	S	S	S	1
	3.51	B	B	S	2
	5.43	B	B	B	3
	6.16	B	B	B	4
	7.09	B	B	B	5
180 x 180 Square Weave	0 to 0.28	S	S	S	16
	0.44	B	B	S	13
	0.45	B	B	S	12
	0 to 0.65	B	B	B	17
	0 to 0.74	B	B	B	14
	1.22	B	B	B	15
* B - Screen layer suffered breakdown during run. S - Screen layer was stable during run.					

The data analysis was based on the multiple-screen barrier performance characteristics depicted by the movie films and the corresponding lateral acceleration environment produced by the centrifuge. The resistance to gas penetration offered by each screen layer was computed, assuming dynamic equilibrium (acceleration body forces are small) from the measurement of the liquid column height supported behind the screen

$$\Delta P_c = \rho(a) \Delta h.$$

The rate of gas ingestion through each screen was estimated from the movie film by measuring the retreat of the liquid in the space between screens as a function of time.

Comparison of the ΔP_c with the bubble point data showed that initial breakdown of each screen in the barrier occurs at its individual bubble point. Then the resistance to gas penetration decays after initial breakdown in a process similar to that observed in the bubble point testing. Typical stress buildup, interface rupture, and resistance decay to gas penetration through multiple-screen barriers under increasing lateral acceleration are plotted for 325 x 2300 Dutch-twill in Fig. IV-11 and for 180 x 180 square weave screen in Fig. IV-12.

Gas penetration characteristics for the 325 x 2300 Dutch-twill multiple-screen barrier are shown in Fig. IV-13. For the 180 x 180 square weave multiple-screen barrier under increasing lateral acceleration, the gas penetration is shown as a function of time in Fig. IV-14. The breakdown behavior observed for the multiple-screen barriers subjected to supercritical lateral accelerations was similar to the breakdown mode of the same barrier under bubble point pressures. The Dutch-twill screens underwent smooth, controlled transition during lateral stability breakdown. The square weave multiple-screen barrier breakdown would shift from smooth gas penetration to sudden, total dropout of the liquid between screens. Erratic, unstable gas penetration on a massive scale was observed for the final square weave screen layer, located next to the bulk liquid and simulating the expulsion channel. After all of the gas accumulation rate data had been reduced as gas penetration flux over the exposed screen area, \dot{q}_g/A , a good correlation was obtained with time after breakdown t for each of the screens in the multiple-screen barriers, with the exception of the innermost (last) screen of the 180 x 180 square weave barrier. These gas penetration flux correlations, plotted in Fig. IV-15 thru IV-21, were essentially independent of the influence of lateral acceleration level, a/a_{cr}^* . Consequently, curve fits of the form

*The critical acceleration for any layer of screen n , is de-

finied on the basis of additive bubble points, $a_{cr} = \frac{\sum_{n=1}^N (\Delta P_c)_n}{\rho L}$.

Then the critical lateral acceleration ratio, $\frac{a}{a_{cr}}$, is the imposed acceleration divided by the critical acceleration.

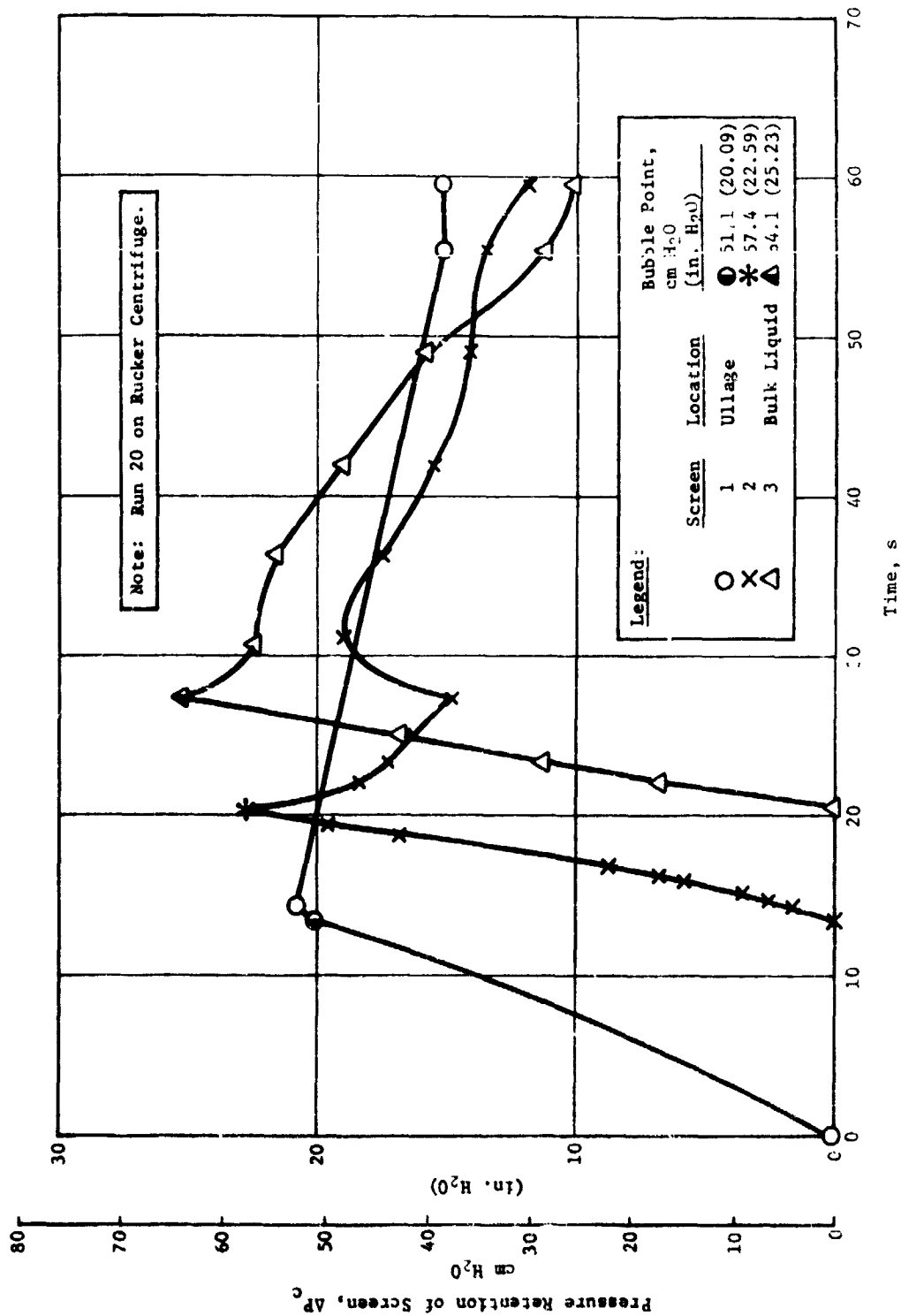


Fig. 11-11 Apparent Pressure Retention Performance of the Multiple 815. 5500
Lateral Acceleration

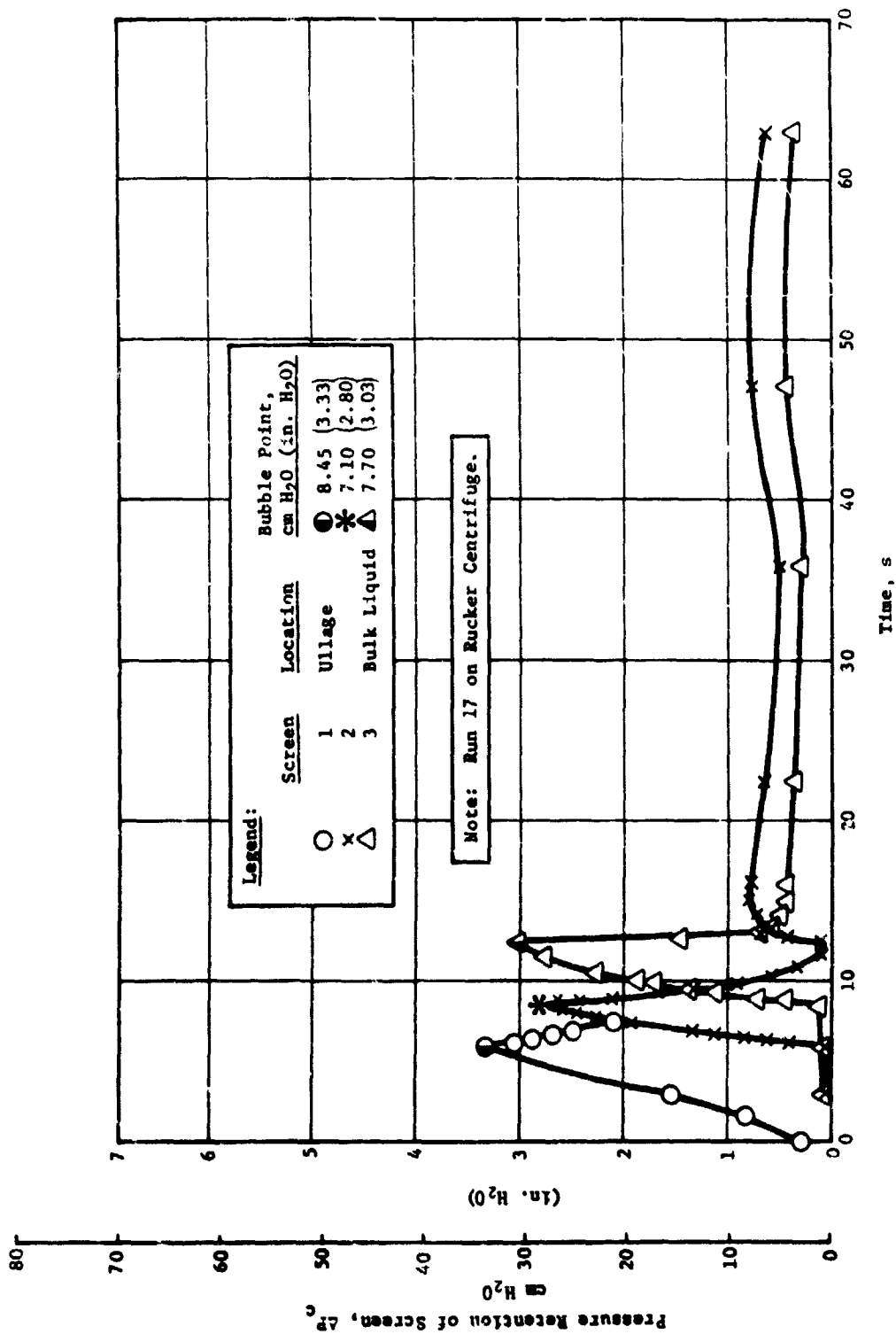


Fig. IV-12 Apparent Pressure Retention Performance of the Multiple 180 x 180 Square Wave Screen Barriers under Lateral Acceleration

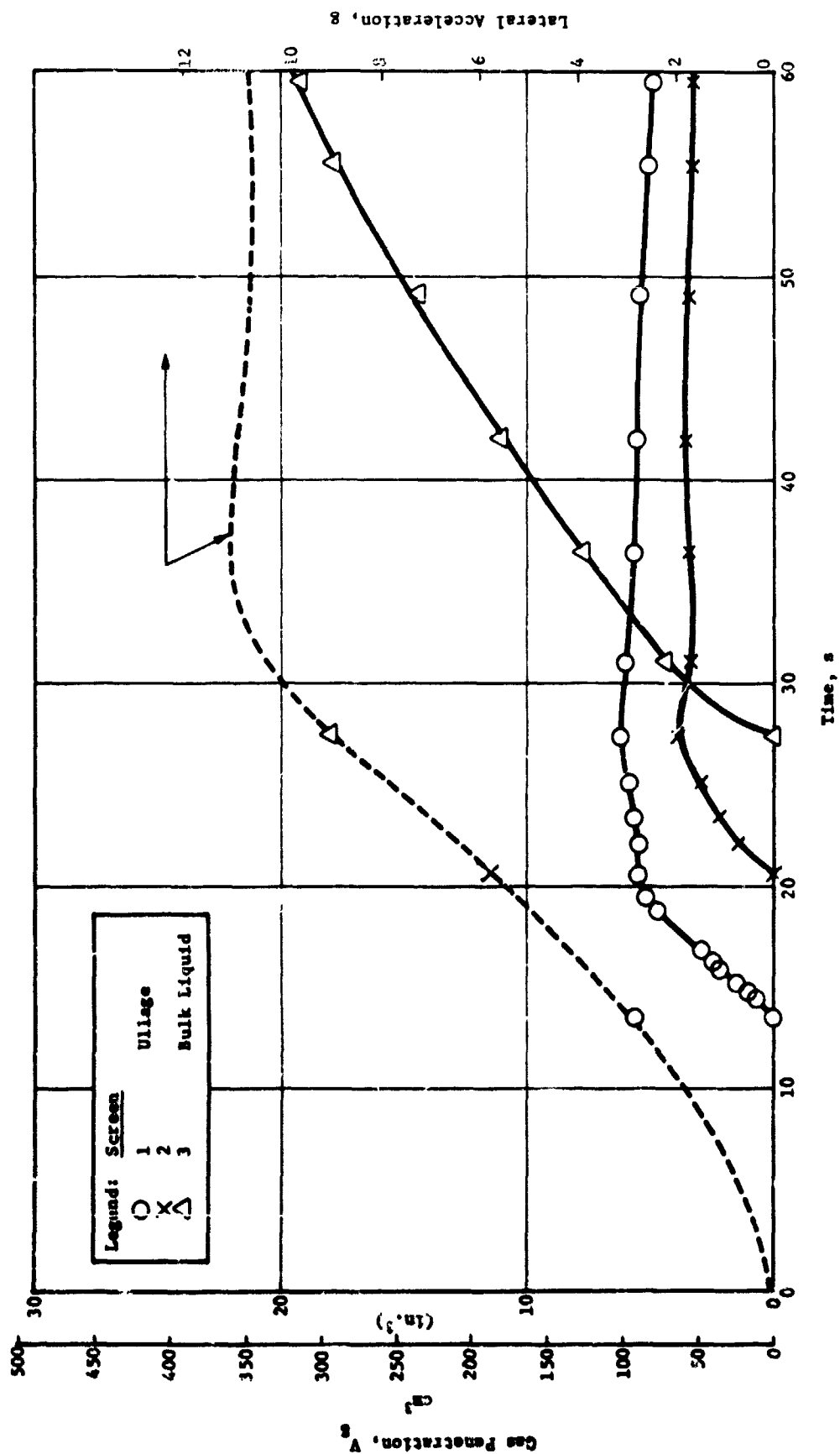


Figure IV-13 Gas Penetration vs. Time, 325 \pm 2300 Dutch Twill (Run 20)

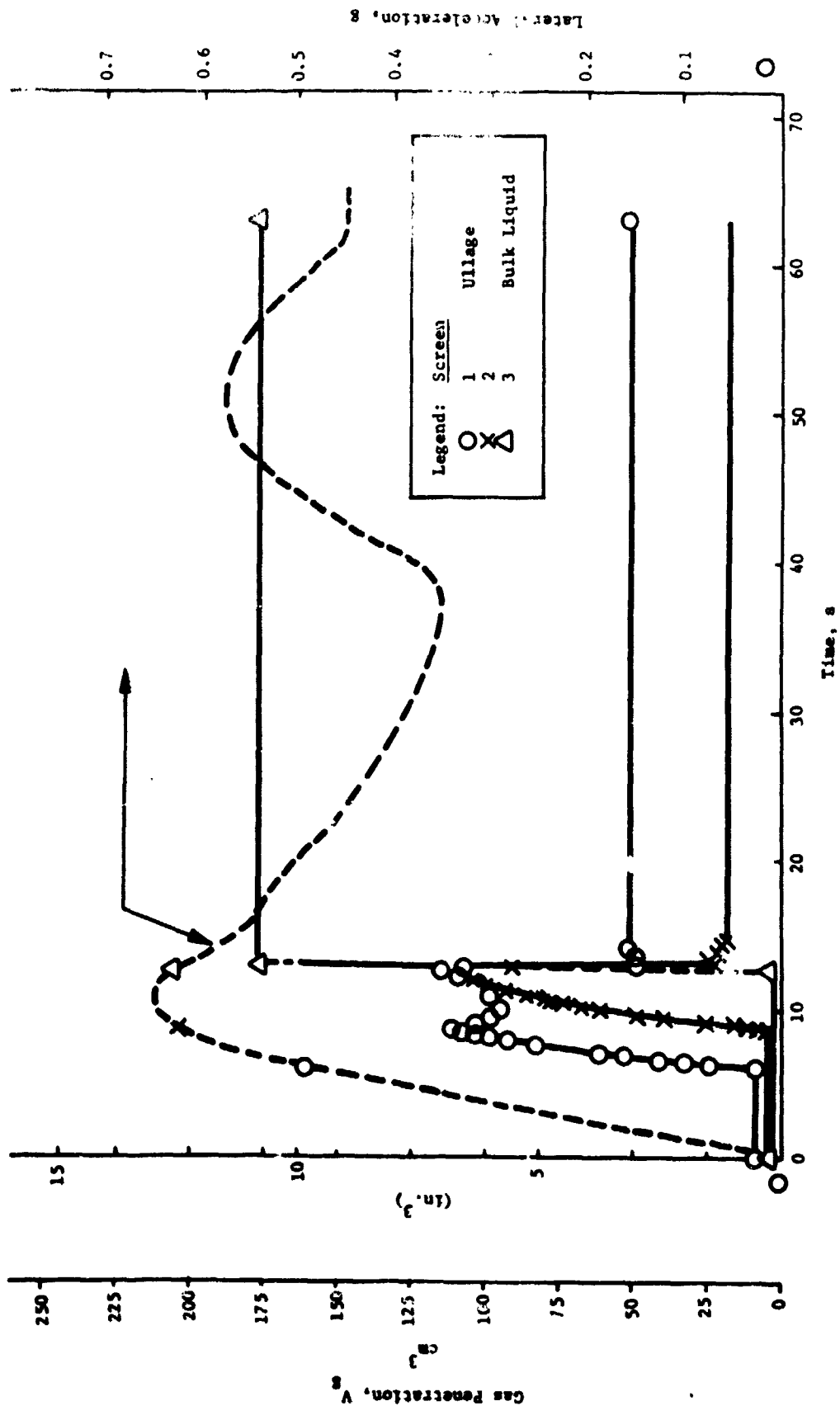


Fig. IV-14 Gas Penetration vs. Time, 180 \pm 180 Square Wave (Run 17)

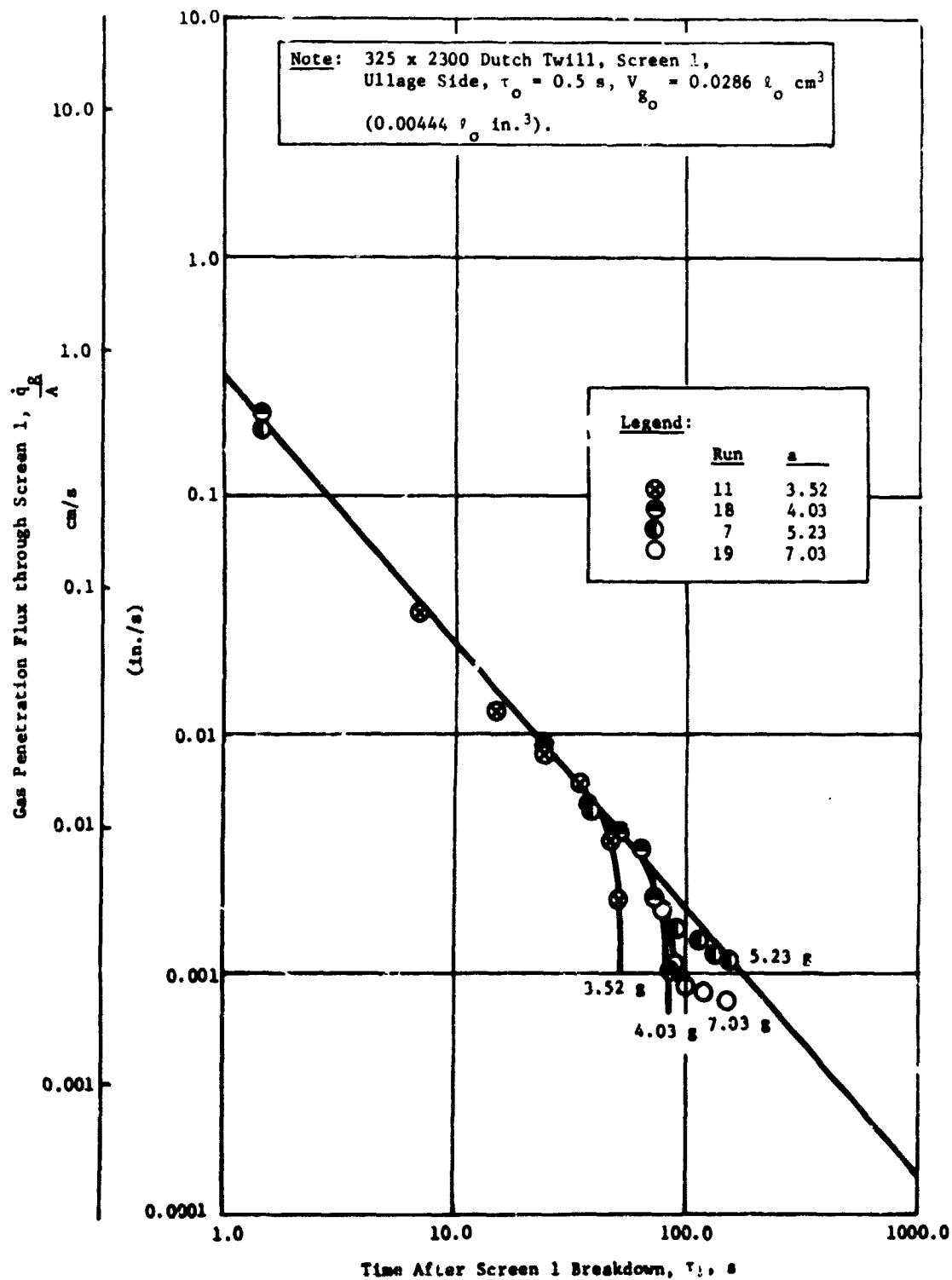


Fig. IV-15 Gas Penetration Flux vs Time (Screen 1)

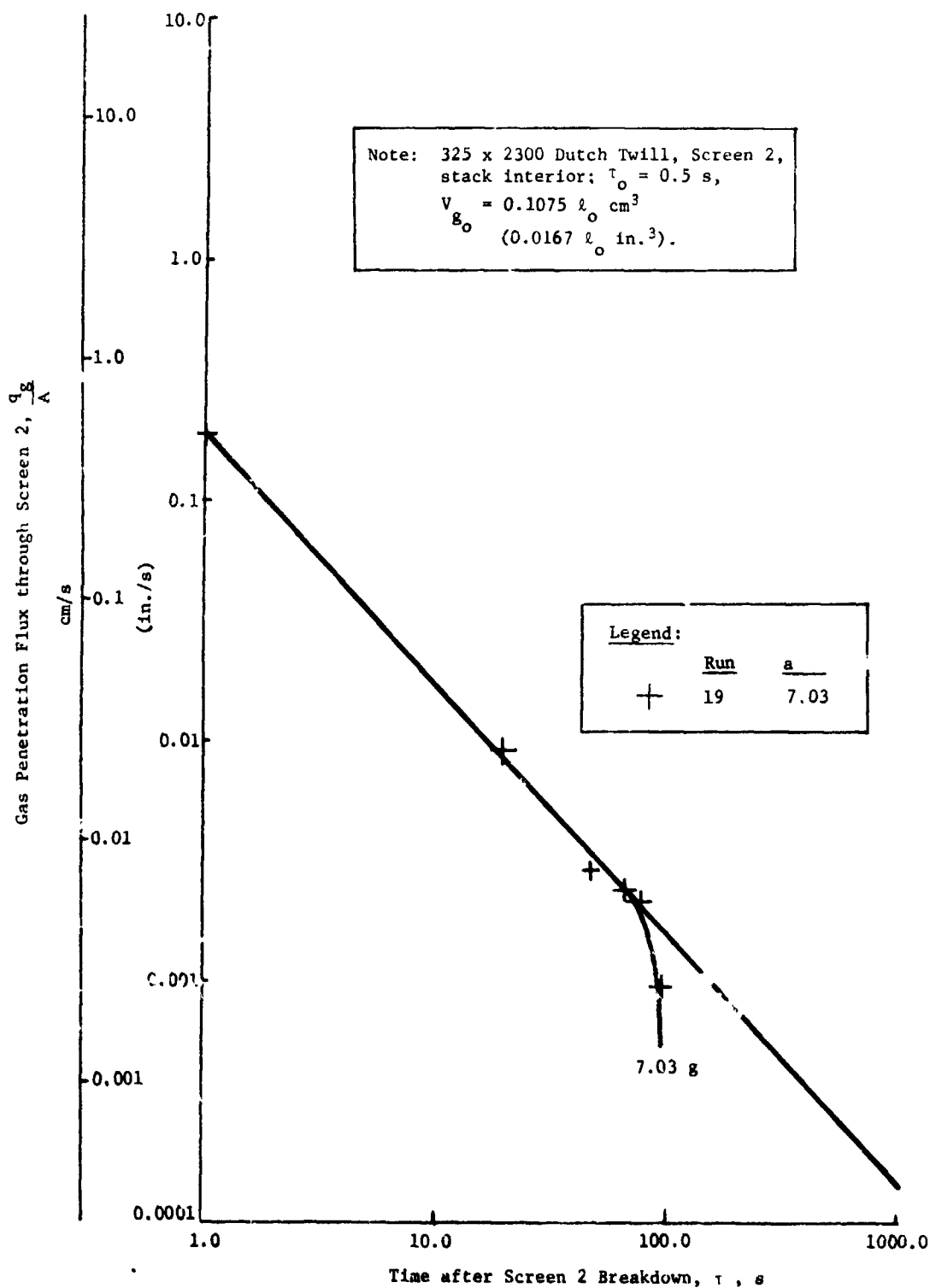


Fig. IV-16 Gas Penetration Flux vs Time (Screen 2)

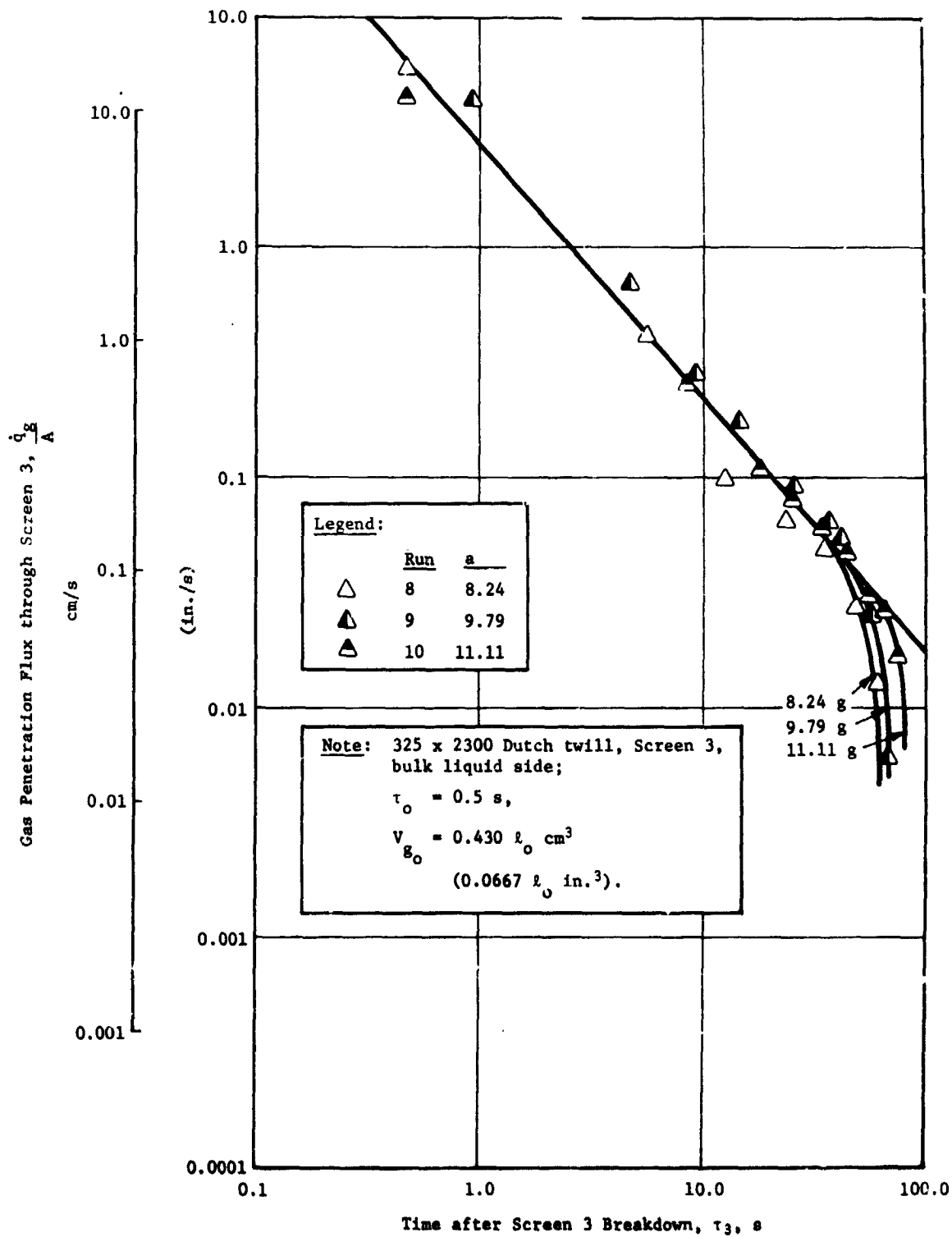


Fig. IV-17 Gas Penetration Flux vs Time (Screen 3)

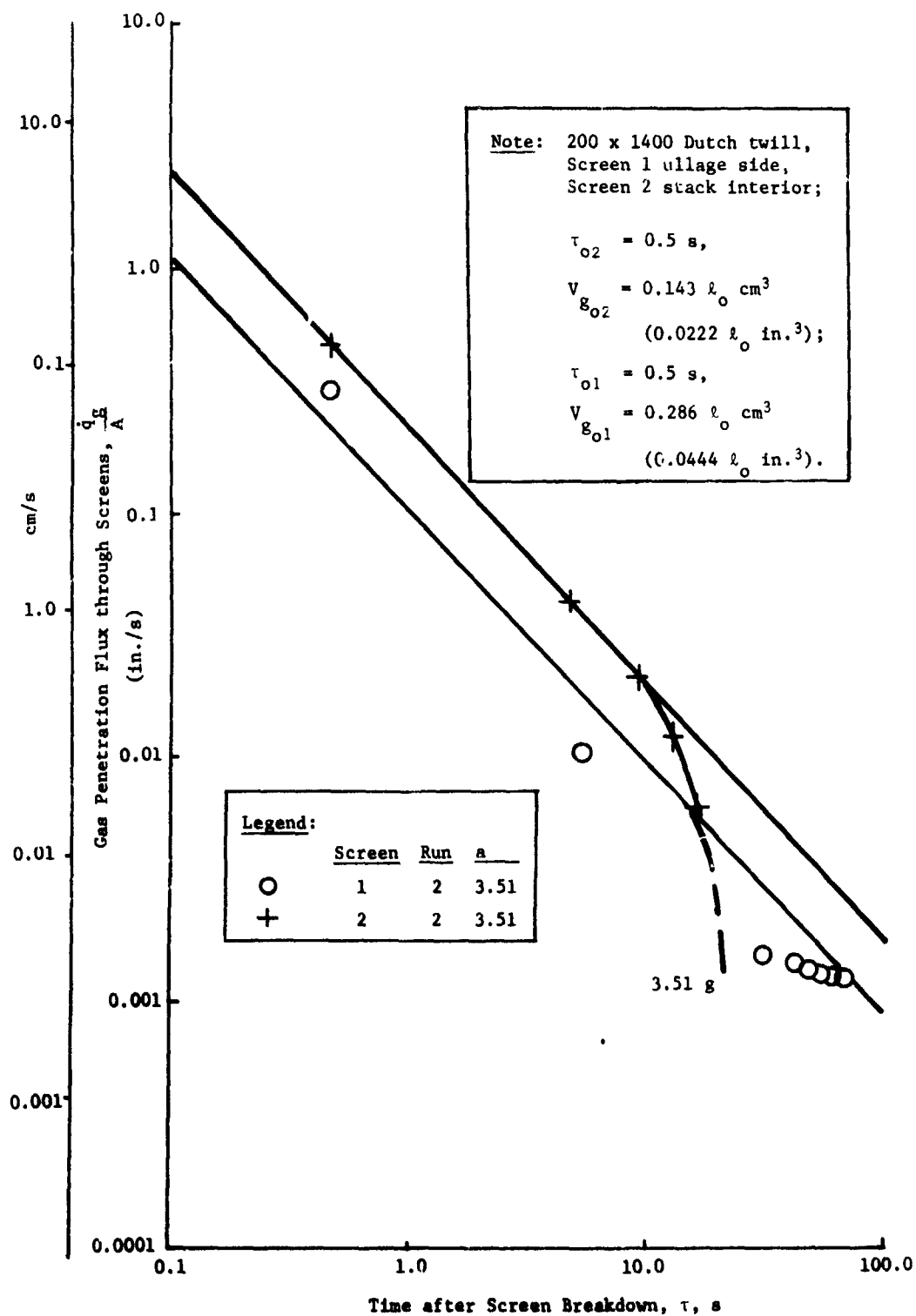


Fig. IV-18 Gas Penetration Flux vs Time (Screens 1&2)

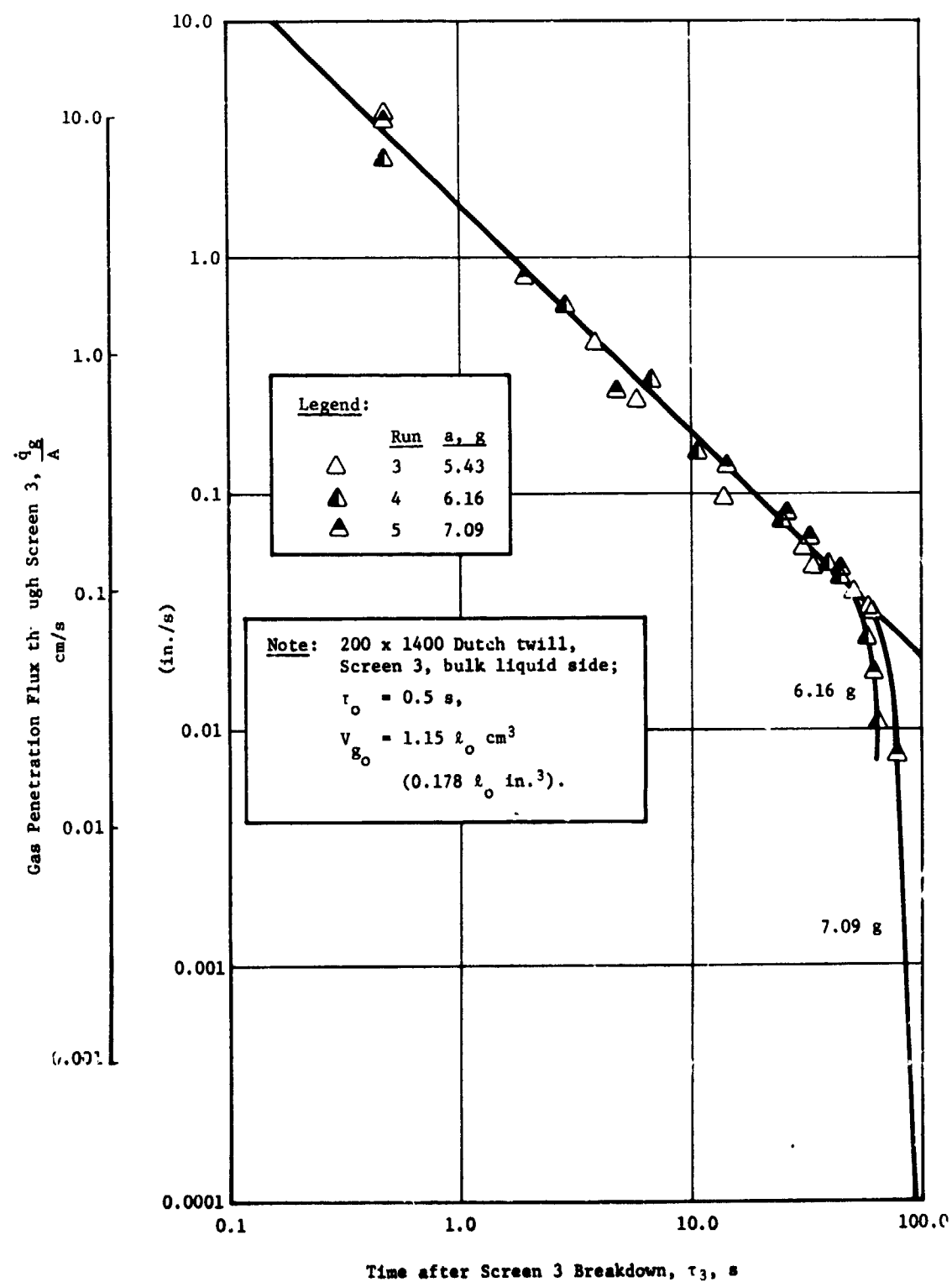


Fig. IV-19 Gas Penetration Flux vs Time (Screen 3)

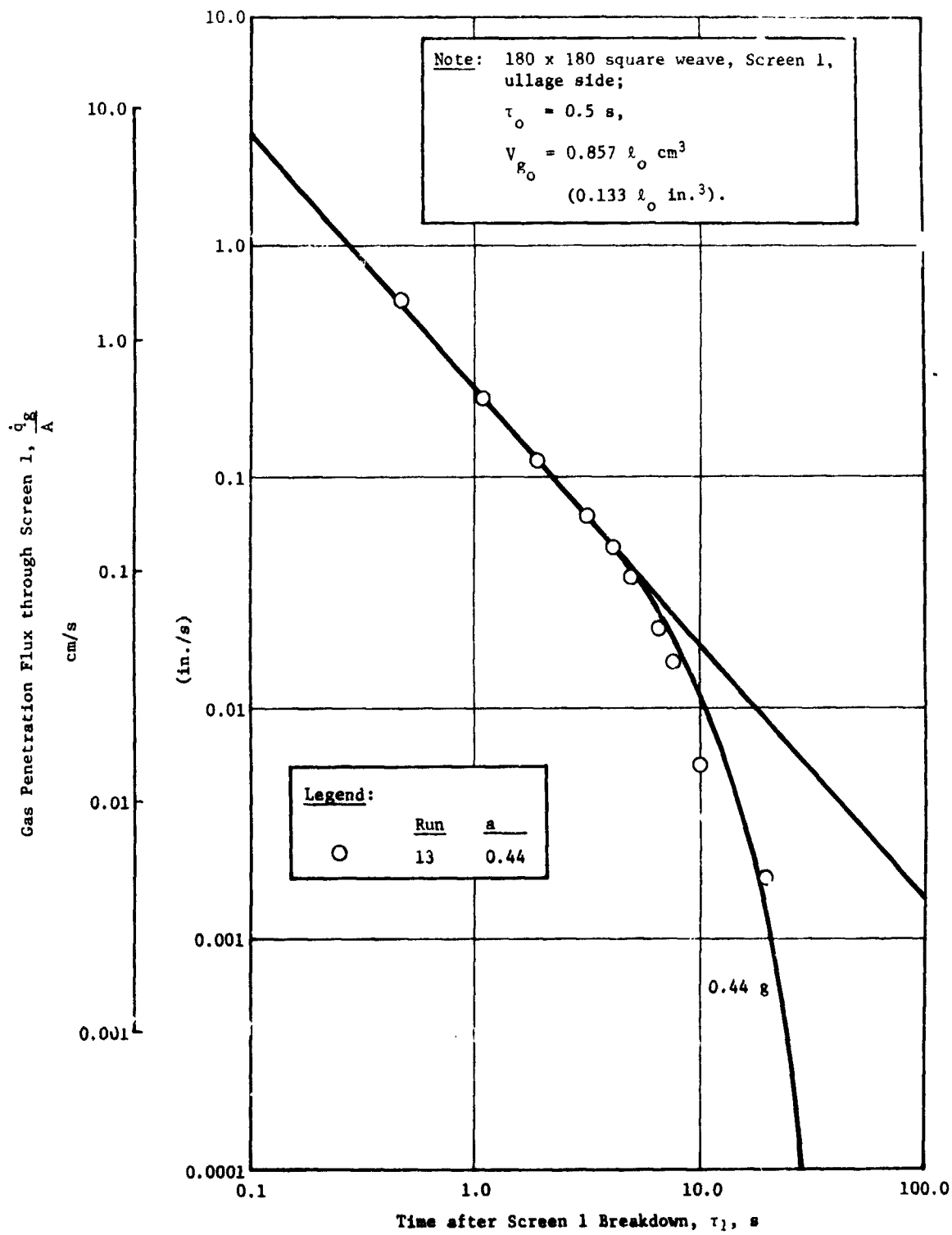


Fig. IV-20 Gas Penetration Flux vs Time (Screen 1)

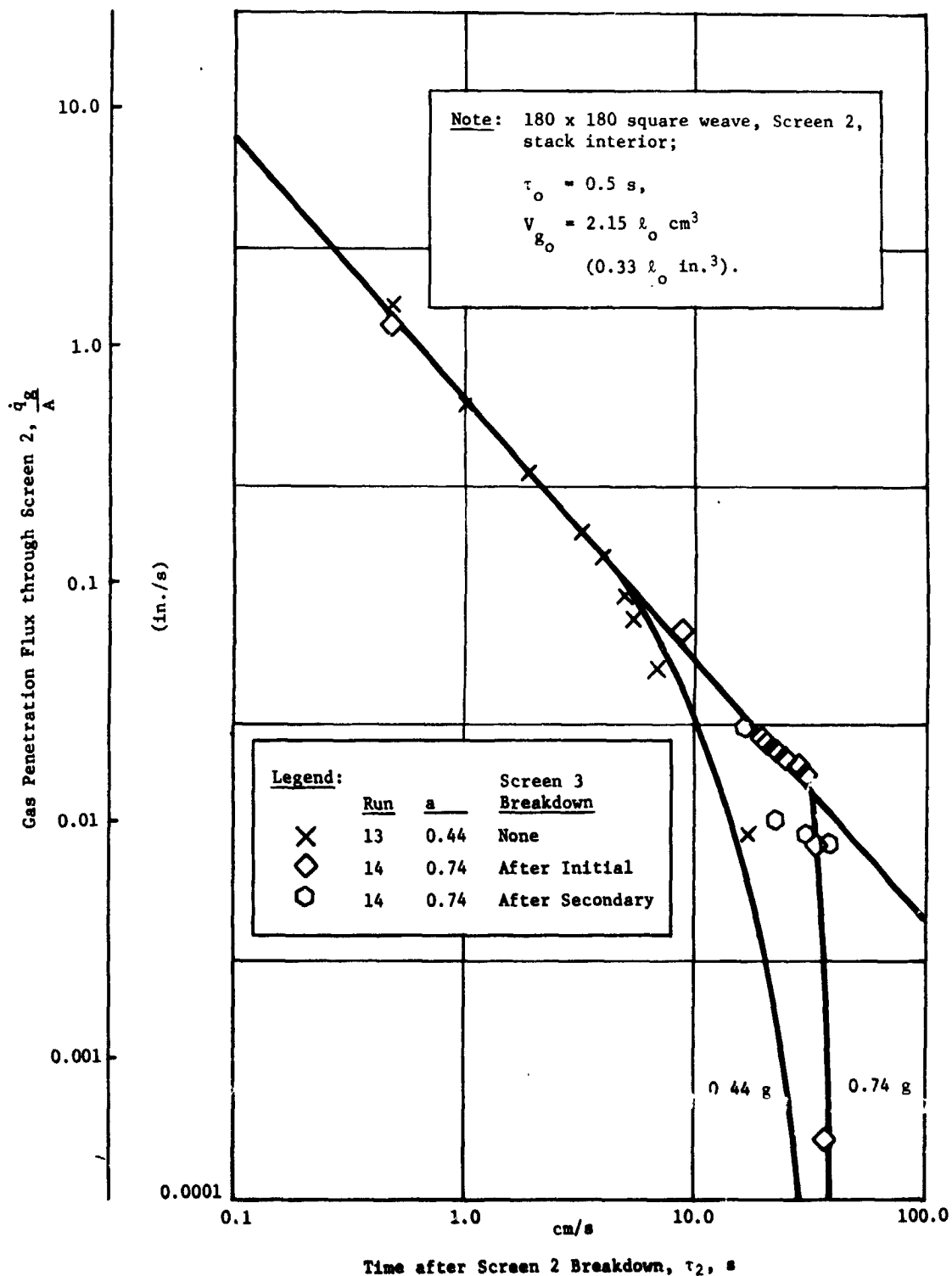


Fig. IV-21 Gas Penetration Flux vs Time (Screen 2)

$$\frac{\dot{q}_g}{A} = \frac{k_n}{\tau_n \gamma_n}$$

represent the generalized gas accumulation behind the nth screen for draining, which is unimpeded by the liquid column proximity to its steady-state height. This steady-state height is based on the residual ΔP_c of the exposed screen and k_n and γ_n are constants for the nth screen. As the gas accumulation volume approaches the steady-state position, the gas penetration flux departs from the universal characteristic and approaches zero.

With the mathematical expression available for the rate at which gas accrues during screen breakdown, it was necessary to determine the magnitude of the gas ingestion during initial breakdown, $V_{g_o}|_n$. Then a simple, empirical formula for multiple-screen barrier performance, such as

$$V_{g_n} = V_{g_o}|_n \left\{ f(\tau) \right\}_n$$

could represent the general gas accumulation through the nth screen under a supercritical lateral acceleration. From the original data for V_{g_n} versus τ_n , a dependence

$$V_{g_o}|_n = v_n \left(\frac{a}{a_{cr}} \right)$$

can be inferred. However, the limited amount of lateral stability testing and the relatively short (60-s) data acquisition period prevented identification of the form of this function from data correlation. Specific tests do provide values for initial gas ingestion, which are generalized to the expression

$$V_{g_o}|_n = C_n \ell_n @ \tau_o|_n$$

These observed values were acquired near $a/a_{cr} \sim 1$ and have been assimilated with the gas penetration flux constants in Table IV-6 to provide a quantitative, basic multiple-screen performance model in terms of breakdown transient duration.

Table IV-6 Constants for Gas Penetration Analysis through Multiple-Layer Screens, Basic Model

Screen	Layer, n	Location	τ_o , s	C_n , cm ² (in. ²)	k_n	γ_n
325 x 2300 Dutch Twill	1	Ullage	0.5	0.0287 (0.00444)	0.320	1.110
	2	Stack Interior	0.5	0.1077 (0.0167)	0.190	1.044
	3	N-Bulk Liquid	0.5	0.4303 (0.0667)	3.00	1.111
200 x 1400 Dutch Twill	1	Ullage	0.5	0.2865 (0.0444)	0.110	1.048
	2	Stack Interior	0.5	0.1432 (0.0222)	0.240	1.062
	3	N-Bulk Liquid	0.5	1.148 (0.178)	1.70	0.9647
180 x 180 Square Weave	1	Ullage	0.5	0.858 (0.133)	0.255	1.115
	2	Stack Interior	0.5	0.858 (0.133)	0.245	1.107
	3	N-Bulk Liquid	0.5	--	--	--
<p><u>Note:</u> $V_{g_o} = C_n \ell_o$, cm³ (in.³);</p> <p>$\frac{\dot{q}}{A} = (\text{in.}/\text{s})$, $\tau = \text{s}$;</p> <p>$V_{g_n} = \text{cm}^3 (\text{in.}^3)$.</p>						

A small sample of initial gas ingestion data was correlated in Fig. IV-22 to provide some definition of the magnitude of the a/a_{cr} influence. This analysis suggests that the effect of a/a_{cr} on $V_{g_o|n}$ may be about first order. Assuming a first-order relationship, the basic model was modified to include the effect of the lateral acceleration ratio

$$V_{g_n|n} = C_{n_o} \left(\frac{a}{a_{cr}} \right)_n \ell_o.$$

Gas penetration flux constants and initial conditions for this generalized relationship are listed in Table IV-7.

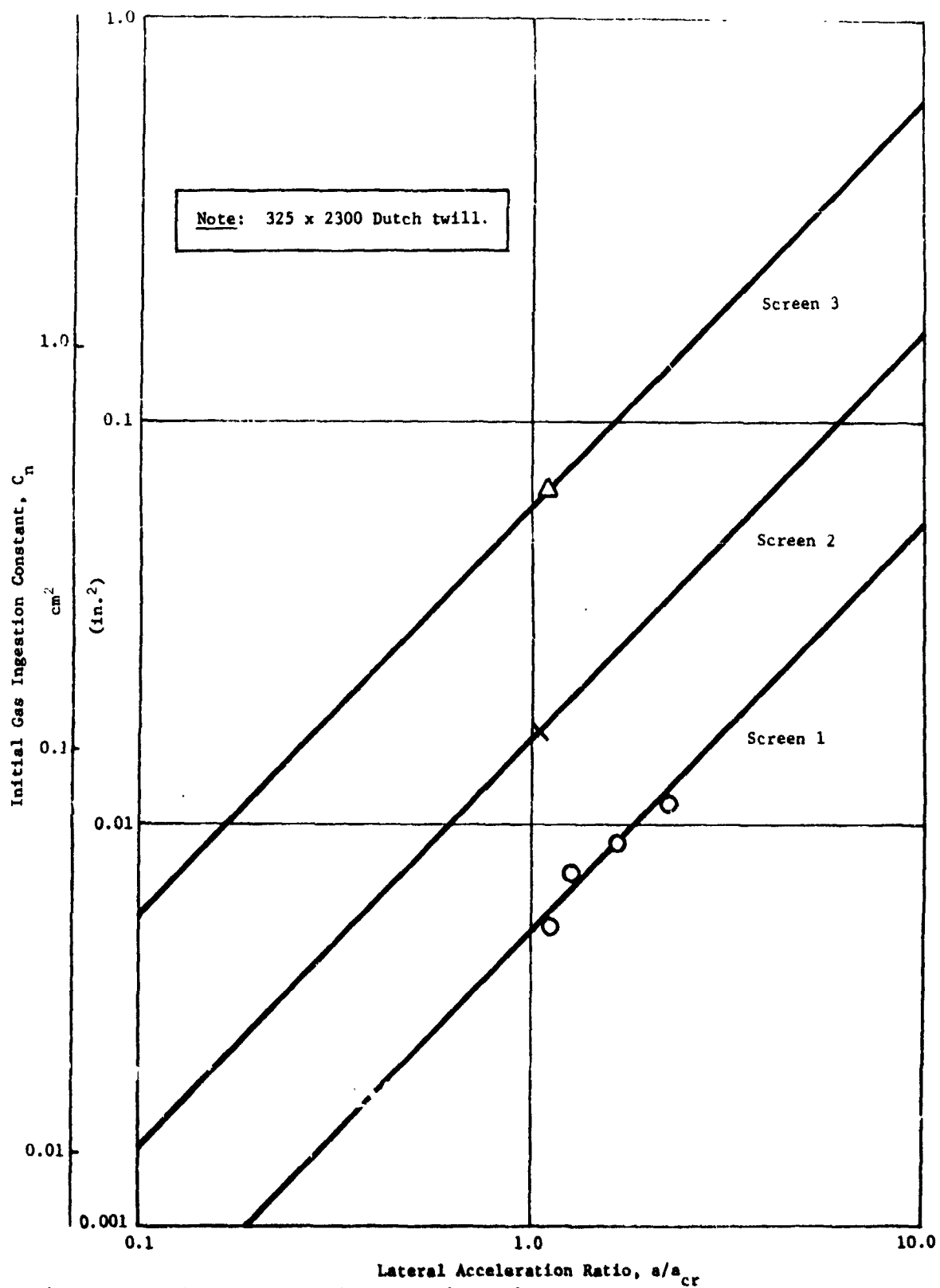


Fig. IV-22 Influence of Lateral Acceleration Ratio on Initial Gas Ingestion Constant

Table IV-7 Constants for Gas Penetration Analysis through Multiple-Layer Screens for Generalized Relationship

Screen	Layer, n	Location	τ_o, s	$C_{n_o}, cm^2 (in.^2)$	k_n	γ_n
325 x 2300 Dutch Twill	1	Ullage	0.5	0.0348 (0.0054)	0.320	1.110
	2	Stack Interior	0.5	0.103 (0.016)	0.190	1.044
	3	N-Bulk Liquid	0.5	0.387 (0.060)	3.00	1.111
200 x 1400 Dutch Twill	1	Ullage	0.5	0.1852 (0.0287)	0.110	1.048
	2	Stack Interior	0.5	0.168 (0.026)	0.240	1.062
	3	N-Bulk Liquid	0.5	1.368 (0.212)	1.70	0.9647
180 x 180 Square Weave	1	Ullage	0.5	0.897 (0.139)	0.255	1.115
	2	Stack Interior	0.5	1.697 (0.263)	0.245	1.107
	3	N-Bulk Liquid	0.5	~40.0 (~6.2)	--	--

Note: $C_n = C_{n_o} \left(\frac{a}{a_{cr}} \right), cm^2 (in.^2);$

$V_{g_o} = C_{n_o} \tau_o, cm^3 (in.^3);$

$\frac{\dot{q}}{A} = (in./s), \tau = s;$

$V_{g_n} = cm^3 (in.^3).$

c. *Analysis of Multiple-Screen Performance Characteristics* - The nearly uniform transverse pressure differences investigated by bubble point testing are developed across multiple-screen barriers during the expulsion operation of a capillary device. However, the effects of hydrostatic pressure gradients along a multiple-screen barrier, which were observed in the lateral stability tests, occur as the result of any dynamic activity on the vehicle. Lateral accelerations can be generated by extraneous forces, boost operation, RCS operation, or OVL maneuvers during either the acquisition or expulsion phases. The bubble point performance of a multiple-screen barrier, measured on any model, is directly applicable to any capillary device using a similar barrier, regardless of scale. By contrast, the lateral stability performance of a prototype capillary device must be scaled from a geometrically and dynamically similar model.

The general characteristics of multiple-screen barrier breakdown under the uniform transverse pressure differences of bubble point tests and under the hydrostatic pressure gradient of lateral stability tests are compared and discussed in Table IV-8.

Table IV-8 Comparison between Breakdown Characteristics for Bubble Point Tests and Lateral Stability Tests

Bubble Point	Lateral Stability
1. Screen 1 breaks down at predicted bubble point, ΔP_{c1}	Screen 1 breaks down at predicted ΔP_{c1} = bubble point.
2. Space 12* empties, but the residual liquid spreads more easily under normal-g. The liquid is displaced from space 12 into the bulk compartment above.	Space 12 starts to empty, but wicking is inhibited by adverse α (both maximum wicking height and wicking flow rate). Space 12 drains to ullage compartment.
3. As space 12 pressure rises toward the ullage pressure less the capillary barrier loss, the pore breakdown (or dryout) due to gas penetration reduces the pressure retention capability of Screen 1 so Screen 2 breaks down at $(P_u - P_a) < 2 \Delta P_{c1}$, depending on the supply of residual liquid in space 12 and its wicking capability. This causes a loss in the apparent ΔP_{c2} for Screen 2. Screen 2 proceeds to break down in the same manner as Screen 1.	As space 12 continues to drain, the increased wicking path allows more and more pores to break down (dry out) so the pressure retention of Screen 1 is continuously reduced toward 0. When the exposed length of Screen 2 reaches its critical height based on bubble point ΔP_{c2} , it breaks down in the same manner as Screen 1.
4. Screen 3 has by this time a larger stable volume of liquid with no superior support so its bubble point suffers only normal drop at breakthrough without dryout deterioration. However, the deterioration of ΔP_{c1} and ΔP_{c2} results in an apparent loss $P_u - P_a < 3 \Delta P_{c1}$.	Screen 3 breaks down in the same manner as Screens 1 and 2 but the deterioration transient is slowed by the larger liquid volume in the bulk compartment to be displaced.
*Denotes the space between Screen 1 and Screen 2.	

Although analogies hold between both breakdown modes, which start at the outer screen and proceed continuously through the stack to the expulsion liquid behind the last screen, characteristic differences should also be noted. The general breakdown under transverse pressure differences is uniformly distributed over the entire screen surface exposed to the gas, and the breakdown of the outer screen is complete before the bubble point of the next screen is reached. The breakdown of a multiple-screen barrier under a hydrostatic pressure gradient, which is uniform across the stack, is initiated at the location of minimum static pressure in the liquid of the outer space and expands over an increasing area of the screen as it is exposed by the retreating liquid in the gap. When the critical height is exposed on the next screen by the bubble formed due to gas penetrating the outer screen, the next screen breaks down despite the situation that the outer screen breakdown may be incomplete. The fact that similar capillary forces resist gas penetration during either mode of breakdown produces many of the analogous characteristics. The differences between the forcing functions causing the bubble point or lateral instabilities result in the characteristic variations.

An analytical model that will predict gas accumulation between the screens of any barrier, regardless of size, is needed. An empirical formula based on the results of the limited centrifuge testing of the multiple-screen test model was derived and provides order-of-magnitude solutions. This empirical formula is applicable only to barriers of constant width (normal to the lateral acceleration vector) because of the limitations imposed by similitude considerations. Complete modeling of a multiple-screen barrier requires that geometric similarity and dynamic similarity be preserved between the full-scale device and the subscale model. Maintaining absolute geometric similarity would entail the scaling of wire sizes and meshes of the capillary material, plus screen-to-screen spacing, in addition to the overall dimensions of the device and tank. Dynamic similarity requires that the ratios between the most influential forces be held constant from prototype to model, e g.,

$$\text{Bond Number (Bo)} = \frac{\text{acceleration forces}}{\text{capillary forces}} = \frac{\rho a L^2}{\sigma}$$

$$\text{Weber Number (We)} = \frac{\text{inertia forces}}{\text{capillary forces}} = \frac{\rho V^2 L}{\sigma}$$

$$\text{Reynolds Number (Re)} = \frac{\text{inertia forces}}{\text{viscous forces}} = \frac{\rho V L}{\mu}$$

Since the screen materials cannot be scaled, it was impossible to maintain geometric similarity. Consequently, a simple one-dimensional analysis, representing the gas accumulation between screens of a general multiple-screen barrier, was examined to formulate realistic scaling parameters for modeling full-scale devices. If the liquid draining is sufficiently slow so the differences in viscous flow losses may be neglected, the dynamics at homologous (similar geometrical) points in the model and full-scale device (prototype) are comparable at times related by

$$\tau = \sqrt{\frac{\beta_l}{\beta_{tl}}} \left(\frac{L_m}{L_p} \right) t$$

where

τ = scaled time or model time,

t = real time,

β = kinematic surface tension,

L = exposed barrier length parallel to acceleration vector,

m = model,

p = prototype,

l = propellant or prototype liquid,

tl = test liquid.

This holds when the model multiple-screen barrier surface is geometrically similar to the full-scale surface, and the barrier screen material and screen spacing are the same as those used in the prototype.

Extending this simple one-dimensional analysis with appropriate time-dependent coefficients to represent the performance of any multiple-screen barrier model provides a general solution for gas accumulation between stacked screens subjected to supercritical lateral accelerations

$$\int_{v_{g_0}}^{v_g} \frac{dv_g}{\phi(v_g)} = \int_{\tau_0}^{\tau} \left(\frac{\dot{q}_g}{A} \right) d\tau .$$

The general solution applied to the model, which is geometrically representative of capillary barriers of constant width l_0 normal to the lateral acceleration vector reduces to

$$\ln \frac{v_g}{v_{g_0}} = \frac{1}{S} \int_{\tau_0}^{\tau} f(\tau) d\tau .$$

The limited test data available apply only to capillary barriers using the same screen materials on the same spacing S . Introducing the correlation for

$$\frac{\dot{q}_g}{A} = \frac{k}{\tau^\gamma}$$

from the results of the lateral stability tests yields an expression of the form

$$v_g = v_{g_0} \left\{ 1 + \exp \left(\frac{k}{S(\gamma-1)} \left[\left(\frac{1}{\tau_0} \right)^{\gamma-1} - \left(\frac{1}{\tau} \right)^{\gamma-1} \right] \right) \right\}$$

for predicting the lateral stability performance of the model.*

The limited lateral stability tests of the model failed to provide quantitative data defining the effect of that lateral acceleration level on the accumulation of gas in an unstable multiple-screen barrier. Measured initial gas ingestion at breakdown was near $a/a_{cr} \sim 1$. Some results of the data analysis indicate a first-order influence of a/a_{cr} on V_{g_0} . Since uncertainty prevails concerning the form of the function $V_{g_0} = v(a/a_{cr})$, the quantitative use of the analytical model is restricted to $a/a_{cr} \sim 1$. For the near-stable barrier environment, the basic model using the constants in Table IV-6 should give realistic performance predictions. When $a/a_{cr} \gg 1$, the basic model predictions only provide a best performance limit. The alternative generalized relationship

$$V_{g_0} = c_{n_0} \left(\frac{a}{a_{cr}} \right)^{n_0}$$

should produce a better estimate of the actual barrier characteristics in the high supercritical acceleration environments. The maximum model accelerations investigated were approximately a/a_{cr} of 3. Therefore, the use of the generalized relationship may or may not be conservative throughout the anticipated OMS acceleration spectrum, $0 < a/a_{cr} < 10$.

*The equivalent form of the equations for gas accumulation behind the nth screen of a multiple-layer barrier depends on the value of γ_n . When

$$\begin{aligned} \gamma_n < 1: \quad V_{g_n} &= V_{g_0} \left\{ 1 + \exp \left[\frac{k_n}{S(1-\gamma_n)} \left(\tau^{1-\gamma_n} - \tau_0^{1-\gamma_n} \right) \right] \right\}, \\ \gamma_n = 1: \quad V_{g_n} &= V_{g_0} \left[1 + \left(\frac{\tau}{\tau_0} \right)^{k_n/S} \right], \\ \gamma_n > 1: \quad V_{g_n} &= V_{g_0} \left\{ 1 + \exp \left(\frac{k_n}{S(\gamma_n-1)} \left[\left(\frac{1}{\tau_0} \right)^{\gamma_n-1} - \left(\frac{1}{\tau} \right)^{\gamma_n-1} \right] \right) \right\}. \end{aligned}$$

After a representative analytical model has been developed for the subscale test device characteristics, the lateral stability performance of similar prototype barriers can be predicted. The similitude criteria permit extrapolation of gas accumulation data from the model to the prototype as

$$v_{g_{\text{prototype}}} = \frac{L_{\text{prototype}}}{L_{\text{model}}} \left(\frac{\ell_{o_{\text{prototype}}}}{\ell_{o_{\text{model}}}} \right) v_{g_{\text{model}}}$$

The modeling derivation is essentially size scaling and time scaling between test model and prototype performance based on equal liquid interface velocities at geometrically similar locations (homologous points). The prototype performance can be estimated using the basic model for $a/a_{cr} \sim 1$ or, using the generalized relationship for $a/a_{cr} \gg 1$, as discussed in the following,

where $\ell_n = \ell_o|_n$:

- 1) Selection of model parameters, k_n , γ_n , and c_n . For the basic model, c_n is a constant and data are taken from Table IV-6. For the generalized relationship $c_n = c_{n_o} \left(\frac{a}{a_{cr}} \right)_n$ and data are taken from Table IV-7;

- 2) Calculation of initial gas ingestion volume during real time t_{o_n} .

$$v_{g_{o_n}} = c_n \ell_n \text{ at } t_{o_n}$$

where $\ell_n = \ell_o|_n$ and the real-time duration t_{o_n} from the breakdown of screen n for $v_{g_{o_n}}$ to be accumulated in space n , is related to comparable model time as

$$t_{o_n} = \sqrt{\frac{\beta_{tl}}{\beta_\ell}} \left(\frac{L_p}{L_m} \right) \tau_{o_n};$$

- 3) Calculation of local time t_n during screen n breakdown transient.

$$t_n = t - t_{n_{cr}}$$

where $t \geq t_{o_1}$ and $t_1 = t$

(note that t_n = real time referenced to screen n breakdown,

t = real time referenced to initial barrier
(Screen 1) breakdown

$t_{n_{cr}}$ = real time, referenced to initial barrier
breakdown, at which screen n breakdown occurs;

- 4) Calculation of scaled time (model time) comparable to real time during Screen n breakdown.

$$\tau_n = \sqrt{\frac{\beta_\ell}{\beta_{t\ell}}} \left(\frac{L_m}{L_p} \right) t_n;$$

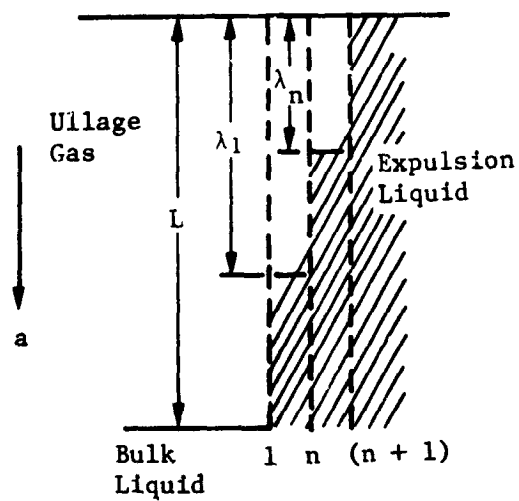
- 5) Calculation of the gas volume accumulated in space n behind screen n during breakdown transient.

$$v_{g_n} = v_{g_{o_n}} \left\{ 1 + \exp \left(\frac{k_n}{S_n(\gamma_n - 1)} \left[\left(\frac{1}{\tau_{o_n}} \right)^{\gamma_n - 1} - \left(\frac{1}{\tau_n} \right)^{\gamma_n - 1} \right] \right) \right\} \frac{L_p}{L_m}$$

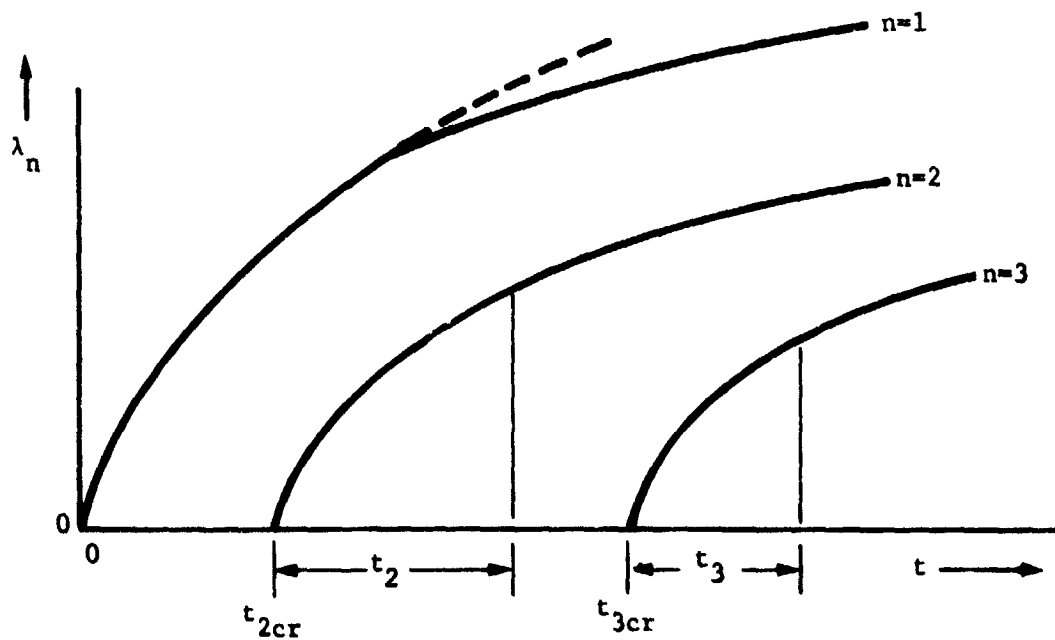
at real time t during barrier breakdown;

- 6) Calculation of gas height behind screen n.

$$\lambda_n = \frac{v_{g_n}}{S_n \ell_n} \text{ as illustrated.}$$



The resulting prototype performance estimate can then be shown as illustrated for $n = 3$:



At $t = t_{3cr}$, gas would be ingested into a liner system composed of 3 layers of screen.

d. *Application to a Simplified OMS Tank* - A hypothetical performance problem was posed to illustrate the use of the gas penetration formulas developed from the lateral stability test data. The prototype configuration chosen was geometrically similar to the test model. The prototype application, design, mission, acceleration environment, and propellant properties are given in Fig. IV-23. The model dimensions

$$L_m = 22.9 \text{ cm (9.0 in.)},$$

$$l_{om} = 11.45 \text{ cm (4.5 in.)},$$

$$S_m = 0.67 \text{ cm (0.25 in.)},$$

result in a model scale for the prototype of

$$\frac{L_m}{L_p} = 12.5\%.$$

The critical lateral acceleration ratios, for which the performance of the prototype multiple-screen liner was calculated, are given in Table IV-9. The barrier breakdown transient predicted by the basic model, which does not consider the lateral accelerations ratio

$\left(\frac{a}{a_{cr}}\right)$, is plotted in Fig. IV-24. The comparable estimate of barrier breakdown characteristics using the generalized relationship

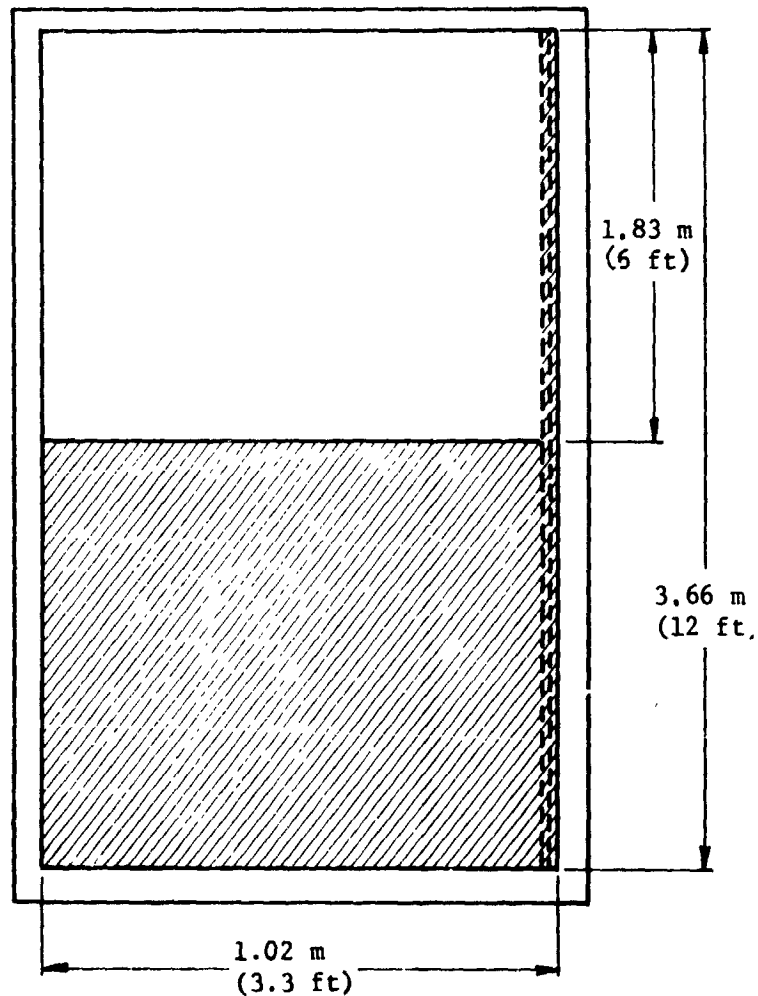
that considers the critical lateral acceleration ratio is plotted in Fig. IV-25.

Based on the results of the bubble point tests and the lateral stability tests, the model logic assumes that after breakdown of screen n , the initial breakdown of screen $(n + 1)$ occurs when

$$\lambda_n > \frac{\Delta P_c |_{(n+1)}}{\rho a}$$

where ΔP_c = individual screen bubble point pressure in the propellant,

ρ = density of the propellant.



- Note:**
1. Three-screen stack, 325 x 2300 Dutch twill, $S = 0.64 \text{ cm}$ (0.25 in.).
 2. $\Delta P_c = 63.5 \text{ cm H}_2\text{O}$ (25.0 in.) in methanol, = 96.3 cm H_2O (37.9 in.) in MMH = 0.945 N/cm^2 (1.37 psi) in MMH.
 3. MMH at 20°C .
 4. $\sigma = 34.3 \text{ dynes/cm}$ ($2.35 \times 10^{-3} \text{ lbf/ft}$),
 $\rho = 8.79 \times 10^2 \text{ kg/m}^3$ (54.9 lbm/ft^3),
 $\mu = 0.86 \times 10^{-3} \text{ Ns/m}^2$ ($0.578 \times 10^{-3} \text{ lbm/ft-s}$),
 $\theta = 0^\circ$.
 5. Launch maxima, $a = 3.0 \text{ g}$.
 6. North polar launch, 50% offload.

Fig. IV-23 Prototype Multiple-Screen Liner for the OMS Monomethylhydrazine Tank

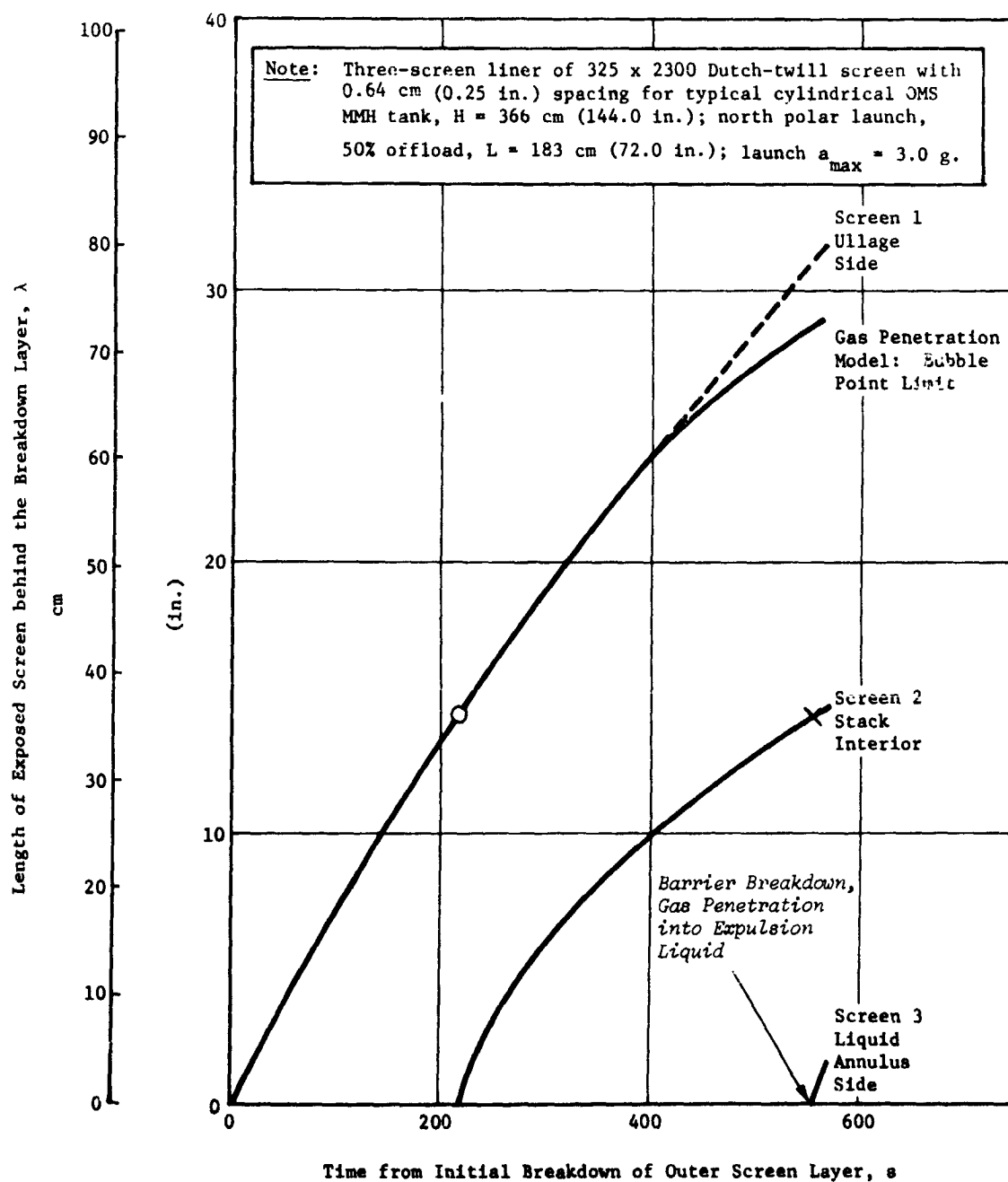


Fig. IV-24 Performance Estimate Based on Multiple Screen Test Model Data

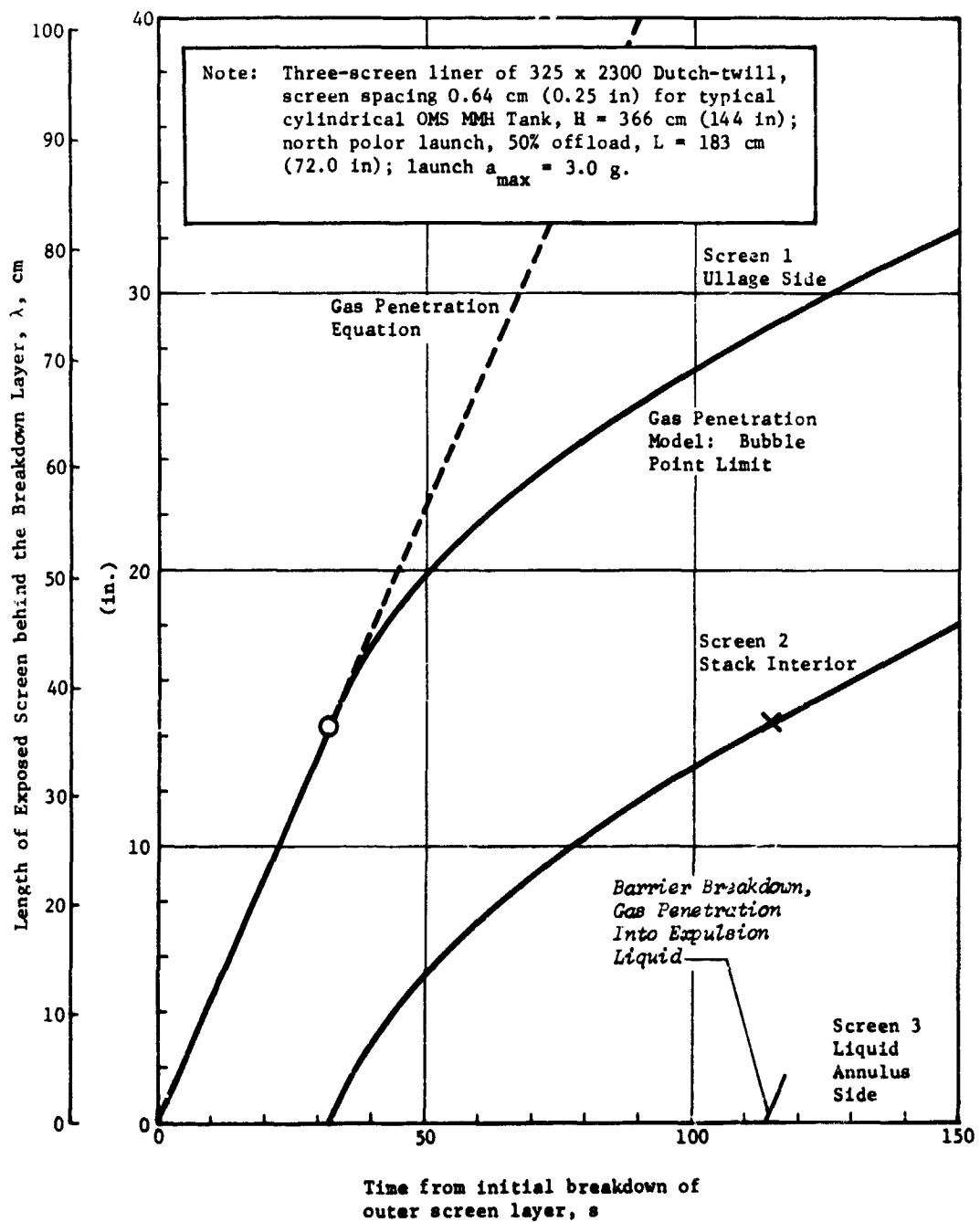


Fig. IV-25 Performance Estimate Based on Multiple-Screen Test Model
Data Modified for Lateral Acceleration Level

Table IV-9 Lateral Acceleration Environment of the Prototype Multiple-Screen Liner

n	a _{cr}	$\frac{a}{a_{cr}}$	C _{n_o} cm ² (in. ²)	C _n cm ² (in. ²)
1	0.60	5.01	0.0348 (0.0054)	0.174 (0.027)
2	1.20	2.50	0.103 (0.016)	0.258 (0.040)
3	1.80	1.67	0.387 (0.060)	0.645 (0.100)
<p>Note: $a_{cr} = \frac{\sum_{c=1}^n \Delta P_c}{\rho L} \Big _m$</p> <p>a = 3.0 g.</p>				

The formulas that predict the gas penetration were derived for liquid draining from space n being unaffected by the dynamics occurring in the (n + 1) space. Since the maximum liquid column that the (n + 1) screen can support is

$$n^{\Delta(n+1)} \lambda_{max} = \frac{\Delta P_c \Big|_{(n+1)}}{\rho a} ,$$

the predicted characteristics for screen n depart from the calculated performance when

$$\left| \lambda_n - \lambda_{(n+1)} \right| > n^{\Delta(n+1)} \lambda_{max}$$

as illustrated by the broken lines for Screen 1 in Fig. IV-24 and IV-25.

Comparison of Fig. IV-24 and IV-25 reveals that the barrier breakdown transient predicted by the basic model is nearly five times as long as that predicted by the generalized relationship, which is felt to be more applicable to the OMS tank example. Regardless of the imprecise knowledge of multiple-screen barrier

breakdown characteristics under high lateral accelerations $a/a_{cr} \gg 1$, a qualitative evaluation of the predicted performance indicates that multiple-screen barriers of fewer layers than required for steady-state lateral stability can be designed to provide barrier breakdown transients on the order of minutes rather than seconds. Multiple-screen barriers designed to the time-dependent acceleration criteria could meet all performance objectives with less weight and more operational flexibility than otherwise possible.

e. *Conclusions* - Analysis of the data from these initial experiments for time-dependent behavior of multiple-screen barriers indicated:

- 1) The gas penetration resistance of a stack of screens is not equal to the sum of the bubble points for the individual screens comprising the barrier. In addition to the nominal bubble point degradation, it was found that violently unstable breakdown is associated with the nonwicking characteristic of the square weave screen, as opposed to the continuous, controlled breakdown observed for the Dutch-twill material;
- 2) The initial breakdown of each layer of screen in a barrier under lateral acceleration can be predicted from the individual bubble point for that layer;
- 3) A quantitative prediction of multiple-screen breakdown performance under lateral accelerations close to the retention capability of the screen $a/a_{cr} \sim 1$ is provided by the basic model;
- 4) A qualitative assessment of the breakdown characteristics of multiple-screen barriers under high lateral accelerations $a/a_{cr} \gg 1$ is provided by the generalized relationship;
- 5) Several minutes of exposure to acceleration environments encountered during normal vehicle operation are required to produce gas penetration through large multiple-screen barriers of relatively few layers.

A review of the test program showed areas of multiple-screen barrier behavior that require further research:

- 1) The gas penetration data measured during the lateral stability tests of the model were limited to one referee liquid (methanol), a constant number of barrier screens ($N = 3$), and a single value for screen spacing [$S = 0.64$ cm (0.25 in.)]. Consequently, these tests provided no information on the effects of liquid properties (σ , θ , μ , and ρ), the number of screens in the stack (N), or the spacing between the screens (S);
- 2) The ability of a screen layer to recover its original capillary retention capability after the initial breakdown acceleration is no longer acting on the barrier has not been investigated;
- 3) The validity of the generalized time parameter and scaling procedures should be verified experimentally.

The results of these preliminary tests and analyses of the dynamics of multiple-screen breakdown suggest that the provision for steady-state control of the liquid may require more layers of screen than previously predicted because of the apparent degradation in additive bubble point. However, steady-state control may not be a design requirement for gas-free liquid acquisition and expulsion in transient high-g environments, as indicated in the OMS tank example. The multiple-screen barrier design criteria may be significantly reduced to a safety factor based on the breakdown time for a capillary barrier whose liquid retention capability is much less than that required under the continuous application of the peak lateral acceleration.

B. ACCEPTANCE, GROUND HANDLING, AND INSPECTION TESTING

The 100- to 500-mission life of the OMS, with up to 30 days of operation per mission, requires simple and efficient ground servicing and maintenance procedures. Positive gas-free propellant loading and complete draining procedures are required for tanks using either liner or trap acquisition/expulsion systems. The expulsion device should not greatly complicate these operations. It should also be compatible with the normal ground handling and transportation environments experienced by the loaded OMS system at the Kennedy Space Center (KSC), where the loading may occur at a remote facility. Mating with the orbiter could then occur at either the Vertical Assembly Building (VAB) or on the launch pad. Propellant would be loaded with the tanks vertical. The tanks would be transported in either the horizontal or vertical position, but probably horizontal. Mating with the orbiter would be with the tanks either horizontal or vertical. In the VAB, the preferred approach would be to install the OMS pods prior to orbiter erection because of the elevations involved; on the pad, the orbiter would be in the launch configuration and the OMS tanks would be installed in the vertical position. Loading could also occur on the launch pad, but the remote loading approach presents the worst-case situation, which should not be constrained by the propellant acquisition device.

The reusability criteria introduce the need for remote inspection techniques between missions. Functional tests of the propellant acquisition/expulsion system installed in the tank must reliably indicate either the flight readiness of the system or the type of any failure present. In addition, simple, effective and dependable acceptance test procedures are needed for the liner and the trap, both prior to and following installation in the tank.

Subscale models of a complete, single-screen liner system and a refillable trap system for the OMS were fabricated and tested under simulated ground handling and transportation operations to demonstrate the compatibility of the systems with these operations. The same liner and trap models were subjected to bench tests designed to evaluate functional inspection, propellant loading and draining, and associated procedures. The ground processing experiments were complemented by additional inspection technique development specifically applicable to acceptance testing. These bench tests were oriented toward direct inspection of the finished device before it is installed in the tank or prior to tank closure.

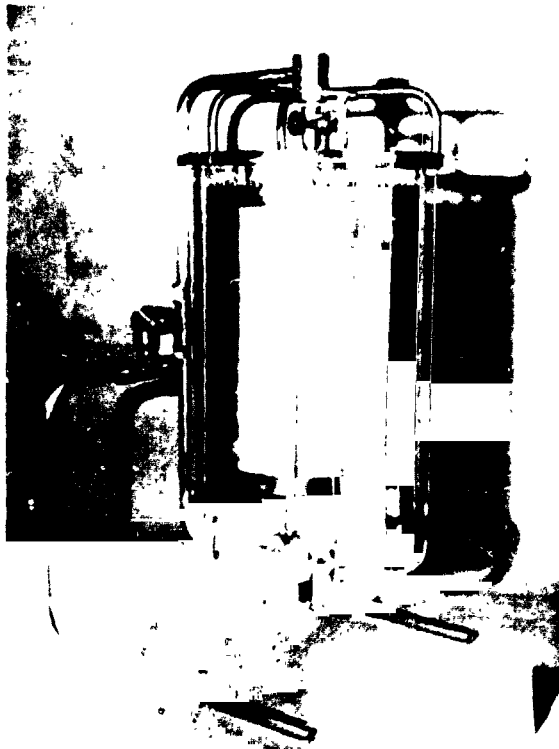
Bubble point checks of the trap system were performed during fabrication, as discussed in Chapter V. System integrity was then demonstrated in the bench tests discussed in this chapter. Acceptance testing of the 325 x 2300-mesh Dutch-twill screen liner resulted in the detection of several flaws in the screen material itself and a leak around one of the sealing gaskets. The system was repaired by soldering the screen flaws and tightening the sealing gasket. Details of the ground operations testing are presented in this section.

1. Liner Device Tests

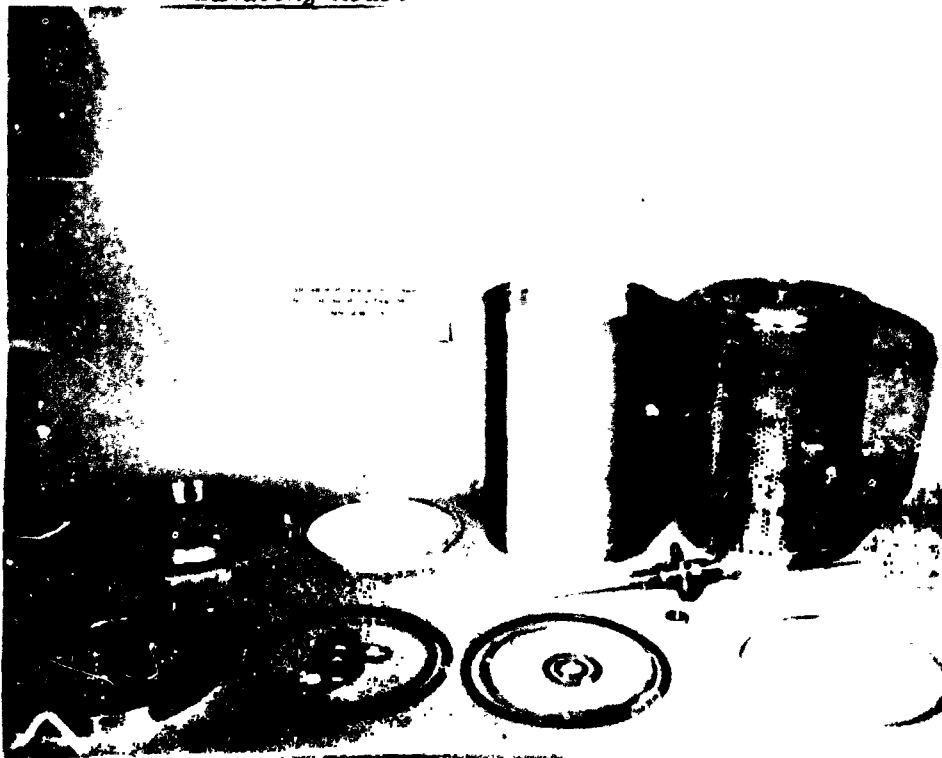
The configuration of the inspection and ground handling model simulates a complete, single-barrier tank liner device. Remote inspection (in-tank) testing provides data applicable to in-service reusability assurance and to acceptance tests for large capillary devices. Liner or channel capillary devices may not become an integral system during manufacture until they are enclosed in the tank. Acceptance testing of such systems may require remote or indirect techniques similar to those investigated during the inspection testing. Acceptance tests appropriate for smaller, unitized capillary devices of all types were demonstrated using the liner (out-of-tank). The implications of reusability and off-vehicle servicing of earth-orbital propulsion systems that employ capillary acquisition/expulsion devices were studied during the ground handling tests. The purposes, procedures, and results of these tests are presented as acceptance tests, ground handling tests, and inspection tests.

a. Test System - The inspection and ground handling test model used in conducting these tests was a 30.5-cm (12-in.) diameter cylinder approximately 46-cm (18-in.) long, as shown in Fig. IV-26. The model consisted of a screen liner inside a clear plastic tank mounted on a stainless steel stand. The stand allowed the test model to be rotated about two mutually perpendicular axes.

The liner assembly, Fig. IV-27, was composed of a stainless steel perforated plate support structure and the fine-mesh Dutch-twill screen cover containing a volume of nearly 18.8 liters (5 gal). The liner comprised three separate pieces of flat screen material, a top disc, a bottom disc, and a cylinder; these were assembled on the liner support structure and sealed with O-rings to allow screen interchangeability. Therefore, any requirement to form the 304L stainless steel screen was avoided. Two 0.315-cm (1/8-in.)



*Fig. IV-26 Inspection and Ground
Handling Model*



*Fig. IV-27 Screen Liner Components of Inspection and Ground
Handling Model*

diameter vent and pressurization lines and a spray nozzle penetrated into the bulk region and were sealed at the liner. The pressurization diffuser, containing 16 orifices, 0.102 cm (0.040 in.) in diameter, was used to spray-wet the screen liner during remote inspection tests. Screen weaves of 325 x 2300, 250 x 1370, and 80 x 700 Dutch-twill were used for the interchangeable liners.

The outer tank was made from annealed polycarbonate sheet (Lexan) since it is more resistant to methanol (Ref IV-2). Polycarbonate is stronger and safer to handle than most other clear materials. The assembly of the inspection and ground handling test model is documented on 16mm color movie film.

Figure IV-28 schematically depicts the internal arrangement and functions of the inspection and ground handling model and support hardware. Methanol was supplied to the model from a large sump tank, which also served as the methanol bath for the liner during the acceptance tests. Liquid expulsion was ordinarily accomplished during testing by draining into a 19-liter (5-gal) glass jar, which is referred to as the catch tank. However, a direct return line was provided from the model to the sump tank for loading or unloading procedures. Three pressure taps were provided on the model:

P_{B1} = static pressure in the bulk volume at 5.4-cm (2.12-in.) depth from the top center of the liner;

P_{A2} = static pressure in the annulus at the ullage end of the tank;

P_{A3} = static pressure in the annulus at the outlet end of the tank.

The instrumentation for the tests consisted of a pressure transducer (± 1.0 psid) and a stripchart recorder with speed set at 2 in./minute. The low-pressure test apparatus (LPTA) shown in Fig. IV-3 was used to control the pressure to the model.

The three liners tested provided a range of lateral stability representative of acquisition/expulsion devices using multiple-screen barriers to obtain steady-state stability throughout their operating environment, small single-screen barriers with low margins of safety, and large capillary barriers that are unstable over portions of their operating spectrum.

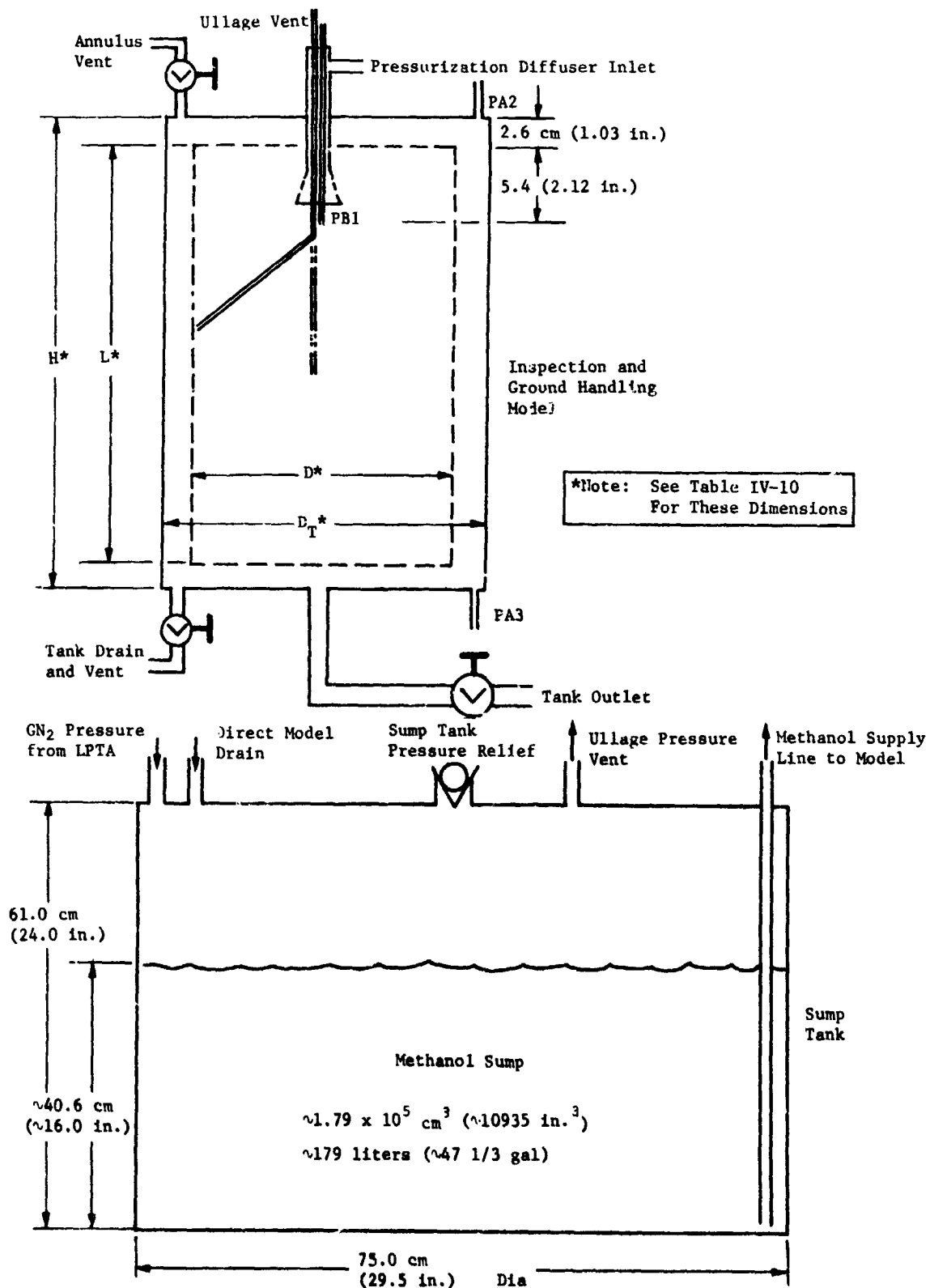


Fig. IV-28 Inspection and Ground Handling Test System Schematic

The lateral stability criteria for the model was formulated as

Stable model in vertical orientation: $\Delta h_{cr} > L$,

Stable model in horizontal orientation: $\Delta h_{cr} > D$

where

$$\Delta h_{cr} = \frac{\Delta P_c}{\rho a}$$

In a static 1-g environment, $a = 980.6 \text{ cm/s}^2$ (32.17 fps^2). The test liquid was methanol. The stability characteristics of the model screens are given in Table IV-10.

Table IV-10 Lateral Stability of the Screen Liners Tested in the Inspection and Ground Handling Model under a Static 1-g Environment

Screen Weave	Nominal Bubble Point of the Screen	Maximum Stable Screen Height	Model Stability for the Orientation in 1-g			
			Vertical Liner		Horizontal Liner	
			Stable Height Margin, $\Delta h_{cr} - L$	Condition*	Stable Height Margin, $\Delta h_{cr} - D$	Condition*
	ΔP_c cm H ₂ O (in. H ₂ O)	Δh_{cr} cm (in.)	cm (in.)		cm (in.)	
325 x 2300	63.5 (25.0)	80.2 (31.6)	42.9 (16.9)	S	54.9 (21.6)	S
250 x 1370	53.3 (21.0)	67.4 (26.5)	30.0 (11.8)	S	41.1 (16.5)	S
80 x 700	16.3 (6.4)	20.5 (8.1)	-16.8 (-6.6)	B	-4.9 (-1.9)	B

TEST LIQUID

Methanol $\sigma = 22.6 \frac{\text{dynes}}{\text{cm}} \left(1.55 \times 10^{-3} \frac{\text{lbf}}{\text{ft}} \right)$

$\rho = 0.791 \frac{\text{gm}}{\text{cm}^3} \left(49.4 \frac{\text{lbm}}{\text{ft}^3} \right)$

LINER DIMENSIONS

$L = 37.3 \text{ cm (14.7 in.)}$

$D = 25.4 \text{ cm (10.0 in.)}$

TANK DIMENSIONS

$H = 43.4 \text{ cm (17.1 in.)}$

$D_T = 29.2 \text{ cm (11.5 in.)}$

*Condition: S - laterally stable liner, no breakdown.

B - laterally unstable liner, breakdown.

The results of the inspection and ground handling model tests attributable to lateral stability behavior can be scaled to prototype devices by

$$\left(\frac{\Delta h_{cr}}{L}\right)_p = \left(\frac{\Delta h_{cr}}{L}\right)_m$$

where p designates prototype and m denotes model. This similitude condition is applicable for propellants having different kinematic surface tension than the test liquid used in the model. Therefore, similar lateral stability effects due to inspection and ground handling can be observed in a subscale model employing material with larger capillary pore size to simulate the prototype barrier.

b. Acceptance Testing - Verification of the acquisition/expulsion device integrity after manufacturing processing is required for every unit produced. A definitive test of the capillary device using the simplest applicable techniques is desirable. Certain types of devices, usually of small size, can be tested as a unit prior to installation in the tank. Others must be integrated with the tank assembly and, consequently, must be acceptance tested in the tank. The remote inspection techniques studied during inspection testing are applicable to the acceptance testing of these systems in the tanks. However, certain simpler tests are possible on the subassemblies or where the capillary device is complete when outside the tank, e.g., a trap device. The liner of the inspection and ground handling model is representative of this smaller class of devices and was used to investigate two acceptance test techniques appropriate for capillary devices outside the tank:

- 1) The submerged bubble point test;
- 2) The liquid retention test, referred to as the drip test.

The object of the acceptance testing was to evaluate the submerged bubble point test and the drip test on the basis of simplicity, accuracy, and range of applicability. In the submerged bubble point test, the location and severity of premature breakdown points are identified by submerging the capillary device in a referee liquid and slowly pressurizing the interior of the device with gas. By manipulating all parts near the liquid surface at each level of pressure to expose all elements (preferentially) to the bubble point pressure, breakdown can be

identified by escaping gas. The drip test provides a measure of the capillary integrity of a device by determining the liquid volumes retained in particular orientations under static 1-g lateral acceleration.

For bubble point testing, the liner was submerged in the methanol sump tank. After complete screen wetting, the liner was pressurized with nitrogen gas at 0.5% of the bulk volume/minute or less, depending on the bubble point of the screen. The pressurant was supplied from the LPTA to the 0.318-cm (1/8-in.) diameter ullage vent line of the liner. It should be noted that significant buoyant force is developed on the capillary device as it begins to pressurize (gas-filled internal volume) so appropriate provisions for maintaining the ability to manipulate the device at the desired immersion depth must be considered. Each element of the liner cylinder was tested by continuously rotating the horizontal liner about its axis of revolution with the liner surface approximately 0.2 cm (5/64 in.) beneath the methanol surface. The end covers were inspected by turning the liner to a vertical position. The locations of screen breakdowns were identified visually and the pressure was recorded.

For drip testing, the liner was completely filled with liquid by submerging the vented liner in the sump tank until methanol overflow was observed. After filling, all ports were closed and tightly capped. The capillary device was oriented to provide the minimum internal hydrostatic pressure, which was horizontal in the case of the liner. The device was then elevated above the methanol and moved over a container sufficiently large to hold the entire contents. If the device is laterally unstable in the minimum-pressure orientation, the barrier breakdown will begin before the device clears the liquid surface. Under these conditions complete recovery of the lost liquid is impossible and a rapid transfer over the recovery container reduces the experimental uncertainty. The capillary device was slowly rotated over the container to progressively greater hydrostatic pressure orientations. The position of the device at the moment of liquid loss provided a quantitative measure of barrier stability. If the capillary device can be oriented to maximum hydrostatic pressure with total liquid retention, a minimum level of barrier stability has been established. The vertical position gives the maximum hydrostatic pressure for the cylindrical liner. To evaluate the liquid retention capability of the capillary device, the liquid lost due to breakdown under any orientation can be measured and correlated with barrier characteristics. The residual liquid at the completion of the drip test can be dumped by venting the bulk volume.

All three screen liners were bubble point tested several times during the program with near nominal results as tabulated.

Material	ΔP_c , cm H ₂ O (in. H ₂ O)
325 x 2300	61.0 (24.0)
250 x 1370	55.9 (22.0)
80 x 700	17.0 (6.7)

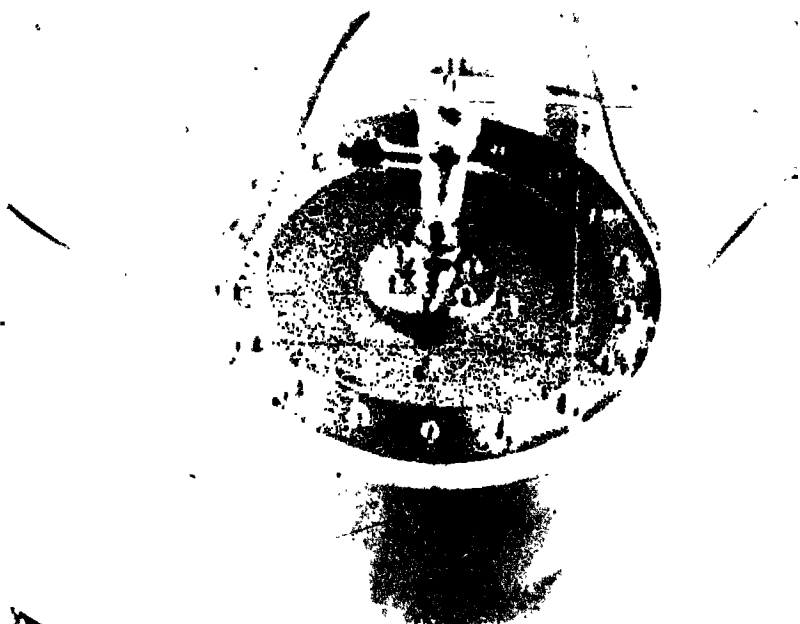
The 325 x 2300 screen and the 80 x 700 screen received the most extensive use and underwent many installations on the liner. A bubble point test was performed after each assembly or to determine baseline barrier performance for evaluating other test results. Representative bubble point test data for the inspection and ground handling model liners are presented in Table IV-11. The 250 x 1370 screen test results are nominal for that liner. The test results shown for the 325 x 2300 screen liner demonstrate the value of the submerged bubble point test for identifying structural problems not associated with screen characteristics. The data for the 325 x 2300 screen liner were taken late in the program and are representative of a degraded or damaged capillary device. The submerged bubble point test was successfully employed to detect degradation in the screen bubble point. Several flaws were located in the screen material. General breakdown of the liner was obtained at the nominal pressure. The flaws located in the screen liner were successfully repaired with Eutectic 157 solder.

Table IV-11 Submerged Bubble Point Test Results

325 x 2300 Dutch Twill Liner, Pressurization Rate = 100 cc/minute of GN ₂		
cm H ₂ O (in. H ₂ O)	ΔP_c , psi	Leak Detected
28.7 (11.3)	0.41	Upper seal ring leak
42.2 (16.6)	0.6	Lower O-ring leak
55.6 (21.9)	0.79	Cylinder electrical capacitance discharge seam weld
57.7 (22.7)	0.82	Cylinder screen 3 to 4 places
62.0 (24.4)	0.88	General cylinder breakdown near seal rings
64.8 (25.5)	0.92	Maximum pressure reached at 100 cc/minute of GN ₂
250 x 1370 Dutch Twill Liner, Pressurization Rate = 100 cc/minute of GN ₂		
56.1 (22.1)	0.80	General breakdown of cylinder with no premature breakdown noted
80 x 700 Dutch Twill Liner, Pressurization Rate = 50 cc/minute		
16.3 (6.4)	0.23	Breakdown at seals
17.5 (6.9)	0.25	General breakdown of cylinder

Structural flaws and enlarged pores in the capillary device can be readily located using the submerged bubble point test. The test is applicable to all types of screen devices. The only problem associated with the submerged bubble point test is that large screen liners cannot be completely submerged in a practical way. However, a large screen device could be installed in a clear tank and tested by partially filling the annulus between the tank and the screen liner. It would be necessary to install a spray nozzle and a pressurization line in the screen device to wet the screen and supply pressure to the bulk region.

The two extremes of the drip test range of application were tested with the inspection and ground handling model liner. Testing with the 250 x 1370 screen liner shown in Fig. IV-29 demonstrated the liquid retention characteristics of a completely stable capillary device. The methanol-filled device supplied all capillary surfaces with sufficient liquid to prevent dryout from evaporation during a period of several minutes of no-drip time. The data for the 250 x 1370 Dutch-twill liner shown in Table IV-12 demonstrate this principle. Since this liner was laterally stable in all orientations under 1-g it did not lose any liquid during the out-of-tank handling with the vents sealed.



(a) *Filling the Screen Liner
with Methanol*

Figure IV-29 Drip Test for 250 x 1370 Dutch-Twill Screen Liner



(b) *Vertical Elevation of
the Stable Screen Liner*



(c) *Measuring the Discharge
after Venting the Liner*

Fig. IV-29 (concl)

Table IV-12 Drip Test Results

Screen Liner	1-g Lateral Stability, cm of Methanol (in. of Methanol)	Liner Position - Condition	Predicted Liquid Loss due to Lateral Instability, liters	Measured Liquid Loss due to Lateral Instability, liters
250 x 1370	Completely Stable 67.4 (26.5)	Vertical-ports closed	0	0
		Vertical-vented	18.8	18.8
80 x 700	Completely Unstable 20.5 (8.1)	Horizontal-ports closed	2.6	11.1*
		Vertical-ports closed	5.9† (0)‡	7.7
		Vertical-vented	10.3	Trace

*Approximately 3.9‡ were lost to the sump before the liner was transferred over the catch tray.

†Based on predicted initial breakdown performance (horizontal)

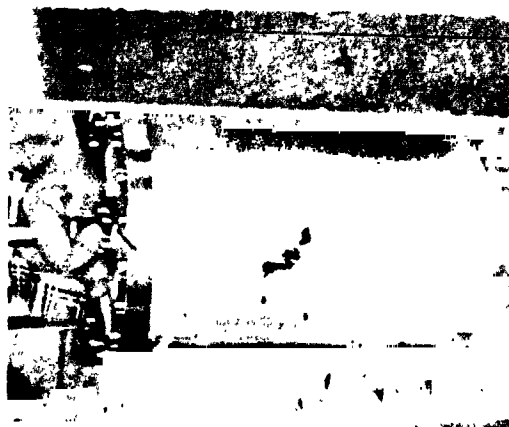
‡Based on measured initial breakdown performance (horizontal).

Testing with the 80 x 700 screen liner shown in Fig. IV-30 demonstrated the breakdown characteristics of a completely unstable capillary device. The liner breakdown began before it had cleared the surface of the methanol sump. Although the initial liquid loss was not recovered for measurement, it was estimated that the actual loss of liquid under 1.23 times the maximum laterally stable head was 4.3 times the volume predicted on the basis of screen bubble point. The residual liquid volume after restabilization of the liner (no liquid drip) in the horizontal orientation was less than the predicted residual liquid for the vertical orientation. However, when the 80 x 700 screen liner was rotated to the vertical, the entire residual contents of the bulk volume were lost. The absence of any draining after the liner was vented verified these results. The drip test data for the 80 x 700 screen liner are also presented in Table IV-12.

The results of the drip tests performed on the 250 x 1370 screen liner and 80 x 700 screen liner are summarized in Fig. IV-31. The drip tests showed that the technique is useful for evaluating capillary devices qualitatively or quantitatively. However, when coarse screen barriers break down (80 x 700), wicking is not rapid enough to reseal the screen at the liquid level of static lateral stability. The ingestion of air through the unstable barrier results in an effective loss in resistance to gas penetration that causes stability (cessation of liquid loss) to be reestablished well below the level predicted on the basis of screen bubble point.



(a) *Filling the Screen Liner
with Methanol*



(b) *Horizontal Elevation of
the Unstable Screen Liner*



(c) *Rotation of the Stabilized
Screen Liner from Horizontal
to Vertical*

Figure IV-30 Drip Test for 80 x 700 Dutch-Twill Screen Liner

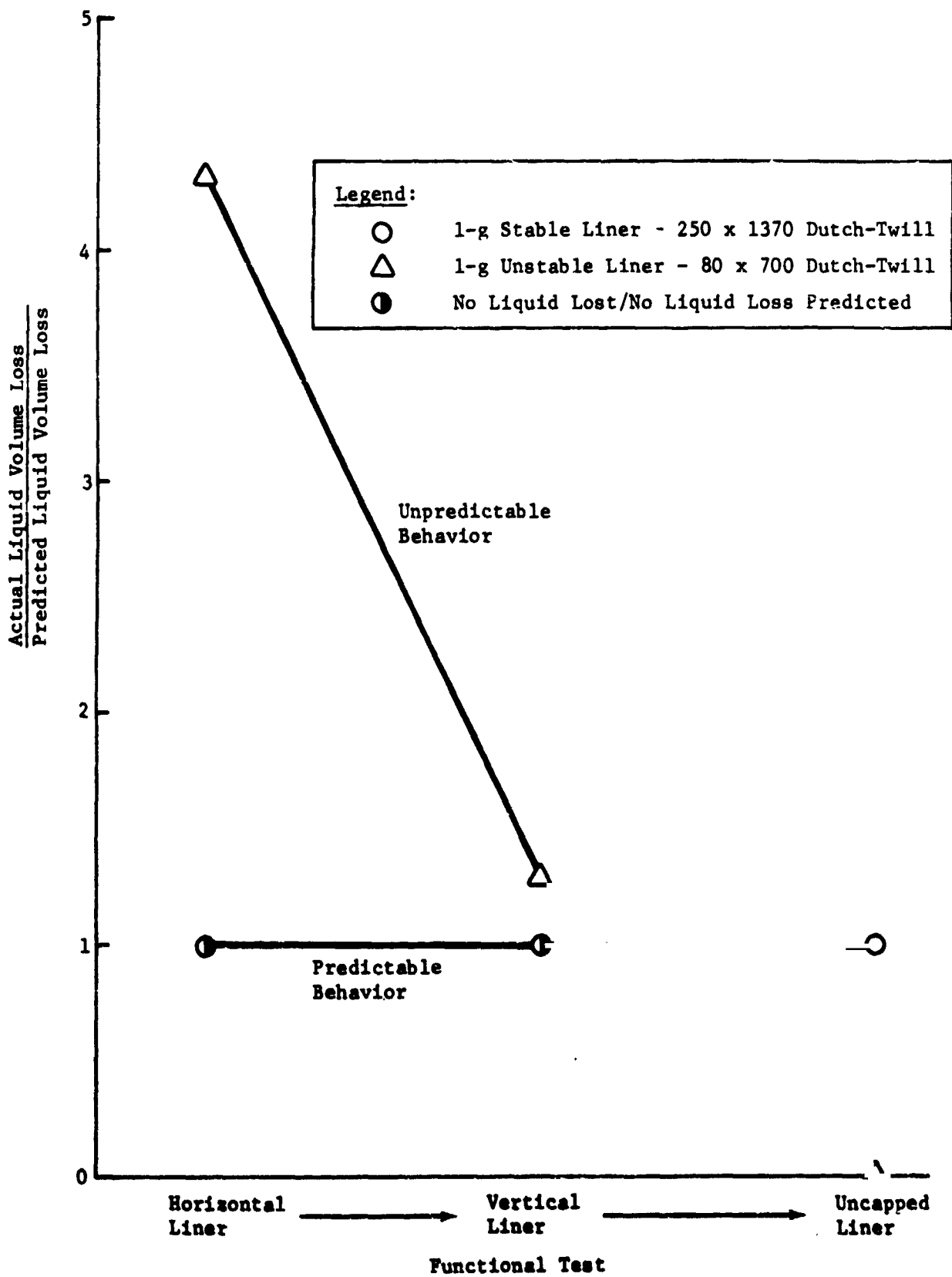


Fig. IV-31 Screen Liner Acceptance Drip Tests, Liquid Methanol in Ambient Air

An uncontrolled dry (unsaturated) test environment contributes to the severity of the rewetting problem. Consequently, the repeatable, correlatable results from drip testing after initial breakdown may be difficult to achieve for valid acceptance testing because of barrier dryout.

The evaluations of the submerged bubble point test and the drip test are summarized in Table IV-13 using the criteria of simplicity, accuracy, and range of application for acceptance testing. The drip test is the easiest test to perform on small devices, but is quantitatively applicable to the limited range of devices that undergo stable to unstable transition with reorientation in 1-g. Although the submerged bubble point test requires additional facilities and time, the results are accurate and thorough.

Table IV-13 Comparison of Acceptance Test Methods

Test	Model	Simplicity	Accuracy	Applicable Range
Submerged Bubble Point Test	325 x 2300 250 x 1370 80 x 700 Inspection and ground handling model liner; subscale OMS refillable trap	Most difficult. Requires more instrumentation, test equipment, and technique.	Excellent. As good as that of the instrumentation and repeatability of the capillary pore dynamics. Careful control of initial wetting, immersion depth, and low pressurization rate required.	Quantitative for all capillary devices that are small enough to be immersed and manipulated.
Drip Test (Liquid Retention)	<u>Completely stable.</u> 250 x 1370 inspection and ground handling model liner. <u>Stable-unstable.</u> Subscale OMS refillable trap. <u>Completely unstable.</u> 80 x 700 inspection and ground handling model liner.	Simplest. Minimal instrumentation, test equipment, and technique.	<u>Completely stable.</u> Qualitative, provides only minimum liquid retention capability. <u>Stable-unstable.</u> Quantitative, satisfactory data from breakdown orientation correlation for slowly manipulated devices under negligible dynamic effects. <u>Completely unstable.</u> Very poor, dispersion of liquid loss data after initial breakdown due to bubble point hysteresis caused by screen dryout.	<u>Completely stable.</u> Qualitative for all capillary devices light and strong enough to be manipulated after liquid filling. <u>Stable-unstable.</u> Quantitative for same as above. <u>Completely unstable.</u> Unsatisfactory for all capillary devices.

c. *Ground Handling Tests* - As discussed previously, the OMS modules may be serviced at a remote hypergolic servicing and loading facility at KSC. To demonstrate the capability of capillary systems to meet the ground handling requirements, tests were conducted with the liner ground handling test model to simulate tank filling, transportation of the loaded tanks to either the VAB or the launch pad, and installation on the orbiter. Both the 250 x 1370 Dutch-twill screen liner and the 80 x 700 Dutch-twill screen liner were tested.

Two test sequences were employed. The first ground handling test sequence is shown in Fig. IV-32 and IV-33. For this case, the liner model was filled in the vertical position with the ullage vented to the atmosphere (Fig. IV-32). After loading [Fig. IV-33(a)], the model was rotated to the horizontal position [Fig. IV-33(b)], placed on a hand cart and transported to simulate moving the loaded propellant tank system from the hypergolic loading facility to the orbiter [Fig. IV-33(c) and IV-33(d)]. The tank was then removed from the transportation cart and rotated back to the vertical position to simulate installation on the orbiter [Fig. IV-33(e)]. This process simulated the conditions associated with ground handling. The second test sequence is shown in Fig. IV-34 and IV-35. In this case, the tank was filled horizontally with the ullage vented [Fig. IV-34 and IV-35(a)], transported vertically [Fig. IV-35(b)], and rotated back to simulate horizontal installation on the orbiter [Fig. IV-35(c)]. The demonstrations were documented on 16mm color movie film. The pictures presented in Fig. IV-33 and IV-35 are individual frames taken from this film.

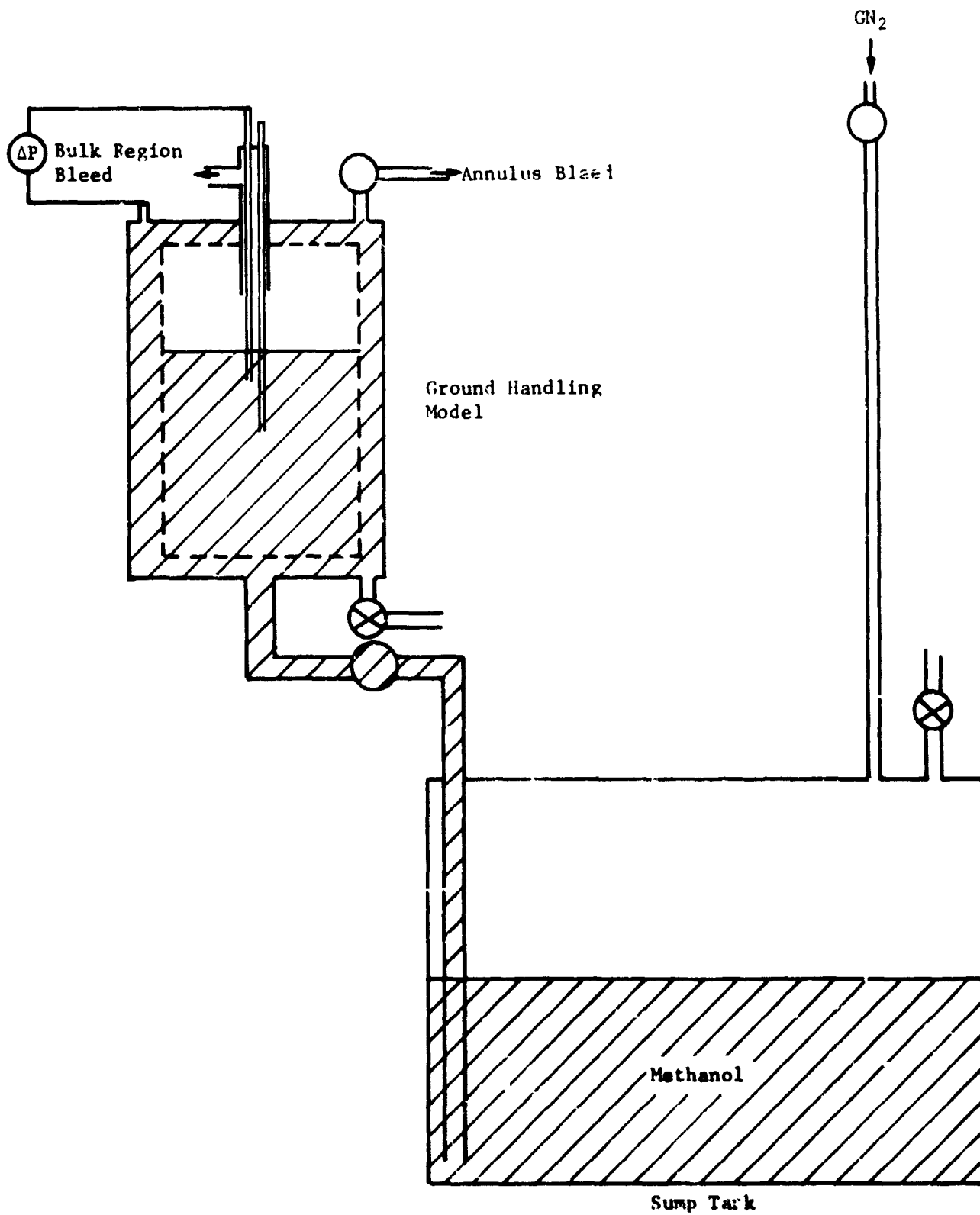


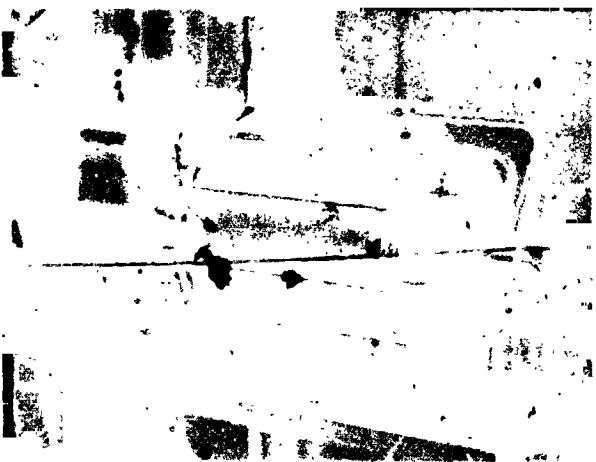
Fig. IV-32 Vertical Fill Test System Schematic



(a) Vertical Filling



(b) Gas Bubble in Annulus
Prior to Transportation



(c) Horizontal Transportation
on Hand Cart



(d) Gas Bubble in Annulus
after Transportation



(e) Vertical Installation
Simulation

Fig. IV-33 Vertical-Horizontal-Vertical Fill-Transport-Install Simulation

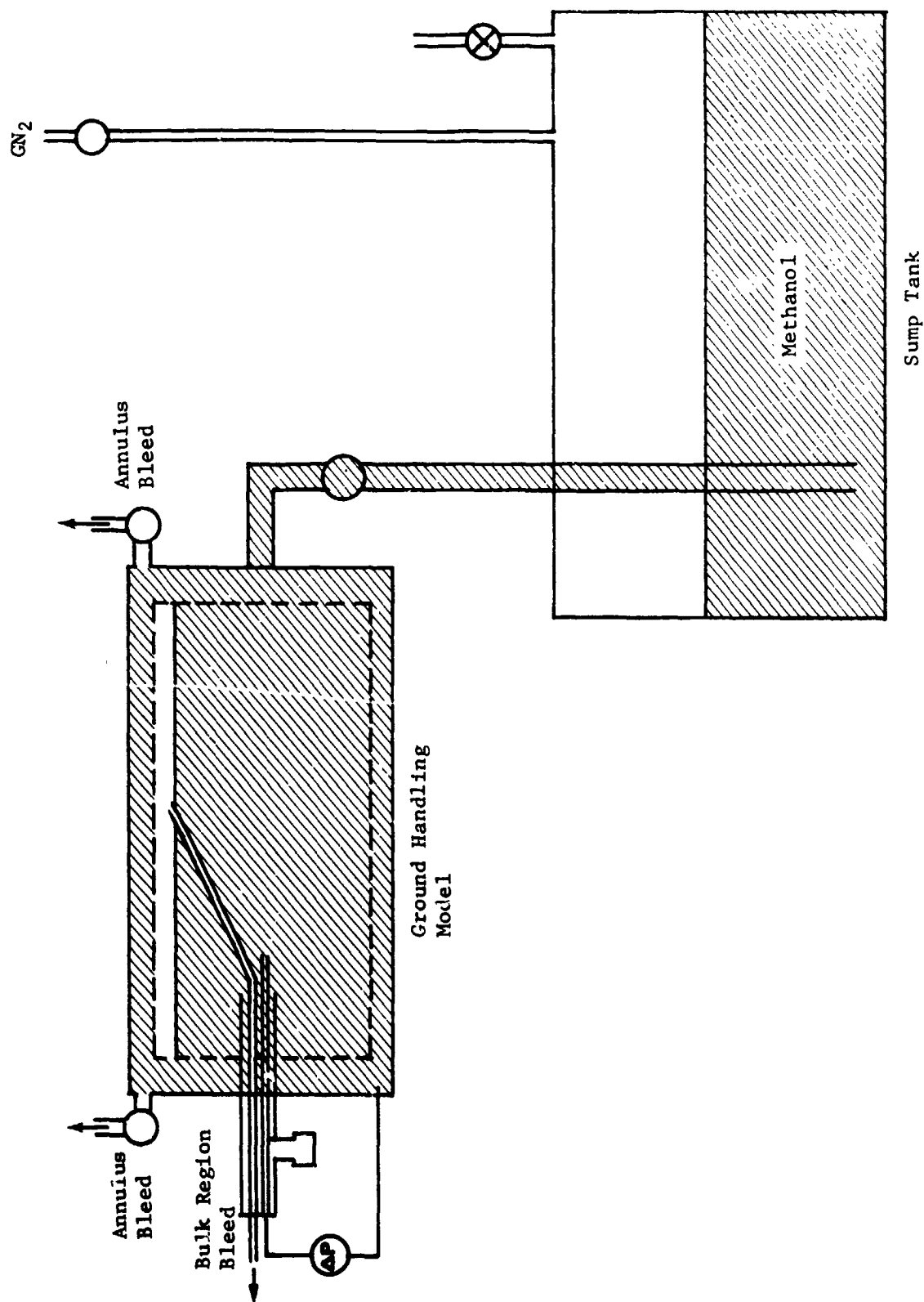
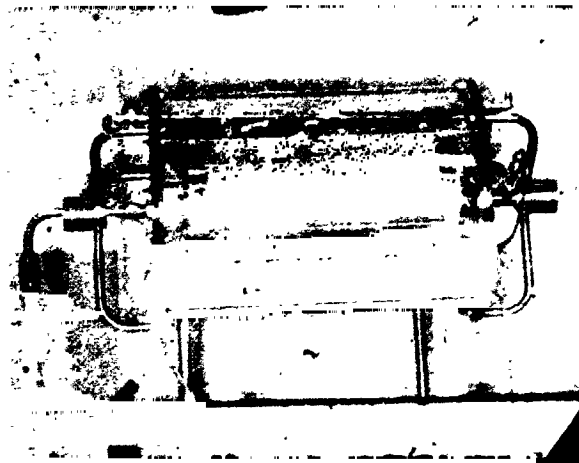
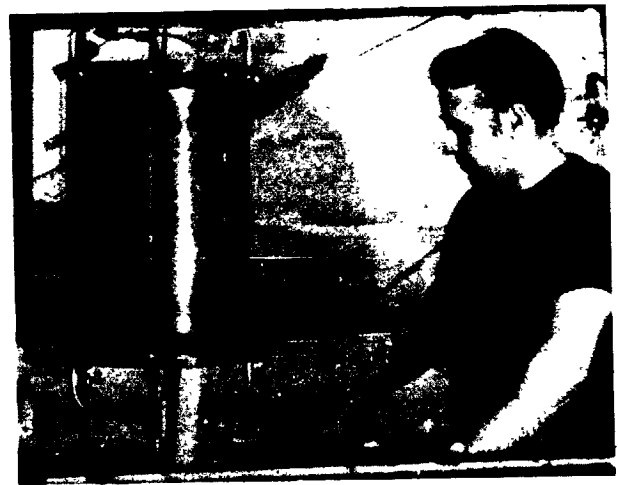


Fig. IV-34 Horizontal Fill Test System Schematic



(a) *Horizontal Filling*



(b) *Vertical Transportation
on Hand Cart*



(c) *Horizontal Installation
Simulation*

*Fig. IV-35 Horizontal-Vertical-Horizontal
Fill-Transport-Install Simulation*

Results of the ground handling tests are summarized in Table IV-14. Both screen liners were filled to a 5% ullage condition by venting from the annulus and bulk propellant regions. The annulus was completely filled with liquid by venting through the bleed line until liquid overflow began. The annulus bleed valve was closed and liquid loading continued into the bulk region until liquid overflow occurred through the bulk region bleed line. The pressurization diffuser line was used as the bulk region bleed line for the vertical filling operation and the ullage vent line was used for the horizontal filling operation. This technique provides a simple, positive fill procedure for the tank.

Table IV-14 Ground Test Results

Screen Liner	Test			Results
	Filling	Transportation	Installation	
250 x 1370 Dutch Twill	Vertical	Horizontal	Vertical	Filled to 5% ullage, no break-down during handling.
250 x 1370 Dutch Twill	Horizontal	Vertical	Horizontal	Filled to 5% ullage, no break-down during handling.
80 x 700 Dutch Twill	Vertical	Horizontal	Vertical	Filled to 5% ullage, no break-down during handling.
80 x 700 Dutch Twill	Horizontal	---	---	Filled to 5% ullage.

Both liners remained stable during transportation and handling as expected [Fig. IV-33(b) and IV-33(d)] since each liner was completely stable at the 5% ullage level. However, if the exposed screen height of the liner to the ullage gas exceeds the stable screen height under the imposed acceleration environment (gravity plus shock and vibration), the liner will break down. This break-down point is completely predictable based on the measured bubble point of the assembled system.

d. *Inspection Tests* - The objectives of these tests were to develop and demonstrate techniques for remote inspection of a capillary device without removing it from the propellant tank and to locate leaks in the system following tank removal. Two methods were used for remote measurement of the system bubble point. In the first method, the bubble point of the system was measured during a negative 1-g liquid methanol expulsion. The other method involved spraying methanol through the combination pressurant diffuser/spray nozzle within the screen liner to wet the screen device and then measuring the bubble point of the system by pressurizing the bulk region. The nozzle represented a spray device that would be installed in the propellant tank for remote measurement of the capillary liquid retention system bubble point.

Once the bubble point of the system has been determined, it will be necessary to locate and repair any premature breakdown points that could occur in seals or the screen itself. Tests were conducted with either partial or total immersion of the screen liner. In both cases, the pressure inside the screen liner was increased with GN₂ pressurant and the breakdown or leak points were located by visual observation of escaping gas bubbles.

For the negative 1-g expulsion tests, the model was set up in the vertical, inverted position as shown in Fig. IV-36 and IV-37.

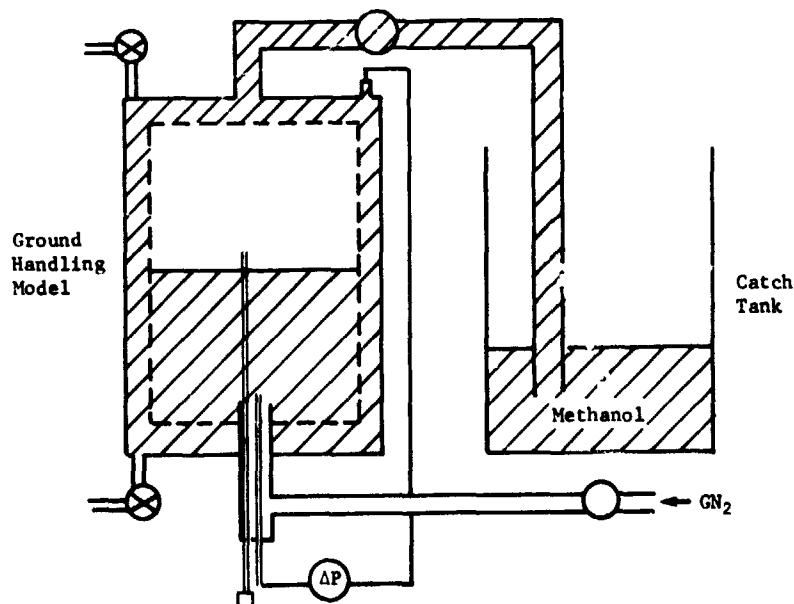
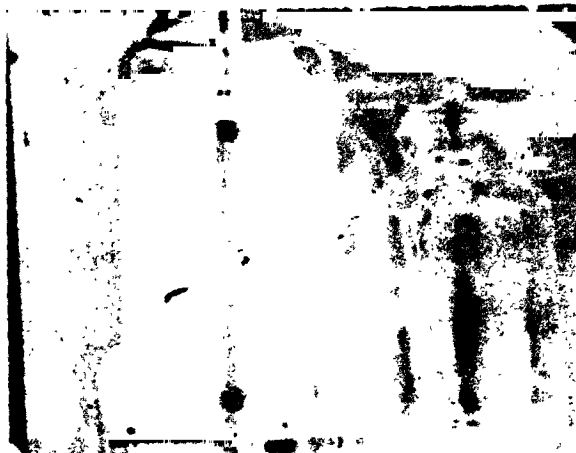
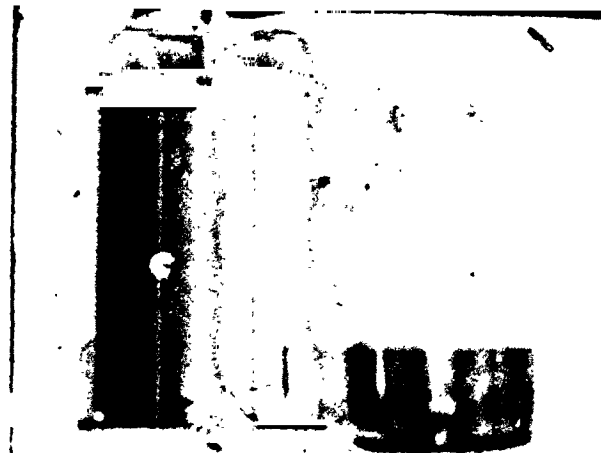


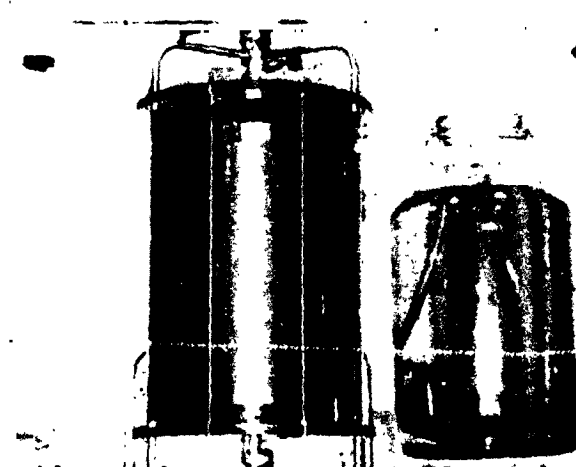
Fig. IV-36 Test System Schematic for Negative 1-g Expulsion Inspection



(a) 250 x 1370 Dutch-Twill Screen Liner System, Outflow Initiation



(b) 250 x 1370 Dutch-Twill Screen Liner System, during Outflow



(c) 250 x 1370 Dutch-Twill Screen Liner System, at Breakdown



(d) 80 x 700 Dutch-Twill Screen Liner System, at Breakdown

Fig. IV-37 Negative 1-g Expulsion Test

The bulk region was pressurized through the pressurant diffuser and the expelled liquid measured. The difference in pressure across the screen was recorded to determine the bubble point of the system at screen breakdown. Methanol was the test liquid and GN_2 was the pressurant.

Figure IV-38 shows the test system used for evaluating the bubble point of the screen liner by the liquid spray remote inspection technique. Methanol was periodically injected through the spray nozzle throughout the test to wet the screen liner. The bulk region was pressurized either continuously or stepwise with GN_2 . During the continuous pressurization test, the bubble point of the system was indicated by the peak in the pressure versus time curve, as shown in Fig. IV-39. In the stepwise pressurization tests, the bulk region was pressurized in increments. The system was sealed off after each pressurization for a period of five minutes. The bubble point was found when the pressure decayed during the lockup period, as shown in Fig. IV-40.

Results of the capillary system remote inspection tests are presented in Table IV-15. These results show that both the negative 1-g expulsion and liquid spray techniques are effective procedures for remotely determining the integrity of a capillary screen acquisition/expulsion system installed in the tank. The bubble points determined in tests 1 and 2, using the negative 1-g expulsion technique, compare favorably with those determined in the previously discussed acceptance tests. During test 3 with the negative 1-g expulsion, a significant drop in the bubble point of the 80 x 700-mesh Dutch-twill screen liner was detected. This result was checked using the liquid spray technique. As shown by the results of test 4, exact agreement between bubble points measured by the two techniques was obtained.

In conducting the remote liquid spray inspection tests, we found that the rate of pressurant inflow must be sufficient to exceed the leak rate of the system when the screen initially breaks down, and low enough to prevent a pressure rise after the initial breakdown. Repetitive, or reproducible, data were obtained with a GN_2 pressurant flow rate between 0.83 cc/s (0.05 in.³/s) and 1.67 cc/s (0.1 in.³/s) as shown by the results for tests 5 and 6 (Table IV-15). Pressurization at a higher flow rate produced general breakdown of the screen liner and yielded an erroneous bubble point (test 7). Stepwise pressurization with the spray inspection technique was used in test 8, producing results comparable to tests 5 and 6.

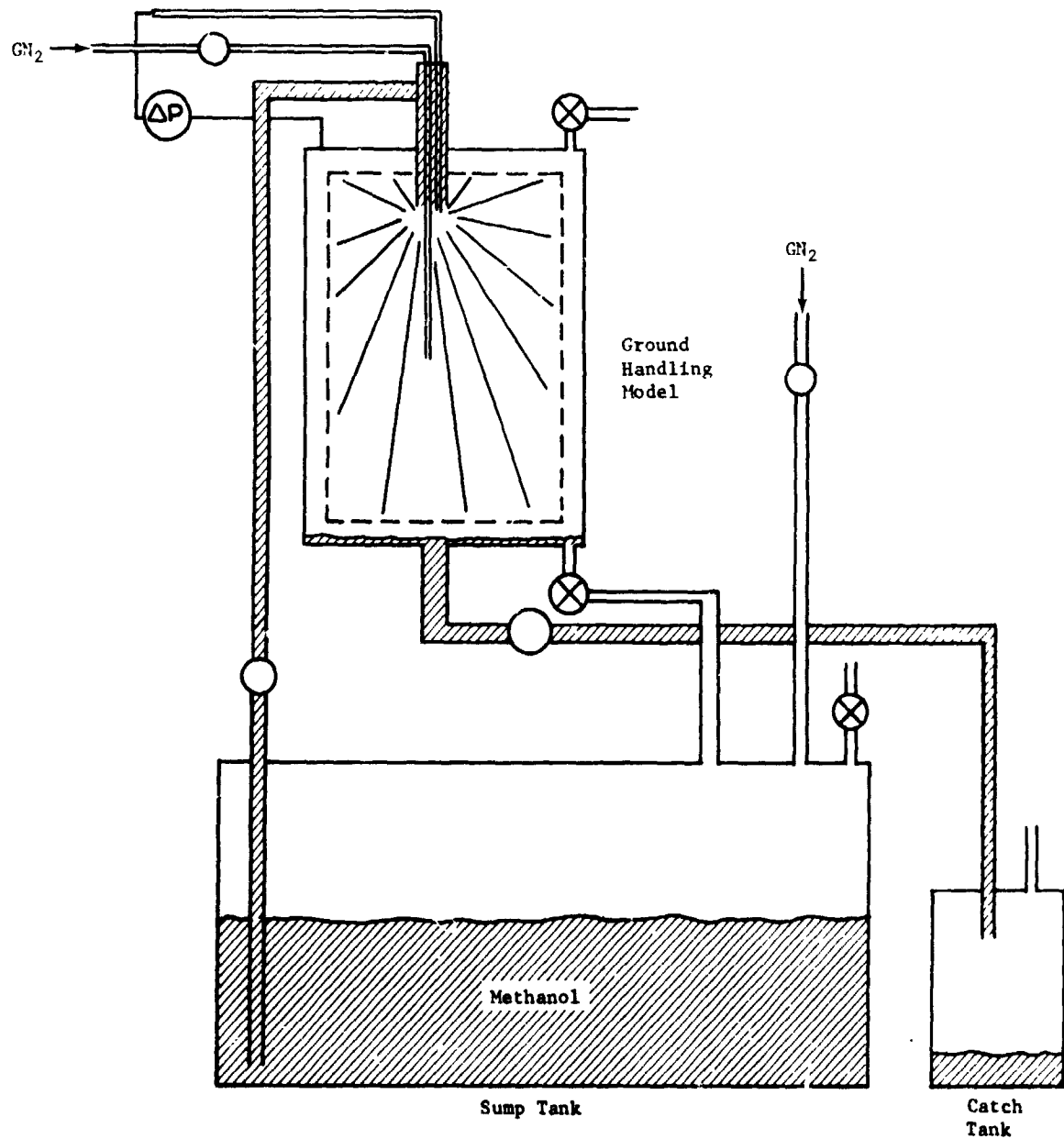


Fig. IV-38 Test System Schematic for Liquid Spray Remote Inspection Technique

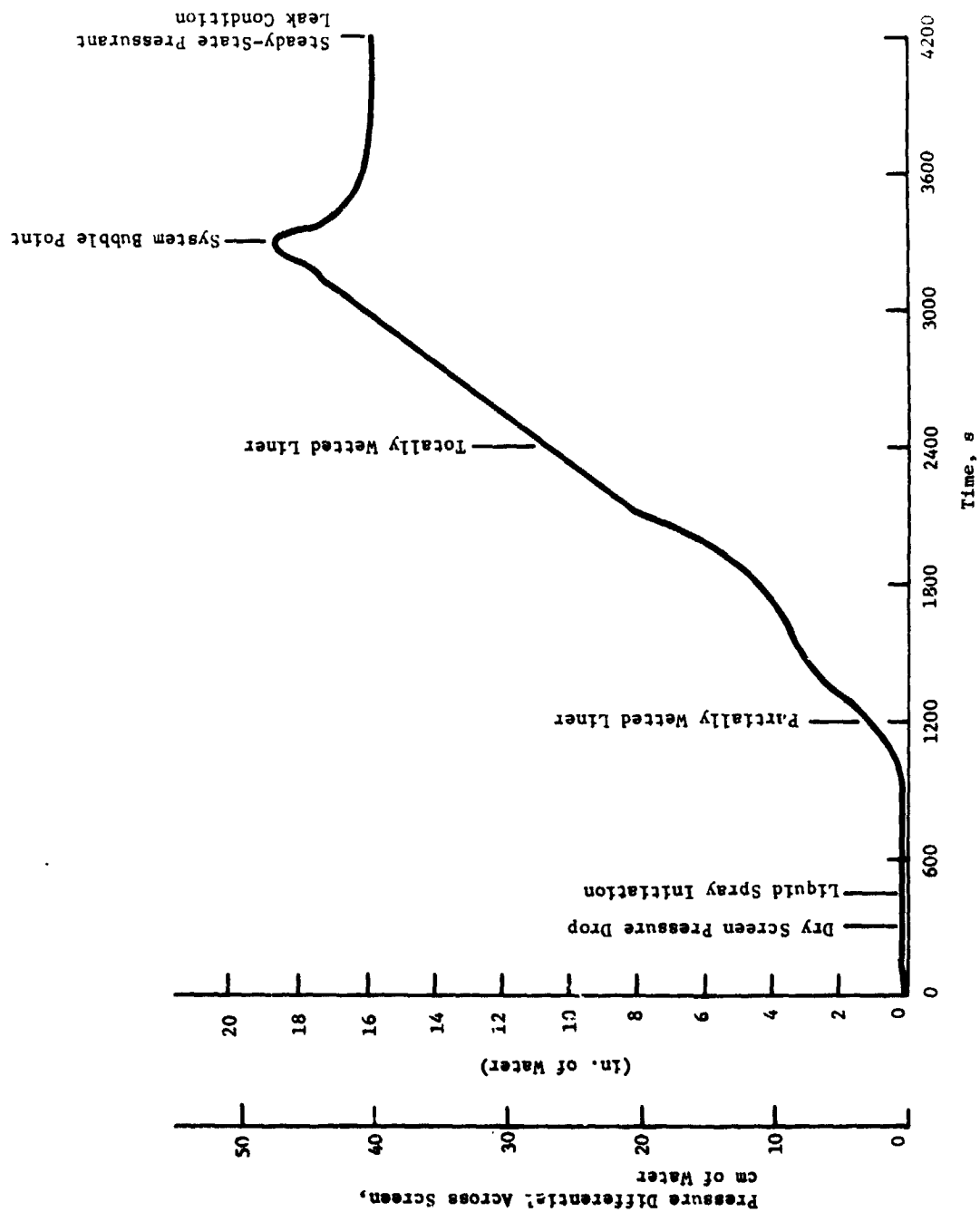


Fig. IV-39 Determination of System Integrity by Liquid Spray Remote Inspection Technique (Continuous Pressurization)

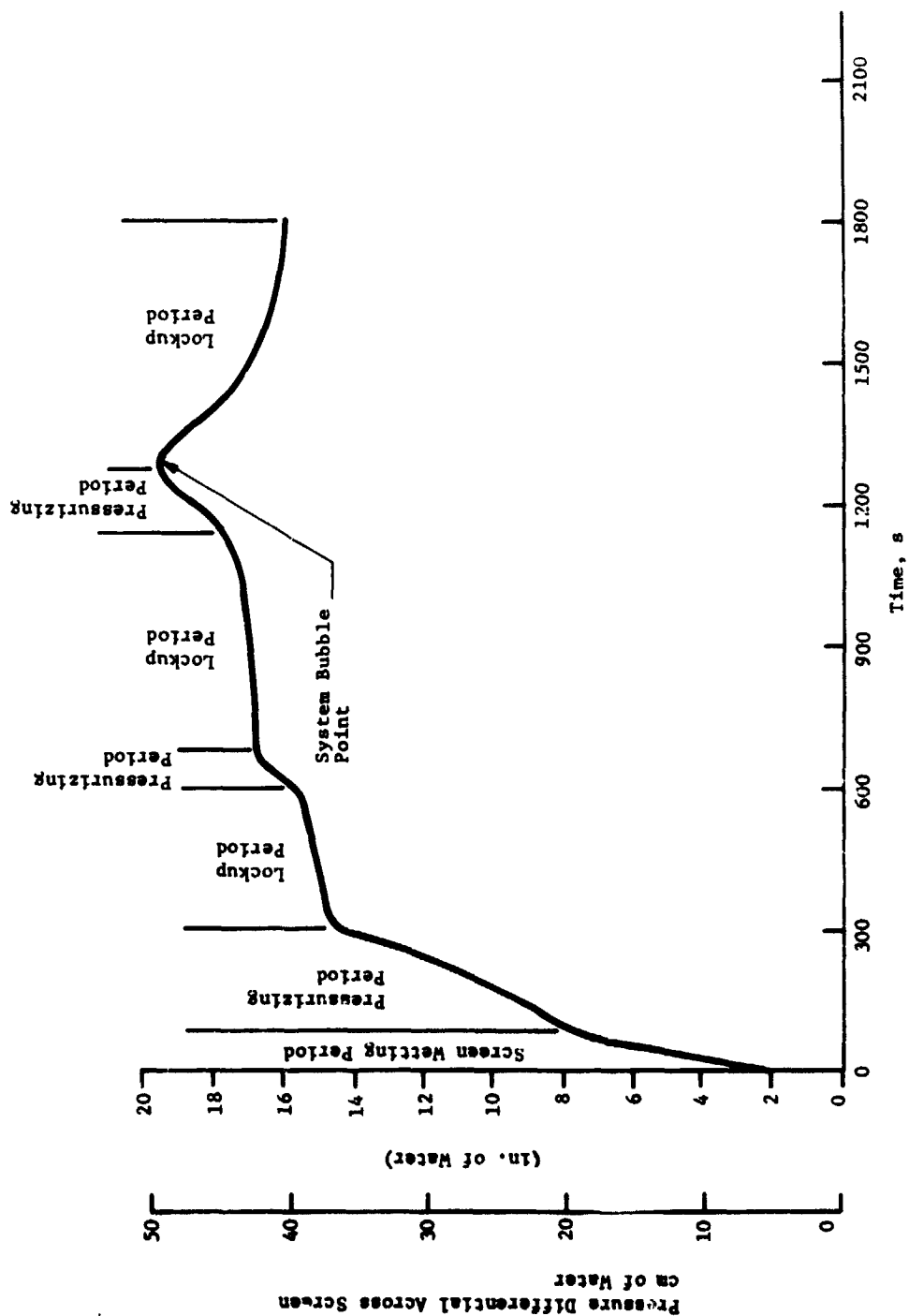


Fig. IV-40 Determination of System Integrity by Liquid Spray Remote Inspection Technique (Stepwise Pressurization)

Table IV-15 Remote Inspection Test Results

(a) Negative 1-g Expulsions

Test Number	Screen Liner	GN ₂ Flow Rate, cc/s (in. ³ /s)	Volume of Methanol Expelled, liters (in. ³)	Measured System Bubble Point, cm of H ₂ O (in. of H ₂ O)
1	250 x 1370	21.3 (1.3)	17.7 (1080)	54.1 (21.3)
2	80 x 700	35.0 (2.1)	10.5 (641)	16.2 (6.4)
3	80 x 700	64.3 (3.9)	5.2 (318)	9.2 (3.6)

(b) Liquid Spray Technique

Test Number	Screen Liner	Type of Pressurization	GN ₂ Flow Rate, cc/s (in. ³ /s)	Measured System Bubble Point, cm of H ₂ O (in. of H ₂ O)
4	80 x 700	Continuous	1.67 (0.1)	9.2 (3.6)
5	325 x 2300	Continuous	0.83 (0.05)	47.5 (18.7)
6	325 x 2300	Continuous	1.67 (0.1)	47.7 (18.8)
7	325 x 2300	Continuous	~16.7 (~1.0)	61.1 (24.1)
8	325 x 2300	Stepwise	1.67 (0.1)	49.5 (19.4)

Following the remote inspection demonstrations, tests were conducted to locate the breakdown areas in the screen liner. The interior of the liner was pressurized with GN₂ and the wetted liner was either totally or partially immersed in methanol, depending on the test to be run. The pressure differential across the screen at breakdown was measured. In both cases, the system was rotated to visually locate the breakdown points of the screen liner.

The data presented in Table IV-16 show that the procedures for pinpointing a leak in a capillary liquid retention device were successful, regardless of orientation. Care must be taken, however, to ensure that the entire liner remains wet when it is only partially submerged.

2. Trap Device Tests

A similar test program was accomplished to evaluate the effect of ground operations and demonstrate performance of the refillable trap capillary device. These tests were conducted under a Martin Marietta-sponsored research task, *Propellant Mass Gaging, Venting and Handling Technology* (Ref IV-3). Pertinent portions of that

study are presented here. The 15-in. diameter subscale trap device, fabricated as a part of the IR&D task, was used for the testing. The trap is shown installed in the foreshortened cylindrical test tank in Fig. IV-41.

Table IV-16 Location of Leak Points

Test	Screen Liner	Model Position	Pressurant Flow Rate	Pressure, cm of H ₂ O (in. of H ₂ O)	Location of Breakdown Points
1	325 x 2300	Vertical, Submerged	1.67 cc/s (0.1 in. ³ /s)	62 (24.4) 66 (26)	Local breakdown in the vicinity of the cylinder seam. General breakdown of the screen liner.
2	325 x 2300	Vertical, Submerged	0.83 cc/s (0.05 in. ³ /s) 1.67 cc/s (0.1 in. ³ /s)	22.8 (9) 53.4 (21) 61 (24)	Leak near upper seal ring. General breakdown of the screen liner. General breakdown of the screen liner.
3	325 x 2300	Horizontal, Submerged	0.83 cc/s (0.05 in. ³ /s)	27.8 (9) 52 (20.5)	Gas leak from upper seal ring. General breakdown during tank rotation.
4	325 x 2300	Vertical upright, Partially Submerged Vertical Inverted, Partially Submerged Horizontal	1.67 to 0.83 cc/s (0.1 to 0.05 in. ³ /s) 1.67 to 0.83 cc/s (0.1 to 0.05 in. ³ /s) 1.67 cc/s (0.1 in. ³ /s)	59.5 (23.5) 27.4 (10.8) 64 (25.2)	12 leaks visible. Top seal leakage. General breakdown.

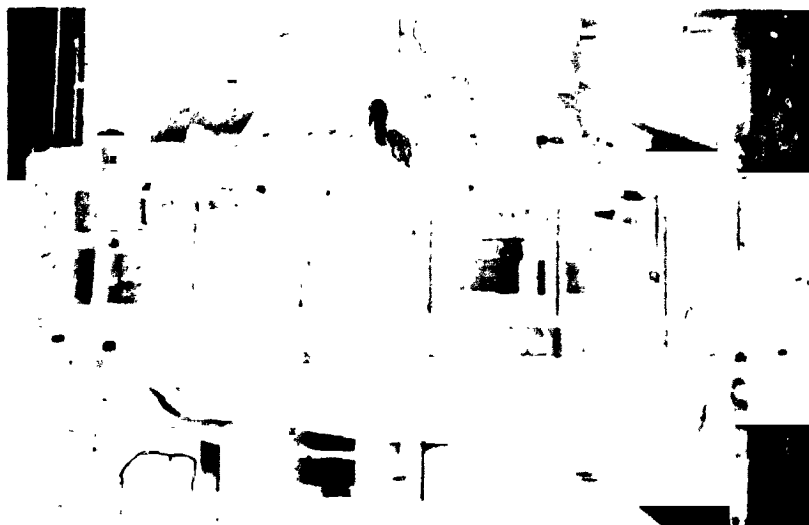


Fig. IV-41 Refillable Trap System Installed in Foreshortened Cylinder Test Tank

The test apparatus for the subscale trap included a fill/catch tank, a four-way control valve, several shutoff valves, a pressure regulator, and a pressurant supply. Transparent plexiglass tanks and Tygon tubing were used to allow visual observation of performance and recording on motion picture film. The fill/catch tank shown in Fig. IV-42 had a liquid outlet at both ends. During the trap filling process, the fill/catch tank was positioned so the ullage was pressurized by bubbling the pressurant through the liquid reservoir, as shown schematically in Fig. IV-43. The fill/catch tank was inverted and the pressurization port in the ullage was vented during the expulsion of liquid from the trap, as shown in Fig. IV-44. The shutoff valves isolated the fill/catch tank from the pressurization system and liquid feedlines during these manipulations. The four-way valve simultaneously directed the pressurization and venting for both the model tank and the fill/catch tank. The pressure regulator controlled the pressure level in the fill/catch tank during the fill mode and in the model tank during the expel mode. Nitrogen gas was used as the pressurant and methanol was used as the test fluid.



Fig. IV-42 Transparent Fill/Catch Tank

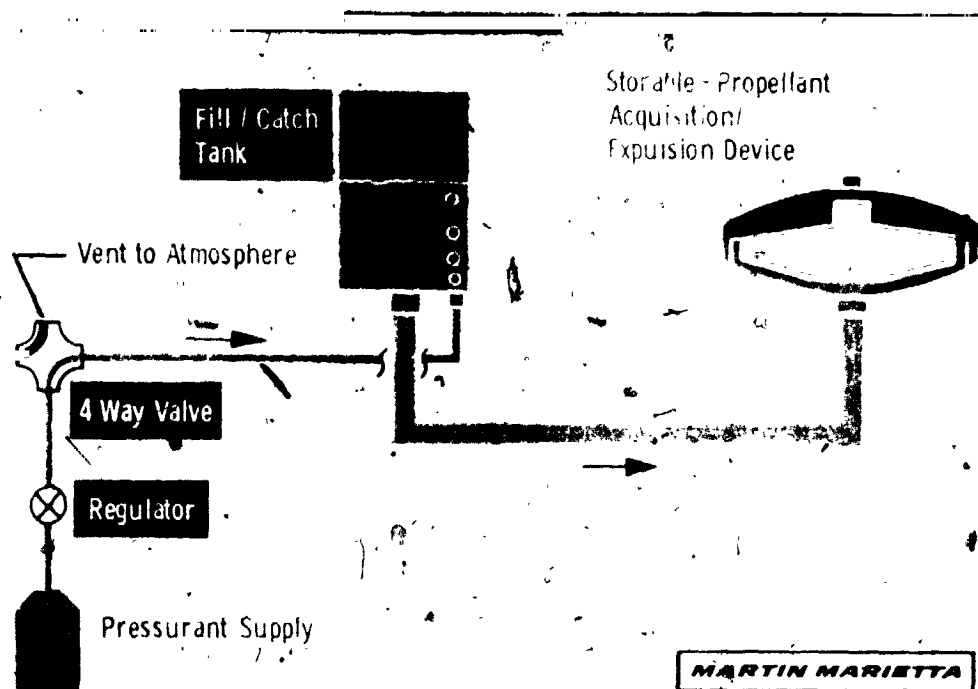


Fig. IV-43 Fill Mode Schematic

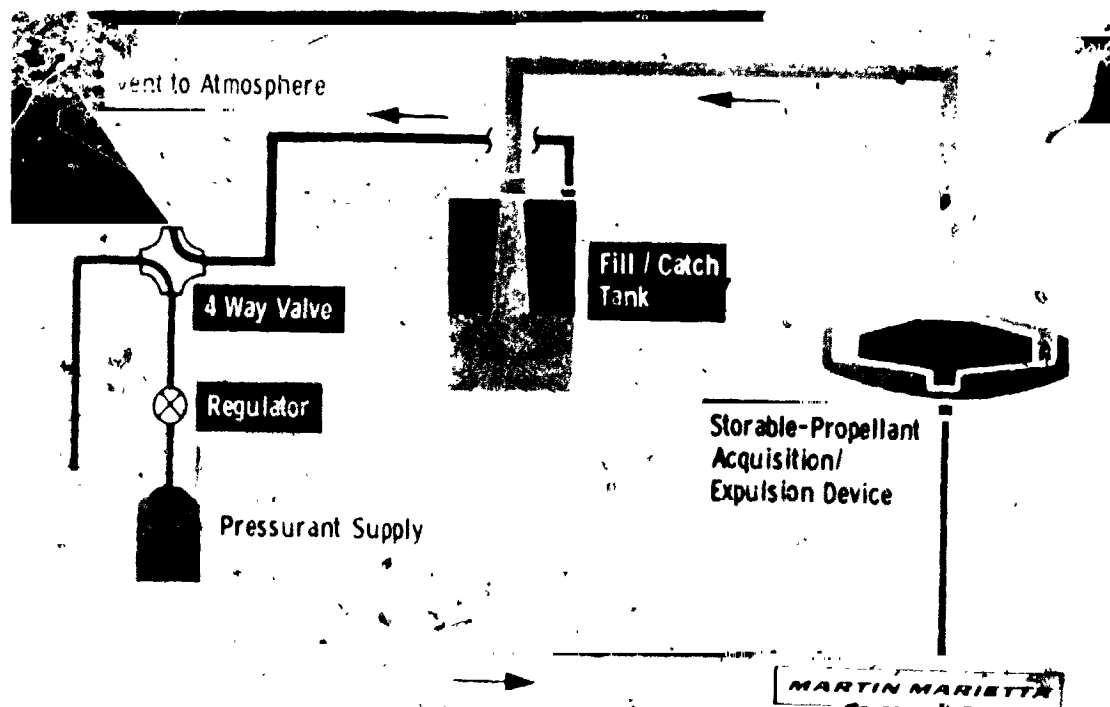


Fig. IV-44 Expel Mode Schematic

Loading of the subscale trap model was demonstrated, as shown in Fig. IV-45. The model tank ullage was vented to the atmosphere while the device, in the plus 1-g orientation (model tank vertical), was filled from the pressurized fill/catch tank (Fig. IV-43). Complete filling of the device was attained. After the device was filled, it was rotated from vertical to horizontal, and then inverted, to demonstrate that the device would not lose any liquid while being handled.

Functional tests of the type that would be accomplished during an acceptance test were demonstrated. The device was configured in both minus 1-g (model tank inverted as in Fig. IV-46) and lateral 1-g (model tank horizontal as in Fig. IV-47) positions. In both cases, gas-free liquid was expelled in this worst-case acceleration environment; minus 1-g and lateral 1-g expulsions are shown in Fig. IV-48 and IV-49, respectively. These tests demonstrated that the coverplate can properly retain the liquid and the annulus can maintain a supply of gas-free liquid to the tank outlet. By reorienting the model tank from inverted to vertical, with the reservoir of the trap nearly empty of liquid, refill of the device during outflow was demonstrated. Gas was purged through the vent tube and the reservoir of the trap refilled, as would occur during an engine burn (Fig. IV-50).

3. Conclusions

Procedures and techniques are available for handling and inspection. The most appropriate test depends on the design, desired performance, and size of the device. Well-established tests, such as bubble point and gas-free expulsion modified for remote monitoring and nonvisual evaluation, are applicable to these reusable systems. The characteristics of barrier breakdown are detectable with conventional instrumentation in available ranges of sensitivity so no new hardware developments or research of capillary behavior are necessary to support these applications of capillary propellant management systems. Ground handling performance is predictable and should present few, if any, constraints on normal ground operations.

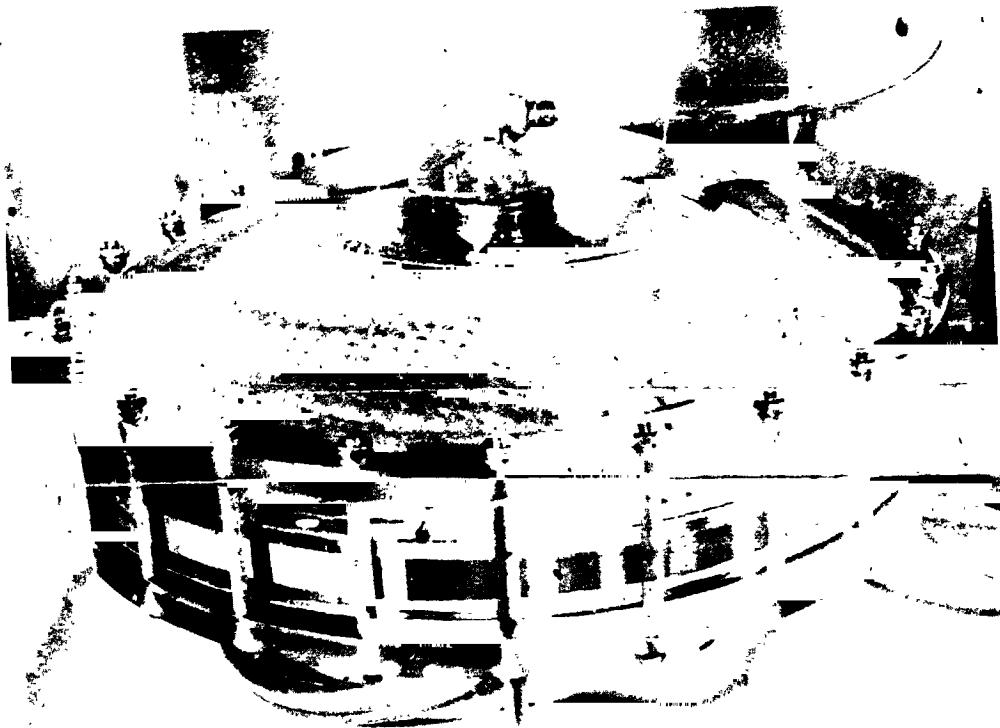


Fig. IV-45 Completion of Device/Tank Fill Operation

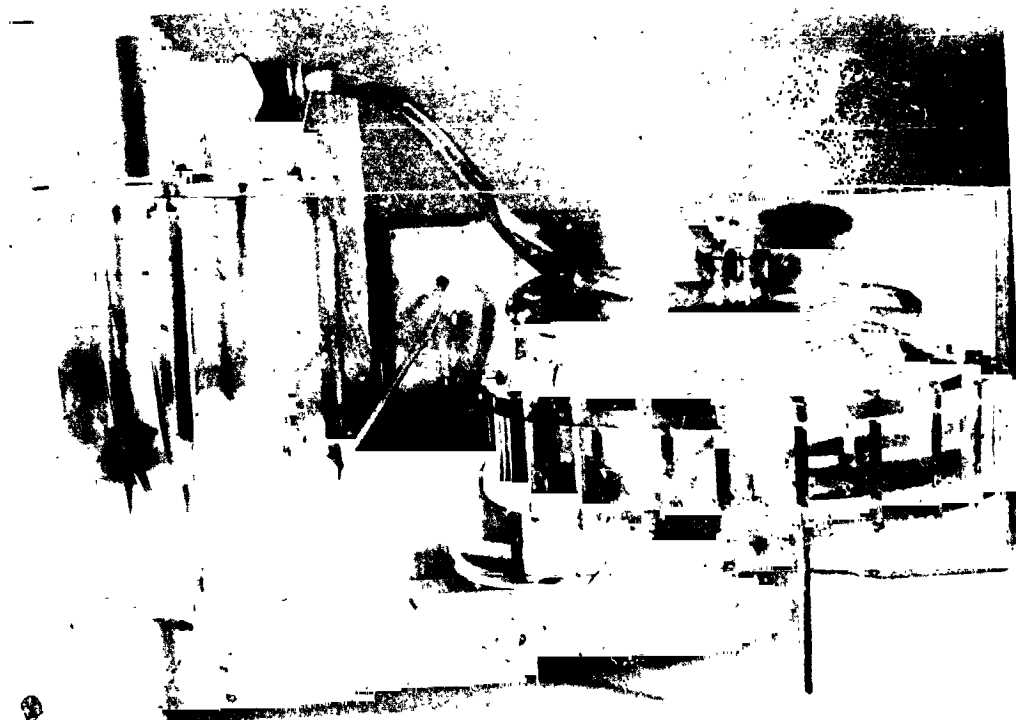


Fig. IV-46 Minus 1-g Test Configuration

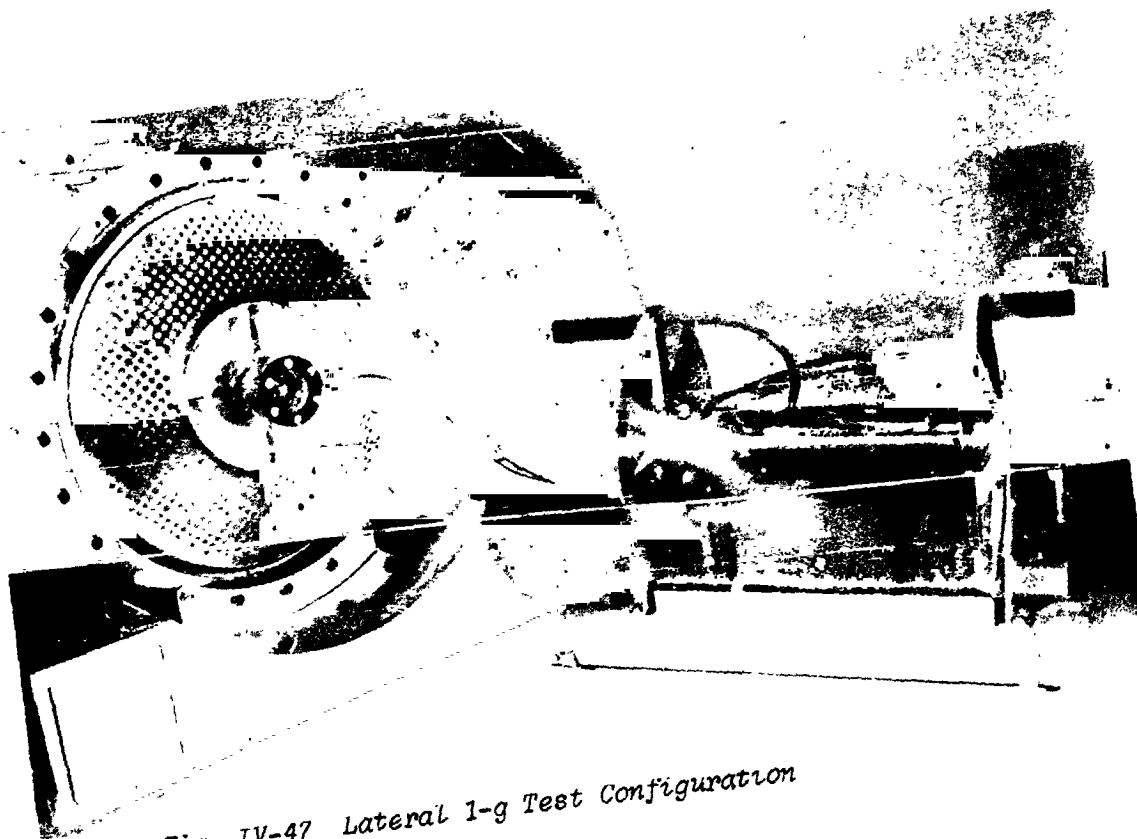
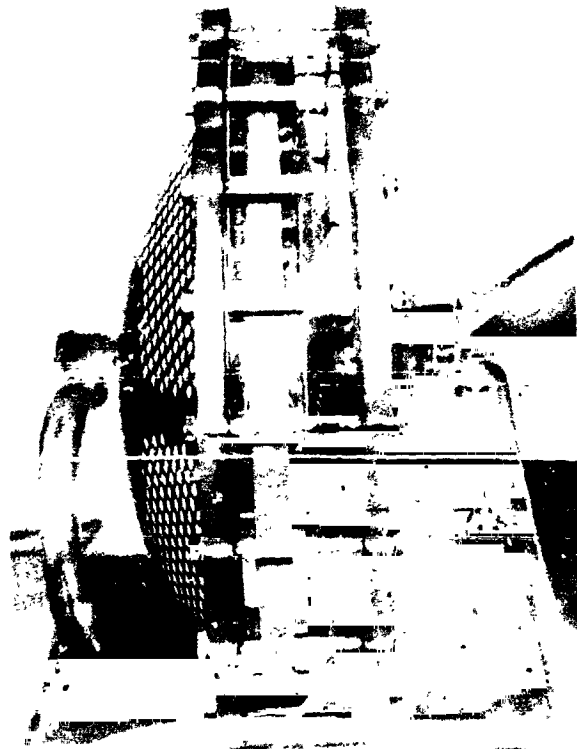


Fig. IV-47 Lateral 1-g Test Configuration



Fig. IV-48 Gas-Free Liquid Expulsion under minus 1-g

IV-85



*Fig. IV-49 Gas-Free Liquid Expulsion
under Lateral 1-g*



*Fig. IV-50 Trap Refill Operation Showing Gas Purging
through Vent Tube*

V. REPRESENTATIVE SYSTEM DESIGNS

Two representative designs for the surface tension devices selected in Chapter III are presented in this chapter. The first is a refillable trap design, and the second is a nonrefillable, enlarged trap. The basic configuration of the refillable trap remains the same for both the fuel and oxidizer tank, but the size of the holes in the vent tube differ, being larger for the fuel. The enlarged trap was designed so the same device could be used in either the fuel or oxidizer tank. The primary purpose of these designs is to show the fabrication details of the devices. The two designs were analyzed from the standpoint of weight, structure, reliability, fabrication, handling, and flight operation. Further analysis of the fluid mechanics and structure would be required before fabrication. These representative designs were used to provide details on performance, flight operation, test, and turnaround procedures. The mission criteria presented in Chapter II, including the specific information of Table II-1, were used in the designs. These designs are representative of the system which would result due to any of the variations in the design criteria specified in Chapter II, i.e., other propellant combinations, tank sizes, etc.

A. REFILLABLE TRAP

The first representative design is a compact refillable trap (Fig. V-1). This system is preferred if the typical missions presented in Chapter II represent the actual missions, with only small variations in number of burns and burn durations.

1. Performance

Table V-1 summarizes the important parameters for this refillable trap design. Both expulsion efficiency and volumetric efficiency are very high, and the device is lightweight.

a. Reservoir Volume - A worst-case condition was used to size the trap volume. The propellant settle time prior to the last burn is the longest. A settle time of 11 s was calculated based on the remaining liquid in the tank being oriented away from the outlet and a single OMS engine operating. A volume of 0.042 m^3 (1.49 ft^3) of liquid would be required to operate the engine during that period of time. To provide an operating margin and the capability to accomplish some short-duration burns, an additional 0.023 m^3 (0.8 ft^3) of volume was added to the basic trap volume. A total reservoir volume of 0.065 m^3 (2.3 ft^3) was obtained, which applies to both the N_2O_4 and MMH tank since their volumetric flow rates are the same.

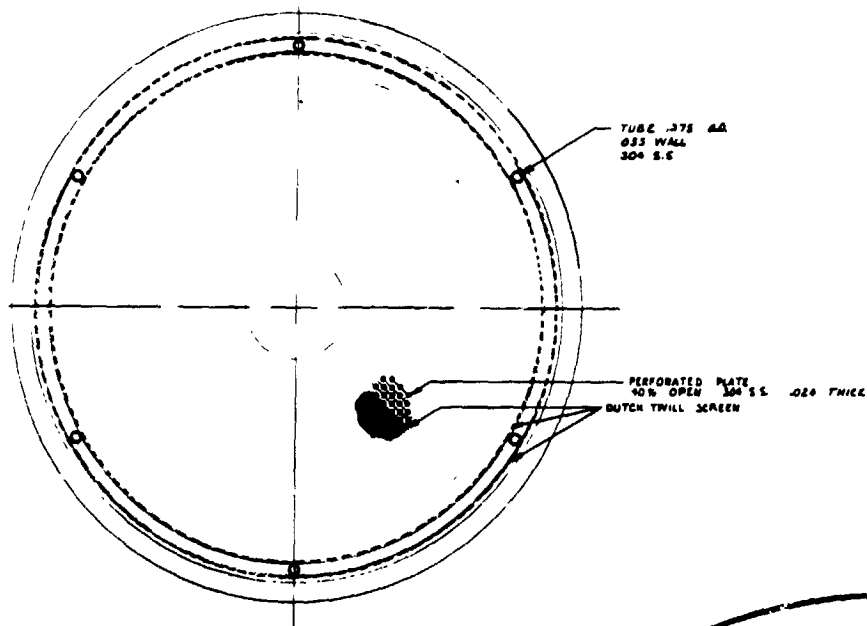
Table V-1 Refillable Trap Parameters

Trap Volume 0.065 m ³ (2.3 ft ³)
Expulsion Efficiency 99.9%
Volumetric Efficiency 99.98%
Material - Stainless Steel
Weight
Device 4.94 kg (10.9 lbm)
Device plus residual (N ₂ O ₄), 9.0 kg (19.9 lbm)
Foraminous Material
Annulus - 200 x 1400 Dutch-twill screen supported with perforated plate
Coverplate - 200 x 1400 Dutch-twill screen supported with perforated plate
Vent Tube - Double perforated plate
Fuel, 2-mm (0.080-in.) diameter holes
Oxidizer, 1-mm (0.040-in.) diameter holes

The additional trap volume could be used to accomplish additional short-duration burns totaling 6 s between complete refills. For example, six 1-s burns or two 3-s burns could be accomplished. Following every complete refill another 6 s of burn time would be available. If it is assumed that refill will be complete in approximately 16 s, this trap could accomplish any number of burns with a duration greater than 16 s, plus the additional 6-s burn time discussed above.

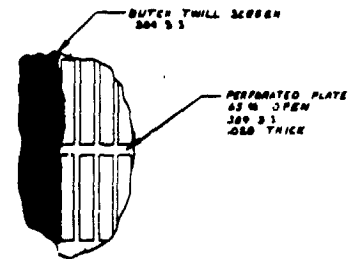
From the standpoint of flight performance, the reservoir sizing is very conservative. A typical OMS would probably have two independent engines. The settling acceleration would then be twice the value used to size the reservoir, while the flow rate of propellant to the engine remains the same. Doubling the acceleration reduces the settle time by about 30% so an additional 30% of propellant is available in the trap when both engines are operating. Also, the settle time is shorter for the burns prior to the last burn (the last burn being the one used to size the reservoir). Unless there is a large offload, the settle time for the first burn could be zero. In addition, the settling calculations are based on the assumption that the liquid is initially oriented away from the device, while it could just as well be in contact with the device.

FOLDOUT FRAME



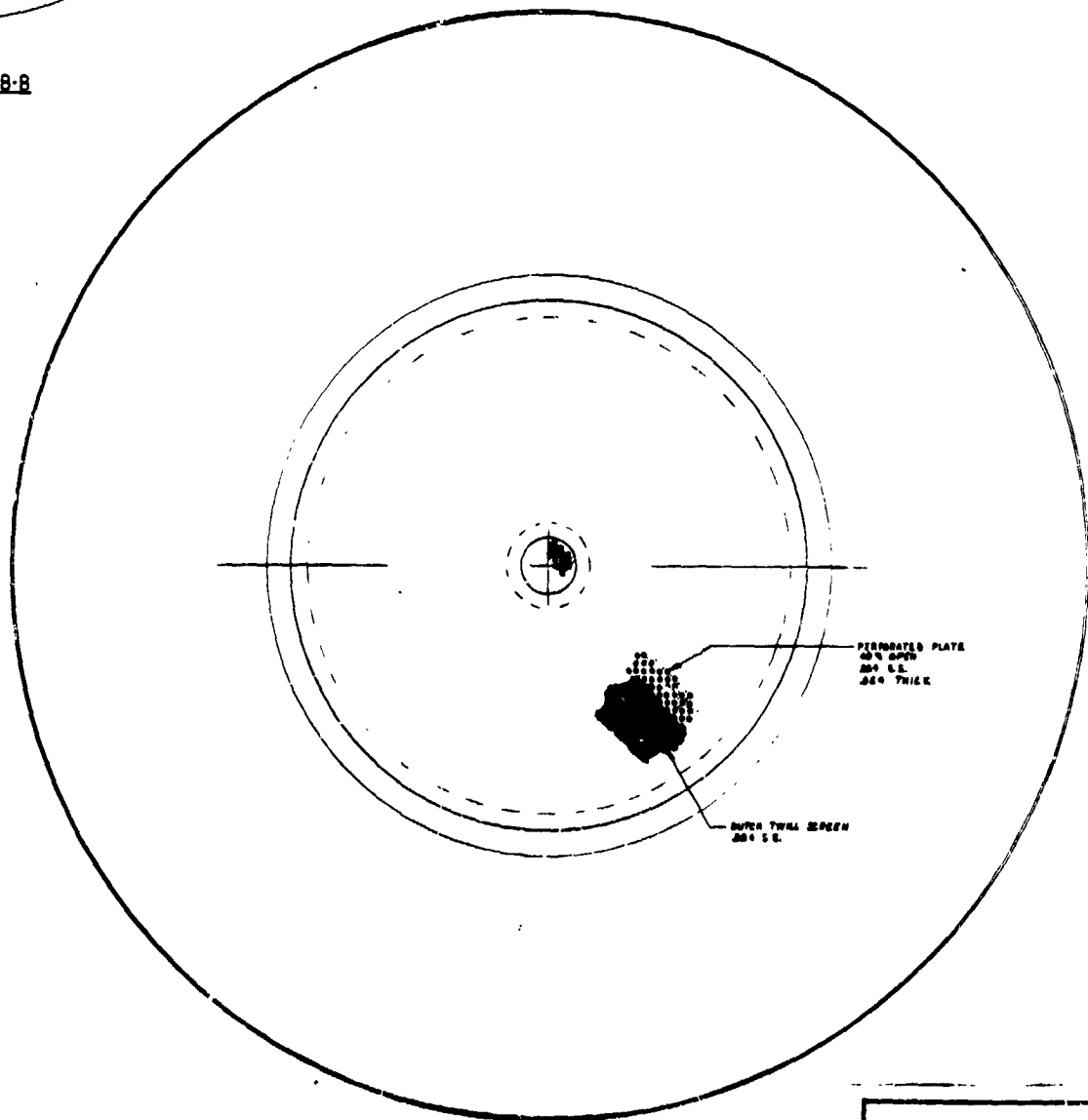
SECTION B-B

scale 1/2



DETAIL 'E'

scale 1/1

PERFORATED PLATE
TO BE TACK WELDED
TO CHANNEL


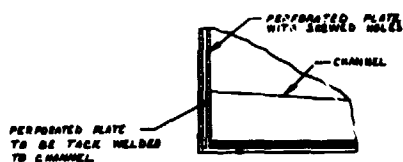
SECTION A-A

scale 1/2

Note: All dimensions
to obtain centi
multiply by 2.54

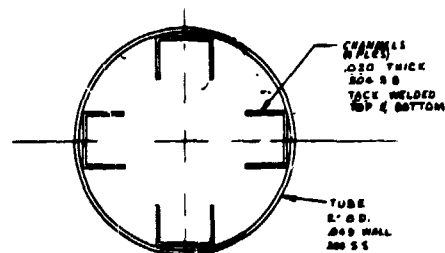
FOLDOUT FRAME

2



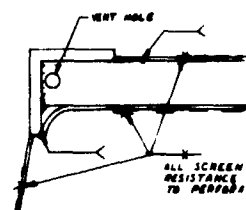
DETAIL 'F'

scale 4/1



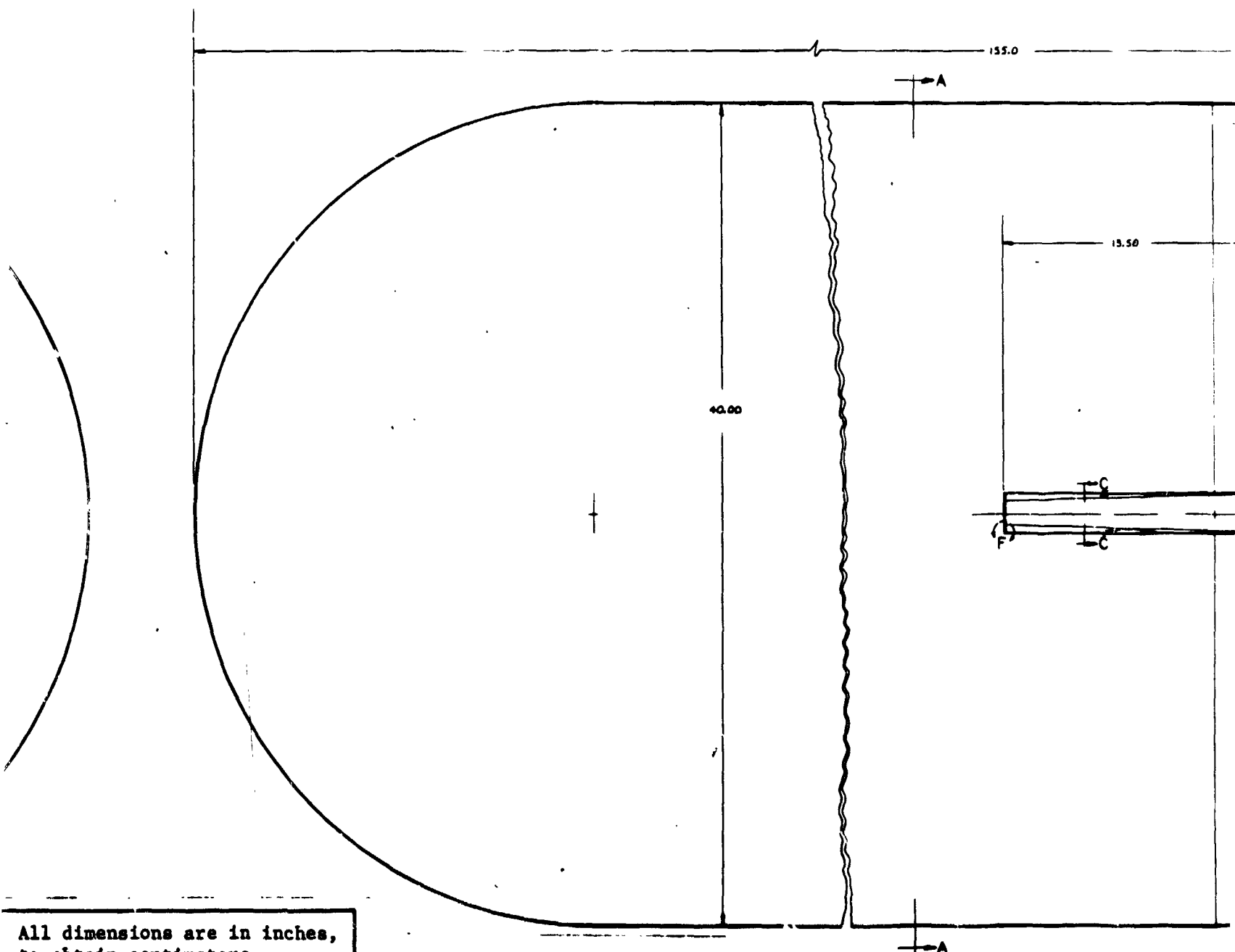
SECTION C-C

scale 4/1



DETAIL 'D'

scale 2/1



All dimensions are in inches,
to obtain centimeters
multiply by 2.54.

FOLDOUT FRAME 3

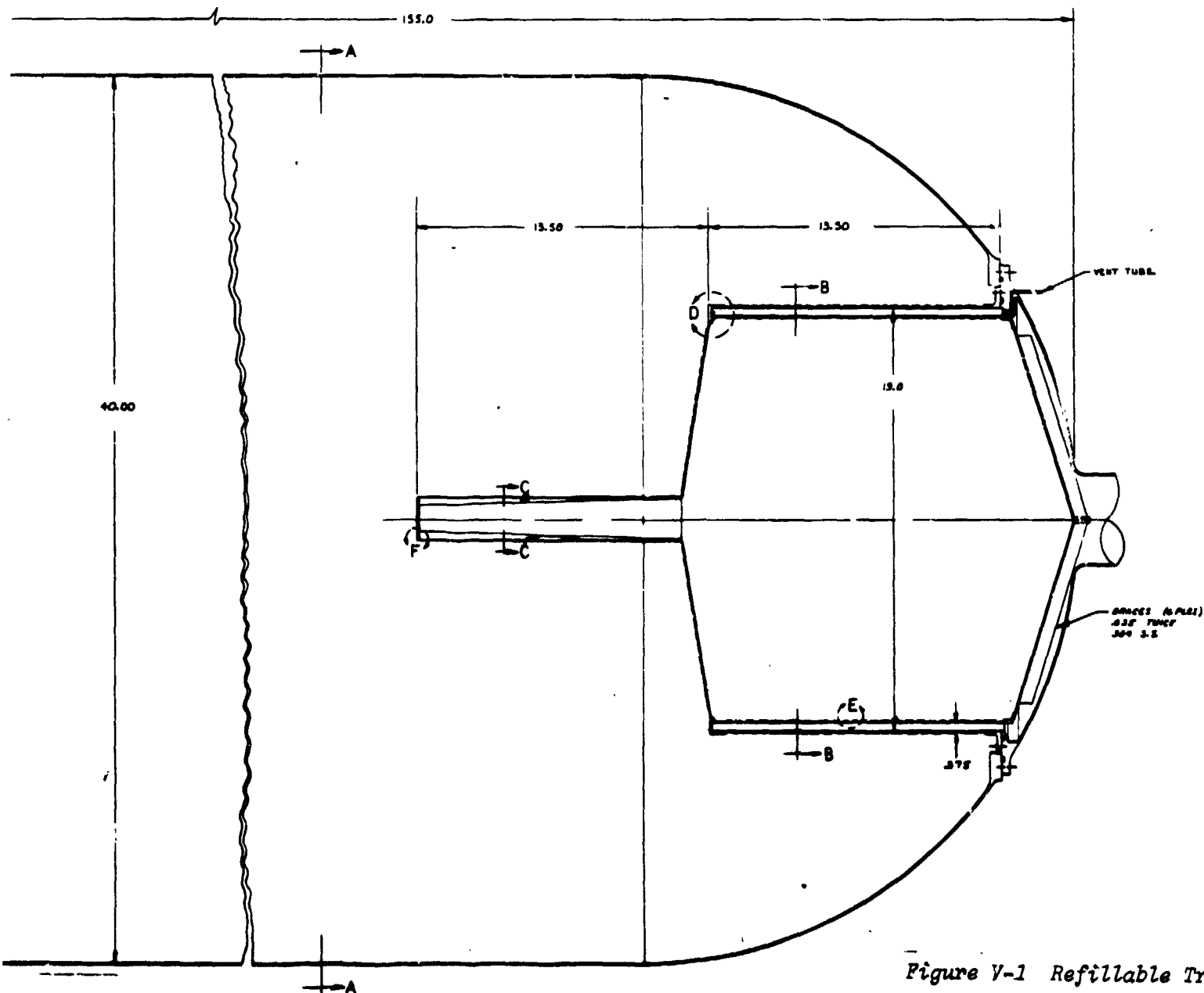
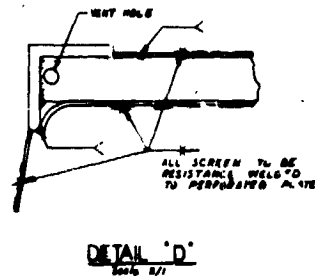
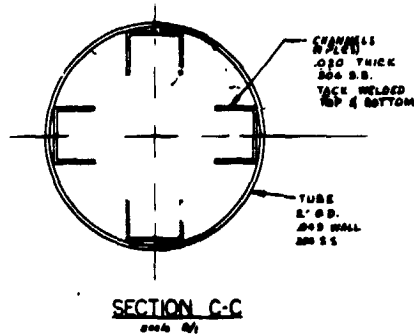


Figure V-1 Refillable Trap

V-3 and V-4

b. *Annulus and Coverplate* - A 200 x 1400-mesh Dutch-twill screen forms the annulus of the device. This screen provides sufficient margin over the maximum pressure losses that occur within the annulus to maintain a gas-free supply of liquid to the engine under all operating conditions. The same screen mesh is used on the coverplate. Both the coverplate and annulus will remain stable when the maximum adverse axial and lateral accelerations are acting on the system.

By using the 200 x 1400-mesh screen, the annulus and coverplate are designed with a safety factor greater than two, as applied to the device for the oxidizer tank. Since the oxidizer, N_2O_4 , imposes the worst case (it has the lower surface tension) and the same screen is being used for the fuel tank device, an even greater design safety factor is applied to the fuel tank device. This overdesign has a negligible effect on refill of the reservoir but significantly improves the stability of the device under the effects of adverse accelerations and vibrations.

c. *Vent Tube* - To make the device refillable, the geometry of the trap must be based on the magnitude of the adverse lateral acceleration and axial settling acceleration, as discussed in Chapter III. For the acceleration environment considered, a vent tube located on the coverplate of the trap provides an efficient means of obtaining the proper geometry. Under the axial settling acceleration, the height of the vent tube increases the hydrostatic head acting at the capillary barrier located on top of the tube. The diameter of the trap was kept as small as possible to reduce the hydrostatic heads imposed by the lateral accelerations.

Double perforated plate is used at the top of the vent tube. The holes in the plate are sized to allow breakdown under the minimum axial vehicle acceleration produced with one OMS engine operating. The vent tube will remain unstable and allow the reservoir region to fill until the liquid level reaches the base of the vent tube. At that point the perforated plate on the vent tube becomes stable and no further filling is possible. The size of the holes in the perforated plate for the oxidizer tank device are different than those of the fuel tank device because the surface tensions of the two propellants are different. In this case, overdesign would degrade the ability of the device to refill. Perforated plate is used in lieu of screen material because the plate will provide a much more uniform and predictable bubble point at the pore sizes required.

Double plate is used to keep this capillary barrier wetted. A reservoir is formed between the plates that remains full of liquid. The holes in the plates are offset so there is no direct path through the two plates. Wicking channels were added to the inside of the vent tube to bring additional liquid from the trap reservoir region to the perforated plate under low-g conditions. This insures that the plate will remain wetted. This device would permit offloads as large as 95%. At that fill level, the tank would be filled to the top of the coverplate of the trap.

2. Fabrication

a. *Material Selection* - Based on the material compatibility discussion presented in Chapter II, Table V-2 presents acceptable surface tension device materials for various tankage materials.

The most desirable screen material would be the same as the tank material. However, in many cases the screen material is not available in the mesh size required by the device design. The availability of screen mesh usually determines which screen material, and therefore which metal, will be used for the device. Based strictly on material compatibility considerations, the differences in using any of the screen materials with any of the tank materials listed in Table V-2 are very minor.

For the representative trap design presented, stainless steel was selected as the material of construction. A typical tank material for an OMS application would be titanium, but titanium screen is not available in a fine enough mesh. Either stainless steel or aluminum are applicable as trap materials, since both of these materials are manufactured in a 200 x 1400-mesh Dutch twill. Because of greater screen fabrication experience with stainless steel than with aluminum, stainless steel was chosen.

Table V-2 *Material Selection*

Tank Material	Screen Material		
	1st Choice	2nd Choice	3rd Choice
Titanium	Titanium	Stainless Steel	Aluminum
Stainless Steel	Stainless Steel	Titanium	Aluminum
Aluminum	Aluminum	Stainless Steel	Titanium

b. *Structural Design* - Structurally the device must permit modular installation and be capable of withstanding the loads imposed throughout the mission. Reusability of the device for up to 500 missions, including the effects of transportation and handling, must also be considered in the structural design. A conservative approach was taken to provide a structurally sound and durable design.

An access cover on which the trap device is mounted was added to the bottom of the tank. The access cover diameter must be considered in establishing the geometry of the device. As the access cover diameter is increased, the tank weight increases because of the flanges. A practical limit is reached when the access cover diameter is approximately one-half the tank diameter. The device is bolted to the access cover and the cover is easily attached to the tank, as described later in this section.

The basic structure of the annulus is two concentric, perforated plate cylinders reinforced with tubes located in the annulus gap. The addition of support rings allows the trap structure to withstand the vibration and high-g levels encountered during boost, reentry, and landing. The screen material is attached to the outer surface of the perforated plate. The plate provides added structural support for the screen.

Perforated plate was also used in the coverplate. A conical shape coverplate was used to improve the rigidity and reduce the effect of settled liquid impacting the device. Even with these conservative approaches, the device was relatively lightweight.

a. *Assembly* - The assembly procedure for the trap device is as follows:

- 1) Weld perforated plate to top cap of vent tube;
- 2) Tack-weld wicking channels to vent tube cap and perforated plate;
- 3) Weld vent tube cap to vent tube;
- 4) Tack-weld wicking channels to bottom of vent tube;
- 5) Resistance-weld screen to upper perforated plate coverplate;
- 6) Weld antivortex baffles to lower coverplate;
- 7) Resistance-weld screen to lower coverplate;

- 8) Weld support tubes to upper and lower coverplate support rings;
- 9) Tack-weld both the outer and inner annulus perforated plates to support tubes, and weld plates to coverplate support rings;
- 10) Resistance-weld screen to both outer and inner annulus plates;
- 11) Weld upper and lower coverplates to support rings;
- 12) Weld completed vent tube assembly to upper coverplate.

After each fabrication step involving the screen, bubble point tests would be conducted to guarantee the pressure retention capability of the trap.

Welding was selected as the only joining method to be used for assembly. This method was chosen because it is the only proven state-of-the-art technique for fabricating propellant acquisition screen systems. Although other joining methods such as brazing, soldering, etc are applicable for some screen systems, they have not received as much development work and therefore were not specified.

An example of the successful use of the all-welded joining method was in the fabrication of the subscale trap discussed in Chapter IV. The fabrication techniques used for that model and the trap presented here are very similar.

A subscale model was fabricated from stainless steel under a separate corporation-sponsored task (Ref V-1). Detailed manufacturing and assembly processes such as resistance seam welding and repair of an enlarged screen port were demonstrated. Checkout procedures, including bubble point checks of subassemblies, were performed. The following paragraphs summarize the fabrication and assembly processes for the subscale model.

The flat patterns of the upper and lower perforated cone barriers are shown in Fig. V-2. Fine-mesh stainless steel screen was welded to the perforated plate. This welding of the screen to the flat pattern of the lower capillary barrier is shown in Fig. V-3.



Fig. V-2 Upper and Lower Perforated Cone Barriers

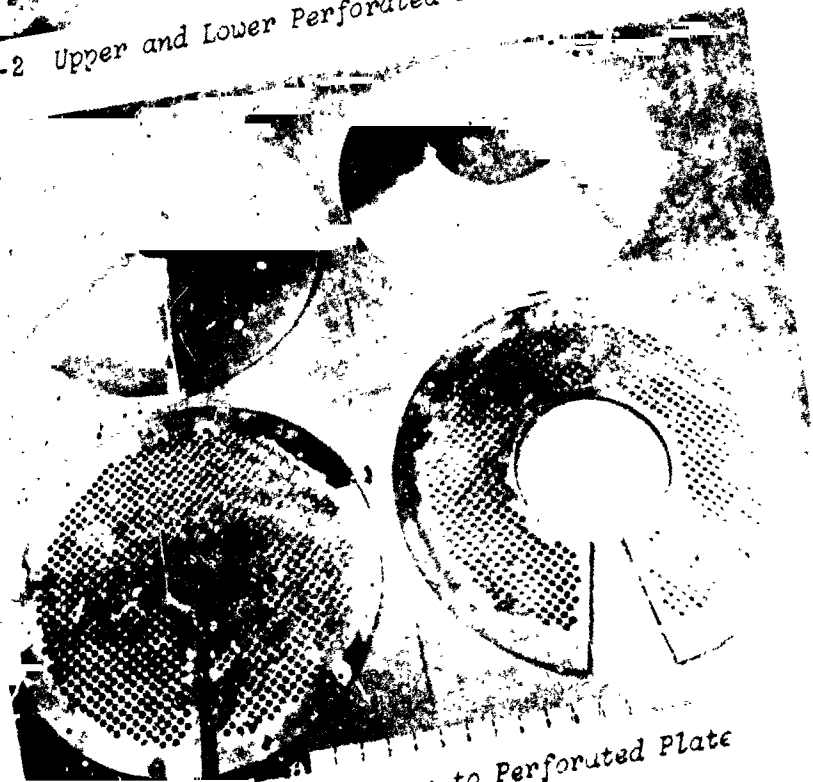


Fig. V-3 Welding of Screen to Perforated Plate

A lip-forming operation was performed after the screen was welded to the flat pattern and after the cones were closed and seam-welded. The cone barriers were trimmed to the desired diameter in their rim lip bending dies. In production, special tooling would be designed to provide the necessary rigidity for the trim operation. A completed lower cone barrier detail ready for bubble point testing is shown in Fig. V-4 (plastic covering is for protection during storage).

The welded outlet assembly is shown in Fig. V-5. The outlet plate was welded to the ring around the pin. The antivortex vanes were skip-arc-welded to reduce distortion and the support tube was resistance-welded from the plate bottom using quarter chills and a chill ring on top. The bottom plate required stress relief (annealing) under a flattening load to alleviate ripples introduced during welding. The support tube and outlet assembly were tungsten-inert-gas (TIG)-welded to the lower cone barrier, as shown in Fig. V-6. Heat was applied from the side opposite the screen with an aluminum chill ring used around the support tube.

The inner and outer perforated side rings before screen attachment are shown in Fig. V-7. Screen material is attached to side rings with tack welds for positioning, followed with resistance welds (overlapping spots) to provide a seal between the rings and screens. Figure V-8 shows the mounting, fixturing, and automatic welding equipment used to weld the lower cone barrier subassembly. The weld sequence was (1) weld inner ring to upper cone barrier, (2) weld inner ring to lower cone barrier, and (3) weld outer ring to upper cone barrier.

Figure V-9 shows the mounting, fixturing, and automatic welding equipment used to automatically weld the vent tube perforated cap to the vent tube (outside) and support tube (inside). The weld sequence was (1) weld the perforated cap to the vent tube, and (2) weld the perforated cap to the support tube.

A top view of the trap with the small vent hole screens attached is shown in Fig. V-10. The screens were welded to the land area along the outer rim. Figure V-11 shows the completed subscale OMS trap from a direct side view where both upper and lower cone barriers are shown.



Fig. V-4 Lower Cone Barrier Ready for Bubble Point Testing



1 2 3 4 5 6 7 8 9

Fig. V-5 Welded Outlet Assembly

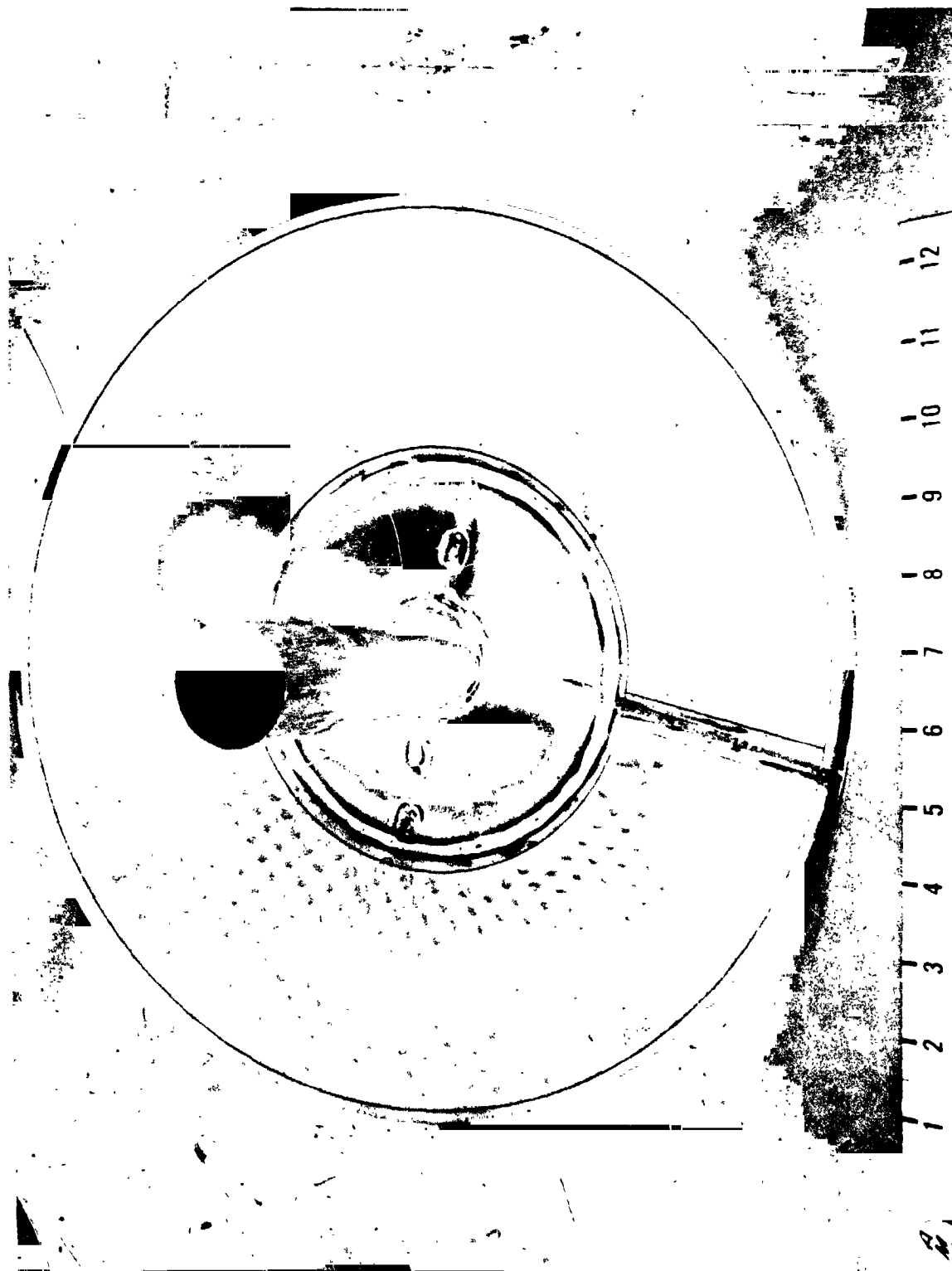


Fig. V-6 Lower Cone Barrier Showing Support Tube/Outlet Assembly



Fig. V-7 Inner and Outer Perforated Side Rings



Fig. V-8 Welding the Lower Cone Barrier Subassembly to the
Inner Ring/Upper Cone Barrier Subassembly

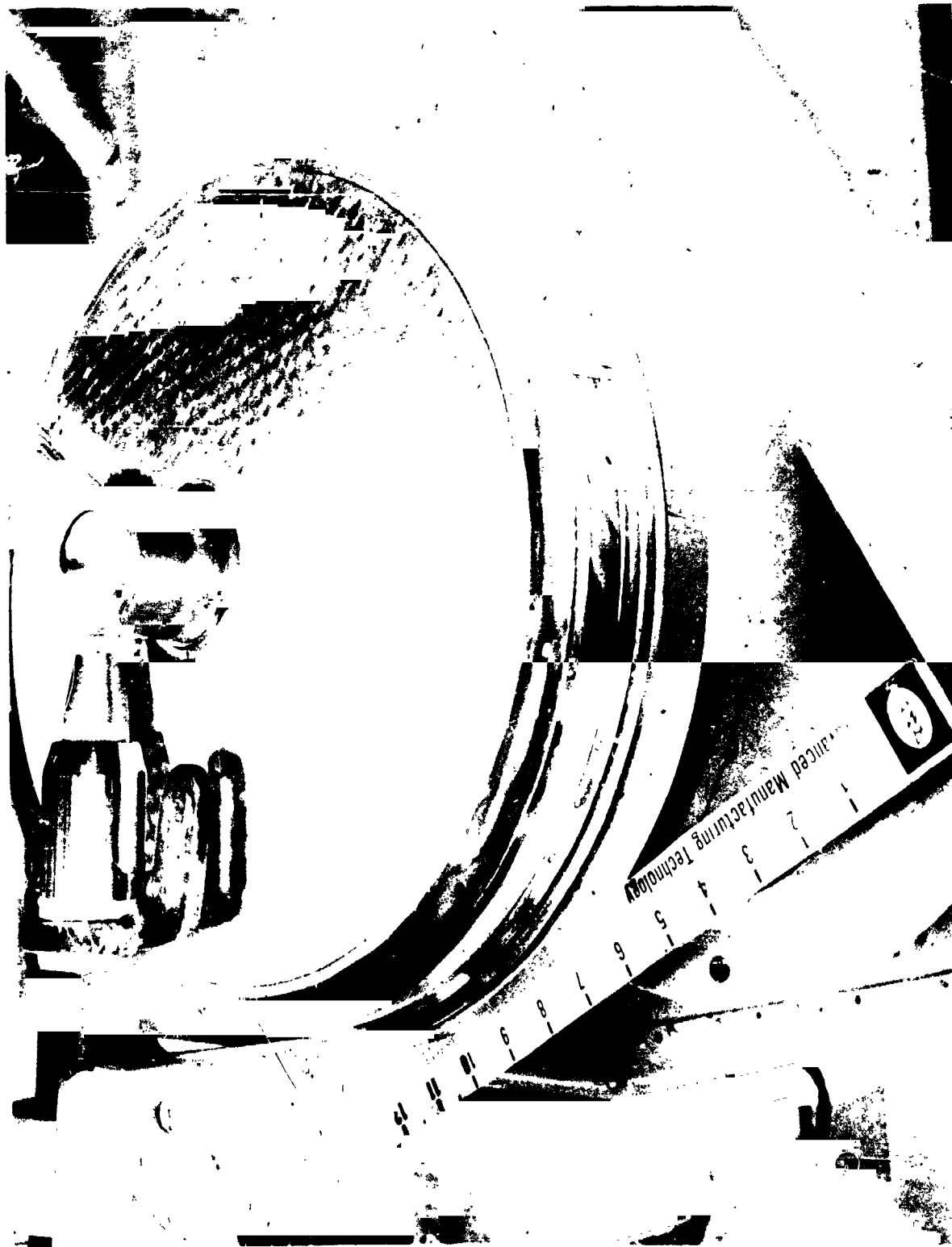


Fig. V-9 Welding the Vent Tube Perforated Cap to the Vent and Support Tube

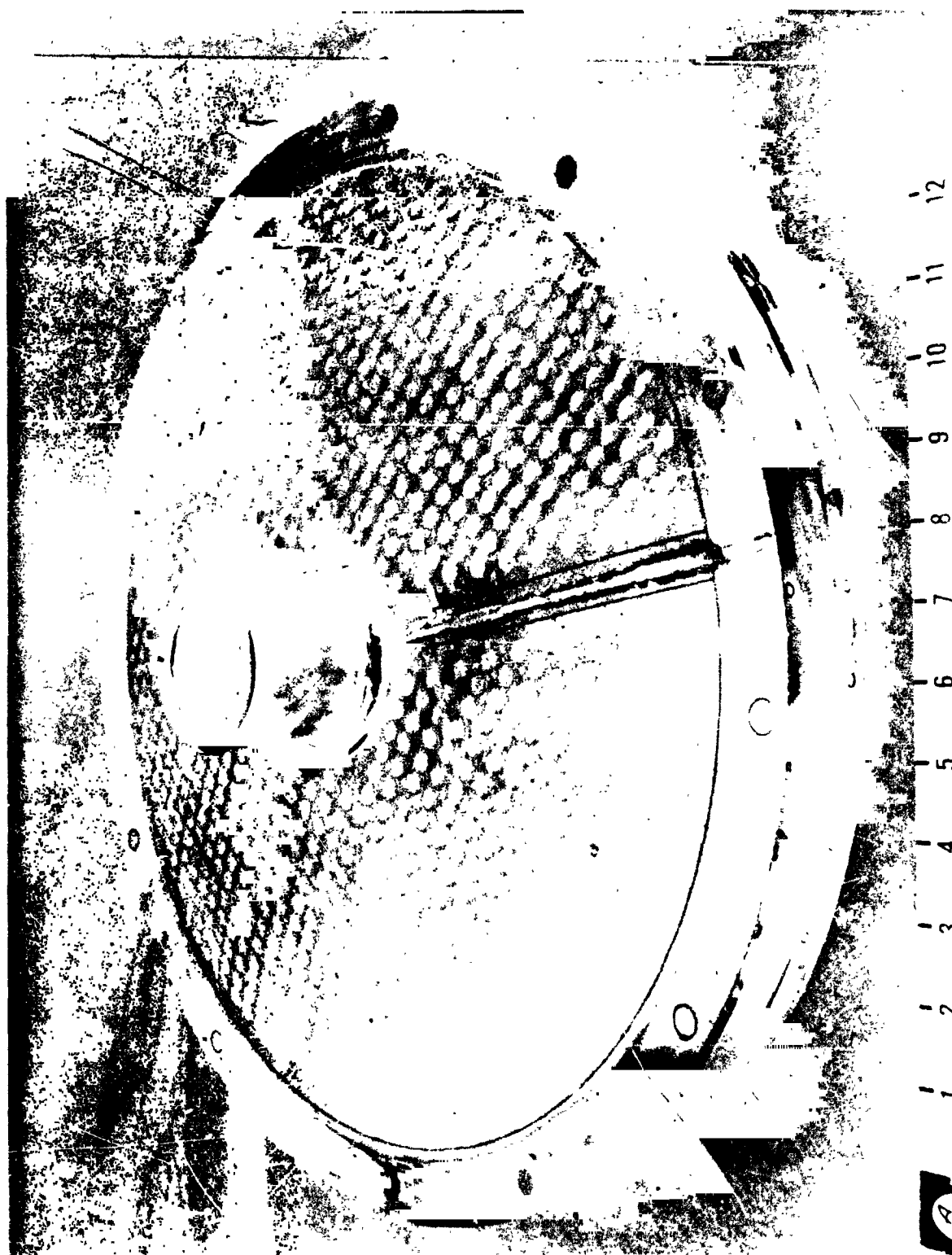


Fig. 1-10 Top View of Trap Showing Small Vent Hole Screens Attached

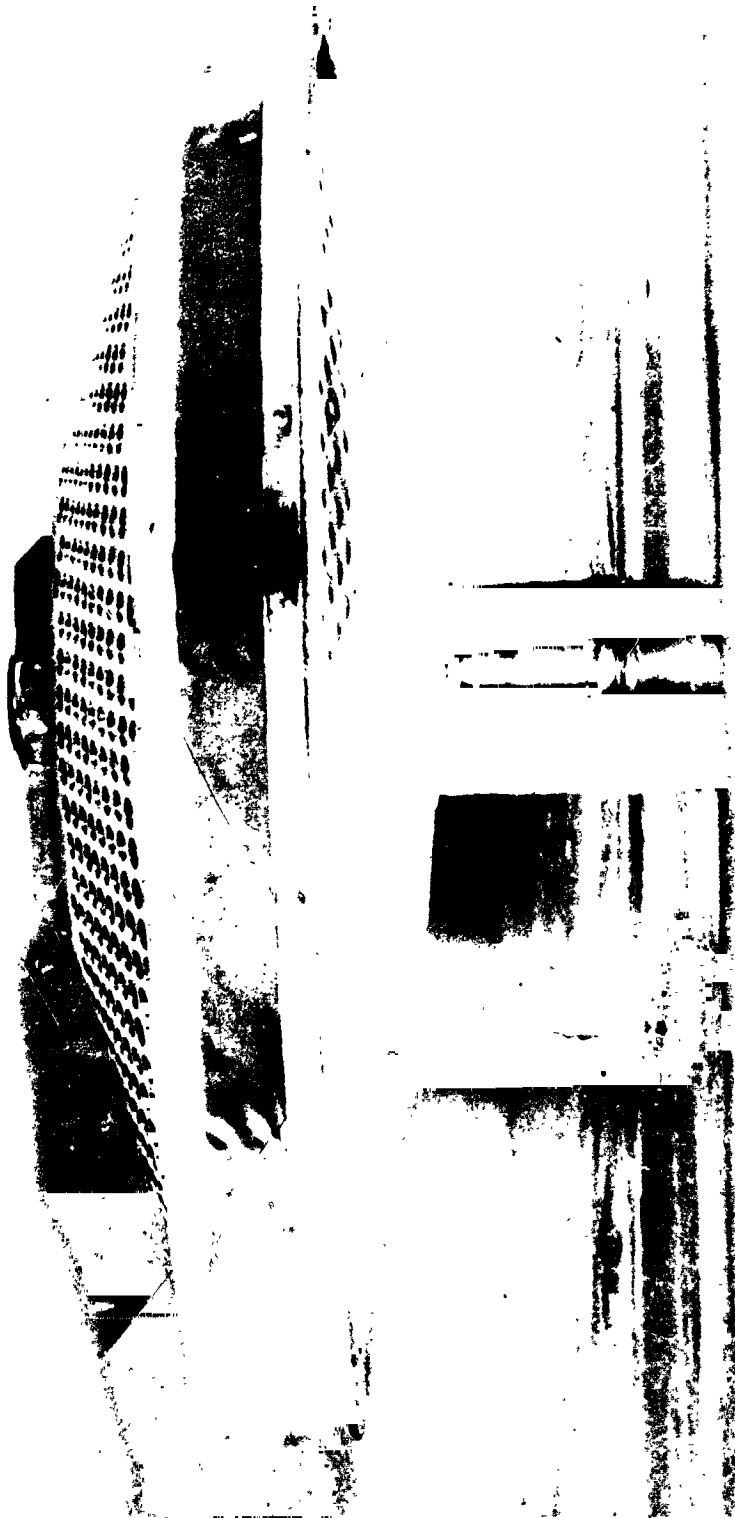


Fig. V-11 Completed Subscale OMS Trap

d. *Trap Installation* - The procedure for device installation is as follows:

- 1) Install access port cover seals;
- 2) Align assembled trap assembly with tank access port cover;
- 3) Bolt trap assembly to access port cover;
- 4) Perform device acceptance tests (see following Subsection f);
- 5) Insert completed trap/access port cover assembly into tank and align;
- 6) Bolt tank access port cover to tank;
- 7) Perform tank leak checks.

One of the support tubes located in the annulus is provided with a hole leading into the annulus region. This was done to provide an annulus venting capability during propellant loading. During alignment of the trap with the access cover, this tube will be positioned so it mates with a vent channel located in the access cover. A small gasket is provided to effect the sealing required.

e. *Cleaning* - Precise cleaning of capillary propellant management devices is mandatory to guarantee proper functioning. Contaminants may combine with the propellants to degrade device performance by either degrading critical device components (corroding, sludging, or clogging of capillary screen) or by degrading the propellants themselves (changing of surface tension or contact angle or by forming sludges). To avoid contamination, proper cleaning procedures must be used both before assembly of the device components as well as after final assembly. In addition, all joining operations should be performed under strict cleanliness conditions.

In general, two types of cleaning procedures are available for cleaning capillary propellant management systems (Ref V-2 and V-3). One procedure uses chemicals, while the other involves a high-temperature vacuum (i.e., vacuum annealing). If performed properly, both procedures can clean components well enough to survive even fluorine use (Ref V-2). However, because the vacuum annealing process anneals the metal, it is generally not as applicable as chemical processes.

Chemical cleaning procedures usually include four types of processes--degreasing, alkaline base cleaning, oxide removal, and etching. The procedures selected depend on the materials being cleaned as well as on the propellant used. Research at Martin Marietta on a cleaning process for the Viking orbiter and for heat pipe operations indicates that the following chemical cleaning processes for titanium and stainless steel systems are adequate for earth-storable propellants (Ref V-3):

- 1) Solvent degrease with acetone;
- 2) Alkaline-clean with Turco 4215;
- 3) Demineralized water rinse;
- 4) Acid deoxidize;
- 5) Demineralized water rinse, checking pH;
- 6) Acid etch with HNO_3/HF solution;
- 7) Demineralized water rinse, checking pH;
- 8) Acid deoxidize;
- 9) Demineralized water rinse;
- 10) Isopropyl alcohol rinse;
- 11) Hot nitrogen dry.

Etching of the metal surface is required for complete cleaning. However, such an etching process cannot be used on fine-mesh screen because it would increase the size of the screen's capillary pores, thus reducing the bubble point. Therefore for screen cleaning, either chemical processes without etching steps or vacuum annealing must be used. Such screen cleaning procedures have been used to clean stainless steel screens used in liquid fluorine (Ref V-2).

f. Acceptance Tests - After fabrication, the device would be acceptance-tested. This test would be a comprehensive checkout of the screen surfaces and weld joints to insure that there are no leaks and that the retention capability of the device is adequate.

The first series of tests would selectively bubble point test each screen surface of the trap. A bubble point test is accomplished by wetting the screen with alcohol and pressurizing one side of the screen with a gas, such as nitrogen. The point at which gas begins to pass through the screen is detected either by visually observing the bubbles forming on the screen surface or by a remote method.

Bubble points are remotely measured by monitoring the differential pressure across the wetted screen. When the screen is pressurized at a slow rate, the ΔP will increase until the bubble point is reached and then will decrease rapidly. Using this approach, screens enclosed within a device that cannot be observed can be bubble point tested. A further discussion of such tests can be found in Chapter IV.

These tests would be accomplished with the trap mounted on the access cover but not installed in the tank. The annulus would be checked by wetting the outer and inner annulus screens, pressurizing the annulus through the feedline, and measuring the bubble point. The reservoir region would be checked by wetting the inner annulus screen and the coverplate and pressurizing through the vent tube. Finally, the perforated plate on the vent tube would be checked by wetting the vent tube cap, coverplate, and outer annulus screen, leaving the inner annulus screen dry. The reservoir would be pressurized through the feedline and the pressure differential across the vent tube would be measured.

Two functional tests would be performed with a test fluid such as alcohol. By expelling with the device inverted against 1-g, worst-case flow conditions, much more severe than those encountered in flight, would be imposed on the device. Starting with the device completely full, alcohol would be expelled until gas was ingested into the feedline. Gas ingestion can be easily detected by observing the liquid flowing through a clear plastic line. The amount of liquid that could be expelled would be compared with predicted performance to determine the success of the test.

An expulsion with the device upright would be performed to determine the total flow impedance of the device to detect any flow restrictions. If the device successfully passed these tests, it would be flushed to remove any residual test fluid and purged with dry nitrogen gas. If any leaks were detected on the outer screen surfaces, they would be repaired. Soldering is a simple method of repairing pinhole leaks, but any large

leaks would require replacing a section of screen. A solder with a high tin content (greater than 98%) is compatible with the propellants. These repair techniques have been verified by Martin Marietta screen fabrication research.

This same acceptance test would also be performed any time the device had to be removed from the tank for periodic inspection, checkout of flight anomalies, etc.

To a certain point in the operational development, the device would be inspected between each flight to demonstrate its integrity. After the system was fully operational, inspections would be performed only when anomalies were detected or on a periodic basis. Since this trap is a modular unit it could be easily removed from the tank, visually inspected, tested, and reinstalled. When the trap was removed from the tank, it would be removed as a complete unit without disturbing any of the joints of the device. Only the seal between the access cover and the tank would be broken during removal.

To facilitate postflight inspection, the device could be modified to allow the bubble point testing while mounted in the tank. The vent tube complicates this test since the pores in the cap are much larger than those in the screen on the remainder of the device. A simple way of sealing off the vent tube while the device is in the tank is to invert the tank and fill it so the cap of the vent tube is submerged.

The screens must be wet to accomplish the bubble point check. By filling the trap with propellant, then draining it and maintaining saturated propellant vapor in the ullage, the screens would remain wetted during the test. Pressures would be monitored using a ground servicing port on the feedline and specially provided tubes that enter the trap reservoir and the tank ullage through the access cover. All screen surfaces could be bubble point checked individually. When the vent tube cap is not submerged, its bubble point can be checked. The tank penetrations must be designed and operated so the tank will not be contaminated during the test.

3. Reliability

The reliability of surface tension devices was discussed in some detail in Chapter III. Using this representative design, the reliability evaluation was continued by performing a failure modes and effects analysis (FMEA).

One of the most significant causes of failure of a surface tension device is enlargement of the holes in the screen material. This can be a slight enlargement due to corrosion of the screen wires, breakage of a few wires, or a substantial tear due to structural failure. A number of causes discussed in the reliability evaluation can lead to this mode of failure. Also, this failure mode is directly related to the basic function of the surface tension device--the retention of liquid by the screen material. The effect of interest is how much gas would be allowed to enter the spacecraft engine due to the enlargement of a pore. Gas can penetrate the capillary barrier of a device under both static or dynamic (liquid flowing) conditions. Only when liquid is flowing can the gas be carried to the outlet and the engine.

As discussed in Chapter II, two criteria must be met before liquid will be retained by a pore in the screen material. The interface at the pore must be stable (Bond number criteria) and the pore must have an adequate pressure retention capability (bubble point of the pore).

N_2O_4 will be used as an example in this discussion since its kinematic surface tension (σ/ρ) is less than that of the other propellants being considered. For any given conditions (acceleration and pore radius), N_2O_4 would have the least stable interface. The stability limits for N_2O_4 are shown in Fig. V-12, plotted as a function of the pore radius and acceleration. Points falling above the critical Bond number are unstable; those below are stable. When the pressure differential between the gas and liquid exceeds the maximum capillary pressure, retention of the liquid is no longer possible. Figure V-13 is a plot of the maximum pressure retention capability versus hole radius. Various screen meshes are noted on the curve.

Both of these criteria--stability and pressure retention--must be satisfied before liquid can be retained by a capillary barrier. When fine-mesh screens that have pore radii on the order of 2.5μ (10^{-4} in.) to 25μ (10^{-3} in.) are used at moderate g-levels, the stability criteria in Fig. V-12 are readily satisfied. In most applications, the requirement for pressure retention is more difficult to satisfy. Therefore, an enlargement of a pore is more likely to cause a loss of pressure retention capability before the interface becomes unstable.

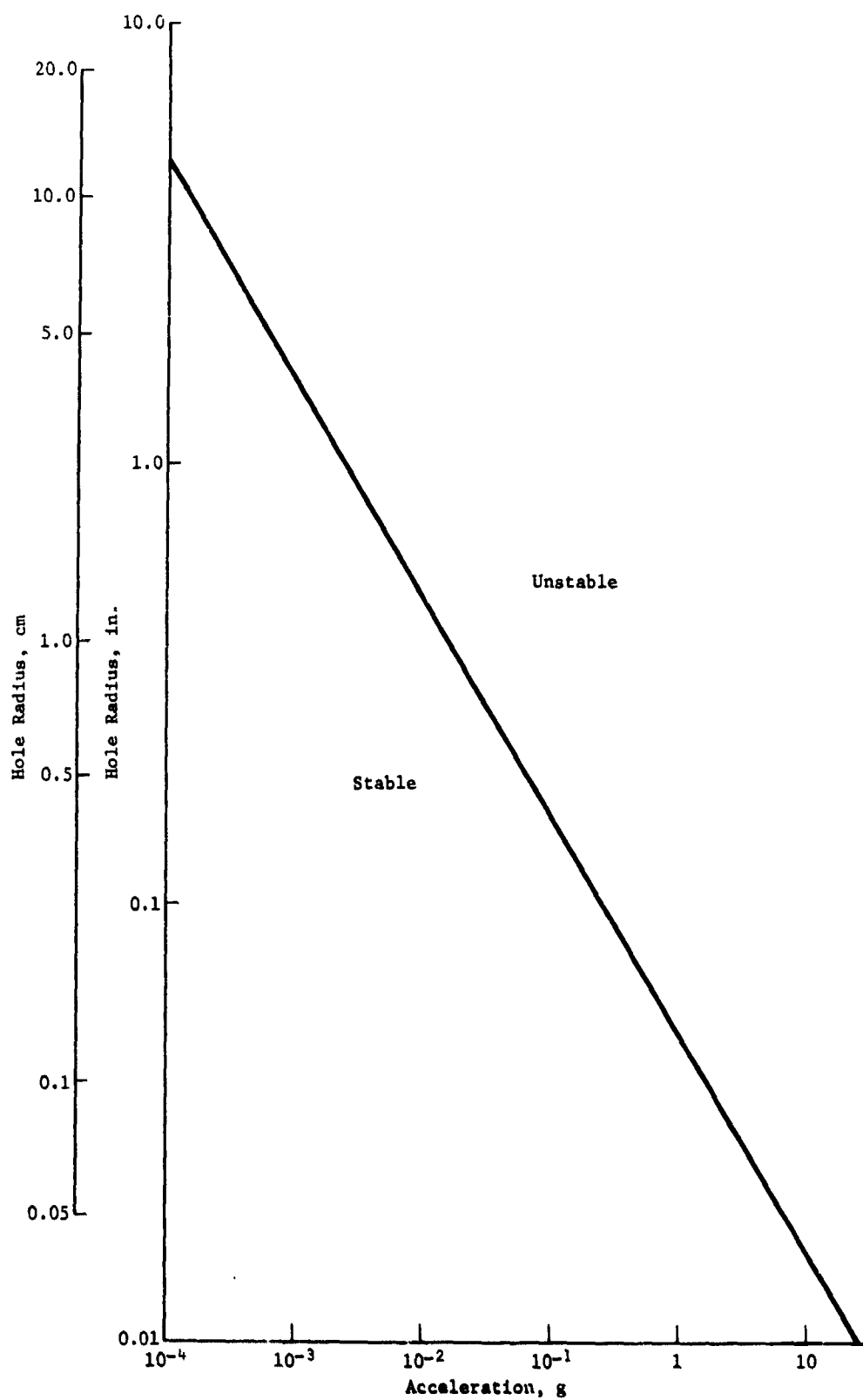


Fig. V-12 Capillary Stability of N_2O_4

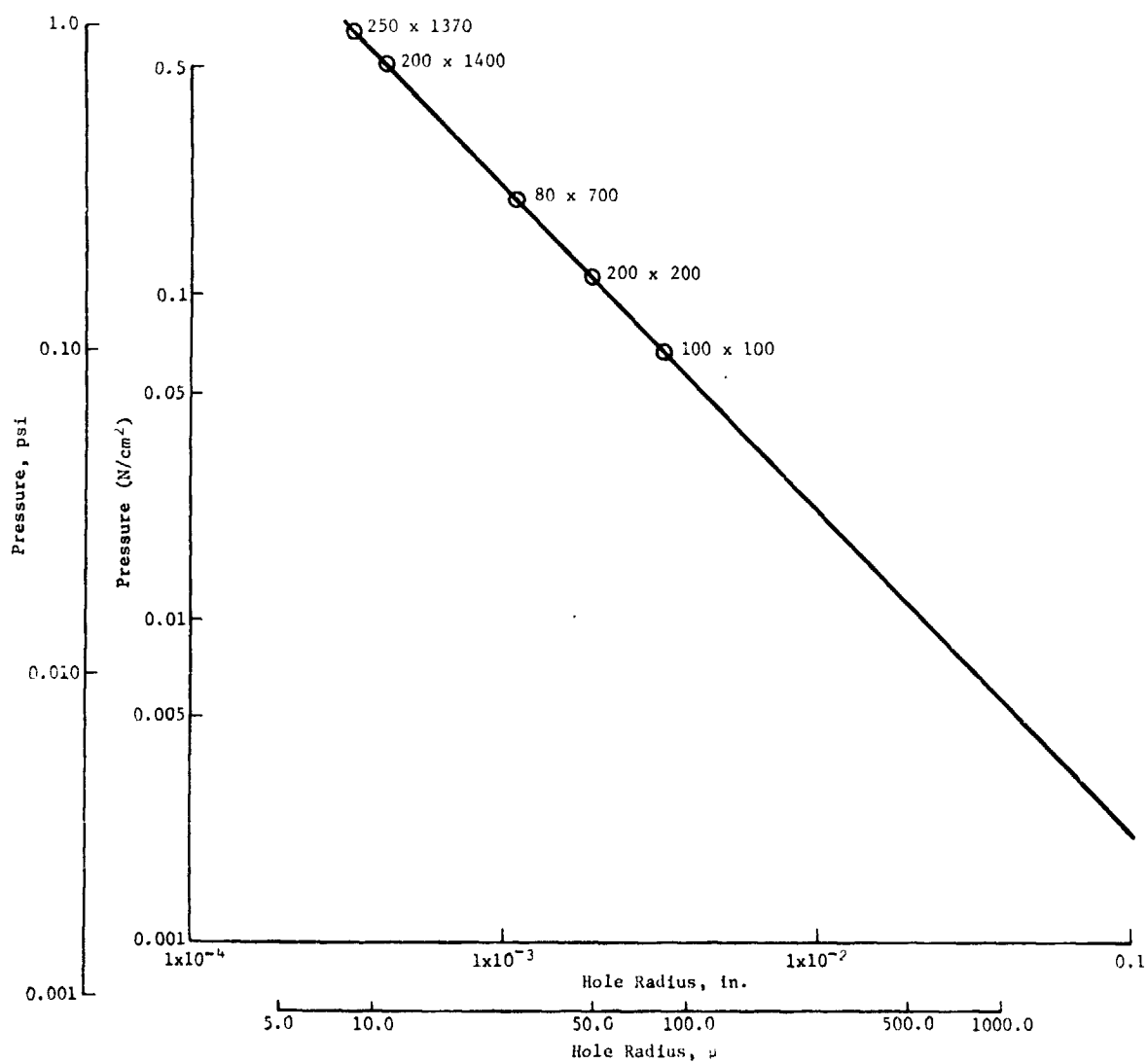


Fig. V-13 Pressure Retention of N_2O_4

For example, consider a fine-mesh screen device that operates in a 0.1-g environment and must retain liquid against a 0.14-N/cm^2 (0.2-psi) pressure differential. According to the stability curve, an enlargement of the pore size by approximately two orders of magnitude would be necessary before the interface became unstable. On the other hand, a 0.069-N/cm^2 (0.1-psi) decrease in pressure retention capability will occur if the pore size were to approximately double, which is a much more significant effect.

The configuration of the screen material within the surface tension device and the orientation of the liquid must be considered before the effect of the enlargement of a pore can be determined. Consider first the case of an enlarged pore in a capillary barrier, which would represent the coverplate of the trap, as shown in Fig. V-14. Liquid is being retained above the barrier under static conditions (no liquid flow) while the container undergoes a constant acceleration. The bottom surface of the barrier is exposed to gas. Because there is no hydrostatic pressure difference along the screen, the pressure retention criterion does not apply to this case. When the Bond number of a pore is below the critical value, the interface is stable and the liquid will be retained above the barrier. If a pore should become enlarged enough to make the interface unstable, liquid will drain through the hole.

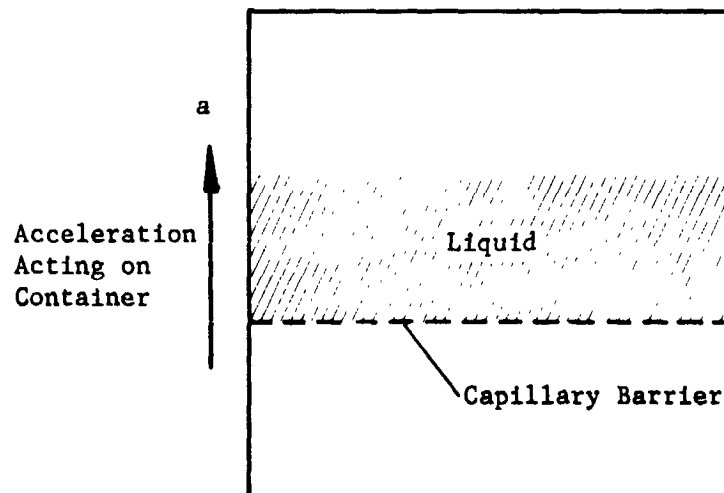


Fig. V-14 Enlarged Pore in Capillary Barrier

The effect of such a failure of a pore to retain liquid depends on the function of the barrier in the surface tension device. Failure of a barrier to retain liquid does not necessarily mean that some gas will be fed to the spacecraft engine. The purpose of the barrier in the trap is to retain liquid in a reservoir. If the enlarged pore allows more liquid to leave the reservoir than permissible, the device could fail to provide gas-free liquid. Consequently, a number of factors influence the amount of gas that actually enters the engine.

A second failure case is the effect of an enlarged pore in the screen forming the trap annulus, as shown in Fig. V-15. The annulus region is full of liquid and the length h_1 is exposed to gas on the right side of the screen. In this case the screen selected for the annulus can support the hydrostatic head h_1 . Although the interface at the pores must also be stable, it will be assumed that this is not the dominant criterion. The effect of an enlarged pore depends on its location in the screen. For the enlarged pore shown in Fig. V-15, liquid will be retained if the pore is capable of supporting the hydrostatic head h_2 since h_2 determines the pressure difference between the gas and liquid at the enlarged pore. If the height h_2 cannot be supported, liquid will drain out of the annulus into the bulk region and gas will enter the annulus through the enlarged pore. When the height of the liquid remaining in the annulus is equal to the height that can be supported by the enlarged pore, gas will stop entering the annulus. Therefore, the amount of gas that enters the annulus depends on the size and location of the enlarged pore. The effect of the enlargement is most significant if it is located at the top of the annulus for the acceleration shown.

In the typical application, the annulus feeds liquid to the tank outlet. If gas enters the annulus under static conditions, it may or may not be drawn into the tank outlet when the engine is operated. Buoyancy forces and fluid momentum forces act in opposition to each other across the gas bubble. The resulting pressure balance on the gas can prevent it from entering the tank outlet.

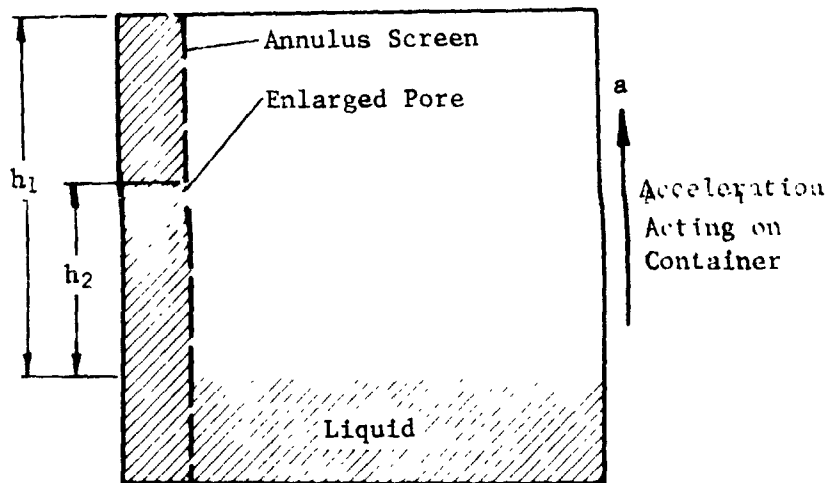


Fig. V-15 Enlarged Pore in Annulus Screen

Under dynamic conditions when liquid is in motion, the principles discussed with respect to the static condition still apply, with the addition of a few new variables. In the case of a capillary barrier, liquid may be reorienting with respect to the barrier. The specific orientation of the liquid and the function of the barrier during the dynamic condition must be considered. For example, with the refillable trap the barrier is designed to become unstable during main-engine operation. An enlarged pore does not degrade the operation of the barrier under these conditions. When the function of the barrier is to retain the liquid against adverse accelerations, the criteria used for the static condition (Bond number) apply in the same manner to the dynamic condition.

When liquid is flowing through an annulus, greater pressure differentials than those experienced under static conditions will usually be established. Due to an increase in the pressure difference, an enlarged pore that could retain liquid under static conditions may not be able to retain liquid under dynamic conditions. When one side of the enlarged pore is exposed to gas, the size of the hole and the pressure differential acting across the hole are the primary factors to be considered. As liquid flows past an enlarged pore through which gas is entering, the gas will be carried along with the liquid. Under these conditions, equilibrium cannot be established as it could be for the static condition.

By selecting some typical operating conditions for an annulus, the amount of gas that could enter the engine can be predicted. The configuration modeled is shown in Fig. V-16. Both the liquid flowing through the annulus and the acceleration acting on the device produce a pressure differential at the enlarged pore. When the pressure retention capability of the hole is exceeded, gas will be drawn into the liquid stream. It is assumed that the hole acts as an orifice, restricting the flow of the gas. N_2O_4 was used as the liquid, either N_2O_4 vapor or helium as the gas, and a typical liquid flow rate of 5.4 kg/s (12 lbfm/s) was selected. Based on these assumptions, the liquid quality versus hole size and the pressure differential that exists at the hole is plotted in Fig. V-17.

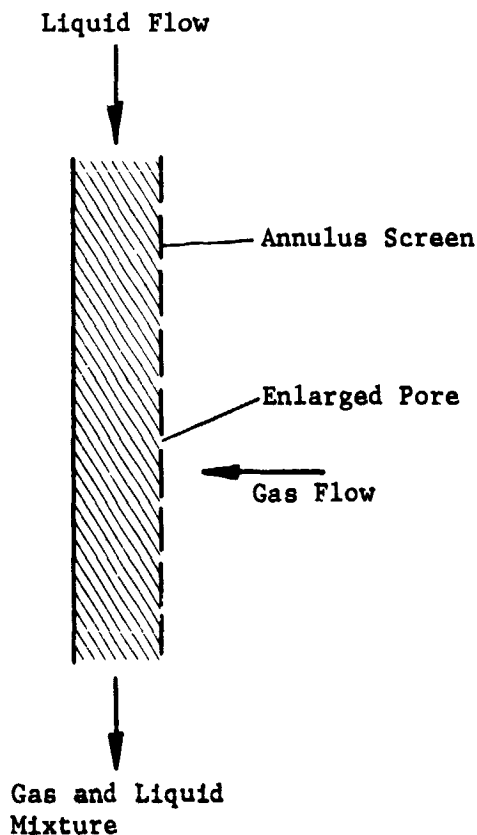


Fig. V-16 Enlarged Pore in Annulus under Flow Conditions

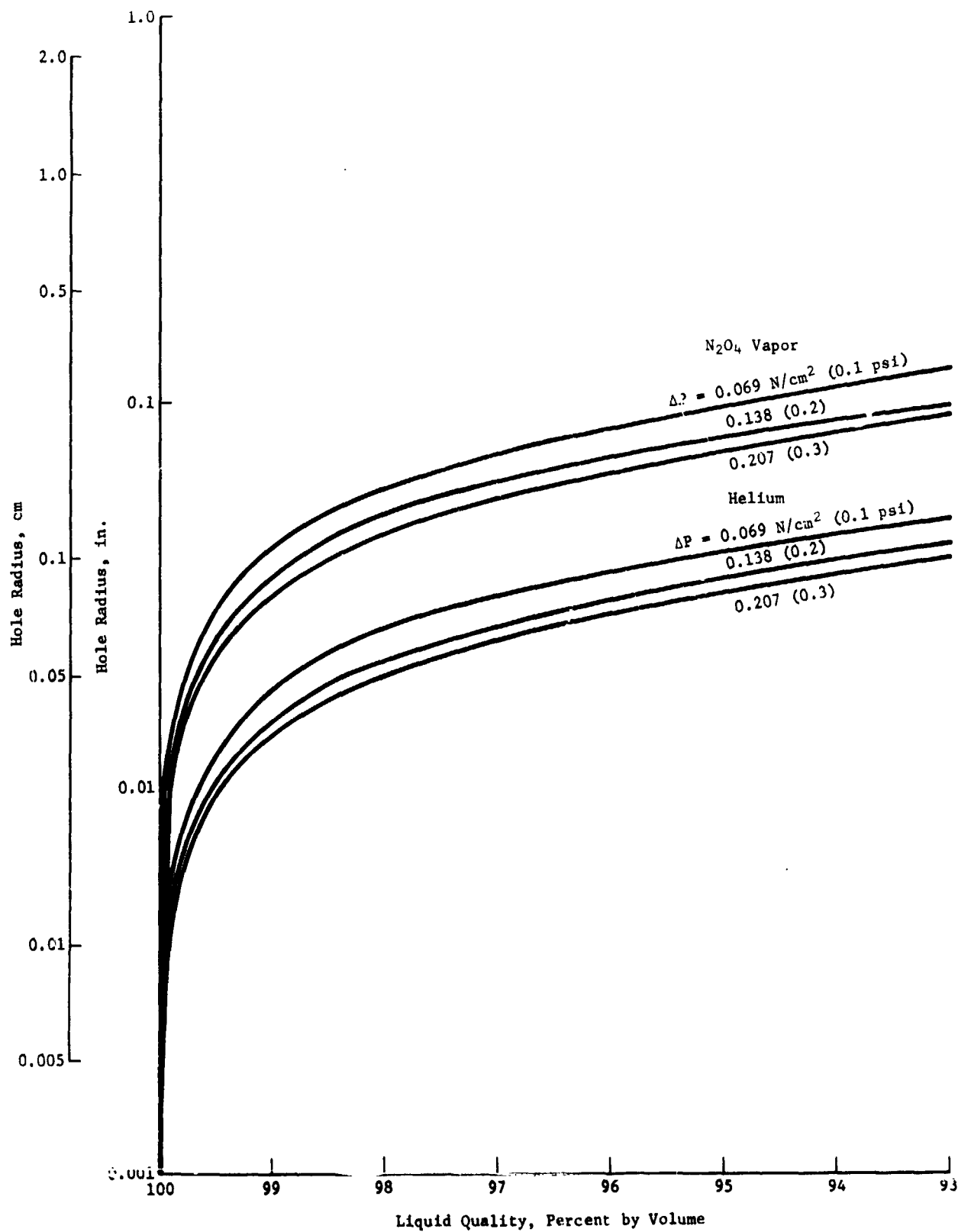


Fig. V-17 Effect of Hole Size on Liquid Quality in a Flowing Annulus
(Liquid N₂O₄)

The pressure retention curve (Fig. V-13) shows that a 76- μ (0.003-in.)-radius hole will retain 0.069 N/cm² (0.1 psi), a 41- μ (0.0016-in.)-radius hole will retain 0.14 N/cm² (0.2 psi), and a 25- μ (0.0010-in.)-radius hole will retain 0.21 N/cm² (0.3 psi). For the given ΔP curves, the above hole sizes are lower limits to the curves, e.g., the liquid quality will be 100% for smaller hole sizes because the hole prevents gas from entering the annulus.

The curve shows that a wide range of hole sizes will not cause any significant reduction in liquid quality. Typical fine-mesh screen pores are on the order of 2.5 μ (10^{-4} in.) to 25 μ (10^{-3} in.) in radius. The 200 x 1400-mesh screen used on the device has a pore radius of 10 μ (4×10^{-4} in.). An annulus screen with a pore enlargement of up to a 0.0254-cm (0.01-in.)-radius (an increase of one to two orders of magnitude), will still provide liquid with a quality greater than 99.5%. However, further increases in the hole size will severely degrade liquid quality. When the hole size exceeds a 0.254-cm (0.1-in.)-radius, corresponding to a small tear or puncture, the rate at which the liquid quality degrades considerably accelerates.

Of course, these results apply only to devices with operating conditions similar to the example. Changing the liquid flow rate will shift the curves. With the fuel, the holes have a higher pressure retention capability and thus a larger hole size will still provide 100% liquid quality. The most important factor is whether the hole is exposed to gas. When the hole is submerged in liquid it is not a concern, regardless of its size.

4. Reusability

The turnaround process for a typical OMS, and how a surface tension device would fit into this process, was outlined in Chapter III. How this trap device would affect the turnaround process is specifically discussed here.

The acceptance test and the procedure for installing the device in the tank have already been discussed. The next step involving the trap device is propellant loading. Propellant would be loaded with the tank vertical to allow venting through the pressurization inlet. Filling of the annulus region of the device is the only additional step that would need to be added to the normal loading procedure. An annulus vent was incorporated in this design to prevent gas entrapment during filling of the annulus. One of the support tubes is open at the top and the base of the tube is connected to a small line that penetrates the tank access cover.

As long as some portion of the annulus screen is dry, gas would leave the annulus as the tank is filled. As the liquid level nears the top of the annulus, wicking of liquid into the screen will precede the liquid level, sealing some gas within the annulus. The purpose of the vent is to remove this remaining volume of gas. By slightly tilting the tank all of the gas will leave through the vent. When liquid is present at the vent outlet, the vent would be capped and sealed for flight.

Since the perforated plate at the top of the vent tube is initially dry and will not wet until the liquid level reaches it, filling the reservoir is not a problem. Even if the vent tube were wetted, it would become unstable in l-g and the reservoir would fill in the same manner as during OMS engine burns.

Unless the surfaces of the loaded trap could become exposed to the ullage gas, handling of the tanks does not have to be restricted. When the tanks are partially loaded and rotated horizontally, surfaces of the screen may become exposed. In such cases the retention of the screen material in l-g must be evaluated. The perforated plate on the vent tube is the weakest point in the device and could easily break down, allowing the liquid to leave the reservoir region of the device. But the reservoir region will always refill when the tank is returned to vertical.

When more than about 33 cm (13 in.) of the annulus is exposed to gas, liquid would be lost from the annulus. If this could happen, the approach would be to bleed the gas from the annulus using the annulus vent and refill the annulus when handling of the tank was complete.

These are the only operations that would affect the device. The device would remain mounted to the tank and continue to be reused. Only if problems were detected or if it were necessary to perform a periodic inspection would the device be removed from the tank.

B. ENLARGED TRAP

The second representative design, the enlarged trap, is shown in Fig. V-18. This one device is applicable to both the fuel and oxidizer tank. This device has a greater degree of flexibility for short-duration burns than the trap discussed in the previous section. Its design is based on the premise that the typical missions presented in Chapter II are only examples of some of the missions that might be required. There may also be other missions that would impose the worst-case conditions as far as sizing the reservoir volume of a trap is concerned. However, it is recognized that all missions will have some basic characteristics, e.g., initial and final long-duration burns.

Performance

Table V-3 summarizes the significant parameters for the enlarged trap design. Expulsion efficiency and volumetric efficiency are high, but somewhat less than the values for the refillable trap design. This is because the device is much larger in size.

A large percentage of the device's weight can be attributed to the flanges on the channels, manifold, and coverplate that are necessary for modular installation. If the device were fabricated as an integral part of the tank, thus eliminating these flanges, its dry weight would be reduced to 7.17 kg (15.8 lbm).

Table V-3 Enlarged Trap Parameters

Trap Volume 0.71 m ³ (25 ft ³)
Expulsion Efficiency 98.9%
Volumetric Efficiency 99.93%
Material - Stainless Steel
Weight - Device 16.5 kg (34.3 lbm)
Device plus Residual (N ₂ O ₄) 64.1 kg (141.4 lbm)
Foraminous Material -
Annulus - 250 x 1370 Dutch-Twill Screen
Coverplate - 250 x 1370 Dutch-Twill Screen
Supported with Perforated Plate

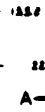
a. *Reservoir Volume* - Sizing of the reservoir volume was based on such factors as device weight and the effect of propellant offload rather than mission duty cycle. The largest possible trap volume, with a reasonable weight and a minimum effect on other factors, was desired. Since a reasonable device weight could be obtained when the reservoir was sized for the minimum propellant load, this volume, 0.71 m^3 (25 ft^3), was selected.

This large a trap volume requires that the coverplate be a capillary barrier that extends completely across the barrel section of the tank. The coverplate remains stable throughout the on-orbit phase of the mission. It would be desirable to design the coverplate so the trap could be refilled, using the criteria presented in Chapter III. Since the settling and lateral accelerations are of the same magnitude and the barrier must extend completely across the tank, the acceleration environment does not permit a reasonable refillable coverplate design. Therefore this trap is nonrefillable. Any gas that enters the trap remains in the trap throughout the mission. It cannot be purged and replaced with liquid during an engine burn as with the refillable trap.

An evaluation of the capability of this trap to accomplish a large number of burns, including those of short duration, shows it is a very flexible concept. The device is dependent on propellant settling.

During engine start, the propellant within the trap is used to supply the engine if the liquid located outside the trap is not in contact with the coverplate. When liquid is not in contact with the coverplate, the coverplate breaks down and gas enters the reservoir region as liquid is used from the trap. When liquid is in contact with the coverplate, liquid will feed in preference to the gas, and the coverplate remains stable. Settling of the liquid outside the trap brings it into contact with the coverplate at some point in time following engine start.

To be conservative, it is assumed that some gas will enter the trap with each engine start. The liquid outside the trap is assumed to be oriented at the top of the tank. The primary concern is that all of the liquid inside the trap could be depleted prior to using the liquid located outside the trap. If this should happen, the trap would not be capable of supplying the engine during propellant settling and all of the propellant in the tank could not be expelled. Short-duration burns tend to use proportionally more liquid from the trap than from outside the trap, while the opposite is true for the long-duration burns.



1. 2020年 12月 25日
 2. 2020年 12月 25日
 3. 2020年 12月 25日
 4. 2020年 12月 25日
 5. 2020年 12月 25日

Source: FBI
Filing: Birmingham

— ١٩٩٤٠٠٠ (١٩٩٤٠٠٠)
١٩٩٤٠٠٠ ١٩٩٤٠٠٠
١٩٩٤٠٠٠ ١٩٩٤٠٠٠

A-

FOLDOUT FRAME

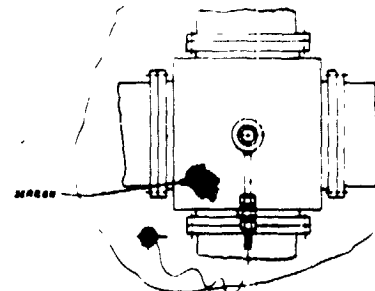
2

ADD 3 1/2 BUTTER FLANK
SHEETS, 10 1/2 THICK
24 1/2" x 72 1/2"

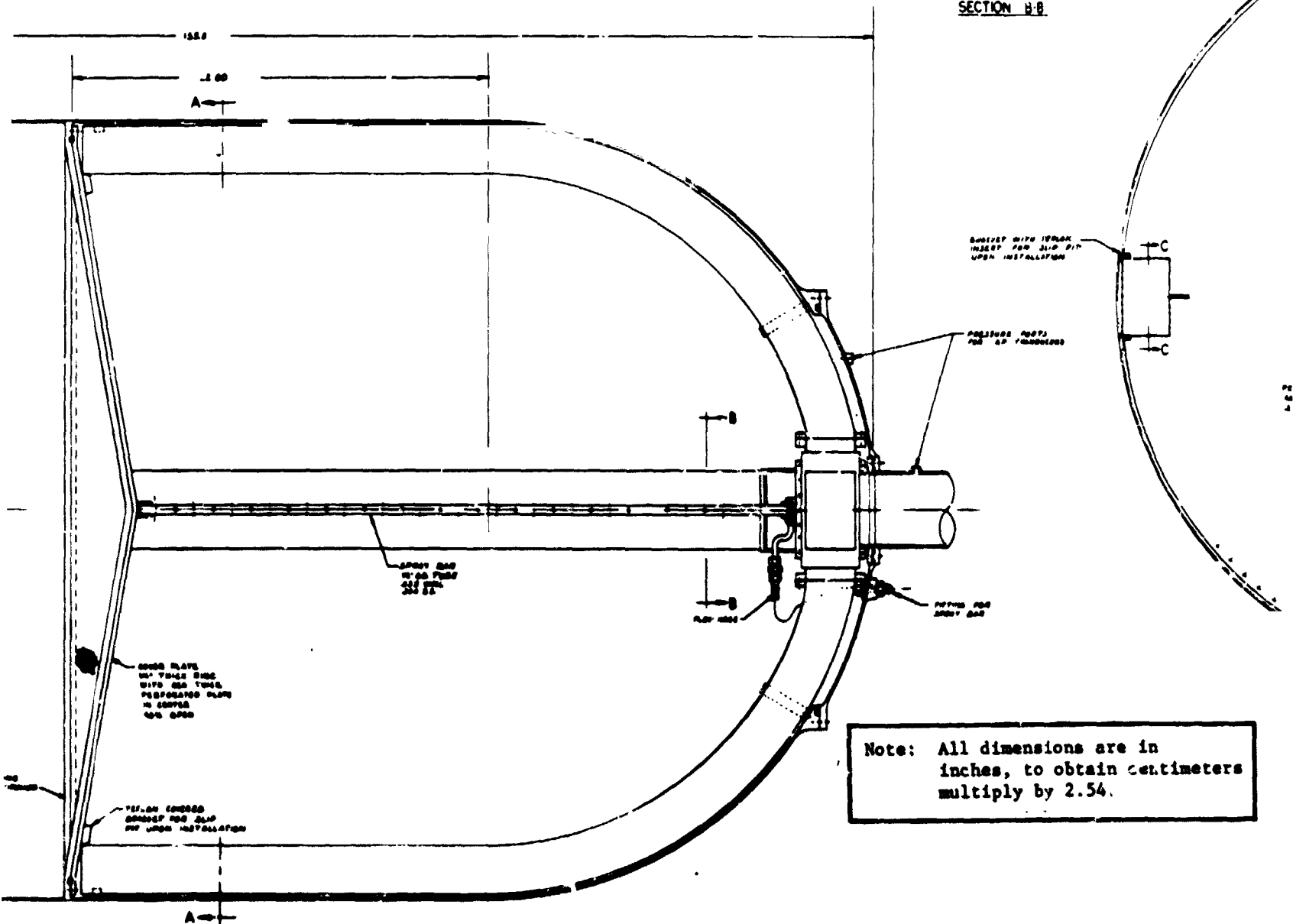


PERFORATED PLATE
20" x 38"
20% OPEN
24" THICK

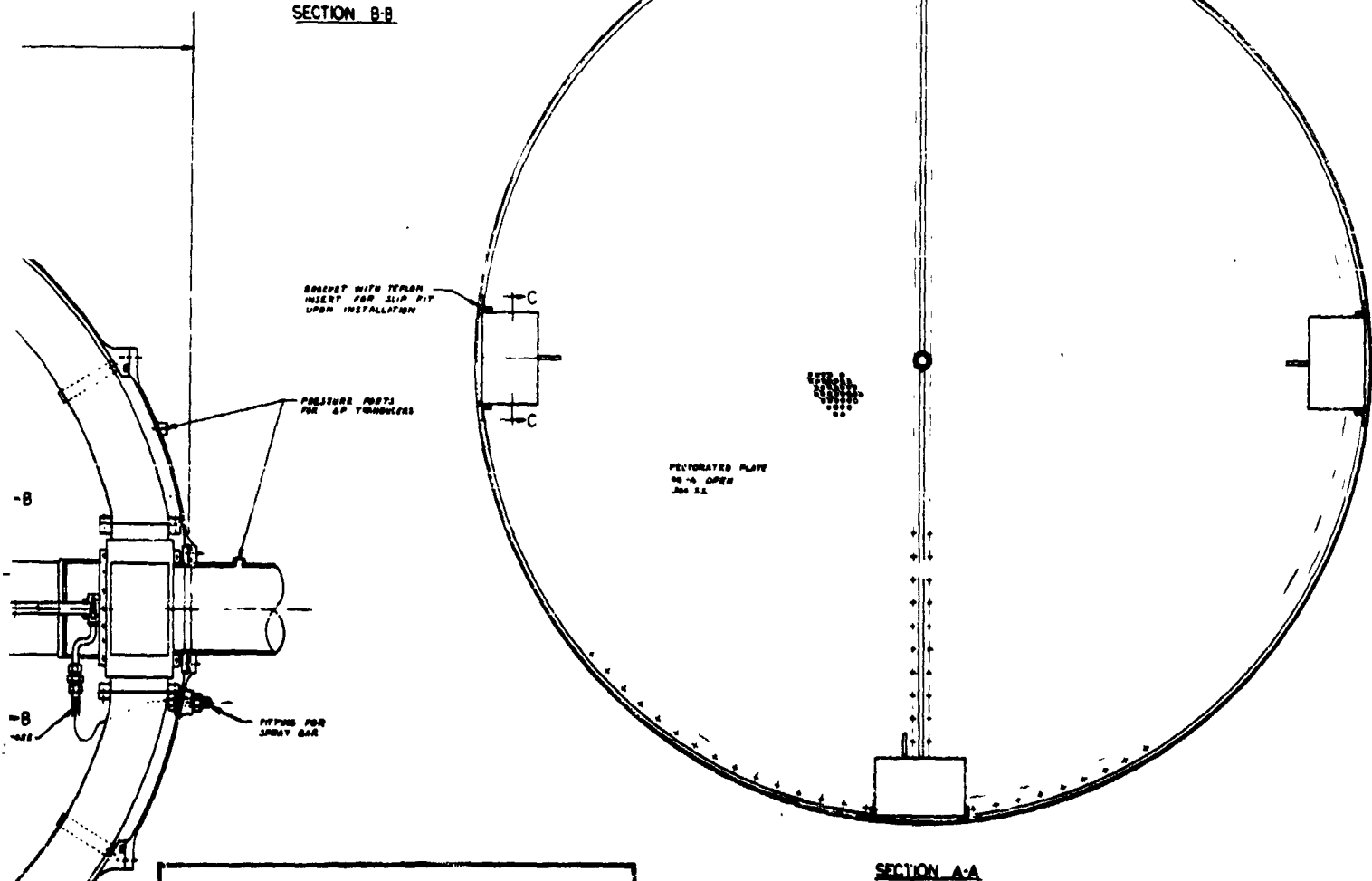
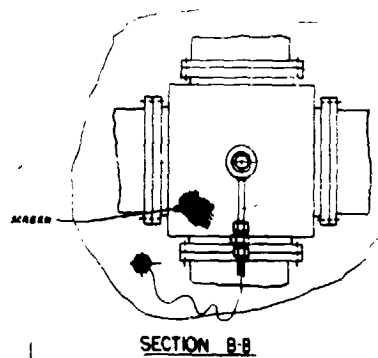
SECTION C-C



SECTION H-H



FOLDOUT FRAME 3



Note: All dimensions are in inches, to obtain centimeters multiply by 2.54.

Figure V-18 Enlarged Trwp
V-35 and V-36

Assuming that all the burns were of equal duration, and using a conservative estimate of the settle time, the burn duration that would simultaneously deplete both the trap and bulk propellant at the end of the last burn can be predicted. For the given trap volume this duration is approximately 25 s. This means that if all the burns were less than 25 s, some liquid that could not be expelled would be left in the bulk region of the tank. If all the burns were greater than 25 s, the bulk region would be depleted before the trap was depleted and all of the liquid could be expelled. An actual mission will consist of burns of varied durations. The long-duration burns, of which there are at least two, would deplete a considerable portion of the liquid outside the trap. There would have to be a very large number of short-duration burns (many more than would be expected for an OMS-type mission) before a problem of incomplete propellant expulsion would be encountered.

Another factor to be considered is that the OMS is intended for long-duration burns, while the reaction control system (RCS) is intended for the smaller translations. Based on efficient use of propellant there is a burn duration limit below which it is better to use the RCS and above which the OMS should be used. This break-even point depends on a number of factors, but a typical value would be a burn duration of about 10 to 15 s. Therefore the number of short-duration OMS burns should be small and their duration will be of a reasonable magnitude.

In contrast to the refillable trap, which could accomplish any number of burns if they were longer than a certain duration, this device can accomplish consecutive burns of any duration as long as their number and total burn time is less than a certain amount. To evaluate the effect of the number of burns, some consideration must also be given to the burn duration. The effect on the use of propellant from the trap is greatest when the burn duration is equal to or slightly less than the settle time. Using a rather conservative approach, burns of this duration would use liquid only from inside the trap and none from outside.

The bulk liquid must be in contact with the device before it will enter the trap in preference to gas, and it has been assumed that the liquid is initially oriented away from the device. For the first burn, the settle time is near zero and for the last burn it could be as long as 11 s. Assume that the settle time would average about 8 s over the entire mission. Based on the volume of liquid in the trap, 23 burns of 8-s duration could be accomplished, which would use all the liquid

in the trap. The typical missions indicate that this would not limit the flexibility of the device since the maximum number of burns is much less than 23 and more on the order of 8. Also, it must be recognized that a large portion of the burns will be of long duration. Based on the typical mission duty cycles, a trap volume of only 0.17 m^3 (6 ft^3) would be required. The device provides four times that amount.

The preceding discussion was primarily concerned with a fully loaded propellant tank. Propellant offloading tends to improve the performance of the trap. As the propellant load is decreased, a greater portion of the liquid is initially located inside the trap. At the minimum propellant load, all the propellant is inside the trap and the device functions as a liner and its flexibility is not limited.

b. Annulus - Four rectangular channels form the annulus of this device. The channels provide a sufficient flow area and allow the device to be adapted to modular installation. Prior to each burn, at least one channel will be in contact with the liquid inside the trap. The channels will continue to feed liquid to the engine as the liquid in the trap orients over the manifold. The screen on the channels, a 250 x 1370-mesh Dutch twill, will retain liquid within the channels under all static and flow conditions encountered in orbit.

c. Coverplate - As discussed previously, the coverplate of this device remains stable while the vehicle is in orbit. Refill of the trap during engine burns is not considered feasible. A 250 x 1370-mesh screen provides more than adequate retention capability for on-orbit operation of the device. In addition to providing structural rigidity, the inverted cone shape of the coverplate preferentially orients the liquid inside the reservoir during low-g coast periods. When the liquid in the reservoir is oriented away from the tank outlet, the coverplate orients it toward the channels. Thus sufficient liquid will be in contact with the channels prior to an engine start. This eliminates the need for the channels to extend across the lower surface of the coverplate.

The previous discussion of reliability and the FMEA for the refillable trap also applies to this device.

2. Structural Design, Fabrication, and Installation

a. *Material Selection* - For the enlarged trap, 250 x 1370-mesh Dutch-twill screen was selected. Mesh sizes this fine are only available in stainless steel. Therefore 300-series stainless steel was selected based on the material selection criteria presented for the refillable trap.

b. *Structural Design* - A conservative structural design approach was also used in the design of the enlarged trap to provide a structure capable of withstanding the loads encountered during handling, liquid impact, mechanical shock, mechanical vibration, boost, pressure differentials, etc. The access port cover was sized based on the same considerations applied to the refillable trap. A cone-shaped coverplate was used to reduce the effect of settled liquid impacting the device. The flow channels were designed as box-like structures to provide structural rigidity.

Unlike the refillable trap, perforated plate was not used exclusively to back up the fine-mesh screen of the device. Two sides of the channels are not designed with perforated plate. Instead, support strips, spaced approximately every 23 cm (9 in.) are used. Between these backup strips the screen is unsupported. Based on screen structural tests conducted in another phase of this contract (Vol III), unsupported screen segments of this size are capable of withstanding the structural loads.

c. *Assembly* - Based on the same criteria presented for the refillable trap, all-welded joining techniques were selected for the enlarged trap. The steps of device assembly for the enlarged trap would be as follows:

- 1) Weld perforated plate to frame of coverplate;
- 2) Resistance-weld screen to perforated plate of coverplate (the coverplate is made in two segments);
- 3) Weld spacers to perforated plate sides to form box structure of flow channels;
- 4) Resistance-weld screen to flow channels;
- 5) Weld together manifold assembly, including attachment of spray probe to top of manifold;
- 6) Resistance-weld screen to manifold assembly.

d. *Installation* - To allow modular installation, the enlarged trap was designed with three main components--coverplate, flow channels, and manifold assembly. Each of these components can be inserted into the propellant tank through the tank access port to form a completely sealed unit when joined together.

The flange on which the two halves of the coverplate are attached is an integral part of the tank. Teflon gaskets are used to seal the coverplate segments to this flange. The four flow channels were designed to fit individually through the tank access port. These channels are attached to the tank using holding slots and brackets. The slots are located on the coverplate and the brackets are located on the flange of the access port. The flanges on the channels mate to like flanges on the manifold. Adequate space is provided between the four flow channels to allow the bolting operation to be easily accomplished through the tank access port. A double bolt ring arrangement was selected to attach the manifold to the access port cover and seal the access port cover to the tank.

The steps of device installation would be as follows:

- 1) Insert the halves of the coverplate into tank and bolt to the coverplate mounting flange;
- 2) Insert flow channels into tank and slip top portions into attachment slots;
- 3) Attach channel holding brackets;
- 4) Insert manifold assembly into tank and bolt channels to manifold;
- 5) Connect spray probe to access port cover;
- 6) Bolt access port cover to tank and manifold assembly.

e. *Cleaning* - The considerations discussed under the refillable trap also apply to the enlarged trap.

f. *Acceptance Test* - This device would be subjected to an acceptance test similar to that for the refillable trap. The channels would be bubble point checked individually. A plate would be mounted over the opening in the channel, where it mates to the manifold, and the test would be accomplished by submerging the entire channel in alcohol. The manifold would be checked in a similar manner. Each half of the coverplate would be attached to a fixture to create a region that can be pressurized and would be bubble point checked.

Since the device is not complete until it is installed in the tank, the remaining tests would be accomplished after tank installation. A spray probe is provided as an integral part of the device, with an inlet located on the access cover. The test fluid, which could be either alcohol or the propellant, would be sprayed through the probe, wetting all the screen surfaces of the device. The coverplate would be bubble point tested by pressurizing through the tank pressurant inlet. The channels would be checked by pressurizing through the feedline. Pressure taps are provided to measure the differential pressures. This test would determine if the mechanical joints of the device were properly sealed. When the tests were finished the inlet for the spray probe would be sealed for flight.

This approach to the bubble point testing allows the device to be tested anytime without removing the device, opening the tank, or disconnecting the feedlines. During the development phase of the propulsion system the device could be checked following each flight without disassembly.

Although the spray probe in this design is an integral part of the device, it could also be removable. A port, through which the probe would be inserted and mounted, would be provided on the tank access cover. This insertable probe would function the same as the integral probe. When the test was complete the probe would be removed and the port capped. While removing the probe from the device reduces its weight, this savings would probably be offset by the weight increase from the port and access cover. The disadvantage of this approach is that the tank must be opened to insert the probe, with the possibility that the system could become contaminated or degraded during the test. Therefore the integral probe is preferred.

This device would be subjected to the same functional tests described for the refillable trap.

3. Reusability

Although the procedures used with this device would be very similar to those used with the refillable trap, a different method of insuring that all gas leaves the annulus during loading was used for this device. A small section of the screen at the top of the channels is isolated so it will not become wetted by wicking of the propellant. Because solid material surrounds these screen sections interrupting the wicking of the liquid, the screen does not become wet until the liquid contacts. Gas leaves through these screen vents, allowing the channels to fill completely. A similar section of screen at the high point of the coverplate allows the reservoir region of the trap to fill completely.

The trap could be handled as required, rotated from vertical to horizontal and vice versa, as long as the offload was not greater than about 40%. At greater offloads the coverplate would not remain stable in 1-g and liquid would be lost from the reservoir region. The 250 x 1370-mesh screen can support 45.7 cm (18 in.) of N_2O_4 in 1-g. The reservoir would not refill when the tank is returned upright. It would be necessary to keep the tank vertical throughout the handling procedures after loading to prevent liquid loss from the reservoir. Since the tanks are not overly large or heavy, this would be a feasible approach.

There are other approaches to design of the coverplate if vertical transportation of the tanks is not feasible. If the cone angle of the coverplate was increased to 20 deg and a coarser screen was used on the coverplate (such as 165 x 800-mesh Dutch twill), the coverplate would become unstable during the boost phase of the mission. The reservoir would be refilled by the time the vehicle reached orbit. While this screen would be adequate for retention of liquid on-orbit, it would not provide the added capability of the 250 x 1370-mesh screen. Launching a system in a nonoperational mode is not a sound approach for a man-rated space vehicle. Designing the coverplate to be unstable in 1-g (this approach allowed the small refillable trap to refill in 1-g) does not yield a reasonable configuration and operation of the device would be compromised.

These are the only operations accomplished during the turnaround process that would affect the device. All other operations would be accomplished in a normal manner.

VI. DEVELOPMENT PLAN

This chapter presents a plan for developing the flight prototype earth-storable OMS propellant acquisition/expulsion system. In addition to developing fabrication, quality control, and acceptance procedures for the specific prototype system, the plan includes development testing, preparation of a final detail design, and documentation. The plan also presents the schedule and budgetary cost estimate for the development program.

A. OBJECTIVE, GUIDELINES, AND APPROACH

1. Objective

The objective of this plan is to define a development program for an earth-storable OMS capillary propellant acquisition/expulsion device.

2. Guidelines

The candidate passive acquisition/expulsion devices considered in this plan are the refillable trap design and the enlarged trap design presented in Chapter V. These designs are based on the mission criteria presented in Chapter II. A nitrogen tetroxide/monomethylhydrazine bipropellant system is baselined.

3. Approach

Extensive analysis, design, fabrication and testing have already been conducted for capillary propellant control devices (Chapters III and V of this volume, Volume III, and Ref VI-1). Passive control devices have been flight-qualified for Transtage, Agena, Apollo LEM and SPS, and the Mariner 9 spacecraft (Ref VI-2). In addition, the Viking orbiter system has been developed and will fly in 1975. Because of the flight-qualified status of these earth-storable surface tension systems and the demonstrated understanding of low-g fluid mechanics, no subscale or full-scale low-g testing is planned for the concepts used in the prototype design. The development plan will instead formulate guidelines for the detail design, fabrication, quality control, and acceptance and development tests of the capillary control device. Guidelines for the detail design will be given in the design criteria document to be prepared. Fabrication guidelines will be

based on the procedures outlined in Chapter V, Section A. Material selection, structural design, assembly, installation, and cleaning procedures are outlined in Chapter V. Quality control guidelines adequate to meet man-rating requirements will be based on, and conform to, the procedures outlined in the Martin Marietta *Quality Assurance Document* (Ref VI-3), and *Quality Procedures Manual* (Ref VI-4). Guidelines for the test program will be based on the system design requirements as outlined in Chapter II of this volume.

B. PROTOTYPE DEVELOPMENT REQUIREMENTS

The development effort required to bring the prototype design to a flight-qualified status is described in the following paragraphs. The two candidate designs (Chapter V, Fig. V-1 and V-18) will be evaluated against updated OMS system/mission requirements. The small, refillable trap is preferred for the 16-s minimum-burn baseline missions. The planned design analysis, fabrication, and testing tasks are detailed in the following paragraphs. Table VI-1 presents the development status of key design features of the two candidate concepts. Table VI-2 shows the development status of the fabrication techniques.

1. Design Analysis

The design analysis conducted during the earth storable effort of this contract is described in Chapters III and V. The refillable trap concept is documented in detail in an IR&D study completed in December 1972 (Ref VI-5). The subscale trap test model used in this study is shown in Figure VI-1. Figure VI-2 shows the same trap being tested in a minus 1-g condition.

The detailed design effort for the prototype device will include analyses of stress, dynamics, and fluid mechanics. The effects of launch accelerations, acoustic loading, tank slosh, and vibration on the operation of the control device will also be included.

Table VI-1 Device/Tank Development Summary

Design Feature	Development Status	Additional Effort Needed
Performance		
Liquid Expulsion	Plus and minus 1-g testing of trap model performed in IR&D Study 48828 successfully demonstrated methanol expulsion. Methanol expulsion was also demonstrated in a 1-g lateral acceleration mode. Other systems have flown.	None*
Reservoir Propellant Control	Propellant support demonstrated in 1-g and KC-135 tests. Systems have flown.	None*
Interface Stability	Ground test, drop tower, and KC-135 test data are available from contractual studies (Contracts NAS9-8939, NAS8-21259 and NAS8-20837). Screens and perforated plate were subjected to acceleration vectors normal and parallel to the capillary material surface.	None*
Liquid Damping	Experimentally evaluated under Contracts NAS8-21259 and NAS8-20837. Slosh modes were investigated under Contract NAS7-754 and VO'75.	None*
Screen Cleaning	Compatibility of device material with the storable propellants was thoroughly investigated under Contracts NAS7-754 and NAS2-6548. This technology is being further advanced in the Viking Orbiter 1975 program under JPL Contract 953261.	None*
Gas Purging/Trap Refill	Satisfactory venting of gas in trap during simulated engine burn accelerations demonstrated (IR&D Study 48828).	None*
Bubble Point	Single and multilayer screens have been tested using methanol. The technique is developed.	None*
Tank Loading	Demonstrated in numerous programs with trap model.	None*
Control		
Fluid Quality	Liquid vapor sensors have given adequate evaluation of fluid quality and would be desirable in the full-scale device/tank prototype test article.	Install in prototype assembly
Mass Gaging	No device has been used to satisfaction yet. Work being done by NASA and the Air Force holds promise for application.	Test data on new devices desirable
Inspection		
Spray Device	Spraying of capillary screen device with liquid to prepare for bubble point check has been demonstrated as an acceptable procedure. It has been used on small tanks and on the 1.78-m (70-in.) diameter experimental tank built under IR&D Task 48735. Remote inspection is discussed in Volume III and Chapters IV and V of this volume.	1-g testing on the prototype device recommended
* Capability of the specific design should be demonstrated in the development test program for the prototype device, however.		

Table VI-2 Fabrication Development Summary

Design Feature	Development Status	Additional Effort Needed
Fine-Mesh Capillary Screen Forming	Single curvature forming presents no degrading of the screen bubble point. Variations before and after forming are less than the variations occurring in "as-received" material.	None
Screen Joining	Brazing, welding, and diffusion bonding have all been successful techniques. More experience has been accumulated with the stainless steel screens.	None for stainless steel. Aluminum and titanium need more development
Dissimilar Metal Joining	The finest mesh screen is presently available only in stainless steel with aluminum screen next. The tanks are frequently made of titanium. This is always an area of concern.	More study desirable
Cleaning Techniques	Acceptable cleaning techniques have been demonstrated without degrading the bubble point of the screen.	None
Screen Support	Extensive experience has been accumulated for techniques to support the fine-mesh screen. Perforated plate, coarse screen, and combinations of screen and plate have been successfully used.	None
Device-to-Tank Attachment	The refillable trap device is an integral part of the removable aft cover of each propellant tank. It is attached to the cover with a bolt/gasket combination (see dissimilar metal joining).	None

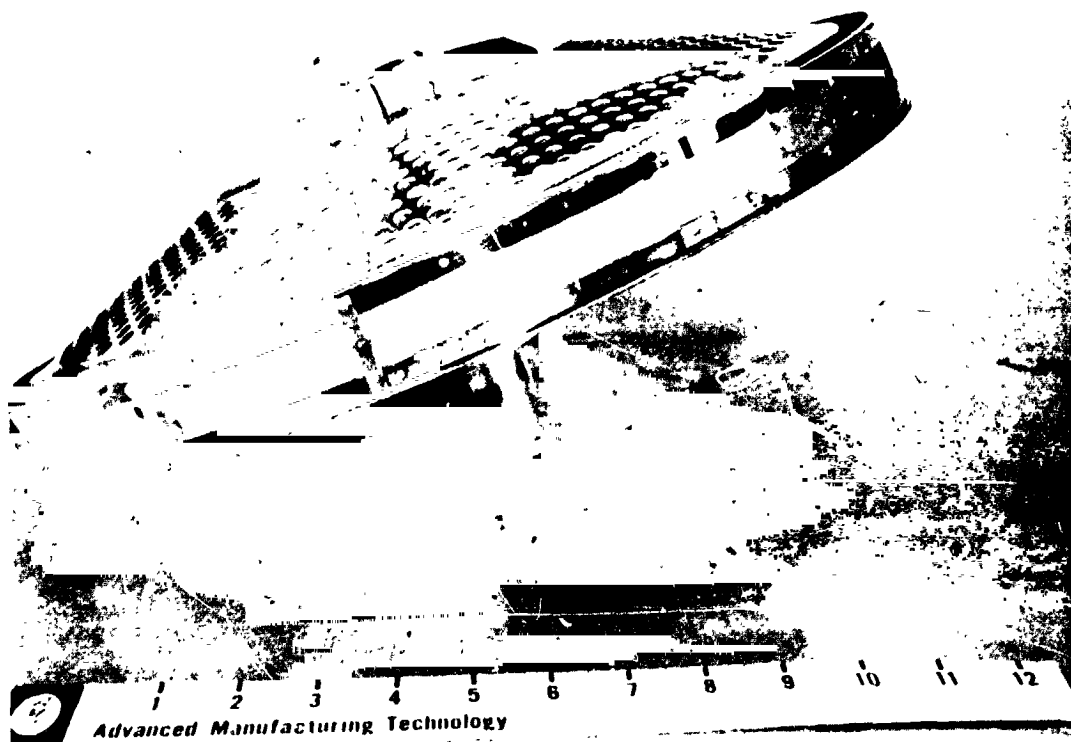


Figure VI-1 Subscale Trap Model



Figure VI-2 Minus 1-g Outflow

2. Fabrication and Test

As part of the fabrication activity, specific manufacturing and inspection techniques will be developed for the full-scale prototype device. Provisions will be made to allow inspection of the device while in the tank. This will enable verification of screen integrity and cleanliness and the absence of any flow blockage without removing the trap module. Quality control of the prototype designs during manufacturing to assure flight qualification of the units will be maintained by adhering to the Martin Marietta *Quality Assurance Document* (Ref VI-3) and *Quality Procedures Manual* (Ref VI-4).

The prototype passive propellant management device/tank assembly will be tested in the laboratory area. In this test area, acceptance tests and conventional fill and drain, outflow, and pressure cycling tests will be performed in the 1-g environment. Launch accelerations will be simulated by placing the prototype/tank on a centrifuge. Fill and drain tests will be performed to demonstrate the adequacy of the proposed ground handling procedures. The tests will show that the trap annulus is completely filled, providing the correct procedures are followed. This filling of the trap annulus must be achieved for either full or offloaded propellant tanks. Adequate draining must be demonstrated for the contingency of launch abort or turnaround. Outflow tests will be performed in both the plus and minus 1-g environments, which present more severe conditions than the orbital flight environment. Satisfactory demonstration therefore will assure low-g performance.

Pressure cycling tests will be performed to show that the anticipated number of flights in the Shuttle mission design life (500 flights) will not be detrimental to the capillary screen.

The full-scale prototype tank/device will be subjected to vibration and centrifuge testing to establish that operational and structural integrity will not be impaired by the accelerations experienced during the mission.

C. DEVELOPMENT PROGRAM SCHEDULE

The development program schedule for the earth-storable OMS propellant acquisition/expulsion system is shown in Fig. VI-3. The 13-month program includes all the necessary tasks from program go-ahead to the end of development testing, final detail design, contractual design review, and documentation of the development effort. At the end of this 13-month period, the acquisition/expulsion system will be ready for system flight qualification.

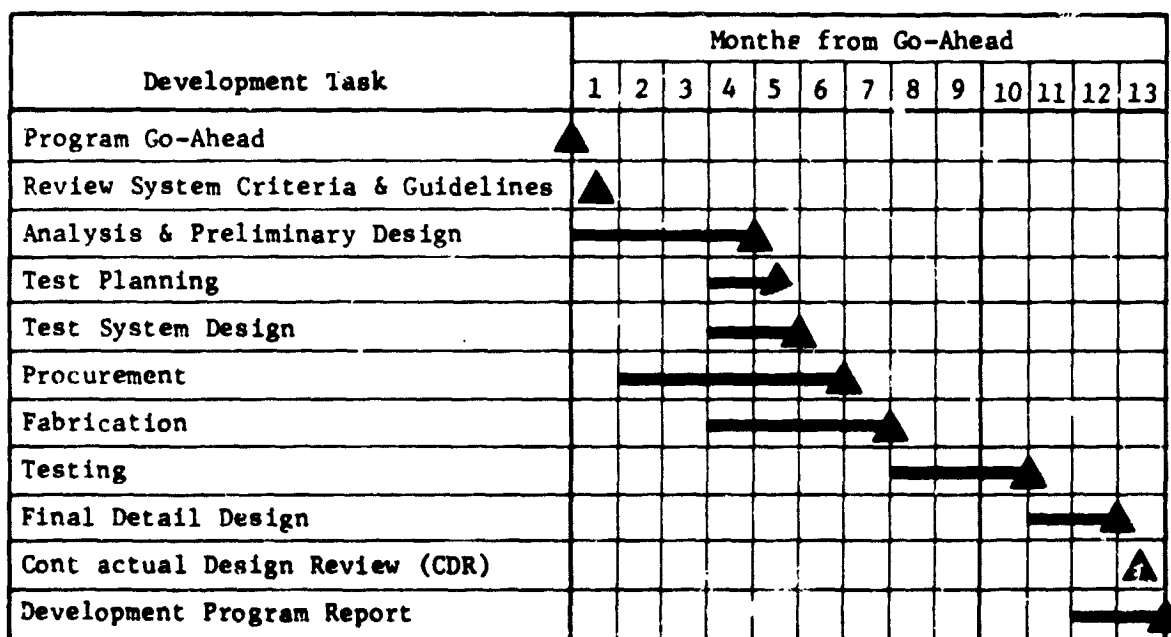


Figure VI-3 Earth-Storable OMS Acquisition/Expulsion System Development Schedule

D. DEVELOPMENT PROGRAM COST

A budgetary cost estimate was prepared for accomplishing the development program outlined in this chapter. The estimate is presented in Table VI-3 in 1973 dollars. These costs include the development of a flightweight propellant acquisition/expulsion system; the remainder of the hardware comprises a full-scale battleship tank and associated ground test system, including valves and other components, lines, and instrumentation.

Table VI-3 Development Program Cost

Analysis and Design	\$105K
Procurement and Fabrication	115K
Development Tests and Final Design	130K
TOTAL COST	\$350K

VII. CONCLUSIONS AND RECOMMENDATIONS

A. CONCLUSIONS

Based on a general set of mission criteria and guidelines for an OMS using earth-storable propellants, the capabilities of various types of surface tension propellant acquisition devices were evaluated. The passive surface tension technique for providing gas-free liquid on demand is superior to other methods. Systems that use capillary pumping to orient the liquid provide insufficient propellant control and are not capable of functioning properly in the given mission environment. Fine-mesh screen systems, in the form of a liner or a trap, are capable of satisfying the mission requirements. Liners, which have unlimited capability with respect to mission duty cycle, are heavy and difficult to install, while trap devices, in general, lack mission duty cycle flexibility. However, if the duty cycle is fairly well defined (as it is in this case), sufficient flexibility can be designed into a trap device to accommodate the expected variations in burn duration and number of burns. In addition, the trap systems are simple, reusable, inspectable, lightweight, insensitive to propellant off-loading, and can be modularly installed. For these reasons, trap devices were selected for this OMS application.

Two representative trap designs were accomplished for both the fuel and the oxidizer. Each design presents a different approach to satisfying the mission requirements. The preferred design is a small trap, refillable during OMS engine burn, and the other is a larger, nonrefillable trap. Performance, fabrication, reliability, and reusability of both the devices were considered in the designs. It was shown that these devices are capable of providing gas-free liquid to the engines, as required, and will satisfy the mission reusability requirements, i.e., loading, handling, and reuse with minimum test and inspection. These earth-storable systems are considered state of the art. Fabrication techniques are developed and the systems can be acceptance tested and the design verified through ground testing. A 13-month program, costing an estimated \$350,000, is required to develop the system.

The results of the test program provided data to aid in definition of the capabilities of the various types of surface tension devices. The performance of a multiple-screen system was established under

both static and dynamic conditions. Test results showed that the rate of gas flow through each screen and the duration of exposure are controlling factors in determining transient performance of multiple-screen systems. Several minutes of exposure to acceleration environments exceeding the static retention capability are required to produce gas penetration through large multiple-screen barriers of relatively few layers. Other tests demonstrated that liner and trap devices can be loaded, handled, and tested as they would be during the ground operations of an OMS system. Acceptance and inspection tests were performed and evaluated; the designs can be verified through ground testing. Remote inspection techniques are available for evaluating the integrity of surface tension propellant acquisition/expulsion systems while installed inside the tank.

B. RECOMMENDATIONS

It is recommended that the surface tension propellant acquisition/expulsion devices selected and designed in this study be considered for any earth-orbital propulsion system having similar mission criteria. The future effort required to take the preliminary designs presented here and develop them into flight-qualified systems is outlined in the development plan. A specific, immediate application of these results is the OMS for the Space Shuttle. The agencies responsible for the selection, design and development of the OMS propellant acquisition system should be guided by the results presented in this report.

Because of the promising results obtained with multiple-screen barriers, additional centrifuge testing should definitely be conducted. An in-depth assessment should be made to substantiate and improve the empirical gas ingestion relationships developed in this program. It is recommended that lateral stability tests be conducted without outflow in a more sophisticated test system. These should then be followed by tests with outflow to determine the effect of liquid flow dynamics on gas ingestion. The experimental study should include determination of the magnitude and effect of any flow blockage due to gas entrapment between screens and the effect of screen spacing. Inspection of these multiple-screen systems should also be considered.

VIII. REFERENCES

- I-1. G. F. Holle: *Earth-Storable Acquisition/Expulsion System Program, Design Requirements Document*. MCR-72-195. Martin Marietta Corporation, Denver, Colorado, July 1972.
- I-2. D. A. Fester, et al.: *Acquisition/Expulsion System for Earth-Orbital Propulsion System Study, Earth-Storable System Comparison, Interim Report*. 1662-73-01. Martin Marietta Corporation, Denver, Colorado, April 1973.
- I-3. G. F. Holle and E. R. Herrington: *Acquisition/Expulsion System for Earth-Orbital Propulsion System Study, Earth-Storable System Test Plan*. MCR-72-279. Martin Marietta Corporation, Denver, Colorado, September 1972.
- II-1. *Orbit Maneuvering System Trade Studies*. Contract NAS9-12755. McDonnell Douglas Corporation, St. Louis, Missouri.
- II-2. H. L. Paynter, et al.: "Zero-G Liquid Propellant Orientation by Passive Control." Paper presented at SAE-ASME Transport and Space Meeting, New York, April 1964, Martin Marietta Corporation, Denver, Colorado.
- II-3. S. B. Brodie, et al.: *Preliminary Design of a Shuttle Docking and Cargo Handling System*. Martin Marietta Corporation, Denver, Colorado, December 1971. (Contract NAS9-11932)
- II-4. J. R. Tewell and C. H. Murrish: *Engineering Study and Experiment Definition for an Apollo Applications Program Experiment on Vehicle Disturbances Due to Crew Activity*. NASA CR-66277. Martin Marietta Corporation, Denver, Colorado, March 1967.
- II-5. E. W. Washburn (Editor): *International Critical Tables of Numerical Data, Physics, Chemistry and Technology*. McGraw-Hill Book Company, New York, N.Y., 1926.
- II-6. *Liquid Propellant Manual (Unclassified)*. Chemical Propulsion Information Agency, Silver Springs, Maryland, December 1966. (Confidential)
- II-7. P. E. Uney and D. A. Fester: *Material Compatibility with Space-Storable Propellants*. MCR-72-26. Martin Marietta Corporation, Denver, Colorado, March 1972.

- II-8. B. Kit and D. S. Evered: *Rocket Propellant Handbook*. The Mac-Millan Company, New York, N.Y., 1960.
- II-9. E. L. White, W. K. Boyd, and W. E. Berry: *Compatibility of Materials with Rocket Propellants and Oxidizers*. Memorandum 201. Defense Metals Information Center, Columbus, Ohio, January 1965.
- II-10. R. J. Salvinski et al.: *Advanced Valve Technology, Volume II - Materials Compatibility and Liquid-Propellant Study*. 06641-6014-R000. TRW Systems Group, Redondo Beach, California, November 1967.
- III-1. T. E. Bowman: *Cryogenic Liquid Experiments in Orbit; Vol I, Liquid Settling and Interface Dynamics*. Martin Marietta Corporation, Denver, Colorado, December, 1966. (Contract NAS8-11328)
- III-2. R. E. Hise and J. R. Tegart: *Interface Stability in a Spherical Tank*, R-72-48631-001. Martin Marietta Corporation, Denver, Colorado, June 1, 1972.
- III-3. H. L. Paynter et al.: *Experimental Investigation of Capillary Propellant Control Devices for Low-Gravity Environments*. MCR-69-585. Martin Marietta Corporation, Denver, Colorado, June 1970. (Contract NAS8-21259)
- III-4. J. A. Salzman et al.: *Low-Gravity Reorientation in a Scale-Model Centaur Liquid-Hydrogen Tank*. NASA TN D-7168. Lewis Research Center, Cleveland, Ohio, February 1973.
- III-5. T. E. Bowman: "Sheet of Liquid Flowing down a Wall." *The Physics of Fluids*, Vol 14, No. 7, July 1971, p 1578.
- III-6. J. A. Salzman and W. J. Masica: *Experimental Investigation of Liquid-Propellant Reorientation*. NASA TND-3789. Lewis Research Center, Cleveland, Ohio, January 1967.
- III-7. H. M. Satterlee and M. P. Hollister: *Engineers Handbook: Low-g Propellant Behavior*. NASA CR-92083. Lockheed Missiles and Space Company, Sunnyvale, California, May 1967.
- III-8. J. F. McCarthy: "Zero-g Propulsion Problems." *Jet, Rocket, Nuclear, Ion, and Electric Propulsion: Theory and Design*. Springer, Verlag, New York, N.Y., 1968, p 644-727. (W. H. T. Loh, Ed.)

- III-9. J. D. Armour and J. N. Cannon: "Fluid Flow through Woven Screens." *AIChE Journal*, Vol 14, No. 3, May 1968, p 415.
- III-10. D. L. Balzer: *Advanced Propellant Management System for Spacecraft Propulsion Systems, Phase II - Detail Design*. MCR-69-436. Martin Marietta Corporation, Denver, Colorado, September 1969. (Contract NAS9-8939)
- III-11. H. L. Paynter: *Investigation of Space-Storable Propellant Acquisition Devices; Vol II, Design and Analysis*. MCR-70-171 (Vol II). Martin Marietta Corporation, Denver, Colorado, December 1970.
- III-12. R. N. Eberhardt: *Propellant Mass Gaging, Venting, and Handling Technology*. S-72-48828-003. Martin Marietta Corporation, Denver, Colorado, December 1972.
- III-13. Meeting at NASA-KSC between Mr. Andy Anderson of NASA and Mr. James Tegart and Mr. Dale Fester of Martin Marietta Corporation, Denver Division, February 6 and 7, 1973.
- IV-1. D. A. Fester et al.: *Main-Tank Injection for Packaged Liquid Missiles, Phase I Report, Volume II - System Feasibility Testing (U)*. AFRPL-TR-66-115 (Vol II). Martin Marietta Corporation, Denver, Colorado, March 1967. (Confidential)
- IV-2. G. Herrington: *Annealing of Plexiglass to Inhibit Methanol Attack*. IDC, Martin Marietta Corporation, Denver, Colorado, December 1, 1972.
- IV-3. R. N. Eberhardt: *Propellant Mass Gaging, Venting, and Handling Technology*. S-72-48828-003. Martin Marietta Corporation, Denver, Colorado, December 1972.
- V-1. R. N. Eberhardt: *Propellant Mass Gaging, Venting, and Handling Technology*. S-72-48828-003. Martin Marietta Corporation, Denver, Colorado, December 1972.
- V-2. H. L. Paynter: *Investigation of Space-Storable Propellant Acquisition Devices, Vol II - Design and Analysis*. MCR-70-171 (Vol II). Martin Marietta Corporation, Denver, Colorado, December 1970.
- V-3. D. A. Fester et al.: *Space-Storable Propellant Acquisition System*. NASA CR114493. Martin Marietta Corporation, Denver, Colorado, October 1972.
- VI-1. *Capillary Screen Device Technology*. M-70-18. Martin Marietta Corporation, Denver, Colorado, July 1970.

- VI-2. D. A. Foster: *Acquisition/Expulsion System for Earth-Orbital Propulsion System Study, Earth-Storable System Comparison*. 1662-73-01. Martin Marietta Corporation, Denver, Colorado, April 1973.
- VI-3. *Quality Assurance Document*. M-64-119 (Rev 3). Martin Marietta Corporation, Denver, Colorado, March 1970.
- VI-4. *Quality Procedures Manual, Vol I, II, and III*. Martin Marietta Corporation, Denver, Colorado.
- VI-5. R. N. Eberhardt: *Propellant Mass Gaging, Venting, and Handling Technology*. S-72-48828-003. Martin Marietta Corporation, Denver, Colorado, December 1972.